VU Research Portal

Design & synthesis of small-molecule modulators of the histamine H1 receptor

Wang, Zhiyong

2021

document version
Publisher's PDF, also known as Version of record

Link to publication in VU Research Portal

citation for published version (APA)
Wang, Z. (2021). *Design & synthesis of small-molecule modulators of the histamine H1 receptor*. s.n.

Design & synthesis of small-molecule modulators of the histamine H$_1$ receptor

Zhiyong Wang

VRIJE UNIVERSITEIT

Design & synthesis of small-molecule modulators of the histamine H$_1$ receptor

ACADEMISCH PROEFSCHRIFT

ter verkrijging van de graad Doctor

aan de Vrije Universiteit Amsterdam,

op gezag van de Rector Magnificus

prof.dr. V. Subramaniam,

in het openbaar te verdedigen

ten overstaan van de promotiecommissie

van de Faculteit der Bètawetenschappen,

op dinsdag 6 april 2021 om 13.45 uur

in de online bijeenkomst van de universiteit,

De Boelelaan 1105

door

Zhiyong Wang

geboren te Hubei, China

promotor: prof.dr. R. Leurs

copromotor: dr. M. Wijtmans

Contents

Chapter 1: Introduction

GPCR modulation by small-molecule ligands: concepts and approaches

Drug discovery

A drug discovery program is a long and complex process. From the initial idea to the approval of a drug can take 12–15 years and has in the past been estimated to cost more than $0.8 billion[1], as shown in Figure 1. More recent data shows an average cost for each newly approved drug of 1.4 billion euro.[2] The initial research starts with the need for suitable medical products for diseases, which drives the motivation of the research program (Figure 1). This firstly requires selection of an appropriate biological target with respect to the disease. Use of a bioinformatics approach with available biomedical data and use of phenotypic screening can help the identification of disease relevant targets.[3] After identification of a possible target, its validation needs to be fully executed. A variety of techniques have been developed, such as antisense technology, transgenic animals, monoclonal antibodies and chemical genomics.[4] Next, screening of compound collections can be performed to give hit molecules which have the desired target activity. Screening strategies include high throughput screening (HTS), virtual screening, phenotypical screening, NMR screening, fragment-based screening, as well as other compound screens. Suitable hits obtained from screening will be retested and evaluated by relevant orthogonal assays. Typically, a small set of hit series is defined which has the required features and these series will be elaborated upon to improve potency and selectivity. These first steps will take a few years and lead to average costs in excess of 24 M$.[1, 3] In the hit-to-lead stage, more potent and selective compounds from the hit series are synthesized and tested. Structure-activity-relationship (SAR) as well as physicochemical properties, for instance, solubility, permeability, and *in vitro* ADME properties, need to be assessed. The average costs for this phase are 49 M$. The final drug discovery phase is lead optimization. Genotoxicity tests (e.g. Ames test), *in vivo* models, metabolic profiling, high-dose pharmacology and PK/PD studies are carried out. In this phase, one or two candidate molecules will typically be obtained from 100 initial compounds. On average, the whole process of lead discovery (meaning hit finding, hit-to-lead and lead optimization) costs 195 M$ and takes 3 years. Once a candidate is selected, subsequently pre-clinical studies are conducted. Safety, pharmacology and toxicology studies are performed to assess pharmacodynamic properties and safety in animals. Moreover, pharmacokinetic and toxicokinetic properties need to be examined.[5] Metabolism and tissue distribution studies are performed. This whole phase may cost 62 M$ with a typical length of 1 year. Human trials will be initiated if pre-clinical studies provide suitable results. A Phase I trial is designed to evaluate the safety and maximum tolerated dose (MTD) of a drug candidate in humans. Phase II trials are designed to test safety, pharmacokinetics, and pharmacodynamics, as well as further determination of optimal doses, dose frequencies and primary administration routes. In the phase III trial, drug efficacy and incidence of common adverse reactions need to be thoroughly studied in a larger and more diverse population.[6] Clinical research takes on average 6 years. Approximately two third of average total development cost of a medicine (548 M$)

supports this stage of studies. After FDA filing the compound can ultimately become a marketed medicine.
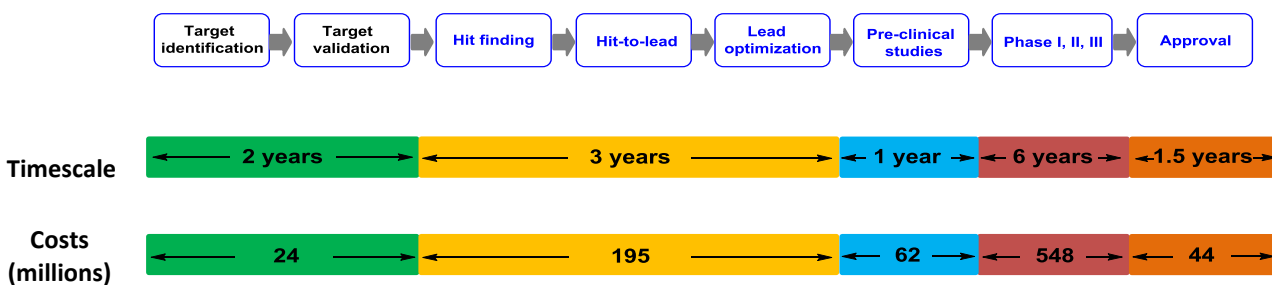
Figure 1. Overview of the drug discovery and development process and associated average timescale and average costs of each phase. The data shown is extracted from Hughes *et al*. and Paul *et al*. [1, 3]

G Protein-Coupled Receptors

Therapeutic relevance

Currently, 34% of all FDA-approved drugs (a total of 475 drugs) target 108 different G protein-coupled receptors (GPCRs).[7, 8] From 2012 to 2017, 69 new drugs targeting GPCRs have been approved by the FDA.[8] Clearly, GPCRs are a protein family of major therapeutic relevance and, in fact, are one of the largest protein families in mammalian genomes.[9] Indeed, this superfamily comprises over 800 GPCRs.[10] GPCRs are membrane-bound receptors and contain seven transmembrane alpha-helices (Figure 2). The specific structure of GPCRs enables cellular communication and these proteins are therefore involved in a diversity of physiological process.[11] Many extracellular signals, including photons, ions, neurotransmitter, small peptides, hormones and synthetic molecules can modulate these receptors. Since GPCRs respond to a large variety of different stimuli and form one of the largest protein families, GPCRs are acknowledged as the largest class of drug targets in drug discovery.[12]
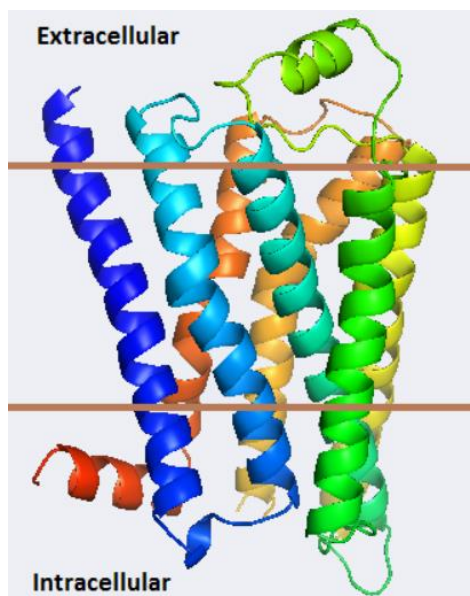
Figure 2. GPCR structure showing the seven transmembrane alpha-helices that pass the cell membrane (schematically indicated by the orange lines). Figure taken from Witter *et al*. [13]

Different classification systems have been developed for the GPCR superfamily with respect to e.g. physiological and structural features. Based on the most commonly used phylogenetic criteria, the human GPCRs superfamily can be divided into 5 classes (Figure 3A): glutamate, rhodopsin, adhesion, frizzled/taste2 and secretin.[10] This so-called GRAFS classification[14] is complementary to the more classical distinction in Family A (rhodopsin-like), Family B (secretin-like), Family C (glutamate-like) and Family F (adhesion frizzled/taste-like) GPCRs (Family D and E are not existing in the human genome). In the past few decades, structural biology on GPCRs has progressed vastly. More than 150 crystal structures of GPCR proteins have been disclosed to date.[15] Of the GPCRs targeted by approved drugs, 46 have such a disclosed structure (Figure 3B)[16] which in many cases helped to provide insights into the binding of the drug. Currently, there are over 142 active compounds in clinical trials targeting 83 distinct GPCRs (Figure 3C).[16] This progress in structural biology together with advances in molecular pharmacology provide a better understanding of signaling modulation and protein-ligand interaction.
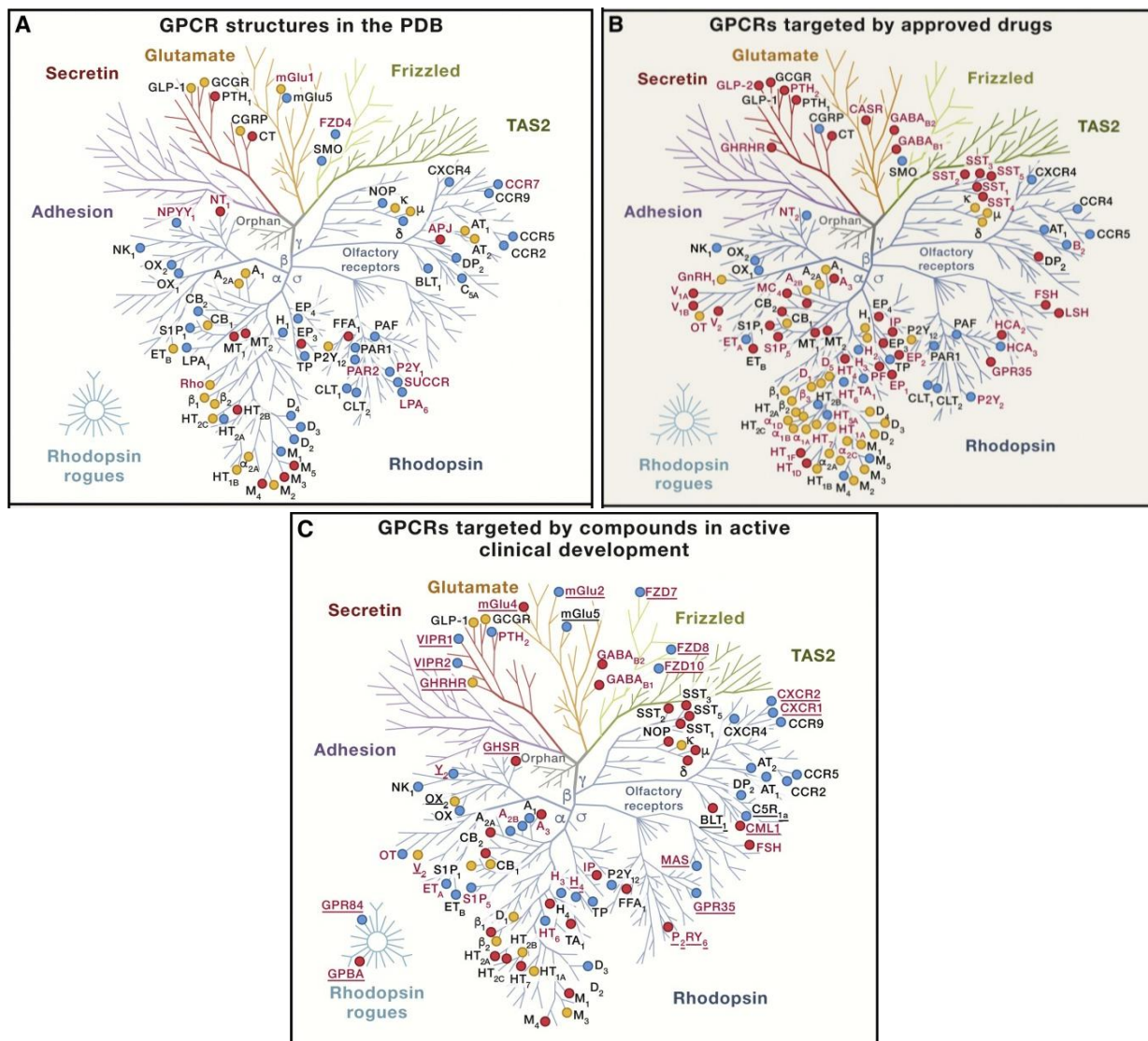
Figure 3. (A) GPCR structures present in the Protein Data Bank (PDB). Colored circles represent structures with ligands in the structure: red, agonist/positive allosteric modulators; blue, antagonist/negative allosteric modulators; yellow, both types. When a crystal structure has been determined, but no drug has been approved or no active compound is in clinical development then the name of target/receptor is colored red. (B) GPCRs targeted by approved drugs. The color scheme is the same as in (A), except for red names: if a structure of receptor has not been determined, the name of the receptor is in red. (C) GPCR with agents in active clinical development. The color scheme is the same as in (A), except for red names: if a structure of receptor has not been determined, the name of the receptor is in red. Figures taken from Congreve *et al*.[16]

GPCR signaling
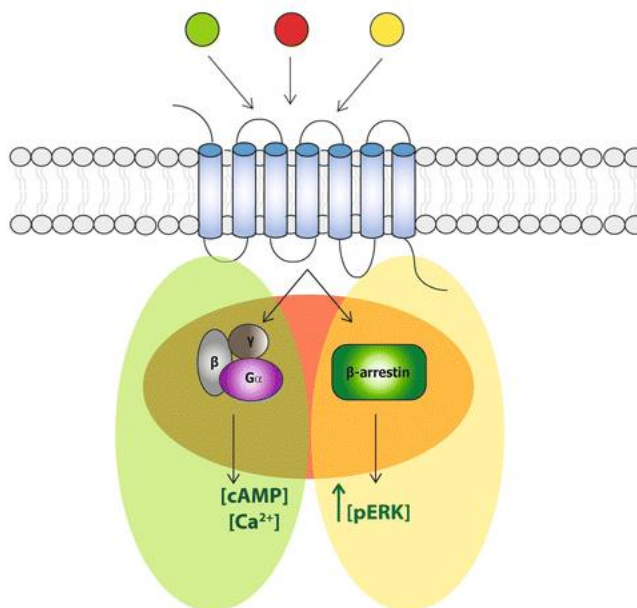
Figure 4. Schematic representation of G protein and β-arrestin activation and biased signaling. Different ligands can induce distinctive signaling pathway via distinctive receptor conformations. *Green* ligand, G protein biased; *red* ligand, non-biased; *yellow* ligand, β-arrestin biased. Figure taken from Mocking *et al*.[17]

Once an external stimulus (green ligand in figure 4) binds and activates a GPCR, this binding event will activate a G protein. Subsequently, secondary messengers (cAMP, IP$_3$ etc) will be generated depending on the G protein involved (Figure 4).[18] Increasing evidence shows that GPCRs can also induce signaling by activation of β-arrestins instead of a G protein (Figure 4).[19] The two processes of activation are distinct. For the G protein pathway, upon heterotrimer activation the G protein subunits dissociate. G$_\alpha$ modulates the production of second messenger such as cAMP and Ca^{2+}, whereas the G$_{\beta\gamma}$ modulates separate downstream signaling networks such as the activation of ion channels, receptor kinases and others. A β-arrestin biased ligand (yellow ligand in figure 4) binds to the receptor, whereafter only β-arrestins are activated. The pathway induces effects such as desensitization or ERK phosphorylation.[20] A non-biased ligand (red ligand in figure 4) can stimulate both G protein and β-arrestin pathways, and further induce effects.

Small molecules in GPCR research

Small molecules are used frequently to modulate GPCRs, both as endogenous molecules, exogenous research tools and therapeutic drugs. Based on their mode of action at the respective GPCR, ligands are pharmacologically classified as shown in Figure 5. Compounds that induce 100% activation are defined as full agonists, such as endogenous agonists (hormones, neurotransmitters, ..). Agonists which do not induce full activation are called partial agonists.

Inverse agonists are antagonists that can decrease any constitutive activity of a GPCR, whereas neutral antagonists only bind to the receptor thereby competing with agonists and inverse agonists, but these ligands do not affect GPCR activity on their own.

Small-molecule GPCR ligands can either interact with orthosteric site (the site where the endogenous ligand binds) or at an allosteric binding site. Allosteric modulators which increase the activity of an agonist are called positive allosteric modulators, whereas negative allosteric modulators decrease the affinity of an agonist.[20] With the emerging evidence for both G protein and β-arrestin signaling pathways, so-called biased ligands can affect one of these two pathways predominantly.
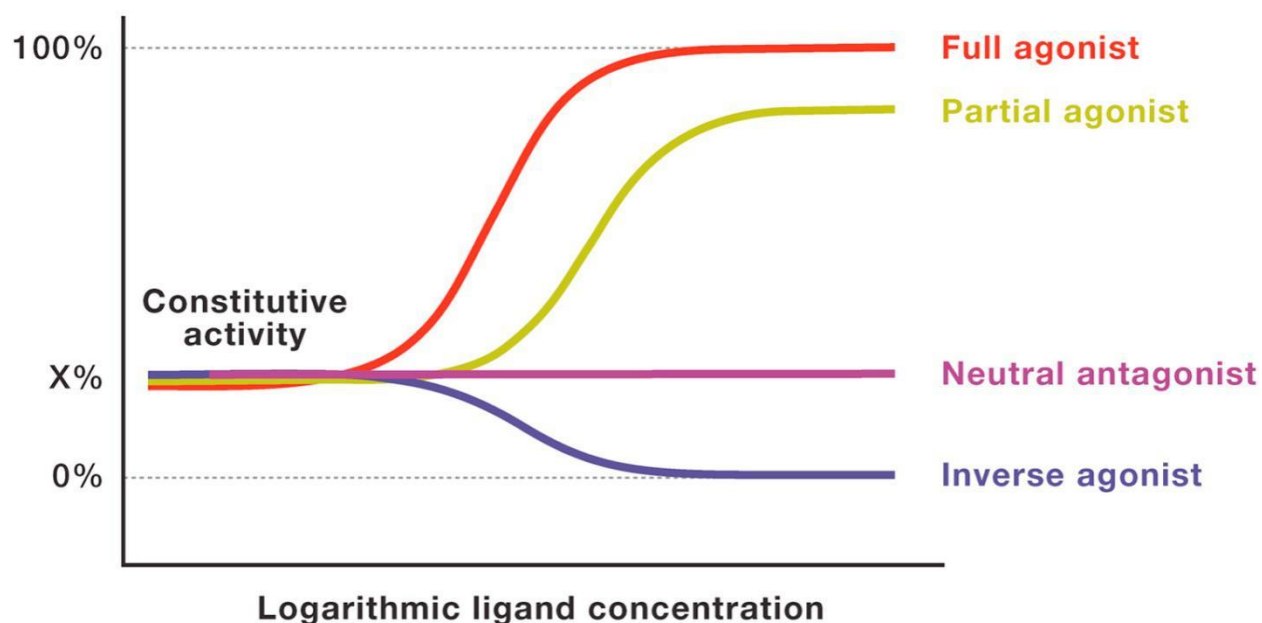
Figure 5. Different activity profiles in GPCRs induced by distinct signal transducers. Figure taken from Wacker *et al*.[20]

The equilibrium binding constant ("affinity") of small molecule binding to a GPCR (expressed as K_D or K_i, or the associated pK_D or pK_i values) has been extremely important for drug discovery as a way to rank their potential following initial screening campaigns. As a result of the widespread utilization of binding affinity in drug discovery, many strategies have been developed to optimize the binding affinity of compounds.[21-23] A classical approach is the development of a structure-activity relationship (SAR), in which the effect of (small) changes in a ligand structure on the K_i value is examined. Another widely applied medicinal chemistry strategy in small-molecule GPCR ligands is that of using isosteres. The size, shape, pK_a, polarity/lipophilicity, electronic distribution and polarizability all potentially contribute to the biological effect of a functional group in a ligand.

Bioisosteres are functional groups that are alike in biological terms once incorporated in ligands rather than in these physical properties. The utility of bioisosteres is broad and ranges from improving potency, and enhancing selectivity to addressing metabolism, modifying toxicophores and acquiring intellectual property.[24] Classical bioisosteres typically encompass simple changes in structures,[25] but the concept can be further expanded by using nonclassical bioisosteres, which involve more subtle and distinct forms of similarity in biochemical effects. Isosteres for the carboxylic acid functionality have been well studied.[26, 27] A classical example in the GPCR field can be found in the development of angiotensin II receptor blockers such as the marketed drug Losartan (Figure 6).[28] An advanced compound with a key acid functionality on a biphenyl moiety has an IC_{50} value of 200 nm. The acid was replaced by a phenyl tetrazole, of which the NH is acidic enough to be deprotonated substantially at pH 7.4. This modification conferred a 7-fold increase in potency compared to the carboxylic acid analogue. Other isosteres of carboxylic acid, i.e. two regioisomeric acyl sulfonamides, either showed 9.5-fold higher or 7-fold less binding affinity compared to the tetrazole. Geometrical analysis indicated that the longer distance between the acidic atom and aryl ring may be beneficial for ligand binding (Fig. 6).[24] The tetrazole compound losartan has been a successful marketed drug for hypertension, diabetic kidney disease and heart failure.[29]
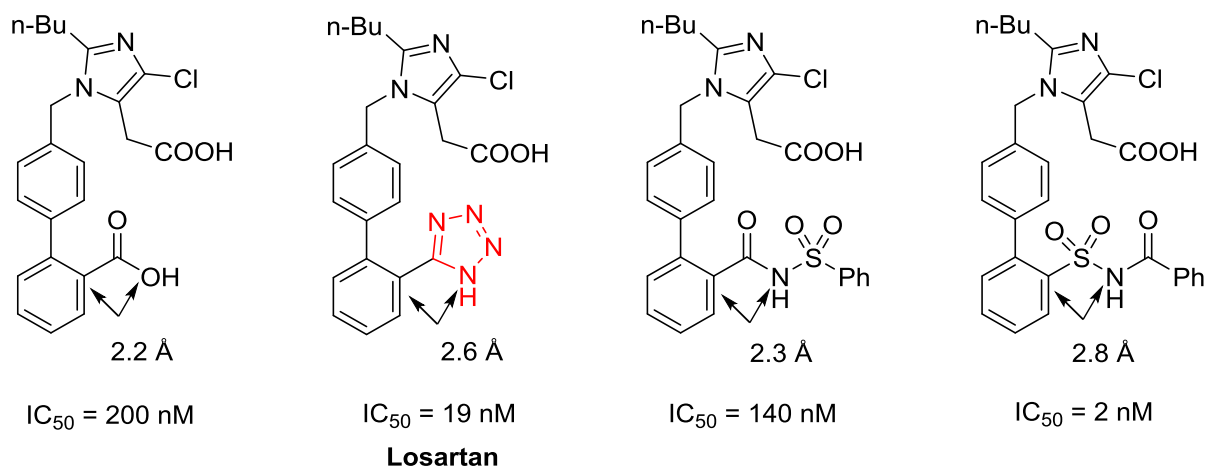
Figure 6. Structures of angiotensin II receptor antagonists and rationale for the use of bioisosteres.[24, 28]

Kinetics of ligand binding to GPCRs

As explained, SAR studies using equilibrium binding parameters on GPCR-targeting small molecules have become important in drug discovery as a way to rank the potential of the ligands. [21-23] However, recently the kinetics of ligand-GPCR binding has been an emerging strategy for describing drug-target interactions.[30, 31]

Binding kinetics in drug discovery

For optimization of the binding kinetics, the drug-target residence time (RT) is a parameter related to the time the compound spends bound to its target. More specifically, it is a measure for the half-life of dissociation of the ligand from the receptor. The parameter RT rather than equilibrium binding affinity is increasingly considered to better predict the *in vivo* efficacy of drugs[32-39], although varying views on the validity of this assumption exist.[40] Studies on ligand binding kinetics have also been performed on GPCRs.[41-46]

In principle, binding kinetics describe how fast a molecule binds to its target and how fast it dissociates from the target. Multiple mechanisms for the ligand binding reaction have been proposed.[32, 36, 46-48] Here, the simple one-step model is described.[32] In Figure 7A, ligand binding of a small molecule (L) to a GPCR is schematically depicted. When a single ligand binds to a receptor (GPCR), it will form a binary ligand-receptor complex (GPCR+L). The rate of ligand association can be described as [L]·[GPCR]·k_{on} (association rate), while the rate of ligand dissociation can be described as [GPCR+L]·k_{off} (dissociation rate). When the dissociation rate equals the association rate, the system reaches a state of equilibrium. The equilibrium dissociation constant (K_d) is described by the ratio of k_{off} over k_{on} (Figure 7B). The residence time (RT) of a ligand, which is an often used metric to describe the half-life of the formed complex, is defined as the reciprocal of the dissociation rate constant ($1/k_{off}$).[32]
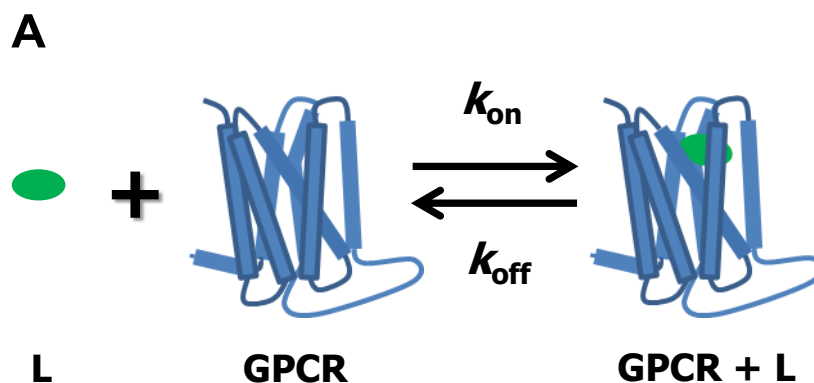
Figure 7. Schematic representation of one-step ligand binding to a GPCR. (A) A ligand binding to a GPCR is a reversible reaction. (B) At equilibrium, the dissociation rate [GPCR+L]·k_{off} is identical to the association rate [L]·[GPCR]·k_{on}. The dissociation constant (K_d) can be described by the ratio of k_{off} over k_{on}. The residence time for the ligand is the reciprocal of the k_{off} value.

Some marketed GPCR drugs have been reported to have a long residence time[46] and long residence time is often hypothesised to lead to long duration of action *in vivo*. For example, tiotropium is an antagonist for the muscarinic M3 receptor and used to treat chronic obstructive pulmonary disease. It was noted that the residence time of tiotropium is over 10 h, which may result in long duration of action *in vivo* as well.[49] Another illustration involves candesartan, an angiotensin receptor antagonist, which is used to treat high blood pressure and congestive heart failure. It binds the receptor with a residence time of 3 h, which can be an explanation of long

duration of action *in vivo*.[50, 51] In general, it is still poorly understood how to design slow dissociation into a molecule and/or how to optimize drug residence-time, but there has been an increasing interest in understanding the molecular determinants that modulate binding kinetics. A study on mostly GPCR and kinase ligands in a Pfizer database shows that there is a trend between ligand flexibility and RT. For ligands with molecular weight (300–500 Da), ligands with less rotatable bonds (≤ 5) more often have a shorter drug-target RT than ligands with more rotatable bonds (≥ 5).[52] In a different study on more than 1800 ligands for the dopamine D_2 receptor by Tresadern *et al*, ligands with a higher number of ring structures were observed to have a long RT.[53] These findings suggest that the number of rotatable bonds and the number of rings can influence the drug-target RT. Recently, other strategies have been applied to optimize drug residence time of small-molecule ligands, such as use of a halogen bond[54], application of a shielded hydrogen bond[55] and covalent binding.[56]

Covalent binding

As mentioned, covalent binders represent one path forward to modulate binding kinetics in a defined way. Most small-molecule drugs bind to their targets reversibly, forming non-covalent interactions during the molecular recognition event (Figure 8A).[57] In contrast, covalent binders are designed to interact with biological targets irreversible. The process of covalent binding can be divided into two steps (Figure 8B). Firstly, the covalent ligand is bound to the target protein via non-covalent interactions. Secondly, given a ligand conformation that enables appropriate orientation of the reactive unit of the ligand toward a nucleophilic center in a protein sidechain, the ligand subsequently forms a covalent bond with this nucleophilic residue.[58] In terms of kinetic parameters, the first step in this binding event can be described similarly to the binding of non-covalent ligands. The second step can be described by k_2/k_{-2} in the case of so-called reversible covalent binding, in which the covalent nucleophile-ligand bond is reversibly. If the covalent bond is irreversibly (i.e. k_{-2} is close to zero), the second step can be described by a single rate constant k_{inact} (Figure 8B).[59, 60] This scenario means that the ligand forms an irreversible covalent bond in the binding site, which will result in permanent occupancy of the target binding site until the complex is degraded.[59, 61] Some critical notes can be mentioned about irreversible covalent binding. It may cause cellular damage and off-target effects as a result of non-specific covalent ligand binding. Due to these associated toxicity issues, covalent drugs have mostly been avoided by pharmaceutical industry. However, covalent drugs can possess many advantages compared to non-covalent drugs, including high potency, high efficiency with lower dose and longer duration of action. In the case of reversible covalent binding, it has a lower possibility of inducing toxic effects and immune responses because it still has a possibility to dissociate when off-target binding occurs. In 2011, Sing *et al*. reported that 39 covalent drugs had been approved by FDA by 2011.[61] Approximately one third of them are anti-infective drugs, one fifth are used to treat cancer, 15% treat gastrointestinal disorders and approximately 15% treat CNS and cardiovascular

indications.[61] Some covalent drugs found their way to the market as blockbuster drugs (Figure 9), including Aspirin, lansoprazole, odanacatib, acalabrutinib and clopidogrel.[60, 61] Clearly, when utilized appropriately, covalent drugs can offer therapeutic benefit.
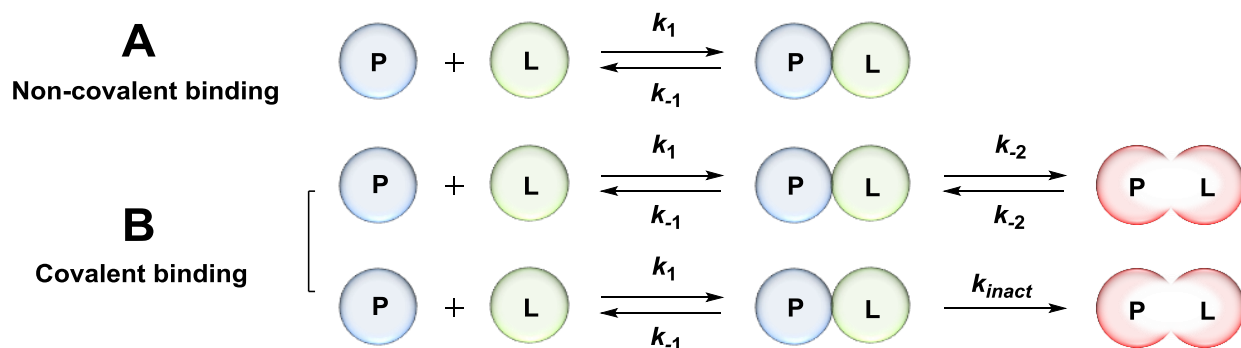
Figure 8. Different modes of binding between protein target P and ligand L. A) reversible binding B) covalent inhibition with reversible covalent binding (top) and irreversible covalent binding (bottom). The image is based on De Cesco et al.[60]
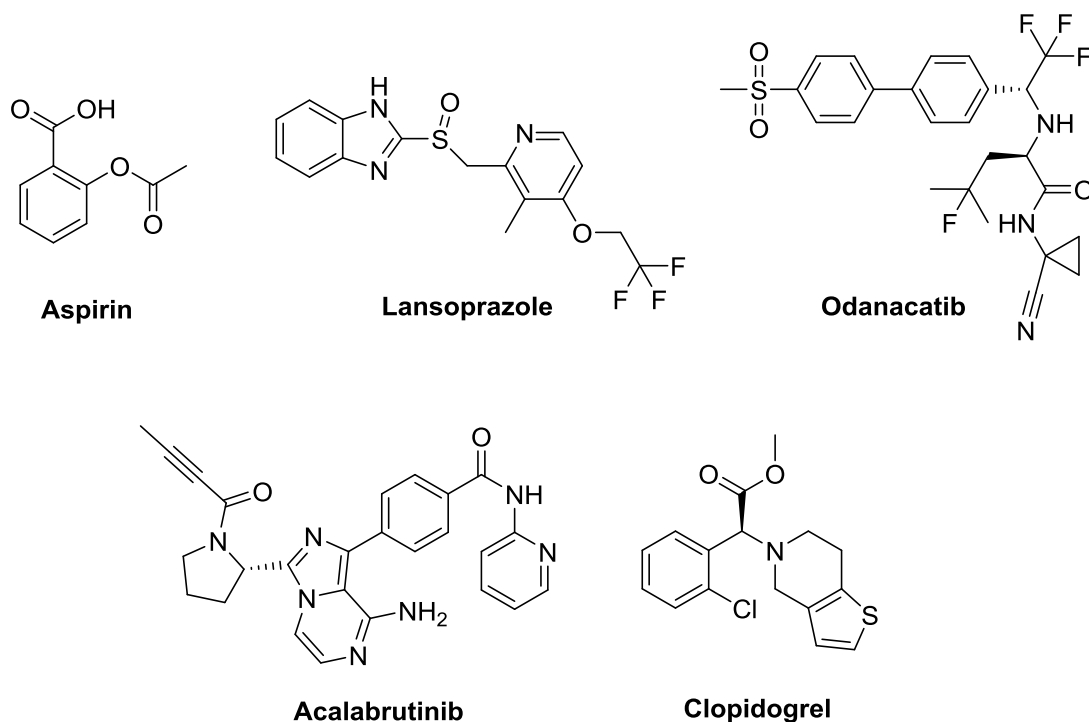
Figure 9. Examples of covalent drugs on the market: aspirin, lansoprazole, odanacatib, acalabrutinib, clopidogrel.[60, 61]

GPCRs, as any protein targets, possess several potential nucleophilic residues, such as cysteine, lysine, serine, cysteine and tyrosine. Not all of these residues are equally applicable to covalent

binding and cysteines tend to be the most targeted nucleophilic residue. Depending on the target residues in binding pocket, suitable electrophilic warheads can be selected with respect to their chemical reactivity.[62] The strategy is then to incorporate such a suitable warhead into a ligand core structure with or without a designed linker between pharmacphore and warhead. clopidogrel (Figure 9) is an example of a covalent drug targeting a GPCR. It was previously found to be a prodrug, which was activated by P450 enzymes to a thiol species which can covalently bind to cysteine residues of P2Y$_{12}$ receptor.[63] Recently, covalent binding has been used to prolong drug-target residence time.[61] Indeed, the use of covalent ligands can be applied to investigate the molecular aspects of GPCR binding kinetics and to help better understand ligand protein interactions.

Photochemical control of GPCR modulation by small molecules

Next to the recent interest in kinetic binding parameters of small-molecule ligands to optimize modulation of GPCR signaling, photochemical modulation (photopharmacology) provides another new approach to GPCR modulation. Photopharmacology is an emerging discipline that addresses the use of photosensitive ligands to study pharmacology. Light is used to control drug activity with, ideally, spatial and temporal regulation of GPCR signalling by light. This remote control can be achieved by incorporating a photosensitive functional group into ligands.[64-66] Two main subareas in this field are photoswitching or photocaging.[67] The field of photopharmacology so far mainly develops new tools for preclinical studies, but some initial clinical translation can be noted. In 2014, Benjamin *et al*. reported that the second-generation photoswitch LiGluR-MAG0$_{460}$ can restore retinal function in rodent and canine models, which can pave the way to clinical translation.[68] Moreover, the approved tyrosine kinase inhibitor axitinib contains a photosensitive stilbene-like moiety, that can be isomerized by UV irradiation, but the optical modulation does not seem to have any role in the clinical use of this drug against renal cell carcinoma.[69]

Photoswitching

The functional groups used in photoswitching are moieties that can photoisomerise, such as azobenzene, stilbene, hemithioindigo, iminothioindindoxyl and spiropyran (Figure 10).[70-74] Upon illumination with a certain wavelength, these moieties can switch between two isomer states (e.g. from the *trans* isomer to the *cis* isomer) which both differ in their structure and properties. The reverse *cis* to *trans* isomerization can be achieved by irradiation with a different wavelength or it occurs thermally. Other classes of photoswitches, such as Stenhouse adducts, dihydroazuelenes and arylhydrazones have been described recently as well.[75-78] The dynamic control of photoswitches enables different modulation of biological targets with ligands that harbor these switches. One of the isomers is intended to bind to a desired biological target,

whereas the other isomer due to its different configuration and properties should bind less to the same target. The concept of this process is depicted in Figure 11. The photoswitchable configurations show different binding affinity, thereby providing pharmacological selectivity. Thus, light offers opportunities to achieve photochemical control via these photoswitchable moieties. Light, if of appropriately low energy, can be relatively harmless. Furthermore, illumination devices with precise spatio-temporal regulation can be enabled, meaning drugs with appropriate photoswitchable features can be activated in some specific area in the body. This can in theory overcome the issue of poor drug selectivity from regular pharmacotherapy. Last but not least, the intensity and wavelength of light can be regulated precisely.[79]

Photoswitching has recently has proven successful for various protein classes, including GPCRs[80, 81] and ion channels.[82-84] Major advancements have been achieved in GPCR photopharmacology and a few examples, including some from our own group, will be described (Figure 12). A structure-activity relationship (SAR) was established using 16 photoswitchable antagonists for the histamine H_3 receptor (H_3R).[85] The synthesized compounds showed moderate to high affinity. Key compound VUF14862 was more active in the *trans* state (pK_i 8.76) than in the *cis* state (pK_i 7.71) in binding and electrophysiology assays. Carreira and co-workers designed and synthesized four photoswitchable compounds based on a parent 3-Br-THC compound.[86] *Trans*-azo-THC-4 showed higher agonist efficacy than its *cis* isomer in whole-cell electrophysiology and FRET-based cAMP assays. A set of photoswitchable ligands were designed and synthesized based on biaryl CXCR3 ligands.[87] Upon illimination, compound VUF16216 gives a switch from antagonism to agonism in G protein activation assays and electrophysiology experiments. In class C GPCRs, application of photopharmacology has also been successful. Alloswitch-1 was designed and synthesized by Llebaria and collaborators as the first potent and selective photoswitchable negative allosteric modulator for the mGlu5 receptor.[88] Significant differences in the pharmacological properties of the *trans* and *cis* compound were shown in functional assays. *In vivo* studies demonstrated that *trans*-Alloswitch-1 induced an inhibitory action on the zebrafish motility.
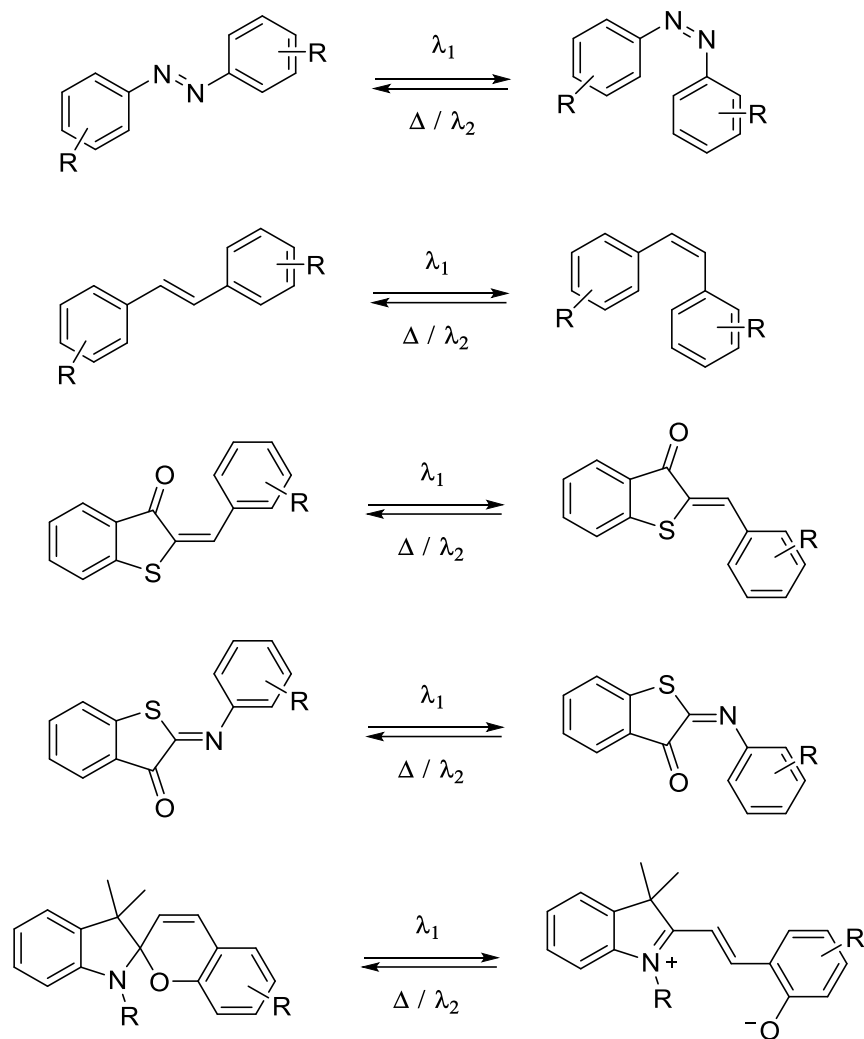
Figure 10. Examples of four types of photoswitches: azobenzene, stilbenes, hemithioindigo, iminothiodindoxyl and spiropyran.
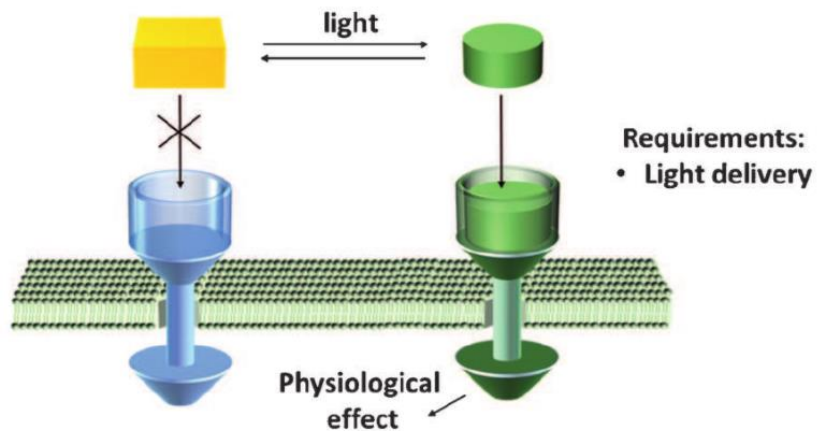
Figure 11. The concept of photoswitching. Different isomeric forms of ligands interact differentially with a target and can induce different physiological effects. Figure taken from Lerch *et al*. [89]

VUF14862

pK_i *trans*: 8.76 ± 0.09

      cis: 7.71 ± 0.09

VUF16216

α_{trans} = 0.16

α_{cis} = 0.99

Azo-THC-4

EC$_{50}$ *trans*: 4 nM

      cis: 55 nM

Alloswitch-1

IC$_{50}$ *trans*   8.6 ± 1.6 nM

      cis   16 ± 1.5 nM
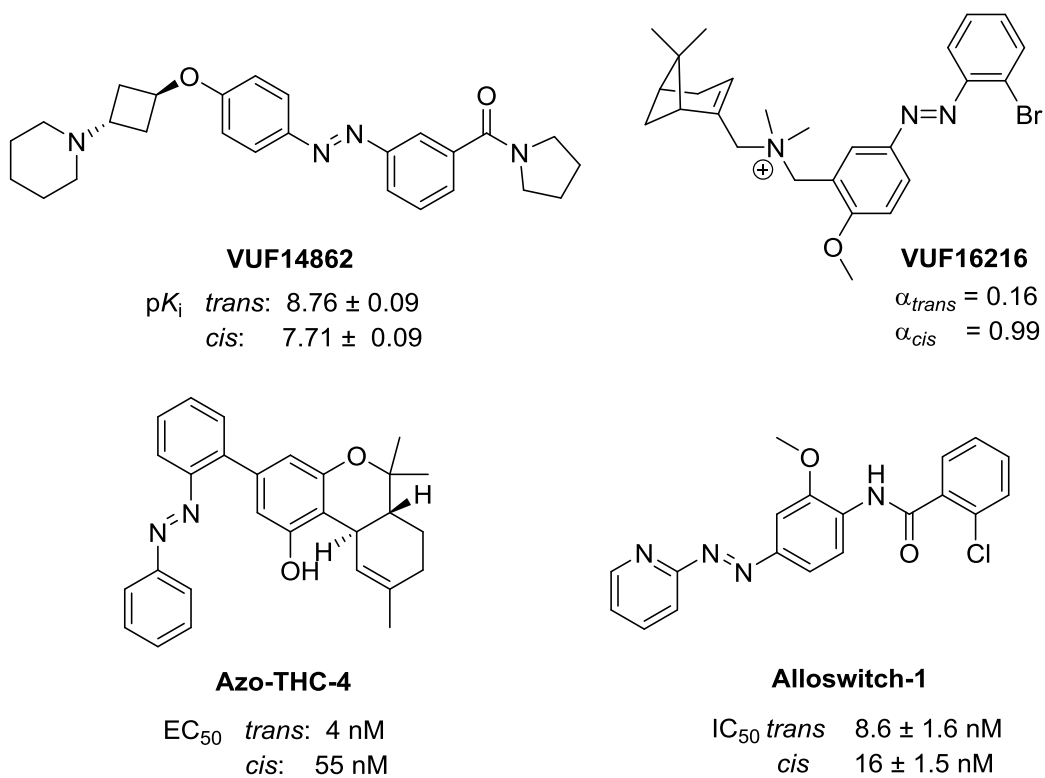
Figure 12. Structures and biological data of exemplary photoswitchable ligands targeting GPCRs: VUF14862[85], VUF16216[87], Azo-THC-4[86], Alloswitch-1.[88]

Photocaging

Another photochemical method for achieving photochemical control is photocaging.[90, 91] It too has the potential to regulate biological processes with a high level of control and temporal resolution, but is not reversible as in the case of photoswitching. The concept of photocaging is depicted in Figure 13. In photocaging, a biologically active molecule is modified with a light-removable protecting group ('caging'), rendering it inactive. The biologically active ligand is formed upon irradiation ('decaging/uncaging'), together with a photoproduct bearing the remnants of the protecting group. Several caging groups (i.e. photoremovable protecting group) have been developed (Figure 14), i.e., coumarin analogs,[92] quinoline-,[93] dibenzofuran-[94] and BODIPY-based structures[95]. Typically, in order to achieve the ability to alter the biological properties, the photoprotecting group is installed at a location as to induce steric blocking of ligand-target interactions or blocking a key interaction such as a salt bridge[96], meaning the caged compound cannot bind its target. The combination of multiple of such effects is likely more common in practice. Upon exposure of the target molecule to light, a photochemical reaction is initiated which releases the biologically active molecule, thereby allowing it to exert its biological activity (Figure 14).
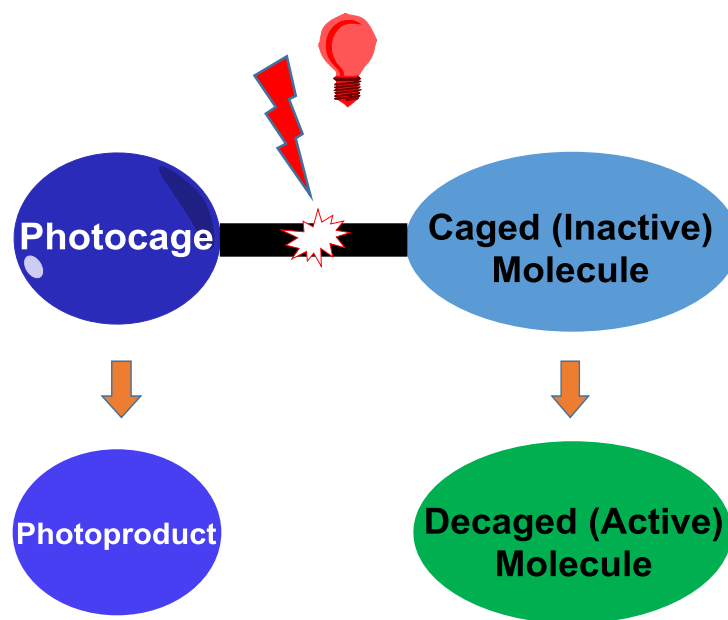
Figure 13. General depiction of the photocaging approach. The image is adapted from Yang *et al*.[97]

Coumarin-based PPG

Quinoline-based PPG

R = Ac or P(O)(OMe)$_2$

Dibenzofuran-based PPG

BODIPY-based PPG
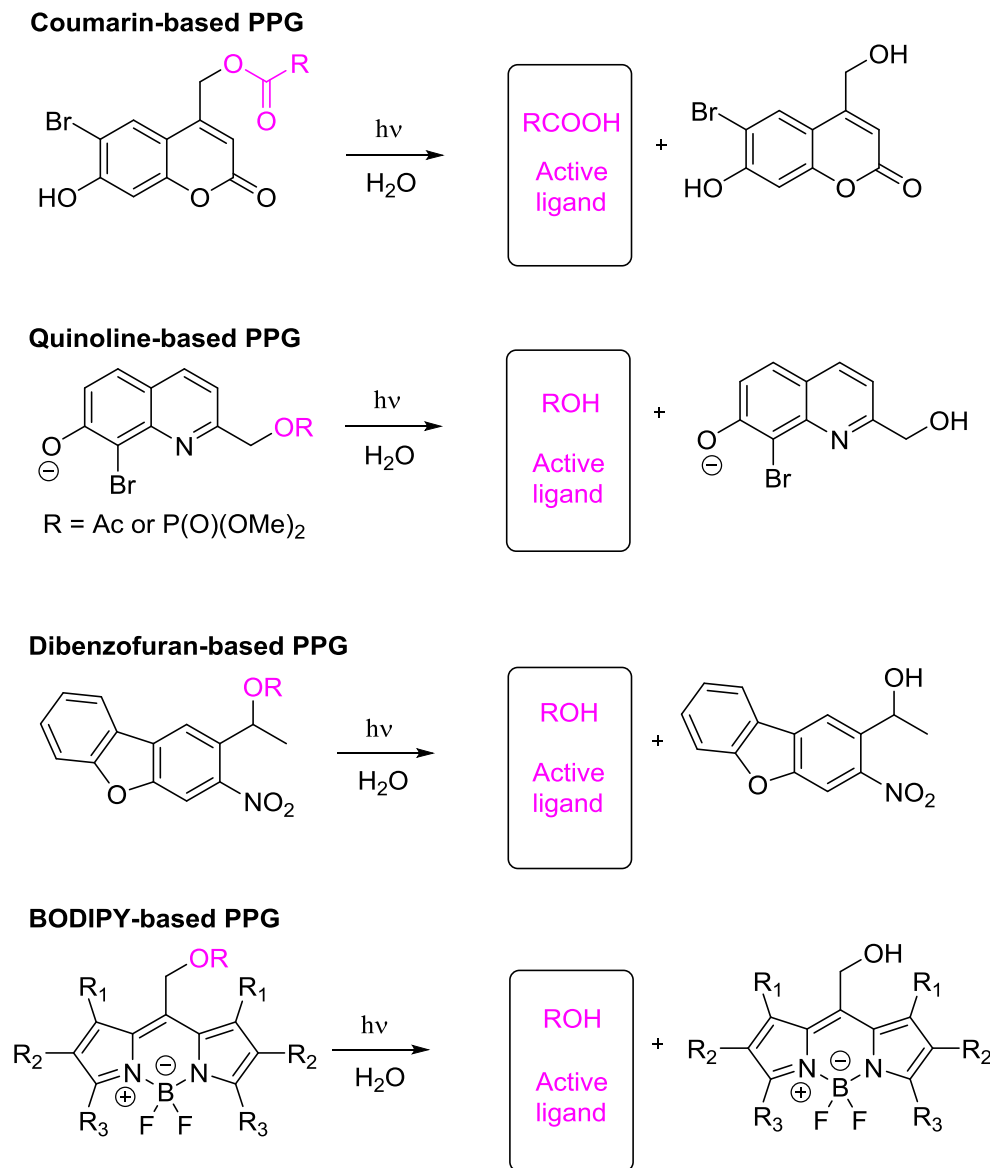
Figure 14. Examples of different photoremovable protecting groups for caged molecules and the decaging process.[92-95]

There are four theoretical scenarios for the use of a photocaging approach (Figure 15).[98] In optimal scenario A, which has been illustrated for e.g. a caged antisense agent[99], a caged isopropyl-beta-D-thio-galactoside (IPTG)[100] and caged toyocamycin[101], the caged ligand is completely inactive. In these cases, full decaging enables restoring of full activity upon irradiation. In scenario B, the molecule is fully inactive when caged. Irradiation can increase the biological activity, yet cannot reach the threshold for induction of biological effect. The reasons for this include, but are not limited to, incomplete decaging or side reactions with the parent uncaged compound induced by irradiation.[102] For scenarios C and D, the caged molecule is still moderately active. The decaging process restores the biological activity to a high (C) or full extent (D).[103, 104]

In scenarios B, C and D, the caged molecule can still be employed if the concentrations used are fine-tuned.[98]
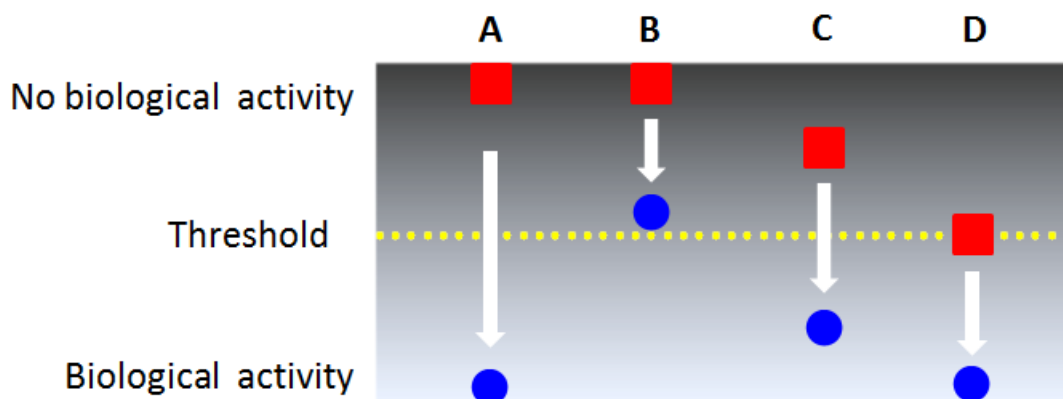
Figure 15. Four scenarios for the outcome of uncaging approaches on small-molecule ligands. (red square) and (blue ball) represent activity before and after irradiation. The figure was adapted from Deiters.[98]

Photocaging has been used in the GPCR field (Figure 16). For example, Muralidharan and Nerbonne used the incorporation of 2-nitrobenzyl group in the adrenergic receptor agonists phenylephrine and epinephrine. The caged phenylephrine shows complete loss of the α-receptor agonist activity of phenylephrine, but agonist activity is regained upon irradiation. The caged epinephrine lacks both α- and β-receptor activity but the agonist activity is regained upon applying flashes of light.[105] Llebaria and co-workers described a caged compound selective for mGlu5 receptor.[106] The photocaged compound JF-NP-026 is a derivative of the mGlu5 receptor negative allosteric modulator raseglurant. The release of the drug upon illumination allowed precisely control of mGlu5 receptor activity both in cultured cells and in striatal primary neurons. Ciruela and collaborators described a light-sensitive caged adenosine A_{2A} receptor antagonist MRS7145.[107] Photoactivation of MRS7145 triggered the local release of the active antagonist SCH442416, resulting in ligand binding and antagonism activity. The efficacy of the active antagonist released upon irradiation was assessed in animal behaviour experiments. Apart from these photocaged ligands targeting synthetic GPCR ligands, natural GPCR ligands can be also equipped with photoremovable protecting groups for photopharmacological study (Figure 17).[108] Examples include aminergic neurotransmitters such dopamine[109], histamine[109] and serotonine[109] as well as lipidic molecules such as lysophosphatidic acid (LPA), platelet activating factor (PAF), and prostaglandin E2 (PGE_2). In all examples, the generation of photo-caged GPCR ligands facilitated optical control of GPCR mediated cellular signaling. This can expand photopharmacological approaches and further provide new perspectives in understanding GPCR mediated (patho)physiology.

phenylephrine

epinephrine

raseglurant
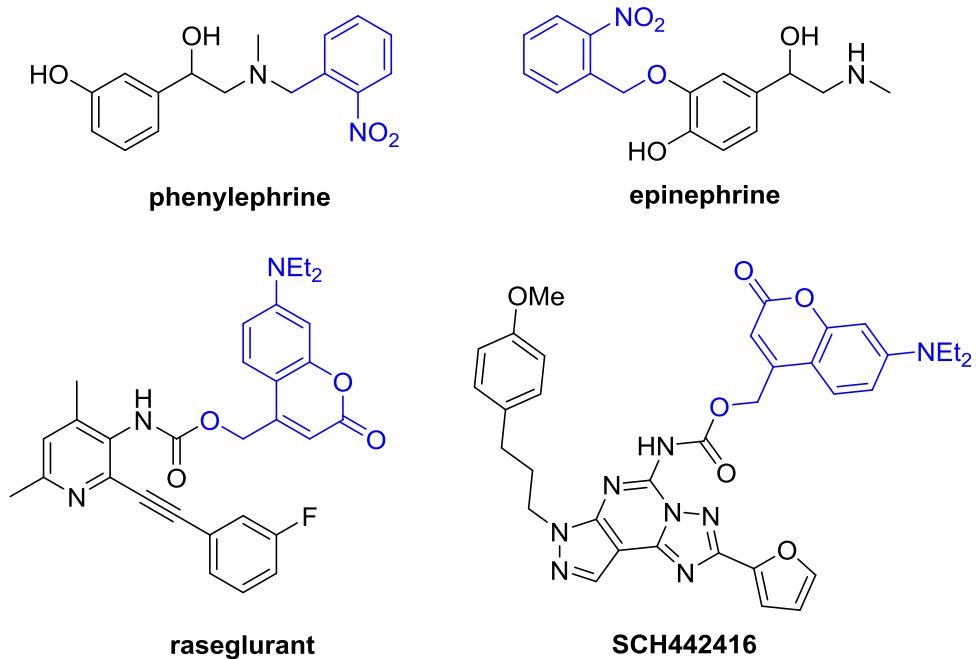
SCH442416

Figure 16. Structure of caged molecules targeting GPCRs with parent compounds being phenylephrine[105], epinephrine[105], raseglurant[106] and SCH442416.[107]
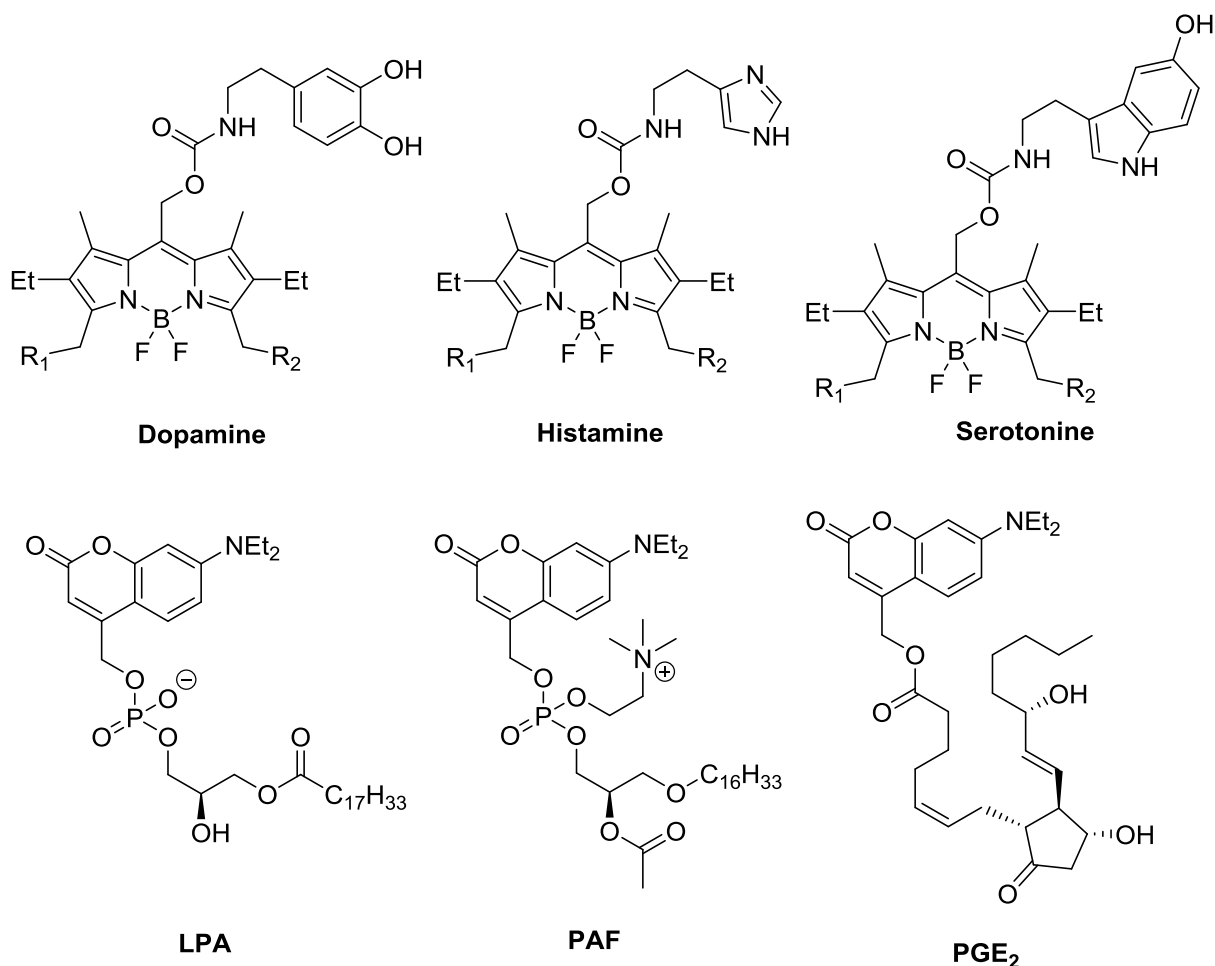
Figure 17. Structures of selected caged derivatives of natural GPCRs ligands: dopamine[109], histamine[109], serotonine[109], LPA[108], PAF[108] and PGE$_2$.[108]

The histamine H$_1$ receptor as an archetypical GPCR

Histamine and histamine receptors

Histamine is the endogenous ligand of four subtypes of histamine receptors, i.e., the histamine H$_1$, H$_2$, H$_3$ and H$_4$ receptor.[110] Interestingly, the affinity of histamine for H$_1$R and H$_2$R is substantially lower than the affinity for H$_3$R and H$_4$R. Each of the four receptors has a distinct physiological function within the human body (Figure 18).[111] The H$_1$R plays a role in many physiological processes, i.e., allergic reactions, sleep-wake cycles and itch.[112] The H$_2$R is mainly expressed in the stomach, CNS and heart. It is known to play a role in the gastric acid production, modulation of circadian rhythm and cognitive function in the brain, as well as in the modulation of glucose metabolism and food intake.[112] The H$_3$R has a key role in the control of neurotransmitter release. including histamine itself. Many neurons express the histamine H$_3$R and it has been postulated to be useful in the therapeutic modulation of e.g. sleep[113] and

cognitive diseases.[112, 114] The histamine H_4 receptor is primarily expressed on mast cells, natural killer cells and dendritic cells. It has been suggested to be involved in the modulation of immune activity.[112]
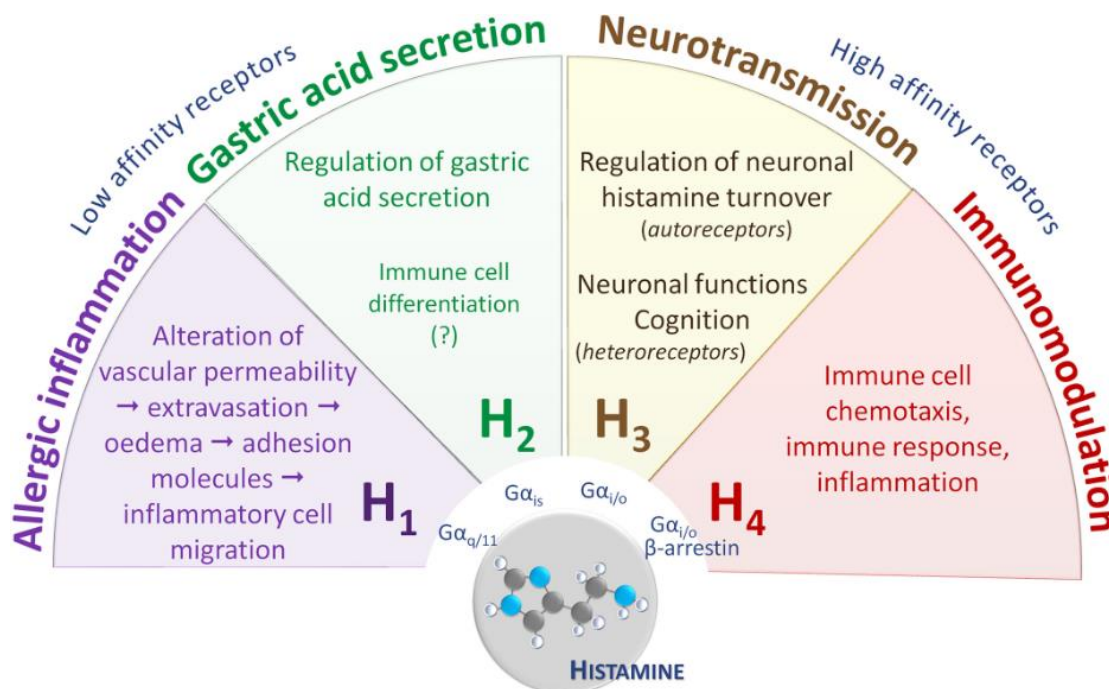
Figure 18. The main function of the four histamine receptors. Figure taken from Tiligada *et al*.[111]

The histamine H₁ receptor and its ligands

The focus in this thesis will be on H_1R. It has proven to be receptor of major therapeutic relevance. H_1R is expressed throughout the human body, including in the lungs, blood vessels, CNS, and immune cells.[112] Through H_1R, cell proliferation and differentiation, regeneration, hematopoiesis and wound healing can be regulated. The H_1R expressed in other cells or organs can also contribute to regulation of neurotransmission, cognition, learning, memory, vigilance, the circadian sleep-wake cycle.[115]

As discussed before in this chapter, GPCR signaling can be transduced after activation of either G protein or β-arrestin. Each pathway will lead to different pharmacological and (patho)physiological effects. Evidence shows that H_1R can also signal through both these pathways. After a ligand binds to H_1R, heterotrimeric $G_{q/11}$ proteins are activated, which results in the increase of intracellular calcium levels via the signaling pathway of phospholipase C (PLC) and inositol 1,4,5-trisphosphate (IP3).[116] H_1R has also been reported to signal through β-arrestin. In 2016, Bosma *et al* reported the development of a real-time assay for H_1R and β-arrestin2 in

living cells. This bioluminescence resonance energy transfer (BRET)-based assay was able to monitor histamine-induced β-arrestin2 recruitment to H_1R.[43]

Many H_1R small-molecule antagonists (sometimes also referred to as antihistamines) have become blockbuster drugs. There are currently more than 45 H_1-antihistamines available worldwide.[115] They comprise the largest class of medications for treatment of allergic diseases like atopic dermatitis, asthma, anaphylaxis, allergic angioedema .[115] More recently they have also been applied to regulate sleep-wakefulness.[117-119] Two categories of antihistamines, first and second- generation antihistamines, are distinguished (Figure 19A-B). First-generation antihistamines often contain two (fused) aromatic rings or a butterfly head structures in combination with a basic amine moiety. Examples are doxepin, mepyramine and triprolidine. Because of their high lipophilicity, the ligands pass the blood-brain-barrier (BBB) easily. As a result of their passage into the brain, these ligands have significant side effects, e.g., sedative effects.[120] The second-generation antihistamines were therefore often designed to have a carboxylic acid moiety (e.g. olopatadine and levocetirizine). As the resulting zwitterions are not expected to pass the BBB significantly, they are more selective and do not cause CNS related sedative effects (Figure 19B).[120] However, it is important to note that definition of a ligand as belonging to the second generation involves the reduced BBB passage and lack of sedative effects, not the presence of the carboxylate moiety. For example, desloratadine and rupatadine (structures in figure 19B) also show little BBB passage.[121, 122]

A

Doxepin
pK_i = 9.6

Mepyramine
pK_i = 8.8

Triprolidine
pK_i = 8.3

B

Olopatadine
pK_i = 8.3

Rupatadine
pK_i = 8.4

Levocetirizine
pK_i = 8.1

Desloratadine
pK_i = 9.1
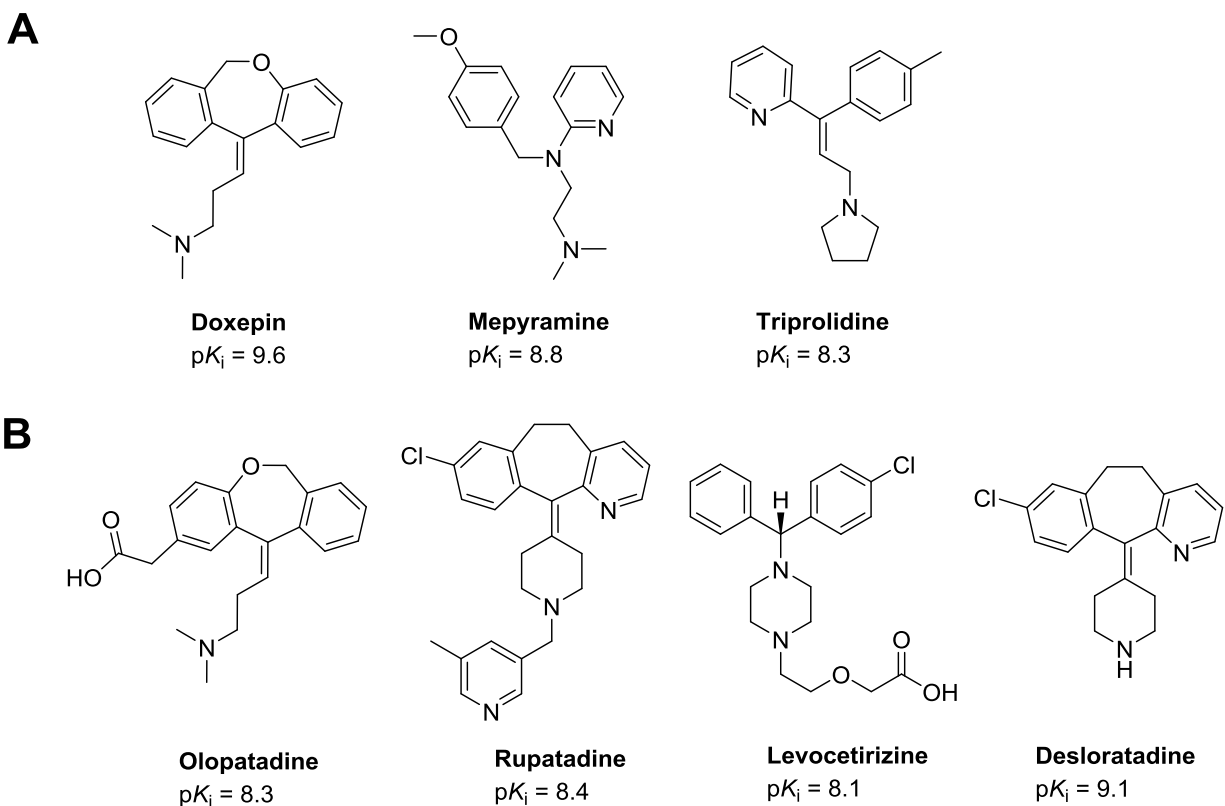
Figure 19. Selected examples for two generations of H_1R antihistamines. (A) First generation of antihistamines and H_1R binding affinity.[42] (B) Second generation of antihistamines and H_1R binding affinity.[41, 42]

It is of interest to discuss small-molecule H_1R ligands in the context of the various concepts described earlier in this chapter. Despite the prominent therapeutic role of H_1R, only a modest number of studies have addressed H_1R ligand-binding kinetics but generally no detailed SKRs were involved.[123-131] Considering the concept of bioisosteres, studies have been performed at histamine H_2R and H_4R[132, 133] but no systematic studies on H_1R have been disclosed. Covalent binding, on the other hand, has been applied at histamine H_1R (Figure 20A). Phenoxybenzamine is an irreversible alpha blocker, which is used to treat symptoms of pheochromocytoma but has also been reported to depress the response of histamine.[134] In later studies, our group discovered that this is because of covalent binding of phenoxybenzamine to H_1R.[135] Another example has been reported by Weichert *et al*. in 2014 using a disulfide warhead to target cysteine.[136] However, none of the covalent ligands was applied to modulate binding kinetics at H_1R. In 2018, Rustler *et al.* reported an example of photoswitching at H_1R in guinea pig ileum (Figure 20B).[137] Azobenzene-based histamine H_1R ligands were designed, synthesized, and pharmacologically investigated. The best ligand of the series shows 46-fold shift on activity between isomers. However, it has overall poor binding affinity, i.e. 630-fold less than the standard antihistamine

mepyramine. To the best of our knowledge, photocaging studies have not been published for H_1R yet.
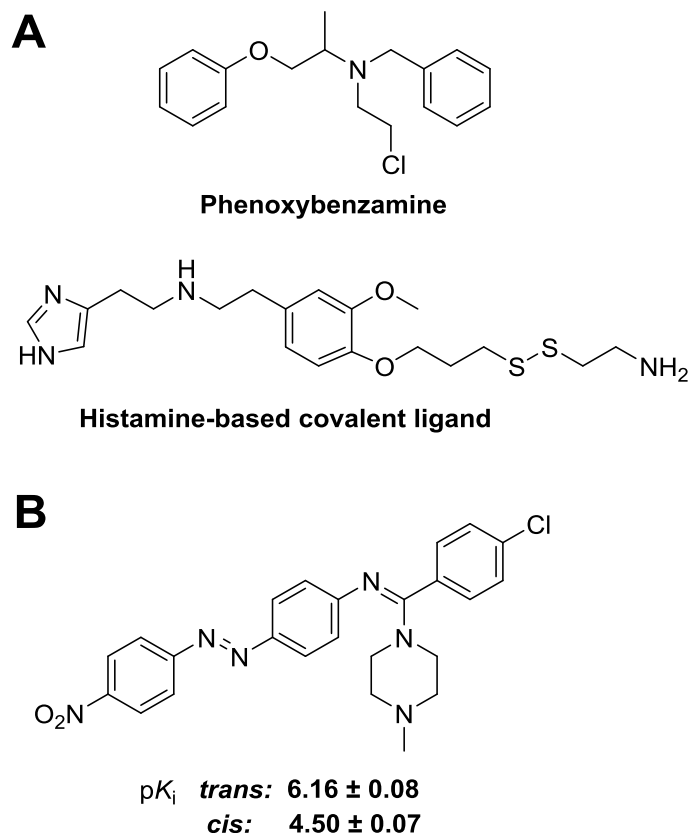
Figure 20. Structures of (A) covalent ligands[136] and (B) a photoswitchable ligand[137] targeting H_1R.

The H_1R binding pocket

In 2011, a co-crystallized structure of H_1R and doxepin was disclosed by Shimamura *et al*.[138] In the binding pocket (Figure 21A, B), different binding regions can be designated, namely the upper and lower aromatic binding regions, the amine-binding region, and the phosphate-binding region. In the co-crystal structure of H_1R with doxepin, the amine-binding region is defined by D107[3.32], I454[7.39], W428[6.48], Y431[6.51], Y458[7.39], Y458[7.43]. D107[3.32] is believed to form an anchor salt bridge with the amine moiety of doxepin. This aspartic acid is conserved in all aminergic GPCRs.[23, 139, 140] Mutation studies of D107[3.32] always result in decreased binding affinity of H_1R ligands.[141-145] Thus, the ionic interaction between D107[3.32] and antihistamines is considered essential for H_1R ligand binding. Mutation of W428[6.48], Y431[6.51], Y458[7.39], Y458[7.43] does not show much difference in binding affinity at the histamine H_1R for tested ligands.[143, 146] F432[6.52], F435[6.55], W158[4.56], Y108[3.33] and Y431[6.51] define the upper aromatic binding region, whereas the lower aromatic region is characterized by F199[5.47], F424[6.44], and W428[6.48]. The butterfly shape of tricyclic heads of several

known H_1R antagonists fit well into the upper and lower aromatic binding region. Efficient recognition of the upper and lower aromatic binding region by such ligands has been underscored by many mutation studies.[141-143, 147] The phosphate-binding region, named as such because of a co-crystallised phosphate anion in the X-ray structure, is positioned close to the amine-binding region and extracellular vestibule. It is defined by H435[7.35], K179[45.49], K191[5.39] and Y431[6.51]. It is suggested that the phosphate-binding region is occupied by anionic carboxylate groups of second-generation antagonists and that this plays a role in governing the dissociation rate.[127, 147] This is suggested by a shorter residence time of the methyl ester of levocetirizine for H_1R (10 min) than the longer residence time of levocetirizine (200 min).[127] Mutation of K191[5.39] results in a slight decrease in binding affinity for levocetirizine.[127]

The determination of a crystal structure can facilitate structure-based ligand discovery. This is illustrated by a customized structure-based virtual fragment screening method that was developed and validated based on the H_1R crystal structure. The optimized screening approach successfully identified a diverse set of novel fragment-like H_1R ligands with a 73% high hit rate. From these hit compounds, the ligand 4-(2-benzylphenoxy)piperidine (VUF14544) (Figure 21C) emerged and it has been used to thoroughly investigate the roles of different binding regions and binding hot spots[148] (Figure 21B).
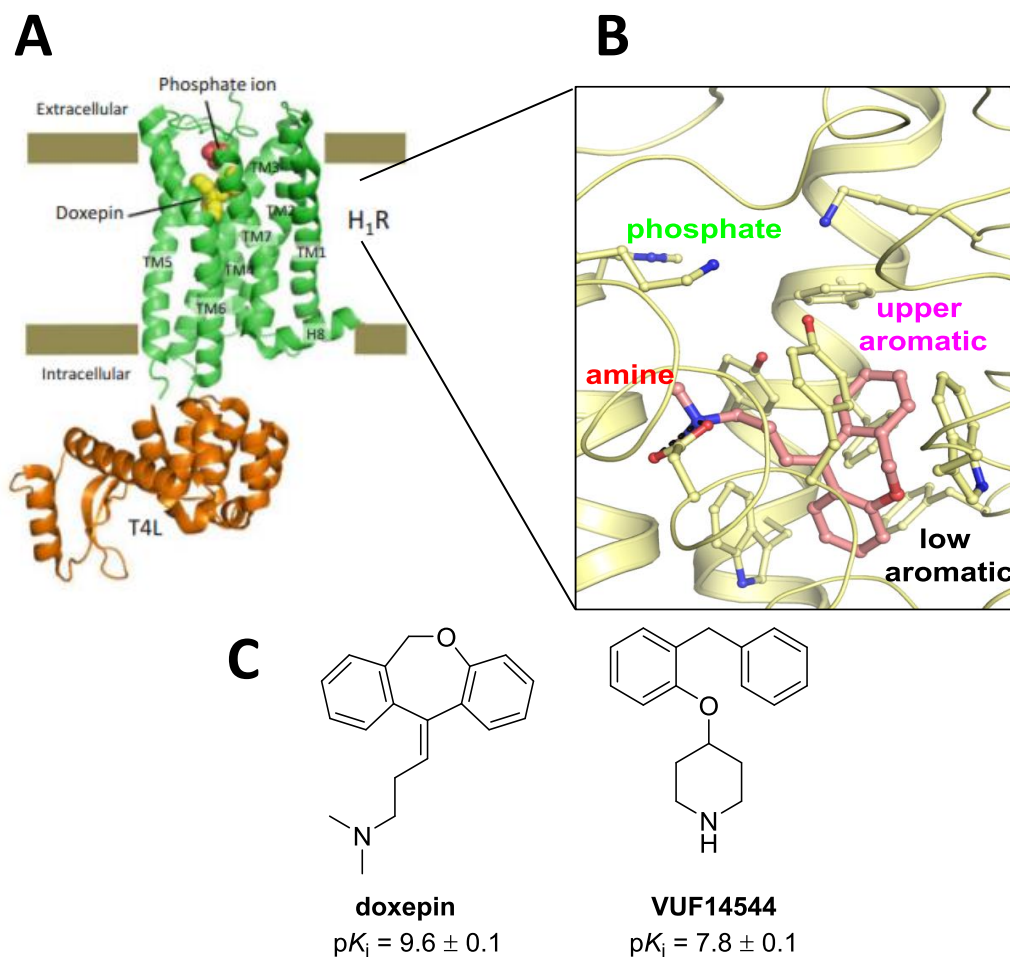
Figure 21. (A) X-ray structure of H_1R co-crystallized with doxepin, also showing the T4L lysozyme appended to facilitate in crystallisation; (B) Structure of the binding pocket of H_1R with doxepin (pink carbon atoms) and different binding regions. (C) Structure of virtual screening hit and doxepin and binding affinity at H_1R.[42, 148] Figure A adapted from Shiroisi *et al*. [149]

Aim of the thesis

The aim of this PhD thesis is to study new ways of small-molecule based modulation of the histamine H_1R, a prototypic family A GPCR. The many ligand chemotypes described for H_1R in combination with the detailed knowledge about the receptor structure and well-developed pharmacology makes this receptor an ideal "work horse" to test new approaches for GPCR modulation. Two main concepts are investigated: binding kinetics and photopharmacology. Several sets of tools compounds have been designed, synthesized and pharmacologically characterized in order to reach the following objectives:

1: To study the H_1R structure-kinetics relationship of

       (a) rupatadine analogs

       (b) tailored tricyclic compounds

       (c) ligands containing classical and novel isosteres of carboxylic acids

2: To identify photocaged small-molecule tools for H_1R

Outline of this thesis

In this thesis, work in **chapter 2** and **6** is related to the amine-binding region of H_1R, while work in **chapter 4** and **5** is related to the phosphate binding region. **Chapter 3** focuses on the aromatic binding region.

Chapter 2 describes structure-kinetics relationship (SKR) studies for a set of rupatadine analogs. Here, it was explored how to modulate residence time by introducing a set of substituents on the amine of rupatadine. Steric hindrance plays a key postulated role in driving the binding kinetics. **Chapter 3** describes the hypothesis that residence time can be modulated by cyclization of the aromatic head group of H_1R ligands. A systematic analysis of SKR shows that antihistamines with tricyclic headgroups tend to have a longer residence time than non-tricyclic antihistamines and tailored synthetic derivatives were used to understand better how to design slow or rapid dissociation into a molecule. **Chapter 4** describes the exploration of isosteres in acid-containing ligands with respect to the binding kinetics at H_1R. Non-acidic and acidic isosteres as well as a tailored set of sulfonyl-containing moieties were probed. An acylsulfonamide was found to be a relevant bioisostere for acid-containing H_1R ligands. **Chapter 5** describes preliminary studies on the binding kinetics of boron-containing ligands for H_1R. A combination of synthesis and bioactivity data is used to investigate whether a proposed reversible covalent binding between boron-containing warheads and a lysine residue may prolong residence time. **Chapter 6** describes the photopharmacological characterization of photocaged ligands for H_1R. The strategy was

applied on three distinct scaffolds. The successful strategy discovered for desloratadine provides a starting point to further investigate photocaging in H_1R. **Chapter 7** summarizes and discusses the general findings and results.

References

1.   Paul, S. M.; Mytelka, D. S.; Dunwiddie, C. T.; Persinger, C. C.; Munos, B. H.; Lindborg, S. R.; Schacht, A. L., How to improve R&D productivity: the pharmaceutical industry's grand challenge. *Nature Reviews Drug Discovery* **2010,** *9* (3), 203-214.

2.   DiMasi, J. A.; Grabowski, H. G.; Hansen, R. W., Innovation in the pharmaceutical industry: New estimates of R&D costs. *Journal of Health Economics* **2016,** *47*, 20-33.

3.   Hughes, J.; Rees, S.; Kalindjian, S.; Philpott, K., Principles of early drug discovery. *British Journal of Pharmacology* **2011,** *162* (6), 1239-1249.

4.   Peet, N. P., What constitutes target validation? *TARGETS* **2003,** *2* (4), 125-127.

5.   Singh, G., Preclinical Drug Development. In *Pharmaceutical Medicine and Translational Clinical Research*; Vohora, D., Singh, G.; Academic Press, Boston, 2018; pp 47-63.

6.   Umscheid, C. A.; Margolis, D. J.; Grossman, C. E., Key concepts of clinical trials: A narrative review. *Postgraduate Medicine* **2011,** *123* (5), 194-204.

7.   Hauser, A. S.; Attwood, M. M.; Rask-Andersen, M.; Schiöth, H. B.; Gloriam, D. E., Trends in GPCR drug discovery: new agents, targets and indications. *Nature Reviews Drug Discovery* **2017,** *16* (12), 829-842.

8.   Jacobson, K. A., New paradigms in GPCR drug discovery. *Biochemical Pharmacology* **2015,** *98* (4), 541-555.

9.   Katritch, V.; Cherezov, V.; Stevens, R. C., Structure-function of the G protein-coupled receptor superfamily. *Annual Review of Pharmacology and Toxicology* **2013,** *53*, 531-556.

10.   Fredriksson, R.; Lagerström, M. C.; Lundin, L.-G.; Schiöth, H. B., The G-protein-coupled receptors in the human genome form five main families. Phylogenetic analysis, paralogon groups, and fingerprints. *Molecular Pharmacology* **2003,** *63* (6), 1256-1272.

11.   Garland, S. L., Are GPCRs still a source of new targets? *Journal of Biomolecular Screening* **2013,** *18* (9), 947-966.

12.   Przydzial, M. J.; Bhhatarai, B.; Koleti, A.; Vempati, U.; Schürer, S. C., GPCR ontology: development and application of a G protein-coupled receptor pharmacology knowledge framework. *Bioinformatics* **2013,** *29* (24), 3211-3219.

13.   Witter, F. R.; Zimmerman, A. W.; Reichmann, J. P.; Connors, S. L., In utero beta 2 adrenergic agonist exposure and adverse neurophysiologic and behavioral outcomes. *American Journal of Obstetrics & Gynecology* **2009,** *201* (6), 553-559.

14.   Schiöth, H. B.; Fredriksson, R., The GRAFS classification system of G-protein coupled receptors in comparative perspective. *General and Comparative Endocrinology* **2005,** *142* (1-2), 94-101.

15.   Piscitelli, C. L.; Kean, J.; de Graaf, C.; Deupi, X., A molecular pharmacologist's guide to G protein–coupled receptor crystallography. *Molecular Pharmacology* **2015,** *88* (3), 536-551.

16.   Congreve, M.; de Graaf, C.; Swain, N. A.; Tate, C. G., Impact of GPCR structures on drug discovery. *Cell* **2020,** *181* (1), 81-91.

17.   Mocking, T., R. Bosma, Rahman, S.N., Verweij, E.W.E., McNaught-Flores, D.A., Vischer, H.F., Leurs, R. (2016) Molecular aspects of histamine receptors. In histamine receptors: preclinical and clinical aspects (eds Blandina, p & Passani, M.B.) 1-49. The receptors, vol. 28. Humana Press, Cham.

18.   Grundmann, M.; Merten, N.; Malfacini, D.; Inoue, A.; Preis, P.; Simon, K.; Rüttiger, N.; Ziegler, N.; Benkel, T.; Schmitt, N. K.; Ishida, S.; Müller, I.; Reher, R.; Kawakami, K.; Inoue, A.; Rick, U.; Kühl, T.; Imhof, D.; Aoki, J.; König, G. M.; Hoffmann, C.; Gomeza, J.; Wess, J.; Kostenis, E., Lack of beta-arrestin signaling in the absence of active G proteins. *Nature Communications* **2018,** *9* (1), 341.

19.   Granier, S.; Kobilka, B., A new era of GPCR structural and chemical biology. *Nature Chemical Biology* **2012,** *8* (8), 670-673.

20.   Wacker, D.; Stevens, R. C.; Roth, B. L., How ligands illuminate GPCR molecular pharmacology. *Cell* **2017,** *170* (3), 414-427.

21.   Wang, L.; Wu, Y.; Deng, Y.; Kim, B.; Pierce, L.; Krilov, G.; Lupyan, D.; Robinson, S.; Dahlgren, M. K.; Greenwood, J.; Romero, D. L.; Masse, C.; Knight, J. L.; Steinbrecher, T.; Beuming, T.; Damm, W.; Harder, E.; Sherman, W.; Brewer, M.; Wester, R.; Murcko, M.; Frye, L.; Farid, R.; Lin, T.; Mobley, D. L.; Jorgensen, W. L.; Berne, B. J.; Friesner, R. A.; Abel, R., Accurate and reliable prediction of relative ligand binding potency in prospective drug discovery by way of a modern free-energy calculation protocol and force field. *Journal of the American Chemical Society* **2015,** *137* (7), 2695-2703.

22.   Hopkins, A. L.; Keserü, G. M.; Leeson, P. D.; Rees, D. C.; Reynolds, C. H., The role of ligand efficiency metrics in drug discovery. *Nature Reviews Drug Discovery* **2014,** *13* (2), 105-121.

23.   Kooistra, A. J.; Kuhne, S.; de Esch, I. J. P.; Leurs, R.; de Graaf, C., A structural chemogenomics analysis of aminergic GPCRs: lessons for histamine receptor ligand design. *British Journal of Pharmacology* **2013,** *170* (1), 101-126.

24.   Meanwell, N. A., Synopsis of some recent tactical application of bioisosteres in drug design. *Journal of Medicinal Chemistry* **2011,** *54* (8), 2529-2591.

25.   Patani, G. A.; LaVoie, E. J., Bioisosterism: A rational approach in drug design. *Chemical Reviews* **1996,** *96* (8), 3147-3176.

26.   Lassalas, P.; Gay, B.; Lasfargeas, C.; James, M. J.; Tran, V.; Vijayendran, K. G.; Brunden, K. R.; Kozlowski, M. C.; Thomas, C. J.; Smith, A. B.; Huryn, D. M.; Ballatore, C., Structure property relationships of carboxylic acid isosteres. *Journal of Medicinal Chemistry* **2016,** *59* (7), 3183-3203.

27.   Ballatore, C.; Huryn, D. M.; Smith III, A. B., Carboxylic acid (bio)Isosteres in drug design. *ChemMedChem* **2013,** *8* (3), 385-395.

28.   Duncia, J. V.; Chiu, A. T.; Carini, D. J.; Gregory, G. B.; Johnson, A. L.; Price, W. A.; Wells, G. J.; Wong, P. C.; Calabrese, J. C.; Timmermans, P. B., The discovery of potent nonpeptide angiotensin II receptor antagonists: a new class of potent antihypertensives. *Journal of Medicinal Chemistry* **1990,** *33* (5), 1312-29.

29.   Ripley, E.; Hirsch, A., Fifteen years of losartan: what have we learned about losartan that can benefit chronic kidney disease patients? *International Journal of Nephrology and Renovascular Disease* **2010,** *3*, 93-98.

30.   Schuetz, D. A.; de Witte, W. E. A.; Wong, Y. C.; Knasmueller, B.; Richter, L.; Kokh, D. B.; Sadiq, S. K.; Bosma, R.; Nederpelt, I.; Heitman, L. H.; Segala, E.; Amaral, M.; Guo, D.; Andres, D.; Georgi, V.; Stoddart, L. A.; Hill, S.; Cooke, R. M.; De Graaf, C.; Leurs, R.; Frech, M.; Wade, R. C.; de Lange, E. C. M.; Ijzerman, A. P.; Müller-Fahrnow, A.; Ecker, G. F., Kinetics for drug discovery: an industry-driven effort to target drug residence time. *Drug Discovery Today* **2017,** *22* (6), 896-911.

31.   Hoffmann, C.; Castro, M.; Rinken, A.; Leurs, R.; Hill, S. J.; Vischer, H. F., Ligand residence time at G-protein-coupled receptors-why we should take our time to study it. *Molecular Pharmacology* **2015,** *88* (3), 552-60.

32.   Pan, A. C.; Borhani, D. W.; Dror, R. O.; Shaw, D. E., Molecular determinants of drug–receptor binding kinetics. *Drug Discovery Today* **2013,** *18* (13), 667-673.

33.   Copeland, R. A.; Pompliano, D. L.; Meek, T. D., Drug–target residence time and its implications for lead optimization. *Nature Reviews Drug Discovery* **2006,** *5* (9), 730-739.

34.   Swinney, D. C., The role of binding kinetics in therapeutically useful drug action. *Current Opinion in Drug Discovery & Development* **2009,** *12* (1), 31-39.

35.   Yin, N.; Pei, J.; Lai, L., A comprehensive analysis of the influence of drug binding kinetics on drug action at molecular and systems levels. *Molecular BioSystems* **2013,** *9* (6), 1381-9.

36.   Tummino, P. J.; Copeland, R. A., Residence time of receptor–ligand complexes and its effect on biological function. *Biochemistry* **2008,** *47* (20), 5481-5492.

37.   Lu, H.; Tonge, P. J., Drug-target residence time: critical information for lead optimization. *Current Opinion in Chemical Biology* **2010,** *14* (4), 467-74.

38.   Zhang, R.; Monsma, F., The importance of drug-target residence time. *Current Opinion in Drug Discovery & Development* **2009,** *12* (4), 488-96.

39.   Copeland, R. A., The drug-target residence time model: a 10-year retrospective. *Nature Reviews Drug Discovery* **2016,** *15* (2), 87-95.

40.   Folmer, R. H. A., Drug target residence time: a misleading concept. *Drug Discovery Today* **2018,** *23* (1), 12-16.

41.   Bosma, R.; Wang, Z.; Kooistra, A. J.; Bushby, N.; Kuhne, S.; van den Bor, J.; Waring, M. J.; de Graaf, C.; de Esch, I. J.; Vischer, H. F.; Sheppard, R. J.; Wijtmans, M.; Leurs, R., Route to prolonged residence time at the histamine H1 receptor: Growing from desloratadine to rupatadine. *Journal of Medicinal Chemistry* **2019,** *62* (14), 6630-6644.

42.   Bosma, R.; Stoddart, L. A.; Georgi, V.; Bouzo-Lorenzo, M.; Bushby, N.; Inkoom, L.; Waring, M. J.; Briddon, S. J.; Vischer, H. F.; Sheppard, R. J.; Fernández-Montalván, A.; Hill, S. J.; Leurs, R., Probe dependency in the determination of ligand binding kinetics at a prototypical G protein-coupled receptor. *Scientific Reports* **2019,** *9* (1), 7906.

43.   Bosma, R.; Moritani, R.; Leurs, R.; Vischer, H. F., BRET-based β-arrestin2 recruitment to the histamine H1 receptor for investigating antihistamine binding kinetics. *Pharmacological Research* **2016,** *111*, 679-687.

44.   Stoddart, L. A.; Vernall, A. J.; Bouzo-Lorenzo, M.; Bosma, R.; Kooistra, A. J.; de Graaf, C.; Vischer, H. F.; Leurs, R.; Briddon, S. J.; Kellam, B.; Hill, S. J., Development of novel fluorescent histamine H1-receptor antagonists to study ligand-binding kinetics in living cells. *Scientific Reports* **2018,** *8* (1), 1572.

45.   Xia, L.; Burger, W. A. C.; van Veldhoven, J. P. D.; Kuiper, B. J.; van Duijl, T. T.; Lenselink, E. B.; Paasman, E.; Heitman, L. H.; Ijzerman, A. P., Structure–affinity relationships and structure–kinetics relationships of pyrido[2,1-f]purine-2,4-dione derivatives as human adenosine A3 receptor antagonists. *Journal of Medicinal Chemistry* **2017,** *60* (17), 7555-7568.

46.   Guo, D.; Hillger, J. M.; IJzerman, A. P.; Heitman, L. H., Drug-target residence time—a case for G protein-coupled receptors. *Medicinal Research Reviews* **2014,** *34* (4), 856-892.

47.   Copeland, R. A., The dynamics of drug-target interactions: drug-target residence time and its impact on efficacy and safety. *Expert Opinion on Drug Discovery* **2010,** *5* (4), 305-310.

48.   Boehr, D. D.; Nussinov, R.; Wright, P. E., The role of dynamic conformational ensembles in biomolecular recognition. *Nature Chemical Biology* **2009,** *5* (11), 789-796.

49.   Dowling, M. R.; Charlton, S. J., Quantifying the association and dissociation rates of unlabelled antagonists at the muscarinic M3 receptor. *British Journal of Pharmacology* **2006,** *148* (7), 927-937.

50.   Vauquelin, G.; Fierens, F.; Liefde, I. V., Long-lasting angiotensin type 1 receptor binding and protection by candesartan: comparison with other biphenyl-tetrazole sartans. *Journal of Hypertension* **2006,** *24*, S23-S30.

51.   Swinney, D. C., Applications of binding kinetics to drug discovery. *Pharmaceutical Medicine* **2008,** *22* (1), 23-34.

52.   Miller, D. C.; Lunn, G.; Jones, P.; Sabnis, Y.; Davies, N. L.; Driscoll, P., Investigation of the effect of molecular properties on the binding kinetics of a ligand to its biological target. *MedChemComm* **2012,** *3* (4), 449-452.

53.   Tresadern, G.; Bartolome, J. M.; Macdonald, G. J.; Langlois, X., Molecular properties affecting fast dissociation from the D2 receptor. *Bioorganic & Medicinal Chemistry* **2011,** *19* (7), 2231-2241.

54.   Heroven, C.; Georgi, V.; Ganotra, G. K.; Brennan, P.; Wolfreys, F.; Wade, R. C.; Fernández-Montalván, A. E.; Chaikuad, A.; Knapp, S., Halogen–aromatic π interactions modulate inhibitor residence times. *Angewandte Chemie International Edition* **2018,** *57* (24), 7220-7224.

55.   Schmidtke, P.; Luque, F. J.; Murray, J. B.; Barril, X., Shielded hydrogen bonds as structural determinants of binding kinetics: Application in drug design. *Journal of the American Chemical Society* **2011,** *133* (46), 18903-18910.

56.   Bradshaw, J. M.; McFarland, J. M.; Paavilainen, V. O.; Bisconte, A.; Tam, D.; Phan, V. T.; Romanov, S.; Finkle, D.; Shu, J.; Patel, V.; Ton, T.; Li, X.; Loughhead, D. G.; Nunn, P. A.; Karr, D. E.; Gerritsen, M. E.; Funk, J. O.; Owens, T. D.; Verner, E.; Brameld, K. A.; Hill, R. J.; Goldstein, D. M.; Taunton, J., Prolonged and tunable residence time using reversible covalent kinase inhibitors. *Nature Chemical Biology* **2015,** *11* (7), 525-531.

57.   Bauer, R. A., Covalent inhibitors in drug discovery: from accidental discoveries to avoided liabilities and designed therapies. *Drug Discovery Today* **2015,** *20* (9), 1061-1073.

58.   Baillie, T. A., Targeted covalent inhibitors for drug design. *Angewandte Chemie International Edition* **2016,** *55* (43), 13408-13421.

59.   Lee, C.-U.; Grossmann, T. N., Reversible covalent inhibition of a protein target. *Angewandte Chemie International Edition* **2012,** *51* (35), 8699-8700.

60.   De Cesco, S.; Kurian, J.; Dufresne, C.; Mittermaier, A. K.; Moitessier, N., Covalent inhibitors design and discovery. *European Journal of Medicinal Chemistry* **2017,** *138*, 96-114.

61.   Singh, J.; Petter, R. C.; Baillie, T. A.; Whitty, A., The resurgence of covalent drugs. *Nature Reviews Drug Discovery* **2011,** *10* (4), 307-317.

62.   Ábrányi-Balogh, P.; Petri, L.; Imre, T.; Szijj, P.; Scarpino, A.; Hrast, M.; Mitrović, A.; Fonovič, U. P.; Németh, K.; Barreteau, H.; Roper, D. I.; Horváti, K.; Ferenczy, G. G.; Kos, J.; Ilaš, J.; Gobec, S.; Keserű, G. M., A road map for prioritizing warheads for cysteine targeting covalent inhibitors. *European Journal of Medicinal Chemistry* **2018,** *160*, 94-107.

63.   Ding, Z.; Kim, S.; Dorsam, R. T.; Jin, J.; Kunapuli, S. P., Inactivation of the human P2Y12 receptor by thiol reagents requires interaction with both extracellular cysteine residues, Cys17 and Cys270. *Blood* **2003,** *101* (10), 3908-3914.

64.   Brieke, C.; Rohrbach, F.; Gottschalk, A.; Mayer, G.; Heckel, A., Light-controlled tools. *Angewandte Chemie International Edition* **2012,** *51* (34), 8446-8476.

65.   Klán, P.; Šolomek, T.; Bochet, C. G.; Blanc, A.; Givens, R.; Rubina, M.; Popik, V.; Kostikov, A.; Wirz, J., Photoremovable protecting groups in chemistry and biology: Reaction mechanisms and efficacy. *Chemical Reviews* **2013,** *113* (1), 119-191.

66.   Ellis-Davies, G. C. R., Caged compounds: photorelease technology for control of cellular chemistry and physiology. *Nature Methods* **2007,** *4* (8), 619-628.

67.   Dcona, M. M.; Mitra, K.; Hartman, M. C. T., Photocontrolled activation of small molecule cancer therapeutics. *RSC Medicinal Chemistry* **2020**.

68.   Gaub, B. M.; Berry, M. H.; Holt, A. E.; Reiner, A.; Kienzler, M. A.; Dolgova, N.; Nikonov, S.; Aguirre, G. D.; Beltran, W. A.; Flannery, J. G.; Isacoff, E. Y., Restoration of visual function by expression of a light-gated mammalian ion channel in retinal ganglion cells or ON-bipolar cells. *Proceedings of the National Academy of Sciences* **2014,** *111* (51), E5574-E5583.

69.   Schmidt, D.; Rodat, T.; Heintze, L.; Weber, J.; Horbert, R.; Girreser, U.; Raeker, T.; Bußmann, L.; Kriegs, M.; Hartke, B.; Peifer, C., Axitinib: A photoswitchable approved tyrosine kinase inhibitor. *ChemMedChem* **2018,** *13* (22), 2415-2426.

70.   Herre, S.; Schadendorf, T.; Ivanov, I.; Herrberger, C.; Steinle, W.; Rück-Braun, K.; Preissner, R.; Kuhn, H., Photoactivation of an Inhibitor of the 12/15-Lipoxygenase Pathway. *ChemBioChem* **2006,** *7* (7), 1089-1095.

71.   Szymański, W.; Beierle, J. M.; Kistemaker, H. A. V.; Velema, W. A.; Feringa, B. L., Reversible photocontrol of biological systems by the incorporation of molecular photoswitches. *Chemical Reviews* **2013,** *113* (8), 6114-6178.

72.   Wiedbrauk, S.; Dube, H., Hemithioindigo—an emerging photoswitch. *Tetrahedron Letters* **2015,** *56* (29), 4266-4274.

73.   Sheng, Y.; Leszczynski, J.; Garcia, A. A.; Rosario, R.; Gust, D.; Springer, J., Comprehensive theoretical study of the conversion reactions of spiropyrans: Substituent and solvent effects. *The Journal of Physical Chemistry B* **2004,** *108* (41), 16233-16243.

74.   Hammarson, M.; Nilsson, J. R.; Li, S.; Beke-Somfai, T.; Andréasson, J., Characterization of the thermal and photoinduced reactions of photochromic spiropyrans in aqueous solution. *The Journal of Physical Chemistry B* **2013,** *117* (43), 13561-13571.

75.   Helmy, S.; Oh, S.; Leibfarth, F. A.; Hawker, C. J.; Read de Alaniz, J., Design and synthesis of donor–acceptor stenhouse adducts: A visible light photoswitch derived from furfural. *The Journal of Organic Chemistry* **2014,** *79* (23), 11316-11329.

76.   Broman, S. L.; Nielsen, M. B., Dihydroazulene: from controlling photochromism to molecular electronics devices. *Physical Chemistry Chemical Physics* **2014,** *16* (39), 21172-21182.

77.   De Waele, V.; Schmidhammer, U.; Mrozek, T.; Daub, J.; Riedle, E., Ultrafast bidirectional dihydroazulene/vinylheptafulvene (DHA/VHF) molecular switches: Photochemical ring closure of vinylheptafulvene proven by a two-pulse experiment. *Journal of the American Chemical Society* **2002,** *124* (11), 2438-2439.

78.   Franks, A. T.; Peng, D.; Yang, W.; Franz, K. J., Characterization of a photoswitching chelator with light-modulated geometric, electronic, and metal-binding properties. *Inorganic Chemistry* **2014,** *53* (3), 1397-1405.

79.   Velema, W. A.; Szymanski, W.; Feringa, B. L., Photopharmacology: Beyond proof of principle. *Journal of the American Chemical Society* **2014,** *136* (6), 2178-2191.

80.   Ricart-Ortega, M.; Font, J.; Llebaria, A., GPCR photopharmacology. *Molecular and Cellular Endocrinology* **2019,** *488*, 36-51.

81.   Berizzi, A. E.; Goudet, C., Strategies and considerations of G-protein-coupled receptor photopharmacology. *Advances in Pharmacology* **2020,** *88*, 143-172.

82.   Stein, M.; Middendorp, S. J.; Carta, V.; Pejo, E.; Raines, D. E.; Forman, S. A.; Sigel, E.; Trauner, D., Azo-propofols: Photochromic potentiators of GABAA receptors. *Angewandte Chemie International Edition* **2012,** *51* (42), 10500-10504.

83.   Frank, J. A.; Moroni, M.; Moshourab, R.; Sumser, M.; Lewin, G. R.; Trauner, D., Photoswitchable fatty acids enable optical control of TRPV1. *Nature Communications* **2015,** *6* (1), 7118.

84.   Broichhagen, J.; Schönberger, M.; Cork, S. C.; Frank, J. A.; Marchetti, P.; Bugliani, M.; Shapiro, A. M. J.; Trapp, S.; Rutter, G. A.; Hodson, D. J.; Trauner, D., Optical control of insulin release using a photoswitchable sulfonylurea. *Nature Communications* **2014,** *5* (1), 5116.

85.   Hauwert, N. J.; Mocking, T. A. M.; Da Costa Pereira, D.; Kooistra, A. J.; Wijnen, L. M.; Vreeker, G. C. M.; Verweij, E. W. E.; De Boer, A. H.; Smit, M. J.; De Graaf, C.; Vischer, H. F.; de Esch, I. J. P.; Wijtmans, M.; Leurs, R., Synthesis and characterization of a bidirectional photoswitchable antagonist toolbox for real-time GPCR photopharmacology. *Journal of the American Chemical Society* **2018,** *140* (12), 4232-4243.

86.   Westphal, M. V.; Schafroth, M. A.; Sarott, R. C.; Imhof, M. A.; Bold, C. P.; Leippe, P.; Dhopeshwarkar, A.; Grandner, J. M.; Katritch, V.; Mackie, K.; Trauner, D.; Carreira, E. M.; Frank, J. A., Synthesis of photoswitchable Δ9-tetrahydrocannabinol derivatives enables optical control of cannabinoid receptor 1 signaling. *Journal of the American Chemical Society* **2017,** *139* (50), 18206-18212.

87.   Gómez-Santacana, X.; de Munnik, S. M.; Vijayachandran, P.; Da Costa Pereira, D.; Bebelman, J. P. M.; de Esch, I. J. P.; Vischer, H. F.; Wijtmans, M.; Leurs, R., Photoswitching the efficacy of a small-molecule ligand for a peptidergic GPCR: from antagonism to agonism. *Angewandte Chemie International Edition* **2018,** *57* (36), 11608-11612.

88.   Pittolo, S.; Gómez-Santacana, X.; Eckelt, K.; Rovira, X.; Dalton, J.; Goudet, C.; Pin, J.-P.; Llobet, A.; Giraldo, J.; Llebaria, A.; Gorostiza, P., An allosteric modulator to control endogenous G protein-coupled receptors with light. *Nature Chemical Biology* **2014,** *10* (10), 813-815.

89.   Lerch, M. M.; Hansen, M. J.; van Dam, G. M.; Szymanski, W.; Feringa, B. L., Emerging targets in photopharmacology. *Angewandte Chemie International Edition* **2016,** *55* (37), 10978-99.

90.   Hansen, M. J.; Velema, W. A.; Lerch, M. M.; Szymanski, W.; Feringa, B. L., Wavelength-selective cleavage of photoprotecting groups: strategies and applications in dynamic systems. *Chemical Society Reviews* **2015,** *44* (11), 3358-77.

91.   Silva, J. M.; Silva, E.; Reis, R. L., Light-triggered release of photocaged therapeutics - Where are we now? *Journal of Controlled Release* **2019,** *298*, 154-176.

92.   Furuta, T.; Wang, S. S.-H.; Dantzker, J. L.; Dore, T. M.; Bybee, W. J.; Callaway, E. M.; Denk, W.; Tsien, R. Y., Brominated 7-hydroxycoumarin-4-ylmethyls: Photolabile protecting groups with biologically useful cross-sections for two photon photolysis. *Proceedings of the National Academy of Sciences* **1999,** *96* (4), 1193-1200.

93.   Zhu, Y.; Pavlos, C. M.; Toscano, J. P.; Dore, T. M., 8-Bromo-7-hydroxyquinoline as a photoremovable protecting group for physiological use: Mechanism and scope. *Journal of the American Chemical Society* **2006,** *128* (13), 4267-4276.

94.   Momotake, A.; Lindegger, N.; Niggli, E.; Barsotti, R. J.; Ellis-Davies, G. C. R., The nitrodibenzofuran chromophore: a new caging group for ultra-efficient photolysis in living cells. *Nature Methods* **2006,** *3* (1), 35-40.

95.   Goswami, P. P.; Syed, A.; Beck, C. L.; Albright, T. R.; Mahoney, K. M.; Unash, R.; Smith, E. A.; Winter, A. H., BODIPY-derived photoremovable protecting groups unmasked with green light. *Journal of the American Chemical Society* **2015,** *137* (11), 3783-3786.

96.   Ieda, N.; Yamada, S.; Kawaguchi, M.; Miyata, N.; Nakagawa, H., (7-Diethylaminocoumarin-4-yl) methyl ester of suberoylanilide hydroxamic acid as a caged inhibitor for photocontrol of histone deacetylase activity. *Bioorganic & Medicinal Chemistry* **2016,** *24* (12), 2789-2793.

97.   Yang, D.; Ma, P. a.; Hou, Z.; Cheng, Z.; Li, C.; Lin, J., Current advances in lanthanide ion (Ln3+)-based upconversion nanomaterials for drug delivery. *Chemical Society Reviews* **2015,** *44* (6), 1416-1448.

98.   Deiters, A., Principles and applications of the photochemical control of cellular processes. *ChemBioChem* **2010,** *11* (1), 47-53.

99.   Young, D. D.; Lusic, H.; Lively, M. O.; Yoder, J. A.; Deiters, A., Gene silencing in mammalian cells with light-activated antisense agents. *ChemBioChem* **2008,** *9* (18), 2937-2940.

100.   Vilar, J. M. G.; Guet, C. l. C.; Leibler, S., Modeling network dynamics: the lac operon, a case study. *Journal of Cell Biology* **2003,** *161* (3), 471-476.

101.   Young, D. D.; Garner, R. A.; Yoder, J. A.; Deiters, A., Light-activation of gene function in mammalian cells viaribozymes. *Chemical Communications* **2009,** (5), 568-570.

102.   Chou, C.; Young, D. D.; Deiters, A., A Light-activated DNA polymerase. *Angewandte Chemie International Edition* **2009,** *48* (32), 5950-5953.

103.   Cambridge, S. B.; Geissler, D.; Calegari, F.; Anastassiadis, K.; Hasan, M. T.; Stewart, A. F.; Huttner, W. B.; Hagen, V.; Bonhoeffer, T., Doxycycline-dependent photoactivated gene expression in eukaryotic systems. *Nature Methods* **2009,** *6* (7), 527-531.

104.   Wu, Y. I.; Frey, D.; Lungu, O. I.; Jaehrig, A.; Schlichting, I.; Kuhlman, B.; Hahn, K. M., A genetically encoded photoactivatable Rac controls the motility of living cells. *Nature* **2009,** *461* (7260), 104-108.

105.   Muralidharan, S.; Nerbonne, J. M., Photolabile "caged" adrenergic receptor agonists and related model compounds. *Journal of Photochemistry and Photobiology B: Biology* **1995,** *27* (2), 123-137.

106.   Font, J.; López-Cano, M.; Notartomaso, S.; Scarselli, P.; Di Pietro, P.; Bresolí-Obach, R.; Battaglia, G.; Malhaire, F.; Rovira, X.; Catena, J.; Giraldo, J.; Pin, J.-P.; Fernández-Dueñas, V.; Goudet, C.; Nonell, S.; Nicoletti, F.; Llebaria, A.; Ciruela, F., Optical control of pain in vivo with a photoactive mGlu5 receptor negative allosteric modulator. *eLife* **2017,** *6*, e23545.

107.   Taura, J.; Nolen, E. G.; Cabré, G.; Hernando, J.; Squarcialupi, L.; López-Cano, M.; Jacobson, K. A.; Fernández-Dueñas, V.; Ciruela, F., Remote control of movement disorders using a photoactive adenosine A2A receptor antagonist. *Journal of Controlled Release* **2018,** *283*, 135-142.

108.   Wagner, N.; Schuhmacher, M.; Lohmann, A.; Nadler, A., A coumarin triflate reagent enables one-step synthesis of photo-caged lipid metabolites for studying cell signaling. *Chemistry – A European Journal* **2019,** *25* (68), 15483-15487.

109.   Kand, D.; Liu, P.; Navarro, M. X.; Fischer, L. J.; Rousso-Noori, L.; Friedmann-Morvinski, D.; Winter, A. H.; Miller, E. W.; Weinstain, R., Water-soluble BODIPY photocages with tunable cellular localization. *Journal of the American Chemical Society* **2020,** *142* (11), 4970-4974.

110.   Leurs, R.; Vischer, H.; Wijtmans, M.; Esch, I., En route to new blockbuster anti-histamines: surveying the offspring of the expanding histamine receptor family. *Trends in Pharmacological Sciences* **2012,** *33*, 49.

111.   Tiligada, E.; Ennis, M., Histamine pharmacology: from Sir Henry Dale to the 21st century. *British Journal of Pharmacology* **2020,** *177* (3), 469-489.

112.   Schneider, E. H.; Seifert, R., Pharmacological characterization of human histamine receptors and histamine receptor mutants in the Sf9 cell expression system. *Handbook of Experimental Pharmacology* **2017,** *241*, 63-118.

113.   Schwartz, J.-C., The histamine H3 receptor: from discovery to clinical trials with pitolisant. *British Journal of Pharmacology* **2011,** *163* (4), 713-721.

114.   Borriello, F.; Iannone, R.; Marone, G., Histamine release from mast cells and basophils. *Handbook of Experimental Pharmacology* **2017,** *241*, 121-139.

115.   Simons, F. E. R.; Simons, K. J., Histamine and H1-antihistamines: Celebrating a century of progress. *Journal of Allergy and Clinical Immunology* **2011,** *128* (6), 1139-1150.e4.

116.   Pinton, P.; Pozzan, T.; Rizzuto, R., The Golgi apparatus is an inositol 1,4,5-trisphosphate-sensitive Ca2+ store, with functional properties distinct from those of the endoplasmic reticulum. *EMBO Journal* **1998,** *17* (18), 5298-5308.

117.   Huang, Z.-L.; Mochizuki, T.; Qu, W.-M.; Hong, Z.-Y.; Watanabe, T.; Urade, Y.; Hayaishi, O., Altered sleep–wake characteristics and lack of arousal response to H3 receptor antagonist in histamine H1 receptor knockout mice. *Proceedings of National Academy of Sciences* **2006,** *103* (12), 4687-4692.

118.   Ikeda-Sagara, M.; Ozaki, T.; Shahid, M.; Morioka, E.; Wada, K.; Honda, K.; Hori, A.; Matsuya, Y.; Toyooka, N.; Ikeda, M., Induction of prolonged, continuous slow-wave sleep by blocking cerebral H1 histamine receptors in rats. *British Journal of Pharmacology* **2012,** *165* (1), 167-182.

119.   Parmentier, R.; Zhao, Y.; Perier, M.; Akaoka, H.; Lintunen, M.; Hou, Y.; Panula, P.; Watanabe, T.; Franco, P.; Lin, J.-S., Role of histamine H1-receptor on behavioral states and wake maintenance during deficiency of a brain activating system: A study using a knockout mouse model. *Neuropharmacology* **2016,** *106*, 20-34.

120.   Simons, F. E.; Simons, K. J., Histamine and H1-antihistamines: celebrating a century of progress. *The Journal of Allergy and Clinical Immunology* **2011,** *128* (6), 1139-1150.e4.

121.   González-Núñez, V.; Bachert, C.; Mullol, J., Rupatadine: global safety evaluation in allergic rhinitis and urticaria. *Expert Opinion on Drug Safety* **2016,** *15* (10), 1439-48.

122.   Agrawal, D. K., Pharmacology and clinical efficacy of desloratadine as an anti-allergic and anti-inflammatory drug. *Expert Opinion on Investigational Drugs* **2001,** *10* (3), 547-60.

123.   Treherne, J. M.; Young, J. M., Temperature-dependence of the kinetics of the binding of [³H]-(+)-N-methyl-4-methyldiphenhydramine to the histamine H1-receptor: comparison with the kinetics of [³H]-mepyramine. *British Journal of Pharmacology* **1988,** *94* (3), 811-822.

124.   Wallace, R. M.; Young, J. M., Temperature dependence of the binding of [³H]mepyramine and related compounds to the histamine H1 receptor. *Molecular Pharmacology* **1983,** *23* (1), 60-66.

125.   Gillard, M.; Chatelain, P., Changes in pH differently affect the binding properties of histamine H1 receptor antagonists. *European Journal of Pharmacology* **2006,** *530* (3), 205-214.

126.   Kanba, S.; Richelson, E., Histamine H1 receptors in human brain labelled with [³H]doxepin. *Brain Research* **1984,** *304* (1), 1-7.

127.   Gillard, M.; Van Der Perren, C.; Moguilevsky, N.; Massingham, R.; Chatelain, P., Binding characteristics of cetirizine and levocetirizine to human H1 histamine receptors: contribution of Lys 191 and Thr194. *Molecular Pharmacology* **2002,** *61* (2), 391-399.

128.   Malany, S.; Hernandez, L. M.; Smith, W. F.; Crowe, P. D.; Hoare, S. R., Analytical method for simultaneously measuring ex vivo drug receptor occupancy and dissociation rate: application to (R)-dimethindene occupancy of central histamine H1 receptors. *Journal of Receptor and Signal Transduction Research* **2009,** *29* (2), 84-93.

129.   Slack, R. J.; Hart, A. D.; Luttmann, M. A.; Clark, K. L.; Begg, M., In vitro characterisation of the duration of action of the histamine-1 receptor antagonist azelastine. *European Journal of Pharmacology* **2011,** *670* (2), 586-592.

130.   Slack, R. J.; Russell, L. J.; Hall, D. A.; Luttmann, M. A.; Ford, A. J.; Saunders, K. A.; Hodgson, S. T.; Connor, H. E.; Browning, C.; Clark, K. L., Pharmacological characterization of GSK1004723, a novel, long-acting antagonist at histamine H(1) and H(3) receptors. *British Journal of Pharmacology* **2011,** *164* (6), 1627-1641.

131.   Wittmann, H.-J.; Seifert, R.; Strasser, A., Influence of the N-terminus and the E2-loop onto the binding kinetics of the antagonist mepyramine and the partial agonist phenoprodifen to H1R. *Biochemical Pharmacology* **2011,** *82* (12), 1910-1918.

132.   Ghorai, P.; Kraus, A.; Keller, M.; Götte, C.; Igel, P.; Schneider, E.; Schnell, D.; Bernhardt, G.; Dove, S.; Zabel, M.; Elz, S.; Seifert, R.; Buschauer, A., Acylguanidines as bioisosteres of guanidines: NG-acylated imidazolylpropylguanidines, a new class of histamine H2 receptor agonists. *Journal of Medicinal Chemistry* **2008,** *51* (22), 7193-7204.

133.   Geyer, R. Hetarylalkyl(aryl)cyanoguanidines as histamine H4 receptor ligands: Synthesis, chiral separation, pharmacological characterization, structure-activity and -selectivity relationships. 2011.

134.   Cook, D. A., Blockade by phenoxybenzamine of the contractor response produced by agonists in the isolated ileum of the guinea-pig. *British Journal of Pharmacology* **1971,** *43* (1), 197-209.

135.   Sansuk, K. Molecular aspects of the histamine H1 receptor (doctoral dissertation), Vrije Universiteit Amsterdam, 2010.

136.   Weichert, D.; Kruse, A. C.; Manglik, A.; Hiller, C.; Zhang, C.; Hübner, H.; Kobilka, B. K.; Gmeiner, P., Covalent agonists for studying G protein-coupled receptor activation. *Proceedings of the National Academy of Sciences* **2014,** *111* (29), 10744-10748.

137.   Rustler, K.; Pockes, S.; König, B., Light-switchable antagonists for the histamine H1 receptor at the isolated guinea pig ileum. *ChemMedChem* **2019,** *14* (6), 636-644.

138.   Shimamura, T.; Shiroishi, M.; Weyand, S.; Tsujimoto, H.; Winter, G.; Katritch, V.; Abagyan, R.; Cherezov, V.; Liu, W.; Han, G. W.; Kobayashi, T.; Stevens, R. C.; Iwata, S., Structure of the human histamine H1 receptor complex with doxepin. *Nature* **2011,** *475* (7354), 65-70.

139.   Shi, L.; Javitch, J. A., The binding site of aminergic G protein–coupled receptors: the transmembrane segments and second extracellular loop. *Annual Review of Pharmacology and Toxicology* **2002,** *42* (1), 437-467.

140.   Surgand, J.-S.; Rodrigo, J.; Kellenberger, E.; Rognan, D., A chemogenomic analysis of the transmembrane binding cavity of human G-protein-coupled receptors. *Proteins: Structure, Function, and Bioinformatics* **2006,** *62* (2), 509-538.

141.   Bakker, R. A.; Dees, G.; Carrillo, J. J.; Booth, R. G.; López-Gimenez, J. F.; Milligan, G.; Strange, P. G.; Leurs, R., Domain swapping in the human histamine H1 receptor. *Journal of Pharmacology and Experimental Therapeutics* **2004,** *311* (1), 131-138.

142.   Bruysters, M.; Pertz, H. H.; Teunissen, A.; Bakker, R. A.; Gillard, M.; Chatelain, P.; Schunack, W.; Timmerman, H.; Leurs, R., Mutational analysis of the histamine H1-receptor binding pocket of histaprodifens. *European Journal of Pharmacology* **2004,** *487* (1), 55-63.

143.   Cordova-Sintjago, T.; Fang, L.; Bruysters, M.; Leurs, R.; Booth, R., Molecular determinants of ligand binding at the human histamine H1 receptor: Site-directed mutagenesis results analyzed with ligand docking and molecular dynamics studies at H1 homology and crystal structure models. *Journal of Chemical and Pharmaceutical Research* **2012,** *ISSN : 0975-7384*, 2937-2951.

144.   Nonaka, H.; Otaki, S.; Ohshima, E.; Kono, M.; Kase, H.; Ohta, K.; Fukui, H.; Ichimura, M., Unique binding pocket for KW-4679 in the histamine H1 receptor. *European Journal of Pharmacology* **1998,** *345* (1), 111-117.

145.   Ohta, K.; Hayashi, H.; Mizuguchi, H.; Kagamiyama, H.; Fujimoto, K.; Fukui, H., Site-directed mutagenesis of the histamine H1 receptor: roles of Aspartic acid107, Asparagine198 and Threonine194. *Biochemical and Biophysical Research Communications* **1994,** *203* (2), 1096-1101.

146.   Michino, M.; Beuming, T.; Donthamsetti, P.; Newman, A. H.; Javitch, J. A.; Shi, L., What can crystal structures of aminergic receptors tell us about designing subtype-selective ligands? *Pharmacological Reviews* **2015,** *67* (1), 198-213.

147.   Wieland, K.; Laak, A. M.; Smit, M. J.; Kühne, R.; Timmerman, H.; Leurs, R., Mutational analysis of the antagonist-binding site of the histamine H(1) receptor. *The Journal of Biological Chemistry* **1999,** *274* (42), 29994-30000.

148.   Kuhne, S.; Kooistra, A. J.; Bosma, R.; Bortolato, A.; Wijtmans, M.; Vischer, H. F.; Mason, J. S.; de Graaf, C.; de Esch, I. J.; Leurs, R., Identification of ligand binding hot spots of the histamine H(1) receptor following structure-based fragment optimization. *Journal of Medicinal Chemistry* **2016,** *59* (19), 9047-9061.

149.   Shiroishi, M.; Kobayashi, T., Structural analysis of the histamine H1 receptor. In *Histamine and Histamine Receptors in Health and Disease*, Hattori, Y.; Seifert, R., Eds. Springer International Publishing: Cham, 2017; pp 21-30.

Chapter 2

Route to prolonged residence time at the histamine H$_1$ receptor: growing from desloratadine to rupatadine[#]

Zhiyong Wang[a1], Reggie Bosma[a1], Albert J. Kooistra[a], Nick Bushby[c], Sebastiaan Kuhne[a], Jelle van den Bor[a], Michael J. Waring[d], Chris de Graaf[a], Iwan J. de Esch[a], Henry F. Vischer[a], Robert J. Sheppard[b], Maikel Wijtmans[a] and Rob Leurs[a]*

[a] Amsterdam Institute for Molecules, Medicines and Systems; Division of Medicinal Chemistry, Faculty of Science, VU University Amsterdam, Amsterdam, the Netherlands.

[b] Medicinal Chemistry, Cardiovascular, Renal, and Metabolic Diseases, IMED Biotech Unit, AstraZeneca, Gothenburg, Sweden

[c] IMED Operations, IMED Biotech Unit, AstraZeneca, Alderley Park, United Kingdom.

[d] Medicinal Chemistry, Oncology, IMED Biotech Unit, AstraZeneca, Alderley Park, United Kingdom.

[1] Authors contributed equally to this manuscript.

Abstract

Drug-target binding kinetics are an important predictor of in vivo drug efficacy. Yet the relationship between ligand structures and their binding kinetics is often poorly understood. We show that both rupatadine (**1**) and desloratadine (**2**) have a long residence time at the histamine H1 receptor (H$_1$R). Through development of a [^{3}H]levocetirizine radiolabel, we find that the residence time of **1** exceeds that of **2** more than 10-fold. This was further explored with 22 synthesized rupatadine and desloratadine analogues. Methylene-linked cycloaliphatic or β-branched substitutions of desloratadine increase the residence time at the H$_1$R, conveying a longer duration of receptor antagonism. However, cycloaliphatic substituents directly attached to the piperidine amine (i.e., lacking the spacer) have decreased binding affinity and residence time compared to their methylene-linked structural analogues. Guided by docking studies, steric constraints within the binding pocket are hypothesized to explain the observed differences in affinity and binding kinetics between analogues.

Introduction

Drugs have to bind a therapeutically relevant target to exhibit a biological effect and, as such, target binding is well characterized during the development process of many drugs. The binding affinity is an often-used parameter to measure drug binding to a target (quantified as K_D or K_i value), implicitly assuming ligand binding occurs under equilibrium conditions. However, drug pharmacodynamics can also be characterized by the drug-target binding kinetics, which provide important details about the mechanism of target binding, unexplained by solely the binding affinity.[1-3] The drug-target residence time, which is a measure for the lifetime of a drug-target complex, is currently discussed as one of the important contributors to the biological efficacy of drugs in vivo.[2, 4-10] It has been postulated that a suitably long drug-target residence time might increase the therapeutic window *in vivo* when clearance of the drug is faster than the dissociation of the drug from the receptor.[11, 12] In such cases, drug action would last longer than the presence of free drug plasma concentrations (i.e. *hysteresis*). Thus, duration of therapeutic action may not only depend on drug absorption, distribution, metabolism, and excretion (and the nature of its metabolites), but can also be a direct effect of prolonged target binding.[13-15]

As the target of 33% of all small molecule drugs, the G-protein coupled receptors (GRCPs) are an important class of proteins in drug discovery.[16] The histamine H$_1$ receptor (H$_1$R) is an archetypical GPCR and is successfully targeted by antagonists for the treatment of, for example, allergic disorders.[17] A long duration of action has been observed *in vivo* for second generation H$_1$R antagonists, like levocetirizine and fexofenadine, which have a long residence time at the H$_1$R.[18, 19] Hysteresis was indeed observed for levocetirizine and fexofenadine.[18-20] A strong *hysteresis* of H$_1$R antagonism was also shown for rupatadine (**1**), which antagonizes the histamine-induced

flare response up to 72 hours after oral administration, whereas plasma levels could only be detected up to 12 hours after administration.[21] This might be explained by the metabolism of rupatadine to metabolites such as desloratadine (**2**), which is a known antihistamine itself with a long H1R residence time (>1 h) and a long plasma half-life in vivo (human).[18, 21-27] Yet, a potentially long drug–target residence time of rupatadine may also be a crucial contributing factor to its observed long duration of action.

Here, we report the measurement of the residence times of rupatadine and desloratadine at the H_1R. It was shown that rupatadine has a ≥ 10 fold longer residence time at the H_1R, relative to desloratadine. As a consequence, rupatadine completely antagonized the histamine-induced calcium mobilization in HeLa cells for > 2 h after removal of unbound antagonist, whereas inspected under the same conditions, desloratadine allowed a time-dependent gradual recovery of the histamine-induced response. To understand the structure-kinetics relationship (SKR) for rupatadine and desloratadine in more detail, the binding kinetics at the H_1R were characterized for newly synthesized analogs (**3**-**24**) that retain the core scaffold of **1** and **2** but contain a diverse set of aromatic and aliphatic N-substituents on the piperidine ring. It was shown that relatively small aliphatic N-substitutions were sufficient for a prolonged H_1R residence time compared to desloratadine, unless this was negated by steric interference in the binding pocket.
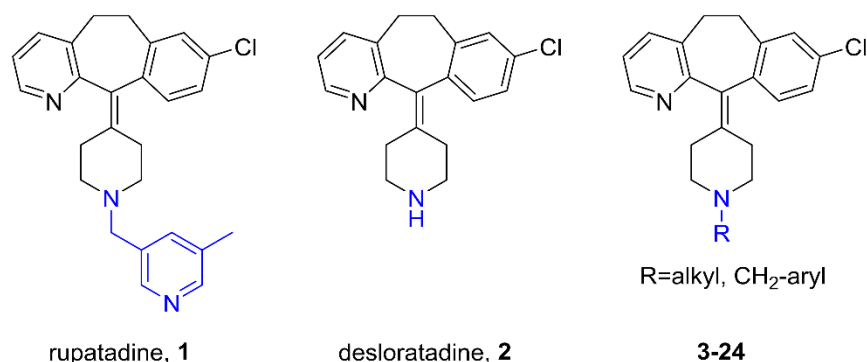
Figure 1-Structures of the investigated H_1R antagonists and synthesized structural analogs.

Results

Binding properties of rupatadine and desloratadine at the H_1R.

Based on the long duration of action of rupatadine *in vivo,*[21] we hypothesized that it would exhibit a long residence time at the H_1R. Therefore, binding of rupatadine and its structural analog desloratadine to the human H_1R was investigated, initially using [^{3}H]mepyramine and standardized competition binding experiments.[26] The H_1R binding affinity of desloratadine (pK_i

9.1 ± 0.1) determined in these experiments was consistent with previously reported affinity values (pK_i= 8.8 – 10[24-26]). Rupatadine (pK_i 8.4 ± 0.1) was shown to have a 5-fold lower binding affinity for the H_1R than desloratadine. To the best of our knowledge, the binding affinity of rupatadine on the human H_1R has not been reported in the literature. Its H_1R activity on guinea pig ileum is known, as well as that for a series of derivatives.[28]

Competitive association experiments were subsequently performed to examine the binding kinetics of rupatadine and desloratadine at the H_1R. Initially, [³H]mepyramine was selected as radioligand and experiments were performed at 25°C with an 80 min incubation time, in the manner described previously.[26] A clear initial overshoot in [³H]mepyramine binding was observed for both unlabeled ligands (Figure 2A), which is indicative of the long residence times of the unlabeled ligands relative to [³H]mepyramine.[29, 30] However, since the binding curves of rupatadine and desloratadine showed similar overshoot patterns, it was difficult to discern differences in their binding kinetics using the Motulsky-Mahan analysis.[30] Desloratadine was found to have a residence time of 190 ± 40 min (similar to that reported in the literature[25, 26]), but for rupatadine the k_{off} value (and thus the residence time) could not be accurately constrained by the model. To overcome this limitation, it was speculated that the residence times of desloratadine and rupatadine at the H_1R might be better discriminated using a radioligand with a longer residence time, and one more closely matched to desloratadine and rupatadine than mepyramine.[31] With this in mind, levocetirizine was considered a better alternative as it is known to have a 100-fold longer residence time at the H_1R than mepyramine.[25] Radiolabeled levocetirizine has previously been disclosed but without synthetic details for its preparation.[25] The radiolabel was prepared by us using a six-step sequence progressing through intermediates **25**-**28**. Separation of the enantiomers of **28**, followed by Pd-catalyzed dehalotritiation of the corresponding aryl iodide delivered the ligand with a specific activity of 956 GBq mmol^{-1} (Scheme 1, and supplementary information).

Scheme 1. Synthesis of [³H]levocetirizine[a]
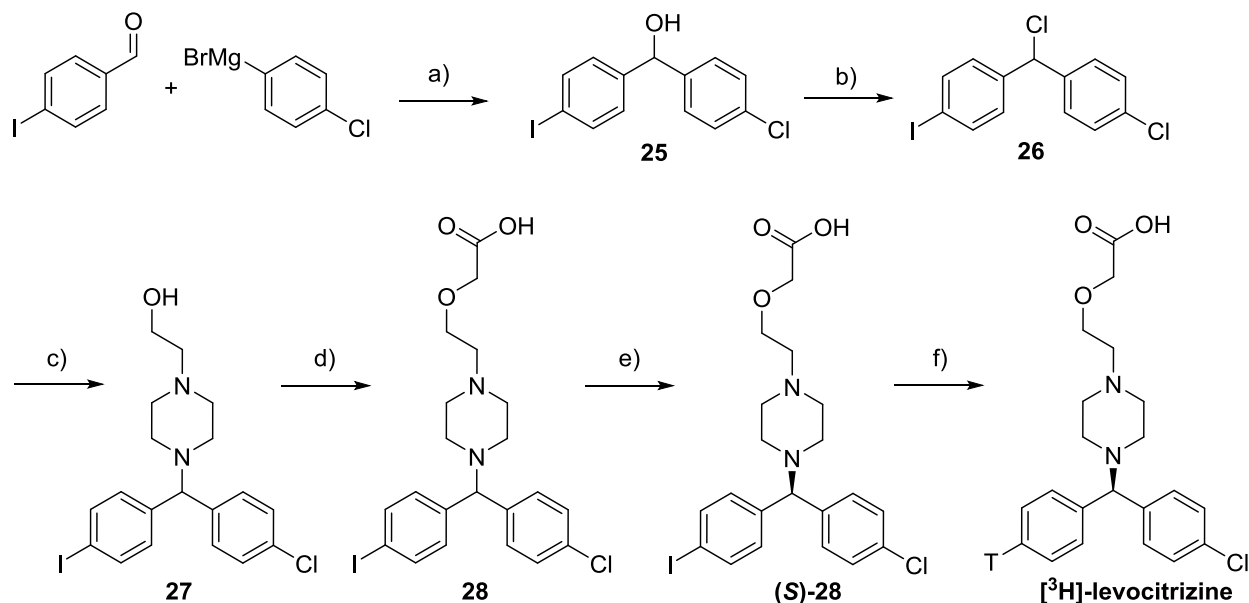
[a]Key: (a) Et₂O, 0 °C to room temperature (rt), 16 h, 88 %; (b) SOCl₂, dichloromethane (DCM), rt, 20 h, 95 %; (c) 2-(piperazin-1-yl)ethanol, PhMe, 80 °C, 20 h, 21 %; (d) (1) KOH, dimethylformamide (DMF), 0 °C, 90 min; (2) sodium 2-chloroacetate, DMF, 0 °C, 3 h, 57 %; (e) chiral separation; (f) T₂, Pd/C (10 %), Et₃N, EtOH.
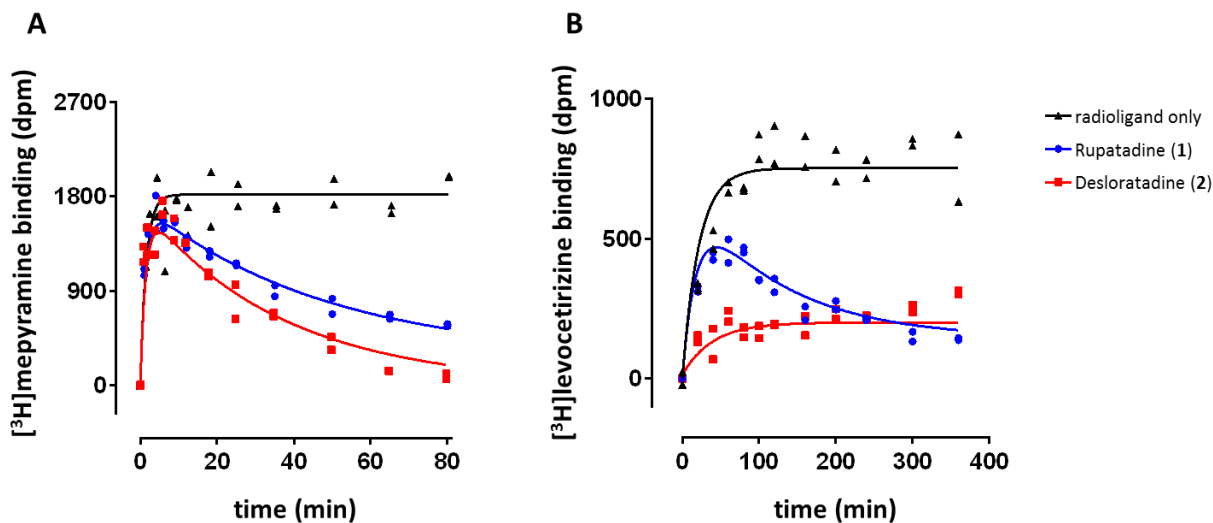
Figure 2 – Radioligand association binding when incubated with rupatadine and desloratadine. A homogenate of HEK293T cells expressing the H_1R was incubated with: (**A**) [³H]mepyramine (3.8 nM) alone, or in the presence of either rupatadine (130 nM) or desloratadine (4 nM); or (**B**), [³H]levocetirizine (6.6 nM) alone, or in the presence of either rupatadine (6 nM) or desloratadine (0.7 nM). Representative graphs of 3 experiments are shown depicting individual measurements with duplicate values per time point.

[^{3}H]levocetirizine was then employed in competitive association experiments to characterize the binding kinetics of rupatadine and desloratadine using an incubation time of 6 h (to ensure a steady state in [^{3}H]levocetirizine binding). In the presence of desloratadine, [^{3}H]levocetirizine binding to the H_1R increased gradually over time, whereas in the presence of rupatadine a clear initial overshoot in [^{3}H]levocetirizine binding was observed (Figure 2). Based on these curve shapes, it is clear that rupatadine has a longer residence time on the H_1R than desloratadine. Fitting the data to the Motulsky-Mahan model[30] did not precise fit of the k_{off} values, but indicated the k_{off} of desloratadine at the H_1R to be > 0.03 min^{-1} (P = 95% in all three experiments) corresponding to a residence time of < 33 min. In the case of rupatadine, the k_{off} value for the binding to the H_1R was < 0.0033 min^{-1} (P = 95% in all three experiments), which corresponds to a residence time of > 300 min. Thus, rupatadine has a very long residence time at the H_1R, which is at least 10-fold longer than observed for desloratadine.

Design and synthesis of rupatadine analogs at the H_1R

To identify the structural features that drive the longer residence time of rupatadine compared to desloratadine at the H_1R, various analogs were synthesized and pharmacologically characterized. Rupatadine contains a 5-methylpyridin-3-yl group connected through a methylene to the basic amine of desloratadine (Figure 1). To study the SKR, we synthesized analogs with the methyl group on different positions of the pyridine ring (**3-5**), and the pyridine analog without the methyl group (**6**). Two positional isomers of **6** (**7**, **8**), and two pyrimidines (**9-10**) were also prepared. Additionally, the pyridine ring of rupatadine was replaced by a phenyl ring with (**11**), or without (**12**), a 3-methyl group. Finally, to gradually bridge the transition to **2**, a set of analogs was synthesized in which the basic amine of desloratadine was substituted with a range of alkyl groups (**13-24**), varying in size, level of constrainment and point of attachment (with or without the one-carbon spacer). Of these, only **3-8**, **12**, **23** and **24** have been reported before.[28, 32-35]

Scheme 2 – Synthesis of rupatadine analogs[a]
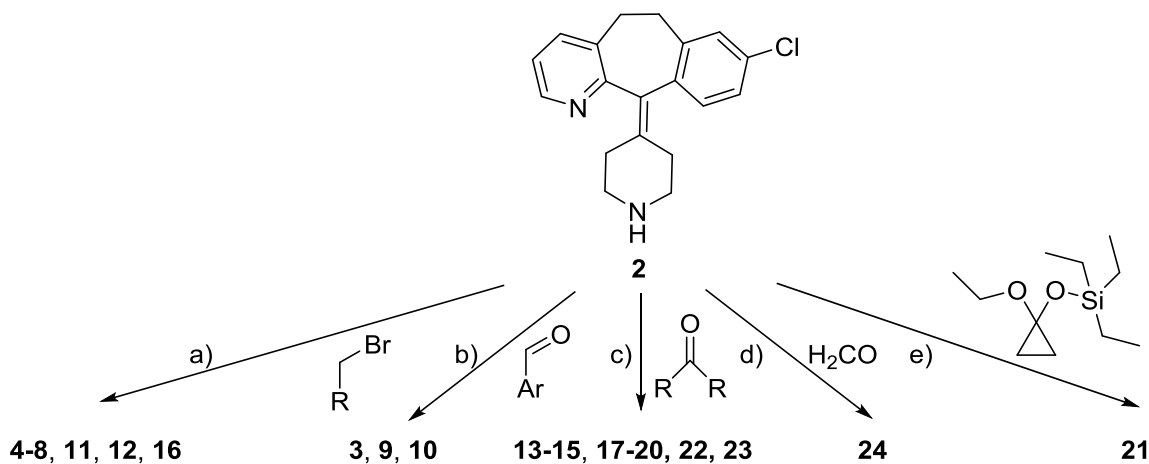
[a]Key: (a) K_2CO_3, DMF, rt, 18 h, 36—86%; (b) NaHB(OAc)$_3$, dichloroethane (DCE), rt, 14 h, 64—88%; (c) NaHB(OAc)$_3$, dichloroethane (DCE), rt, 14 h, 52—71%; (d) NaHB(OAc)$_3$, MeOH, DCM, AcOH, rt, 1.5 h, 60% as fumarate salt; (e) NaHB(OAc)$_3$, AcOH, DCM, rt, 48 h, 17%.

All rupatidine analogues were efficiently obtained in one step from commercially available desloratidine (**2**), as depicted in Scheme 2. Compounds **4**-**8**, **11**-**12** and **16** were obtained *via* nucleophilic substitution of the corresponding alkyl bromides in moderate to good yields (36-86%). Reductive alkylation of **2** with different aromatic aldehydes afforded **3**, **9** and **10** (64-88% yield). Compounds **13**-**15, 17**-**20**, **22** and **23** were synthesized by reductive alkylation using aliphatic carbonyl compounds in acceptable to good yields (52-71%). Methyl-derivative **24** was obtained as the fumarate salt from aqueous formaldehyde and NaBH(OAc)$_3$ in 60% yield. Attempted synthesis of cyclopropyl-substituted analogue **21** via alkylation of **2** with cyclopropylbromide failed. However, reductive alkylation of **2** with (1-ethoxycyclopropoxy)triethylsilane delivered the desired product, albeit in low isolated yield (17%).[36]

Pharmacological characterization

H₁R binding affinity
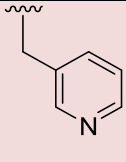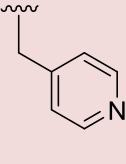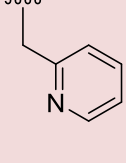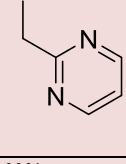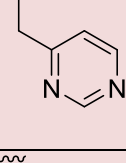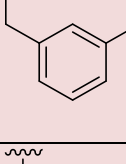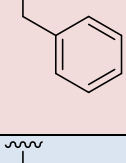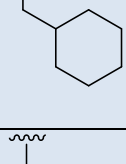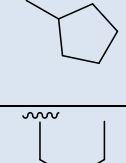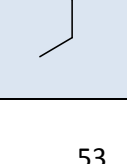
All rupatadine analogs containing an aromatic group (**3**-**12**) had comparable binding affinities at the H$_1$R (pK_i 7.9 – 8.5) as rupatadine, which were 4-16 fold lower than the binding affinity of desloratadine (pK_i = 9.1). Substituting the benzene of **12** for a cyclohexane (**13**) did not affect the binding affinity (<2-fold). However, substituting the benzene of **12** for smaller methylene-linked cycloaliphatic N-substituents (**14**, **16** and **17**) resulted in 2-6 fold higher binding affinities at the H$_1$R, similar to the binding affinity of desloratadine. Likewise, analogs **22**-**24** with small acyclic
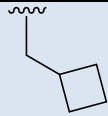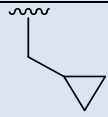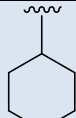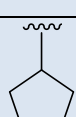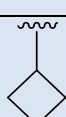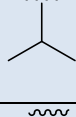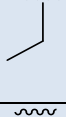
aliphatic substituents had a high binding affinity at the H_1R as well (pK_i 9.0-9.4), again similar to that of desloratadine (pK_i 9.1). Interestingly, the one-carbon linker between the basic amine and the cyclic aliphatic substituents of **13**, **14**, **16** and **17** is important for a high affinity binding, since a 2-8 fold reduced binding affinity is observed for analogs that lack this spacer (**18**-**21**, respectively).

Table 1 – H_1R binding of rupatadine and desloratadine analogs.
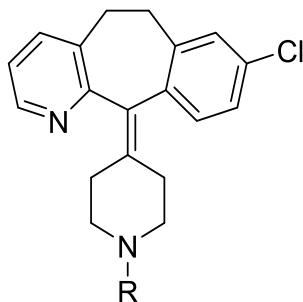
Cmpd#	Name	R	pK_i	KRI
1	rupatadine		8.4 ± 0.1	2.3 ± 0.2
2	desloratadine		9.1 ± 0.1	0.82 ± 0.04
3[b]	VUF15718		7.89 ± 0.05	2.4 ± 0.4
4[b]	VUF15769		8.05 ± 0.04	5.4 ± 3.5
5[b]	VUF15717		8.12 ± 0.04	5.8 ± 1.7

6[b]	VUF15713		8.3 ± 0.1	4.3 ± 1.5
7[b]	VUF15712		8.1 ± 0.3	3.8 ± 0.5
8[b]	VUF15714		8.5 ± 0.1	2.4 ± 0.5
9	VUF15877		8.5 ± 0.1	1.3 ± 0.1
10	VUF15886		8.3 ± 0.1	1.3 ± 0.1
11	VUF15716		8.1 ± 0.1	3.3 ± 0.9
12[b]	VUF15715		8.4 ± 0.1	1.9 ± 0.5
13	VUF16138		8.6 ± 0.2	1.9 ± 0.3
14	VUF16140		8.9 ± 0.2	1.6 ± 0.2
15	VUF16141		8.75 ± 0.05	1.4 ± 0.2

16	VUF16137		9.1 ± 0.2	1.2 ± 0.1
17	VUF16139		9.2 ± 0.1	1.7 ± 0.1
18	VUF16136		7.7 ± 0.1	0.9 ± 0.1
19	VUF16135		8.4 ± 0.2	0.7 ± 0.1
20	VUF16142		8.67 ± 0.04	0.81 ± 0.04
21	VUF 16219		8.5 ± 0.1	0.76 ± 0.03
22	VUF16143		9.0 ± 0.1	1.1 ± 0.3
23[b]	VUF16144		9.38 ± 0.03	1.2 ± 0.1
24[a,b]	VUF15007		9.4 ± 0.1	1.1 ± 0.2

[a] **Fumarate salt.** [b] **Previously reported (see text for references).** [c]Binding affinity (pK_i) values were determined by competition binding experiments using [^{3}H]mepyramine and KRI-values were determined by dual-point competition association experiments using [^{3}H]levocetirizine. Depicted values represent the mean ± SEM of ≥ 3 experiments.

Analysis of binding kinetics

To explore the relative residence time of all analogs, a dual-point competition association was performed to determine the kinetic rate index (KRI).[29] This methodology is based on the observed initial overshoot in radioligand binding when co-incubated with an unlabeled ligand, which is an indicator of a relatively long residence time of the unlabeled ligand compared to that of the radioligand (Figure 2). The overshoot is quantified by measuring the radioligand binding at two time points. The ratio in [^{3}H]levocetirizine binding at both time points (1 and 6 h) is > 1 for

unlabeled ligands that cause an initial overshoot in [³H]levocetirizine binding and hence have a relatively long residence time compared to [³H]levocetirizine. Using this assay setup, a KRI value of 0.9 ± 0.1 was obtained for unlabeled levocetirizine, demonstrating that, as expected, it has a residence time essentially the same as the radioligand. Desloratadine does not cause an initial overshoot in [³H]levocetirizine binding (Figure 2B) and has a KRI value of 0.82 ± 0.04. In contrast, rupatadine binds the H_1R with a much longer residence time (Figure 2B), which is indeed reflected by its KRI value of 2.3 ± 0.2 (Table 1). The KRI values for all analogs are given in Table 1. All analogs with an aromatic substituent (**3**-**12**) show KRI values > 1, indicative of a long residence time at the H_1R (Table 1). More notably, among the analogs with aliphatic substitutions on the piperidine ring (**1**, **2**, **13**-**24**), large differences in the KRI values were observed (Figure 3). This intriguing SKR in the aliphatic series, in combination with the lack thereof in the aromatic series, led us to focus on the former series.
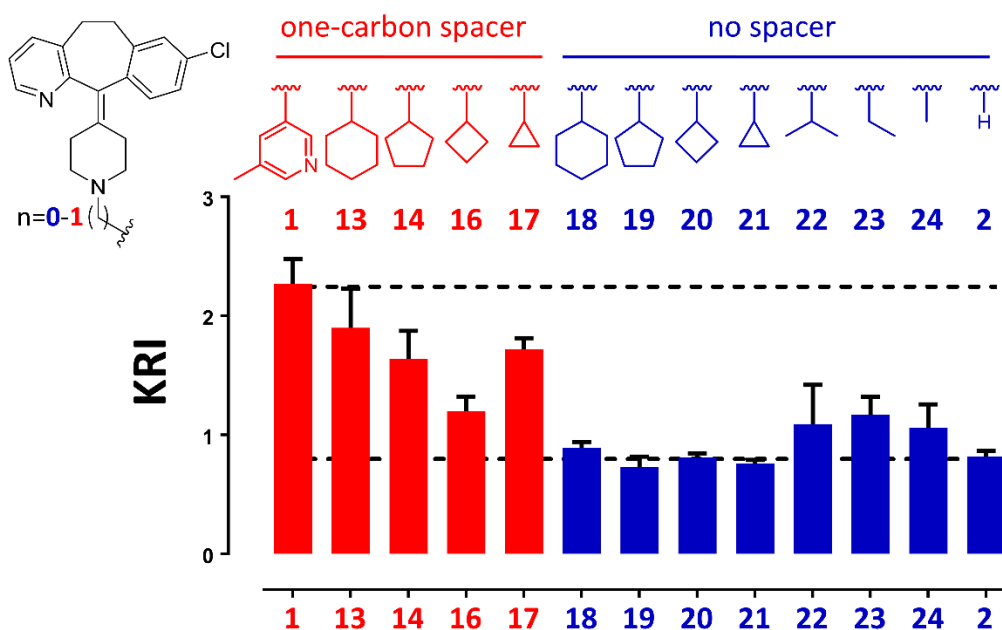
Figure 3– Aliphatic substituents on the basic amine of desloratadine cause differential binding kinetics at the H_1R. A homogenate of HEK293T cells expressing the H_1R was incubated with [³H]levocetirizine and the respective ligands. Binding of [³H]levocetirizine was determined after 1 and 6 h, and the KRI value was determined as the ratio in [³H]levocetirizine binding at both time points (6/1h). The bars depict the mean and SEM of ≥ 3 experiments. The top and bottom dotted lines represent the KRI of reference ligands **1** and **2**, respectively.

Analogs with cycloaliphatic groups and a one-carbon spacer (**13**, **14**, **16** and **17**) show high KRI values, also indicating a long residence time on the H_1R. However, structural analogs with the same cycloaliphatic group without the one-carbon spacer (**18**-**21**) show similar KRI values to desloratadine, indicative of a shorter residence time at the H_1R. Additionally, analogs with small

acyclic aliphatic substituents (**22**-**24**) had an average KRI value slightly larger than 1, implying an increased residence time at the H_1R compared to desloratadine. The correlation between affinity and residence time parameters of GPCR ligands and physiochemical descriptors of the ligands has been investigated, including affinities for H1R receptor antagonists,[37, 38] by various research groups.[39-46] Therefore, we investigated whether correlations exist between our pK_i/KRI values and key physiochemical parameters (log D7.4, polar surface area, van der Waals volume, pK_a value of the conjugate acid of the piperidine nitrogen atom). However, Figure S1, Table S1 and S2, show that no strong correlations are evident.

Duration of functional H_1R-antagonism

Since large differences were observed in the KRI values of the aliphatic rupatadine analogues, these differences were explored in more detail by measuring the kinetics of functional H_1R antagonism following a preincubation with the selected analogues of interest. The functional recovery time (RecT) of the H1R was previously shown to be correlated with the residence time of antagonists.[47] As such, HeLa cells, with endogenous expression of the H_1R, were preincubated with 10 times the K_i-concentration of the respective compound. Unbound ligands were then depleted by washing the cells, which were subsequently stimulated after different incubation times with 10 µM histamine. The intracellular calcium mobilization following administration of histamine was determined with the calcium sensitive fluorescent-dye (Fluo4 NW). Preincubating HeLa cells with desloratadine, which has a low KRI value (<1), resulted in functional recovery of the H_1R over time (Figure 4A and Table S1). However, cells pretreated with rupatadine were completely unresponsive to histamine, for at least for 2 hours after removing unbound rupatadine, suggesting very persistent target engagement by rupatadine. In Figure 4B, the functional recovery of the H_1R is compared after pretreating the cells with analogs containing cycloaliphatic N-substituents on the piperidine with or without a one-carbon spacer. Analogs with a one-carbon spacer (**14**, **16** and **17**) completely abolished the histamine-induced calcium response for at least 2 hours, similarly to rupatadine. In contrast, and in line with the measured KRI values, removing the one-carbon spacer (**19**-**21**), allowed a relatively fast functional recovery of the histamine response.
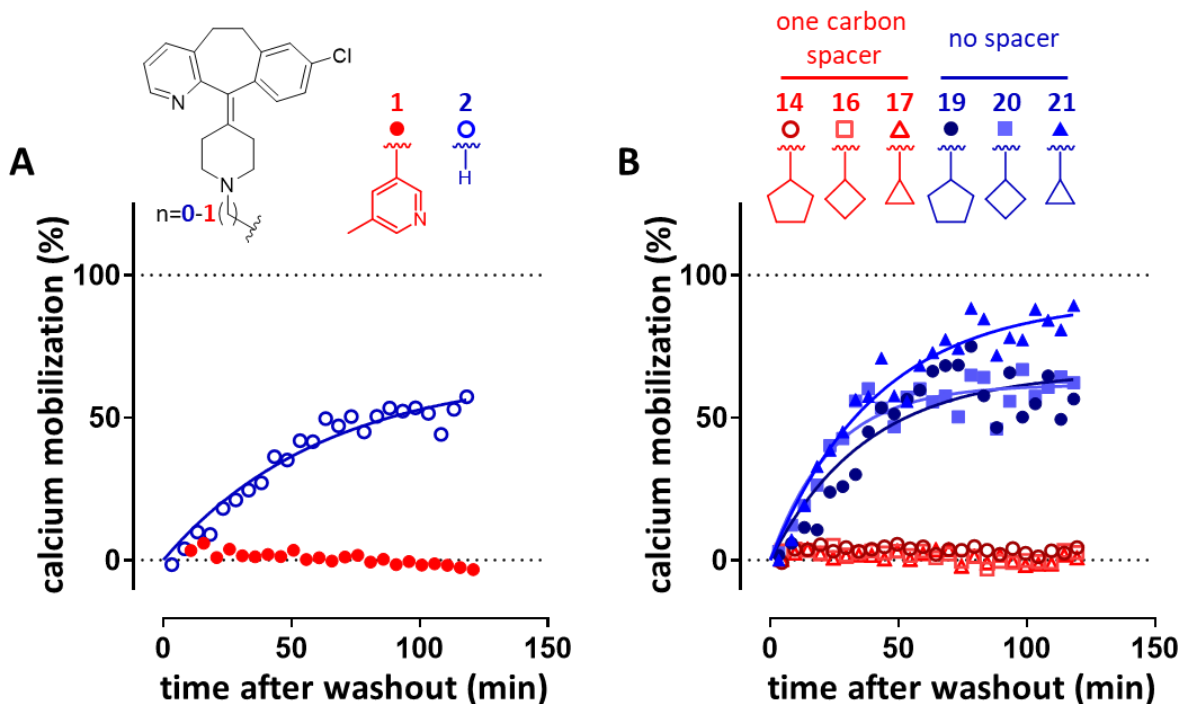
Figure 4– Functional recovery of histamine-induced calcium mobilization after a preincubation with ligands that bind the H_1R. HeLa cells were preincubated for 18-20 h with the respective H_1R ligand, reaching stable and high (±90%) occupancy of the endogenously expressed H_1R. The cells were then labeled with Fluo4NW in the presence of the respective ligands for 1 h. All excess Fluo4NW and unbound ligands were removed by wash steps and cells were subsequently stimulated with histamine (10^{-5} M) after different incubation times. Representative graphs of ≥ 3 experiments are shown, which depict the normalized calcium mobilization that was measured at each time point after washout. **(A)** Cells were preincubated with the reference H_1R antagonists: rupatadine (**1**) and desloratadine (**2**). **(B)** Cells were preincubated with compounds having various cycloalkyl substituents on the basic amine with (**14, 16, 17**) or without (**19, 20, 21**) a one-carbon spacer.

The differences in the combined kinetic/affinity binding profiles of the compounds were further explored on a structural level with docking studies. Using the X-ray crystal structure of the H_1R with the structurally-related ligand doxepin bound,[48] reference compounds desloratadine, rupatadine, as well as all analogs (**3**-**24**) were docked using PLANTS.[49] Figure 5 shows the postulated binding modes of desloratadine, rupatadine, and the representative pair **14/19**, in comparison to the binding mode of the co-crystallized ligand doxepin. Desloratadine likely adopts a similar binding pose to that observed for doxepin in the H_1R crystal structure (Figure 5A). Rupatadine was also found to adopt a similar binding mode to doxepin, but its (5-methylpyridin-3-yl)methyl moiety targets an additional area of the H_1R binding pocket towards the extracellular vestibule (Figure 5B). Since the available space in the H_1R pocket next to the amine-binding region is limited by I454[7.39] and Y458[7.43], it is postulated that the cyclopentyl substituent of **19** encounters greater steric hindrance than the cyclopentlymethyl substituent of **14** (Figure 5C), in line with the altered H_1R binding characteristics of **19.** (Figure 3 and Figure 4B). This steric

hindrance results in a tilted binding mode compared to desloratadine, which is not observed for optimal binding of analogs with a methylene spacer between the desloratadine scaffold and the cyclopentyl group (**14**, Figure 5D). The spacer allows the aliphatic group to turn towards the extracellular vestibule (in the direction of H450$^{7.35}$) where more room is available, possibly preventing a steric clash with I454$^{7.39}$ and Y458$^{7.43}$ (Figure 5D).
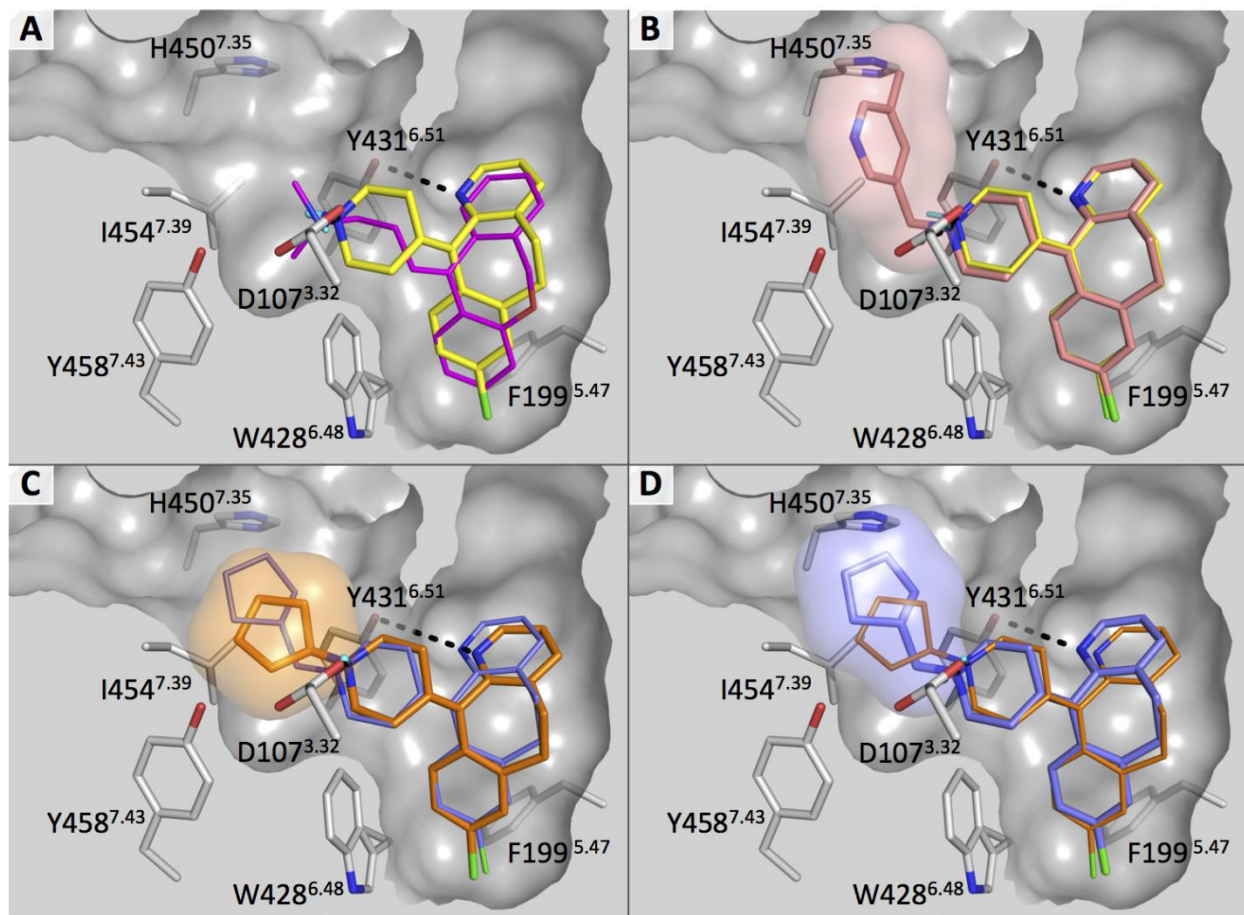
Figure 5– Proposed binding modes of (A) Desloratadine (yellow), (B) Rupatadine (salmon), and (C, D) compound 19 (orange) in comparison to compound 14 (blue) based on docking[49] into the crystal structure (PDB-code 3RZE[48]) of the H$_1$R in complex with Doxepin (magenta, see A). The clipped molecular surface of H$_1$R highlights the limited space for growing from the amine of desloratadine due to I454$^{7.39}$ and Y458$^{7.43}$. To highlight the fit of the substituents of rupatadine (**2**, B), **19** (C), and **14** (D) compared to desloratadine in the H$_1$R binding pocket, they are shown as transparent surfaces.

Discussion and conclusion

A long drug-target residence time has been postulated to benefit the *in vivo* efficacy of several drugs for a broad number of drug targets, among which is the H$_1$R.[4, 7, 50, 51] Affinity-based optimization of drug binding does not necessarily reflect differences in target residence time,[52,

[53] and a discrepancy between affinity and residence time at the H_1R was previously described. Moreover, in the case of ligands that do not reach a binding equilibrium within the time frame of a binding experiment, i.e. ligands with a very slow off rate like rupatadine, the pK_i will be underestimated.[54] The drug-target residence time can therefore provide additional information for the optimization of drugs that would be lost by focusing on only the binding affinity. Since the residence time is not routinely incorporated in drug development, design strategies for optimizing the drug-target residence time of lead compounds are not widely available. Since rupatadine is shown here to have a much longer residence time at the H_1R than its close structural analog desloratadine, despite a reduced binding affinity, it provides an opportunity for a detailed investigation of the SKR for this GPCR. Towards this end, we synthesized [^{3}H]levocetirizine which proved to be a useful tool to map the differences in the KRIs between the two antihistamines. It was therefore employed to determine the relative residence times of structural analogs **3**-**24**. Several analogs of rupatadine were designed to replace the (5-methylpyridin-3-yl)methyl group with other aromatic moieties (**3**-**12**). Interestingly, the K_i values of **3**-**12** are within 4-fold of the K_i value of rupatadine. Additionally, all aromatic analogs have a long apparent residence time, as is reflected by the KRI > 1. Removing the aromatic character of the functional group of **12** by replacing it with a cyclohexyl group (**13**) does not affect the observed H_1R binding properties either. Hence, the strong effect on the residence time by the (5-methylpyridin-3-yl)methyl group of rupatadine (compared to desloratadine) cannot be explained by the aromatic character, nor by the pyridine nitrogen atom and the methyl substituent.

To further probe the SKR between rupatadine and desloratadine, a series of analogs was characterized that had different aliphatic substituents on the piperidine group (**13**-**24**). Strikingly, most aliphatic moieties afford an increase in the KRI compared to desloratadine, whereas the binding affinity remains similar or even decreases. For example, **13**-**15** contain relatively large aliphatic substituents ($\geq$ 6-carbons) and have a slightly reduced binding affinity (pK_i 8.6 – 8.9) and a high KRI (> 1.4) compared to desloratadine. Moreover, analogs with small ($\leq$ 3-carbons) acyclic aliphatic substituents (**22**-**24**) have a similar binding affinity but still a slightly higher KRI compared to desloratadine. This suggests that growing an aliphatic group from the piperidine increases the residence time at the H_1R. This trend is disrupted, however, for analogs that contain cycloaliphatic groups directly substituted on the amine (**18**-**21**) instead of being separated from the amine by a one-carbon spacer (**13**, **14**, **16** and **17**). Analogs without the methylene spacer (**18**-**21**) are marked by a diminished KRI and binding affinity compared to analogs with a methylene spacer, whereas the KRI values are of the same magnitude as desloratadine.

This cliff in the SKR trend was validated for a subset of analogs by studying the kinetics of functional H_1R antagonism, which is known to reflect differential residence times at the H_1R.[47] Representative analogs in which the cycloaliphatic group is substituted with a one-carbon spacer (**14**, **16** and **17**) completely inhibit the functional response of the H_1R for at least 2 h after removal

of unbound ligands, as was observed for rupatadine. In contrast, analogs with the same cycloaliphatic groups without a one-carbon spacer (**19**-**21**) allowed a clear recovery of the H_1R functional response, as was also observed for desloratadine. Hence, the relevance of the methylene-spacer for the binding kinetics of analogs with relatively large N-substituents was confirmed by the duration of functional H_1R inhibition.

The observed residence time/affinity cliff correlated with the binding poses of the representative pair **14** and **19** in the H_1R binding pocket. Our docking studies suggest that the reduced flexibility of the cycloaliphatic group without a spacer (**19**) might lead to a suboptimal fit due to steric hindrance (Figure 5C, D). The increase in ligand residence time at the H_1R, as was observed for most analogs with an aliphatic group on the basic amine of desloratadine (*vide supra*), seems therefore to be mitigated when the shape of the H_1R binding pocket, i.e. the steric constraints imposed by residues I454[7.39] and Y458[7.43], is interfering with the binding position of the desloratadine scaffold.

Recently, it was shown that N-methylation of H_1R ligands with a primary or secondary amine increased the binding affinity at the H_1R by displacing a water molecule near I454[7.39].[43] However, this effect on the binding affinity was not observed for analogs with a chlorine moiety on the aromatic rings. Consistent with this finding, N-methylation of desloratadine (which contains a chlorine group), affording **24**, had only modest effects on the H_1R binding affinity. Interestingly, **24** did have a higher KRI compared to desloratadine but not to the same extent as was observed for larger aliphatic substituents (for example, **13**-**17**). Substitution with aliphatic or aromatic groups on the piperidine possibly reduces the resolvation of both the ligand and binding site during a dissociation event. For ligand dissociation from the CRF_1R, for example, a low degree of ligand solvation during egress from the pocket was related to a long residence time at the receptor.[41] Moreover, hydrophobic shielding of H-bonds can increase the lifetime of such interactions and consequently result in an increased residence time.[40] This is corroborated by the fact that ligands with a relatively high KRI (>1.5) were relatively lipophilic (logD7.4, Figure S1). Considering that N-substitution of H_1R ligands was shown to interfere with the water network in the binding site[43] and that the salt bridge between the basic amine of ligands and D107[3.32] is crucial for a high binding affinity at the receptor,[42] shielding this interaction pair might prevent a rapid egress of the ligands from the binding site.

Compared to desloratadine, rupatadine has an extremely long residence time at the H_1R despite an apparent loss in binding affinity, resulting in a longer duration of functional H_1R antagonism. Development of a [³H]levocetirizine radiolabel allowed a detailed SKR study, which shows that aliphatic N-substitution of the piperidine ring from desloratadine is enough to obtain antagonists with a long residence time at the H_1R without increasing the observed binding affinity. Analogs with large flexible cycloaliphatic or aromatic substituents, like the (5-methylpyridin-3-yl)methyl

substituent of rupatadine, have a long residence time at the H_1R. Notably, analogs with cycloaliphatic substituents required an additional methylene spacer on the amine for an optimal binding of the H_1R. Modeling studies suggest that the combined affinity/kinetics profiles of analogs without a methylene spacer are possibly linked to the steric complementarity in the ligand-H_1R complex. Aliphatic N-substitution of H_1R antagonists is a new potential strategy to optimize the residence time at the receptor. The presented SKR highlights that subtle structural changes of small-molecule ligands can have a profound effect on the binding kinetics at GPCRs.

Methods

Pharmacological assays

Pharmacological Assays. All compounds that were tested in pharmacological assays (**1**–**24**, **28**) are confirmed to pass a publicly available pan-assay interference compounds filter.[55, 56]

Radioligand binding experiments

Radioligand binding experiments were performed as described before, with minor alterations.[26] Cell pellets were produced from HEK293T cells expressing the N-terminally HA-tagged H_1R, and pellets were stored at -20 °C. Upon experimentation, cells were thawed, resuspended in radioligand binding buffer [Na_2HPO_4 (50 mM) and KH_2PO_4 (50 mM), pH 7.4] and homogenized with a Branson sonifier 250 (Branson Ultrasonics, Danbury, CT, USA). Cell homogenates (0.5 – 3 µg/well) were then incubated with the respective ligands under gentle agitation, as specified for the various assay formats below. After the incubation time, binding reactions were terminated with the cell harvester (Perkin Elmer) using rapid filtration and wash steps over PEI-coated GF/C filter plates. Filter bound radioligand was then quantified by scintillation counting using Microscint-O and the Wallac Microbeta counter (Perkin Elmer).

In *competition binding experiments*, cell homogenates were incubated for 4 h at 25 °C with a single concentration of [^{3}H]mepyramine (1.5 – 4nM) and increasing concentrations unlabeled ligands (10^{-5} M – 10^{-13} M). IC_{50} values were obtained by analyzed the displacement curves with GraphPad Prism 7.03 (GraphPad Software, San Diego, USA) and were converted to K_i values using the Cheng-Prusoff equation.[57]

The binding rate constants of [^{3}H]levocetirizine were determined using the previously described methodology, by using four different concentrations of [^{3}H]levocetirizine (1 – 35 nM) for a total incubation time of 360 min, with an incubation temperature of 37 °C (data not shown).[26] This resulted in a k_{on} of 3.7 ± 0.4 $10^6 \cdot$min$^{-1} \cdot$M^{-1} and a k_{off} of 0.022 ± 0.003 min^{-1}. In *competitive association experiments* with [^{3}H]levocetirizine as radioligand, cell homogenates were incubated at 37°C for various incubation times with a single concentration of [^{3}H]levocetirizine (5 – 8 nM)

in the absence of unlabeled ligand as well as with three different concentrations of either desloratadine (2 – 60 nM) or rupatadine (0.1 – 7 nM). The k_{on} and k_{off} values for the binding of [³H]levocetirizine are constrained during the analysis of the H_1R binding kinetics of desloratadine and rupatadine. Kinetic binding rate constants as well as their asymmetrical 95% confidence intervals (95% CI) were determined using GraphPad Prism 7.03. Since the 95% CI values were very broad, values are depicted to be higher or lower than the 95% CI boundary value observed over all individually performed experiments. Graphs depict a representative graph with mean and SD of duplicate values showing, for clarity, only a single concentration unlabeled ligand.

Competitive association experiments with [³H]mepyramine as radioligand were performed as described before, with minor alterations.[26] Briefly, cell homogenates were incubated at 25°C for various incubation times with a single concentration of [³H]mepyramine (2.5 nM – 5.5 nM) in the absence or presence of a single concentration unlabeled ligand (desloratadine [4 – 8 nM] or rupatadine [80 – 250 nM]).

In *dual-point competition association* experiments the kinetic rate index (KRI) value at the H_1R is determined. Cell homogenates were incubated on a 96-well plate for 1 h and 6 h at 37°C, with a single concentration of [³H]levocetirizine (4 – 11 nM) together with a single concentration of unlabeled ligand that equals the respective K_i-value of that ligand at the H_1R. All conditions were measured in triplicate per experiment (n=3). Additionally, for each 96-well plate, [³H]levocetirizine was incubated with a large excess of mianserin (10^{-5} M) to determine non-specific binding levels of the radioligand (n=6) and, as a positive control, [³H]levocetirizine binding was determined in the absence of competitor (maximal binding, n=6). [³H]levocetirizine binding levels were baseline corrected by subtracting non-specific binding levels and KRI values were then calculated by the ratio of [³H]levocetirizine binding after a 1 h incubation time over the [³H]levocetirizine binding after a 6 h incubation time. KRI-values are a quantitative measure for the overshoot in radioligand binding, which results from incubating the radioligand with an unlabeled ligand that has a relatively low k_{off}.[29, 30] It is therefore crucial that the concentrations of unlabeled ligands are comparable and lead to a sub-maximal inhibition of the radioligand binding. Therefore KRI-values were only accepted when the %-inhibition of [³H]levocetirizine binding (compared to the maximal [³H]levocetirizine binding) was (1) less than 80% after either 1 or 6 h and (2) more than 20% inhibition after 6 h. In the case that data points had to be excluded, the concentration unlabeled ligands were attenuated (ranging from 1 x K_i to 3 x K_i concentrations). All experiments were performed in triplicate or more.

Intracellular calcium mobilization assay

The functional recovery of the H_1R following antagonism was measured as described before.[47] In short, HeLa cells, endogenously expressing the H_1R, were seeded $2 \cdot 10^4$ cells/well in a clear bottom 96-well plate which were pre-incubated overnight with a concentration antagonist

corresponding to 10 times the respective K_i at the H_1R (24 wells per antagonist). After 18-20 h, cells were labeled with the Fluo-4NW dye in the presence of the respective concentration antagonist for an hour. Both the excess dye-solution as well as the unbound antagonists were removed by washing the cells two times and cells were then reconstituted in HBSS buffer supplemented with probenecid (2.5 mM) (**t₀**). Following the wash step, cells were stimulated every 5 min by histamine injection, into a single well, using the NOVOstar plate reader (BMG Labtech, Ortenberg, Germany), while simultaneously detecting the calcium mediated Fluo4NW fluorescence ($\lambda_{excitation}$ 494 nm and $\lambda_{emission}$ 516 nm). For each well stimulated with histamine, a consecutive triton-x100 injection after 65 sec was used to lyse the cells leading to saturation of the Fluo4 NW with calcium. The histamine-induced peak-response was then normalized to basal levels of fluorescence (prior to histamine injection; 0) and saturated Fluo4 NW fluorescence (following Triton X-100 injection; 1). This led to a reproducible histamine induced response over time for HeLa cells pretreated with vehicle condition, which was set to a 100%. Histamine-induced peak-responses were plotted against the difference in time between **t₀** and the subsequent histamine injection. The recovery time (RecT) was determined for antagonists by non-linear regression using the one-phase association model in GraphPad Prism 7.03.

Molecular modeling

Simplified molecular-input line-entry system for compounds **1**-**24** were obtained from ChemBioDraw Ultra (version 16.0.1.4), and were subsequently used as input for ChemAxon's calculator for protonation (pH = 7.4). A 3D conformation was then generated using Molecular Networks' CORINA (version 3.49) and stored in Tripos MOL2 format (gold extension). The doxepin-bound H_1R structure was obtained from the protein data bank (PDB-code 3RZE) after which the fused T4-lysozyme was removed from the structure. The complex was further prepared for docking using MOE (Chemical Computing Group, version 2016.0802). Using PLANTS (version 1.2),[49] each compound was docked into the H_1R binding pocket 3-times with the following settings: search speed 1, cluster rmsd 1.0, cluster structures 10, and scored using the ChemPLP scoring function. The binding site was defined by the center of the co-crystallized ligand doxepin with a radius of 11Å. The resulting docking poses were visually inspected and the poses with the best overlap with each other as well as the doxepin reference compounds, which were also the highest-ranking poses for each compound. The binding mode figures were created with PyMol (version 1.8.0). Moreover, using an interaction fingerprint similarity analysis,[58] all docking poses were compared to the binding mode of the co-crystallized compound doxepin. All selected docking poses have an interaction fingerprint similarity of at least 0.72 compared to the binding mode of doxepin and are depicted in the Supporting Information (Figures S2 and S3). The binding mode figures were created with PyMol (version 1.8.0).

Chemistry

*General Procedures. Synthesis of Rupatadine Analogues **3**–**24**.*

Anhydrous tetrahydrofuran, DCM, DMF, and Et$_2$O were obtained by elution through an activated alumina column prior to use. All other solvents and chemicals were acquired from commercial suppliers and were used as received. ChemBioDraw Ultra 16.0.1.4 was used to generate systematic names for all molecules. All reactions were performed under an inert atmosphere (N2). Thin-layer chromatography analyses were carried out with alumina silica plates (Merck F254) using staining and/or UV visualization. Column purifications were performed manually using SiliCycle UltraPure silica gel or automatically using Biotage equipment. NMR spectra (1H, 13C, and two-dimensional) were recorded on a Bruker 300 (300 MHz), Bruker 500 (500 MHz), or Bruker 600 (600 MHz) spectrometer. Chemical shifts are reported in parts per million (ppm) (δ), and the residual solvent was used as internal standard (δ ^{1}H NMR: CDCl$_3$ 7.26; dimethyl sulfoxide (DMSO)-d_6 2.50; CD$_3$OD 3.31; δ ^{13}C NMR: CDCl$_3$ 77.16; DMSO-d_6 39.52; CD$_3$OD 49.00). Data are reported as follows: chemical shift (integration, multiplicity (s = singlet, d = doublet, t = triplet, q = quartet, br = broad signal, m = multiplet, app = apparent), and coupling constants (Hz)). A Bruker microTOF mass spectrometer using electrospray ionization (ESI) in positive-ion mode was used to record high-resolution mass spectrometry (HRMS) images. A Shimadzu LC-20AD liquid chromatograph pump system linked to a Shimadzu SPD-M20A diode array detector with MS detection using a Shimadzu LC-MS- 2010EV mass spectrometer was used to perform liquid chromatography–mass spectrometry (LC–MS) analyses. An Xbridge (C18) 5 µm column (50 mm, 4.6 mm) was used. The solvents that were used were the following: solvent B (acetonitrile with 0.1% formic acid) and solvent A (water with 0.1% formic acid), flow rate of 1.0 mL min−1, start 5% B, linear gradient to 90% B in 4.5 min, then 1.5 min at 90% B, then linear gradient to 5% B in 0.5 min, then 1.5 min at 5% B; and total run time of 8 min. All compounds have a purity of ≥95% (unless specified otherwise), calculated as the percentage peak area of the analyzed compound by UV detection at 254 nm (values are rounded). Reverse-phase column chromatography purifications were performed using Buchi PrepChrom C-700 equipment with a discharge deuterium lamp ranging from 200 to 600 nm to detect compounds using solvent B (acetonitrile with 0.1% formic acid), solvent A (water with 0.1% formic acid), flow rate of 15.0 mL min−1, and a gradient (start 95% A for 3.36 min, then linear gradient to 5% A in 30 min, then at 5% A for 3.36 min, then linear gradient to 95% A in 0.5 min, and then 1.5 min at 95% A).

The Supporting Information lists all detailed experimental procedures and chemical analyses including ^{1}H-NMR and ^{13}C-NMR spectroscopy as well as high-resolution mass spectroscopy and LC-MS chromatography.

Synthesis of [3H]Levocetirizine (**25–28**). Column chromatography was carried out using prepacked silica gel cartridges (SiliCycle, Quebec, Canada) on an Isco Companion (Teledyne Isco, NE). ^{1}H NMR spectra were recorded on a Bruker (600 or 400 MHz) using the stated solvent. Chemical shifts (δ) in ppm are quoted relative to CDCl$_3$ (δ 7.26 ppm) and DMSO-d_6 (δ 2.50 ppm). Liquid chromatography–mass spectrometry (LC–MS) data were collected using a Waters Alliance LC (Waters Corporation, MA) with Waters ZQ mass detector. Analytical high-performance liquid chromatography (HPLC) data were recorded using Agilent 1200 HPLC system with a β-Ram Flow Scintillation Analyser, using the following conditions: Waters Sunfire C18, 3.5 μm, 4.6 × 100 mm2 column at 40 °C, eluting with 5% acetonitrile/water + 0.1% trifluoroacetic acid (TFA) to 95% acetonitrile/water + 0.1% TFA over a 32 min gradient. Specific activities were determined gravimetrically with a Packard Tri-Carb 2100CA Liquid Scintillation Analyser (Packard Instrument Company Inc., IL) using Ultima Gold cocktail. Reactions with tritium gas were carried out on a steel manifold obtained from RC Tritec AG (Teufen, Switzerland). Specific activity was calculated by comparison of the ratio of tritium/hydrogen or carbon-14/carbon-12 for the tracer against the unlabeled reference. [3H]Methyl nosylate was obtained from Quotient Bioresearch as a solution in toluene at 3150 GBq mmol−1. Tritium gas was supplied and absorbed onto a depleted uranium bed by RC Tritec AG (). All other reagents and solvents obtained from Sigma-Aldrich and Fisher and were used without further purification.

Experimental Procedures

8-Chloro-11-(1-((4-methylpyridin-3-yl)methyl)piperidin-4-ylidene)-6,11-dihydro-5H-benzo-[5,6]cyclohepta[1,2-b]pyridine (3)

A mixture of 4-methylnicotinaldehyde (93 mg, 0.77 mmol), desloratadine (200 mg, 0.643 mmol), and NaBH(OAc)$_3$ (218 mg, 1.027 mmol) in DCE (10 mL) was stirred at room temperature for 12 h. The resulting solution was diluted with water and extracted with DCM. The organic phase was washed with satd. aq NaHCO$_3$ solution. The organic layer was dried over Na$_2$SO$_4$, filtered, and concentrated under vacuum. The crude mixture was purified by reverse-phase column chromatography (H$_2$O/MeCN/HCOOH). The product fraction was evaporated, extracted with DCM/satd. aq Na$_2$CO$_3$ solution, dried (MgSO$_4$), and concentrated to yield the title compound as a pink foam (170 mg, 64% yield). ^{1}H NMR (500 MHz, CDCl$_3$) δ 8.42–8.22 (m, 3H), 7.39 (dd, J = 7.6, 1.3 Hz, 1H), 7.15–6.97 (m, 5H), 3.48–3.25 (m, 4H), 2.87–2.60 (m, 4H), 2.51–2.20 (m, 7H), 2.19–2.04 (m, 2H). ^{13}C NMR (126 MHz, CDCl$_3$) δ 157.46, 150.18, 148.22, 147.40, 146.49, 139.49, 138.86, 137.76, 137.35, 133.43, 132.62, 132.56, 132.41, 130.79, 128.94, 125.98, 125.43, 122.13, 57.98, 54.80, 54.71, 31.79, 31.40, 30.97, 30.76, 18.81. HRMS: C$_{26}$H$_{27}$ClN$_3$ (M + H)$^+$ calcd: 416.1894, found: 416.1883. LC–MS: t_R = 3.0 min, purity >96% (254 nm), m/z: 416.2 (M + H)$^+$.

8-Chloro-11-(1-((2-methylpyridin-3-yl)methyl)piperidin-4-ylidene)-6,11-dihydro-5H-benzo[5,6]cyclohepta[1,2-b]pyridine (4)

A mixture of desloratadine (155 mg, 0.50 mmol), 3-(chloromethyl)-2-methylpyridine hydrochloride (116 mg, 0.65 mmol), and K_2CO_3 (180 mg, 1.30 mmol) in DMF (10 mL) was stirred at room temperature for 18 h. The mixture was diluted with EtOAc, washed with water (2×) and brine, dried over Na_2SO_4, filtered, and concentrated under vacuum. The crude mixture was purified by reverse-phase column chromatography (H₂O/MeCN/HCOOH) to yield the title compound as a pink foam (120 mg, 58% yield). ^{1}H NMR (500 MHz, CDCl₃) δ 8.42–8.31 (m, 2H), 7.59 (d, J = 7.0 Hz, 1H), 7.42 (d, J = 7.6 Hz, 1H), 7.16–7.02 (m, 5H), 3.49–3.29 (m, 4H), 2.88–2.65 (m, 4H), 2.60–2.45 (m, 4H), 2.45–2.26 (m, 3H), 2.23–2.06 (m, 2H). ^{13}C NMR (126 MHz, CDCl₃) δ 157.62, 157.44, 147.40, 146.61, 139.50, 138.78, 137.76, 137.32, 137.01, 133.37, 132.69, 132.59, 131.89, 130.78, 128.92, 125.98, 122.11, 121.00, 59.61, 54.92, 54.84, 31.77, 31.41, 30.95, 30.72, 22.26. HRMS: $C_{26}H_{27}ClN_3$ (M + H)⁺ calcd: 416.1888, found: 416.1906. LC–MS: t_R = 2.9 min, purity >98% (254 nm), m/z: 416.2 (M + H)⁺.

8-Chloro-11-(1-((6-methylpyridin-3-yl)methyl)piperidin-4-ylidene)-6,11-dihydro-5H-benzo[5,6]cyclohepta[1,2-b]pyridine (5)

A mixture of desloratadine (200 mg, 0.643 mmol), 5-(bromomethyl)-2-methylpyridine hydrobromide (224 mg, 0.836 mmol), and K_2CO_3 (231 mg, 1.67 mmol) in DMF (10 mL) was stirred at room temperature for 18 h. The mixture was diluted with EtOAc, washed with water (2×) and brine, dried over Na_2SO_4, filtered, and concentrated under vacuum. The crude mixture was purified by reverse-phase column chromatography (H₂O/MeCN/HCOOH). The product fraction was evaporated, extracted with DCM/satd. aq Na_2CO_3 solution, dried (MgSO₄), and concentrated to yield the title compound as a pink foam (170 mg, 64% yield). ^{1}H NMR (500 MHz, CDCl₃) δ 8.41–8.33 (m, 2H), 7.60 (d, J = 7.3 Hz, 1H), 7.41 (d, J = 7.6 Hz, 1H), 7.16–7.02 (m, 5H), 3.50 (s, 2H), 3.42–3.28 (m, 2H), 2.86–2.68 (m, 4H), 2.57–2.48 (m, 4H), 2.47–2.12 (m, 5H). ^{13}C NMR (126 MHz, CDCl3) δ 157.41, 157.37, 149.71, 146.60, 139.51, 138.20, 137.70, 137.42, 137.32, 133.38, 133.00, 132.69, 130.70, 130.1, 128.95, 126.01, 123.01, 122.14, 59.62, 54.56, 54.45, 31.76, 31.42, 30.64, 30.39, 24.10. HRMS: $C_{26}H_{27}ClN_3$ (M + H)⁺ calcd: 416.1894, found: 416.1886. LC–MS: t_R = 3.0 min, purity >98% (254 nm), m/z: 416.2 (M + H)⁺.

8-Chloro-11-(1-(pyridin-3-ylmethyl)piperidin-4-ylidene)-6,11-dihydro-5H-benzo[5,6]cyclohepta[1,2-b]pyridine (6)

A mixture of desloratadine (500 mg, 1.61 mmol), 3-(bromomethyl)-pyridine hydrobromide (529 mg, 2.09 mmol), and K_2CO_3 (579 mg, 4.19 mmol) in DMF (10 mL) was stirred at room temperature for 18 h. The mixture was diluted with EtOAc, washed with water (2×) and brine, dried over Na_2SO_4, filtered, and concentrated under vacuum. The crude mixture was purified by reverse-phase column chromatography (H_2O/MeCN/HCOOH) to yield the title compound as a pink foam (430 mg, 66% yield). ^1H NMR (500 MHz, CDCl$_3$) δ 8.54–8.43 (m, 2H), 8.37 (d, J = 4.6 Hz, 1H), 7.67 (d, J = 7.7 Hz, 1H), 7.41 (d, J = 7.6 Hz, 1H), 7.25– 7.20 (m, 1H), 7.15–7.02 (m, 4H), 3.49 (s, 2H), 3.43–3.27 (m, 2H), 2.88–2.64 (m, 4H), 2.55–2.46 (m, 1H), 2.45–2.25 (m, 3H), 2.21– 2.02 (m, 2H). ^{13}C NMR (126 MHz, CDCl$_3$) δ 157.44, 150.40, 148.60, 146.63, 139.51, 138.60, 137.73, 137.34, 136.81, 133.63, 133.40, 132.79, 132.63, 130.81, 128.96, 126.01, 123.37, 122.15, 60.04, 54.73, 54.66, 31.80, 31.42, 30.89, 30.65. HRMS: $C_{25}H_{25}ClN_3$ (M + H)$^+$ calcd: 402.1737, found: 402.1733. LC–MS: t_R = 3.0 min, purity >99% (254 nm), m/z: 402.1 (M + H)$^+$.

8-Chloro-11-(1-(pyridin-4-ylmethyl)piperidin-4-ylidene)-6,11-dihydro-5H-benzo[5,6]cyclohepta[1,2-b]pyridine (7)

A mixture of desloratadine (500 mg, 1.61 mmol), 4-(bromomethyl)-pyridine hydrobromide (529 mg, 2.09 mmol), and K_2CO_3 (579 mg, 4.19 mmol) in DMF (10 mL) was stirred at room temperature for 18 h. The mixture was diluted with EtOAc, washed with water (2×) and brine, dried over Na2SO4, filtered, and concentrated under vacuum. The crude mixture was purified by reverse-phase column chromatography (H_2O/MeCN/HCOOH) to yield the title compound as a pink foam (229 mg, 36% yield). ^1H NMR (500 MHz, CDCl$_3$) δ 8.49 (d, J = 5.6 Hz, 2H), 8.35 (d, J = 4.6 Hz, 1H), 7.39 (d, J = 7.6 Hz, 1H), 7.24 (d, J = 5.4 Hz, 2H), 7.16–7.00 (m, 4H), 3.46 (s, 2H), 3.42–3.24 (m, 2H), 2.85–2.60 (m, 4H), 2.57–2.23 (m, 4H), 2.20–2.04 (m, 2H). ^{13}C NMR (126 MHz, CDCl$_3$) δ 157.38, 149.64, 147.76, 146.58, 139.50, 138.46, 137.69, 137.38, 133.41, 132.82, 132.63, 130.78, 128.96, 126.00, 123.89, 122.18, 61.56, 54.85, 54.82, 31.77, 31.40, 30.89, 30.67. HRMS: $C_{25}H_{25}ClN_3$ (M + H)$^+$ calcd: 402.1737, found: 402.1741. LC–MS: t_R = 3.0 min, purity >99% (254 nm), m/z: 402.1 (M + H)$^+$.

8-Chloro-11-(1-(pyridin-2-ylmethyl)piperidin-4-ylidene)-6,11-dihydro-5H-benzo[5,6]cyclohepta[1,2-b]pyridine (8)

A mixture of desloratadine (500 mg, 1.61 mmol), 2-(bromomethyl)-pyridine hydrobromide (529 mg, 2.09 mmol), and K_2CO_3 (579 mg, 4.19 mmol) in DMF (10 mL) was stirred at room temperature for 18 h. The mixture was diluted with EtOAc, washed with water (2×) and brine, dried over Na_2SO_4, filtered, and concentrated under vacuum. The crude mixture was purified by reverse-phase column chromatography (H_2O/MeCN/HCOOH) to yield the title compound as a pink foam (399 mg, 62% yield). ^{1}H NMR (500 MHz, $CDCl_3$) δ 8.52 (d, J = 4.5 Hz, 1H), 8.36 (d, J = 4.6 Hz, 1H), 7.62 (t, J = 7.6 Hz, 1H), 7.40 (d, J = 7.2 Hz, 2H), 7.18–6.98 (m, 5H), 3.63 (s, 2H), 3.45–3.27 (m, 2H), 2.87–2.68 (m, 4H), 2.59–2.40 (m, 2H), 2.40–2.27 (m, 2H), 2.26–2.10 (m, 2H). ^{13}C NMR (126 MHz, $CDCl_3$) δ 158.54, 157.56, 149.24, 146.60, 139.52, 138.86, 137.75, 137.28, 136.44, 133.43, 132.62, 132.57, 130.87, 128.96, 125.97, 123.22, 122.11, 122.06, 64.46, 55.07, 55.05, 31.82, 31.40, 30.94, 30.71. HRMS: $C_{25}H_{25}ClN_3$ (M + H)$^+$ calcd: 402.1737, found: 402.1738. LC−MS: t_R = 3.1 min, purity >99% (254 nm), m/z: 402.1 (M + H)$^+$.

8-Chloro-11-(1-(pyrimidin-2-ylmethyl)piperidin-4-ylidene)-6,11-dihydro-5H-benzo[5,6]cyclohepta[1,2-b]pyridine (9)

A mixture of pyrimidine-2-carbaldehyde (91 mg, 0.84 mmol), desloratadine (218 mg, 0.7 mmol), and NaBH(OAc)$_3$ (237 mg, 1.12 mmol) in DCE (10 mL) was stirred at room temperature for 12 h. The resulting solution was diluted with water and extracted with DCM. The organic phase was washed with satd. aq $NaHCO_3$. The organic layer was dried over Na_2SO_4, filtered, and concentrated under vacuum. The crude mixture was purified by column chromatography (EtOAc/MeOH/triethylamine (TEA) = 94:4:2, v/v/v) to yield the title compound as a pink foam (240 mg, 85% yield). ^{1}H NMR (500 MHz, $CDCl_3$) δ 8.71 (d, J = 4.9 Hz, 2H), 8.37 (dd, J = 4.7, 1.4 Hz, 1H), 7.41 (dd, J = 7.7, 1.4 Hz, 1H), 7.17 (t, J = 4.9 Hz,1H), 7.14–7.02 (m, 4H), 3.86–3.74 (m, 2H), 3.44–3.30 (m, 2H), 2.89–2.71 (m, 4H), 2.65–2.47 (m, 2H), 2.42–2.25 (m, 4H). ^{13}C NMR (126 MHz, $CDCl_3$) δ 167.63, 157.64, 157.20, 146.59, 139.48, 138.78, 137.73, 137.20, 133.43, 132.61, 132.59, 130.89, 128.96, 125.97, 122.07, 119.32, 65.09, 55.25, 55.21, 31.85, 31.40, 30.75, 30.50. HRMS: $C_{24}H_{24}ClN_4$ (M + H)$^+$ calcd: 403.1684, found: 403.1680. LC−MS: t_R = 2.9 min, purity >99% (254 nm), m/z: 403.2 (M + H)$^+$.

8-Chloro-11-(1-(pyrimidin-4-ylmethyl)piperidin-4-ylidene)-6,11-dihydro-5H-benzo[5,6]cyclohepta[1,2-b]pyridine (10)

A mixture of pyrimidine-4-carbaldehyde (91 mg, 0.84 mmol), desloratadine (218 mg, 0.7 mmol), and $NaBH(OAc)_3$ (237 mg, 1.12 mmol) in DCE (10 mL) was stirred at room temperature for 12 h. The resulting solution was diluted with water and extracted with DCM. The organic phase was washed with satd. aq $NaHCO_3$, dried over Na_2SO_4, filtered, and concentrated under vacuum. The crude mixture was purified by column chromatography (EtOAc/MeOH/TEA = 94:4:2, v/v/v) to yield the title compound as a pink foam (248 mg, 88% yield). ^1H NMR (500 MHz, $CDCl_3$) δ 9.11 (s, 1H), 8.67 (d, J = 5.2 Hz, 1H), 8.38 (dd, J = 4.7, 1.2 Hz, 1H), 7.53 (d, J = 5.0 Hz, 1H), 7.42 (dd, J = 8.8, 1.2 Hz, 2H), 7.17–7.02 (m, 4H), 3.62 (s, 2H), 3.44–3.31 (m, 2H), 2.87–2.71 (m, 4H), 2.61–2.52 (m, 1H), 2.51–2.42 (m, 1H), 2.41–2.31 (m, 2H), 2.30–2.19 (m, 2H). ^{13}C NMR (126 MHz, $CDCl_3$) δ 167.86, 158.57, 157.38, 157.09, 146.59, 139.52, 138.13, 137.71, 137.37, 133.42, 133.05, 132.71, 130.74, 128.96, 126.03, 122.17, 120.13, 63.36, 55.10, 31.79, 31.44, 30.92, 30.70, one signal overlapping or not visible. HRMS: $C_{24}H_{24}ClN_4$ (M + H)$^+$ calcd: 403.1684, found: 403.1681. LC–MS: t_R = 2.9 min, purity >99% (254 nm), m/z: 403.2 (M + H)$^+$.

8-Chloro-11-(1-(3-methylbenzyl)piperidin-4-ylidene)-6,11-dihydro-5H-benzo[5,6]cyclohepta[1,2-b]pyridine (11)

Desloratadine (500 mg, 1.61 mmol) was added to 3-methylbenzyl bromide (387 mg, 2.09 mmol) and TEA (326 mg, 3.22 mmol) in DCM (10 mL). The resulting mixture was stirred at room temperature for 18 h. The solution was then diluted with DCM, washed with a 5% $NaHCO_3$ solution, then with H_2O, dried over Na_2SO_4, filtered, and concentrated under vacuum. The crude mixture was purified by reverse-phase column chromatography (H_2O/MeCN/HCOOH). The product fraction was evaporated, extracted with DCM/satd. aq Na_2CO_3 solution, dried (MgSO$_4$), and concentrated to yield the title compound as a pink foam (432 mg, 65% yield). ^1H NMR (500 MHz, $CDCl_3$) δ 8.39 (dd, J = 4.8, 1.5 Hz, 1H), 7.41 (d, J = 7.7 Hz, 1H), 7.22–6.99 (m, 8H), 3.53–3.28 (m, 4H), 2.90–2.68 (m, 4H), 2.58–2.25 (m, 7H), 2.21–2.04 (m, 2H). ^{13}C NMR (126 MHz, $CDCl_3$) δ 157.69, 146.64, 139.52, 139.18, 138.09, 137.84, 137.78, 137.23, 133.42, 132.57, 132.49, 130.92, 129.97, 128.97, 128.06, 127.79, 126.33, 125.99, 122.08, 62.99, 54.89, 54.85, 31.87, 31.44, 30.99, 30.75, 21.46. HRMS: $C_{27}H_{28}ClN_2$ (M + H)$^+$ calcd: 415.1941, found: 415.1938. LC–MS: t_R = 3.6 min, purity >99% (254 nm), m/z: 415.2 (M + H)$^+$.

11-(1-Benzylpiperidin-4-ylidene)-8-chloro-6,11-dihydro-5Hbenzo[5,6]cyclohepta[1,2-b]pyridine (12)

Desloratadine (500 mg, 1.61 mmol) was added to benzyl bromide (358 mg, 2.09 mmol) and TEA (326 mg, 3.22 mmol) in DCM (10 mL). The resulting mixture was stirred at room temperature for 18 h. The solution was then diluted with DCM and H_2O and extraction was performed. The organic layer was dried over Na_2SO_4 and filtered. The crude mixture was purified by reverse-phase column chromatography (H_2O/MeCN/HCOOH). The product fraction was evaporated, extracted with DCM/satd. aq Na_2CO_3 solution, dried (MgSO$_4$), and concentrated to yield the title compound as a pink foam (484 mg, 75% yield). ^{1}H NMR (500 MHz, CDCl$_3$) δ 8.38 (dd, J = 4.8, 1.2 Hz, 1H), 7.42 (dd, J = 7.3, 1.1 Hz, 1H), 7.33–7.20 (m, 5H), 7.17–7.00 (m, 4H), 3.51 (s, 2H), 3.45–3.28 (m, 2H), 2.87–2.69 (m, 4H), 2.58–2.26 (m, 4H), 2.23–2.07 (m, 2H). ^{13}C NMR (126 MHz, CDCl$_3$) δ 157.64, 146.62, 139.51, 139.04, 138.09, 137.81, 137.26, 133.42, 132.58, 132.54, 130.89, 129.23, 128.96, 128.21, 127.06, 125.99, 122.10, 62.91, 54.79, 54.74, 31.85, 31.42, 30.94, 30.71. HRMS: $C_{26}H_{26}ClN_2$ (M + H)$^+$ calcd: 401.1785, found: 401.1779. LC−MS: t_R = 3.4 min, purity >99% (254 nm), m/z: 401.1 (M + H)$^+$.

8-Chloro-11-(1-(cyclohexylmethyl)piperidin-4-ylidene)-6,11-dihydro-5H-benzo[5,6]cyclohepta[1,2-b]pyridine (13)

A mixture of cyclohexanecarbaldehyde (95 mg, 0.84 mmol), desloratadine (218 mg, 0.70 mmol), and NaBH(OAc)$_3$ (238 mg, 1.12 mmol) in DCE (10 mL) was stirred at room temperature for 12 h. The resulting solution was diluted with water and extracted with DCM. The organic phase was washed with satd. aq NaHCO$_3$ solution. The organic layer was dried over Na_2SO_4, filtered, and concentrated under vacuum. The crude mixture was purified by column chromatography (cyclohexane/EtOAc/TEA = 40/58/2, v/v/v) to yield the title compound as a pink foam (180 mg, 63% yield). ^{1}H NMR (500 MHz, CDCl$_3$) δ 8.39 (d, J = 4.6 Hz, 1H), 7.42 (d, J = 7.6 Hz, 1H), 7.16–7.09 (m, 3H), 7.07 (dd, J = 7.7, 4.8 Hz, 1H), 3.46–3.29 (m, 2H), 2.86–2.74 (m, 2H), 2.74–2.63 (m, 2H), 2.55–2.46 (m, 1H), 2.44–2.25 (m, 3H), 2.14–1.97 (m, 4H), 1.80–1.60 (m, 5H), 1.50–1.38 (m, 1H), 1.26–1.07 (m, 3H), 0.91–0.78 (m, 2H). ^{13}C NMR (126 MHz, CDCl$_3$) δ 157.77, 146.74, 139.66, 137.96, 137.35, 133.54, 132.70, 132.55, 130.96, 129.07, 126.10, 122.18, 65.45, 55.51, 55.41, 35.32, 32.16, 32.13, 31.94, 31.55, 30.87, 30.62, 26.82, 26.25, one aromatic signal overlapping or not visible. HRMS: $C_{26}H_{32}ClN_2$ (M + H)$^+$ calcd: 407.2249, found: 407.2231. LC−MS: t_R = 3.6 min, purity >99% (254 nm), m/z: 407.2 (M + H)$^+$.

8-Chloro-11-(1-(cyclopentylmethyl)piperidin-4-ylidene)-6,11-dihydro-5H-benzo[5,6]cyclohepta[1,2-b]pyridine (14)

A mixture of cyclopentanecarbaldehyde (83 mg, 0.84 mmol), desloratadine (218 mg, 0.70 mmol), and NaBH(OAc)$_3$ (238 mg, 1.12 mmol) in DCE (10 mL) was stirred at room temperature for 12 h. The resulting solution was diluted with water and extracted with DCM. The organic phase was washed with satd. aq NaHCO$_3$ solution. The organic layer was dried over Na$_2$SO$_4$, filtered, and concentrated under vacuum. The crude mixture was purified by column chromatography (cyclohexane/EtOAc/TEA = 40/58/2, v/v/v) to yield the title compound as a pink foam (162 mg, 59% yield). ^{1}H NMR (500 MHz, CDCl$_3$) δ 8.39 (d, J = 4.6 Hz, 1H), 7.41 (d, J = 7.7 Hz, 1H), 7.15−7.08 (m, 3H), 7.06 (dd, J = 7.6, 4.9 Hz, 1H), 3.45−3.29 (m, 2H), 2.86−2.69 (m, 4H), 2.55−2.45 (m, 1H), 2.44− 2.27 (m, 3H), 2.25 (d, J = 7.2 Hz, 2H), 2.16−1.96 (m, 3H), 1.77−1.67 (m, 2H), 1.61−1.43 (m, 4H), 1.22−1.12 (m, 2H). ^{13}C NMR (126 MHz, CDCl$_3$) δ 157.87, 146.72, 139.60, 137.98, 137.26, 133.50, 132.63, 132.30, 131.03, 129.03, 126.06, 122.11, 64.50, 55.36, 55.30, 37.60, 31.96, 31.77, 31.52, 31.09, 30.85, 25.30, one aromatic signal overlapping or not visible. HRMS: C$_{25}$H$_{30}$ClN$_2$ (M + H)$^+$ calcd: 393.2092, found: 393.2091. LC−MS: t_R = 3.2 min, purity >98% (254 nm), m/z: 393.2 (M + H)$^+$.

8-Chloro-11-(1-(2-ethylbutyl)piperidin-4-ylidene)-6,11-dihydro-5H-benzo[5,6]cyclohepta[1,2-b]pyridine (15)

A mixture of 2-ethylbutanal (85 mg, 0.84 mmol), desloratadine (218 mg, 0.70 mmol), and NaBH(OAc)$_3$ (238 mg, 1.12 mmol) in DCE (10 mL) was stirred at room temperature for 12 h. The resulting solution was diluted with water and extracted with DCM. The organic phase was washed with satd. aq NaHCO$_3$ solution. The organic layer was dried over Na$_2$SO$_4$, filtered, and concentrated under vacuum. The crude mixture was purified by column chromatography (cyclohexane/EtOAc/TEA = 40/58/2, v/v/v) to yield the title compound as a pink foam (186 mg, 67% yield). ^{1}H NMR (500 MHz, CDCl$_3$) δ 8.39 (dd, J = 4.9, 1.7 Hz, 1H), 7.42 (dd, J = 7.7, 1.6 Hz, 1H), 7.16−7.11 (m, 3H), 7.08 (dd, J = 7.7, 4.8 Hz, 1H), 3.46−3.29 (m, 2H), 2.88−2.69 (m, 4H), 2.61−2.03 (br m, 8H), 1.49−1.24 (m, 5H), 0.84 (t, J = 7.4 Hz, 6H). ^{13}C NMR (126 MHz, CDCl$_3$) δ 157.95, 146.74, 139.83, 139.63, 138.06, 137.25, 133.51, 132.64, 132.27, 131.04, 129.04, 126.06, 122.10, 62.44, 55.60, 55.52, 38.06, 31.99, 31.56, 31.15, 30.92, 24.33, 10.99. HRMS: C$_{25}$H$_{32}$ClN$_2$ (M + H)$^+$ calcd: 395.2249, found: 395.2244. LC−MS: t_R = 3.3 min, purity >98% (254 nm), m/z: 395.2 (M + H)$^+$.

8-Chloro-11-(1-(cyclobutylmethyl)piperidin-4-ylidene)-6,11-dihydro-5H-benzo[5,6]cyclohepta[1,2-b]pyridine (16)

A mixture of (bromomethyl)cyclobutane (208 mg, 1.40 mmol), desloratadine (218 mg, 0.70 mmol), and 60% NaH dispersion (41.6 mg, 1.05 mmol) in DMF (10 mL) was stirred at room temperature for 10 h. The resulting solution was diluted with water and extracted with DCM. The organic phase was washed with satd. aq NaHCO$_3$ solution. The organic layer was dried over Na$_2$SO$_4$, filtered, and concentrated under vacuum. The crude mixture was purified by column chromatography (cyclohexane/EtOAc/TEA = 40/58/2, v/v/v) to yield the title compound as a pink foam (150 mg, 56% yield). ^{1}H NMR (500 MHz, CDCl$_3$) δ 8.38 (d, J = 4.9, 1.4 Hz, 1H), 7.41 (d, J = 7.6 Hz, 1H), 7.15–7.08 (m, 3H), 7.06 (dd, J = 7.7, 4.8 Hz, 1H), 3.44–3.30 (m, 2H), 2.85–2.73 (m, 2H), 2.74–2.66 (m, 2H), 2.56–2.44 (m, 2H), 2.43–2.25 (m, 5H), 2.12–1.96 (m, 4H), 1.92– 1.80 (m, 1H), 1.79–1.70 (m, 1H), 1.69–1.58 (m, 2H). ^{13}C NMR (126 MHz, CDCl$_3$) δ 157.78, 146.73, 139.60, 139.24, 137.93, 137.29, 133.49, 132.66, 132.46, 130.99, 129.03, 126.07, 122.13, 65.28, 55.13, 55.07, 34.36, 31.94, 31.53, 31.05, 30.80, 28.32, 18.93. HRMS: C$_{24}$H$_{28}$ClN$_2$ (M + H)$^+$ calcd: 379.1936, found: 379.1923. LC−MS: t_R = 3.1 min, purity >96% (254 nm), m/z: 379.2 (M + H)$^+$.

8-Chloro-11-(1-(cyclopropylmethyl)piperidin-4-ylidene)-6,11-dihydro-5H-benzo[5,6]cyclohepta[1,2-b]pyridine (17)

A mixture of cyclopropanecarboxaldehyde (59 mg, 0.84 mmol), desloratadine (218 mg, 0.70 mmol), and NaBH(OAc)$_3$ (238 mg, 1.12 mmol) in DCE (10 mL) was stirred at room temperature for 12 h. The resulting solution was diluted with water and extracted with DCM. The organic phase was washed with satd. aq NaHCO$_3$ solution. The organic layer was dried over Na$_2$SO$_4$, filtered, and concentrated under vacuum. The crude mixture was purified by column chromatography (cyclohexane/EtOAc/TEA = 40/58/2, v/v/v) to yield the title compound as a pink foam (132 mg, 52% yield). ^{1}H NMR (500 MHz, CDCl$_3$) δ 8.39 (dd, J = 4.8, 1.6 Hz, 1H), 7.42 (dd, J = 7.7, 1.6 Hz, 1H), 7.16–7.09 (m, 3H), 7.07 (dd, J = 7.6, 4.7 Hz, 1H), 3.44–3.30 (m, 2H), 2.93–2.73 (m, 4H), 2.59–2.50 (m, 1H), 2.48–2.31 (m, 3H), 2.24 (d, J = 6.5 Hz, 2H), 2.21–2.12 (m, 2H), 0.92–0.79 (m, 1H), 0.53–0.43 (m, 2H), 0.06 (app q, 2H). ^{13}C NMR (126 MHz, CDCl$_3$) δ 157.78, 146.76, 139.61, 139.24, 137.94, 137.32, 133.51, 132.70, 132.58, 131.01, 129.05, 126.10, 122.17, 63.74, 55.10, 55.05, 31.96, 31.55, 31.05, 30.80, 8.52, 4.11, 4.09. HRMS: C$_{23}$H$_{26}$ClN$_2$ (M + H)$^+$ calcd: 365.1779, found: 365.1773. LC−MS: t_R = 2.9 min, purity >99% (254 nm), m/z: 365.1 (M + H)$^+$.

8-Chloro-11-(1-cyclohexylpiperidin-4-ylidene)-6,11-dihydro-5Hbenzo[5,6]cyclohepta[1,2-b]pyridine (18)

A mixture of cyclohexanone (82 mg, 0.84 mmol), desloratadine (218 mg, 0.70 mmol), and NaBH(OAc)$_3$ (238 mg, 1.12 mmol) in DCE (10 mL) was stirred at room temperature for 12 h. The resulting solution was diluted with water and extracted with DCM. The organic phase was washed with satd. aq NaHCO$_3$ solution. The organic layer was dried over Na$_2$SO$_4$, filtered, and concentrated under vacuum. The crude mixture was purified by column chromatography (cyclohexane/EtOAc/TEA = 40/58/2, v/v/v) to yield the title compound as a pink foam (192 mg, 70% yield). ^{1}H NMR (500 MHz, CDCl$_3$) δ 8.39 (dd, J = 4.8, 1.5 Hz, 1H), 7.42 (d, J = 7.6, 1H), 7.16−7.09 (m, 3H), 7.06 (dd, J = 7.7, 4.8 Hz, 1H), 3.44−3.30 (m, 2H), 2.86−2.71 (m, 4H), 2.53−2.44 (m, 1H), 2.44− 2.23 (m, 6H), 1.88−1.69 (m, 4H), 1.60 (app d, J = 13.6 Hz, 1H), 1.27−1.12 (m, 4H), 1.12−1.00 (m, 1H). ^{13}C NMR (126 MHz, CDCl$_3$) δ 157.92, 146.74, 139.86, 139.60, 137.96, 137.25, 133.52, 132.64, 132.24, 131.10, 129.05, 126.06, 122.12, 63.76, 50.71, 50.59, 32.00, 31.64, 31.54, 31.38, 29.05, 28.91, 26.47, 26.17. HRMS: C$_{25}$H$_{30}$ClN$_2$ (M + H)$^+$ calcd: 393.2092, found: 393.2083. LC−MS: t_R = 3.1 min, purity >99% (254 nm), m/z: 393.2 (M + H)$^+$.

8-Chloro-11-(1-cyclopentylpiperidin-4-ylidene)-6,11-dihydro-5Hbenzo[5,6]cyclohepta[1,2-b]pyridine (19)

A mixture of cyclopentanone (70 mg, 0.84 mmol), desloratadine (218 mg, 0.70 mmol), and NaBH(OAc)$_3$ (238 mg, 1.12 mmol) in DCE (10 mL) was stirred at room temperature for 12 h. The resulting solution was diluted with water and extracted with DCM. The organic phase was washed with satd. aq NaHCO$_3$ solution. The organic layer was dried over Na$_2$SO$_4$, filtered, and concentrated under vacuum. The crude mixture was purified by column chromatography (cyclohexane/EtOAc/TEA = 40/58/2, v/v/v) to yield the title compound as a pink foam (189 mg, 71% yield). ^{1}H NMR (500 MHz, CDCl$_3$) δ 8.38 (d, J = 4.8, 1H), 7.41 (d, J = 7.6 Hz, 1H), 7.15−7.08 (m, 3H), 7.06 (dd, J = 7.7, 4.8 Hz, 1H), 3.44−3.29 (m, 2H), 2.87−2.72 (m, 4H), 2.57−2.39 (m, 3H), 2.38− 2.29 (m, 2H), 2.19−2.07 (m, 2H), 1.87−1.74 (m, 2H), 1.70−1.59 (m, 2H), 1.55−1.45 (m, 2H), 1.45−1.33 (m, 2H). ^{13}C NMR (126 MHz, CDCl$_3$) δ 157.81, 146.73, 139.59, 139.45, 137.87, 137.26, 133.52, 132.66, 132.27, 131.05, 129.04, 126.07, 122.13, 67.41, 54.13, 54.10, 31.98, 31.53, 31.13, 30.85, 30.70, 24.34. HRMS: C$_{24}$H$_{28}$ClN$_2$ (M + H)$^+$ calcd: 379.1936, found: 379.1921. LC−MS: t_R = 3.0 min, purity >99% (254 nm), m/z: 379.1 (M + H)$^+$.

8-Chloro-11-(1-cyclobutylpiperidin-4-ylidene)-6,11-dihydro-5Hbenzo[5,6]cyclohepta[1,2-b]pyridine (20)

A mixture of cyclobutanone (59 mg, 0.84 mmol), desloratadine (218 mg, 0.70 mmol), and NaBH(OAc)$_3$ (238 mg, 1.12 mmol) in DCE (10 mL) was stirred at room temperature for 12 h. The resulting solution was diluted with water and extracted with DCM. The organic phase was washed with satd. aq NaHCO$_3$ solution. The organic layer was dried over Na$_2$SO$_4$, filtered, and concentrated under vacuum. The crude mixture was purified by column chromatography (cyclohexane/EtOAc/TEA = 40/58/2, v/v/v) to yield the title compound as a pink foam (145 mg, 57% yield). ^{1}H NMR (500 MHz, CDCl$_3$) δ 8.39 (d, J = 4.6 Hz, 1H), 7.42 (d, J = 7.6 Hz, 1H), 7.15–7.09 (m, 3H), 7.09–7.05 (m, 1H), 3.45–3.30 (m, 2H), 2.87–2.74 (m, 2H), 2.74–2.60 (m, 3H), 2.55–2.46 (m, 1H), 2.46–2.28 (m, 3H), 2.05–1.86 (m, 6H), 1.74–1.57 (m, 2H). ^{13}C NMR (126 MHz, CDCl$_3$) δ 157.78, 146.77, 139.60, 139.01, 137.89, 137.33, 133.53, 132.78, 132.74, 130.99, 129.09, 126.12, 122.21, 60.32, 51.24, 51.23, 31.97, 31.53, 30.65, 30.38, 27.42, 14.35. HRMS: C$_{23}$H$_{26}$ClN$_2$ (M + H)$^+$ calcd: 365.1779, found: 365.1772. LC–MS: t_R = 2.9 min, purity >99% (254 nm), m/z: 365.2 (M + H)$^+$.

8-Chloro-11-(1-cyclopropylpiperidin-4-ylidene)-6,11-dihydro-5H-benzo[5,6]cyclohepta[1,2-b]pyridine (21)

A mixture of (1-ethoxycyclopropoxy)trimethylsilane (347 mg, 2.00 mmol), desloratadine (622 mg, 2.00 mmol), AcOH (111 mg, 2.00 mmol), and sodium triacetoxyborohydride (604 mg, 3.20 mmol) in DCM (10 mL) was stirred at room temperature for 48 h. The resulting solution was diluted with water and extracted with DCM. The organic phase was washed with satd. aq NaHCO$_3$ solution. The organic layer was dried over Na$_2$SO$_4$, filtered, and concentrated under vacuum. The crude mixture was purified by reverse-phase column chromatography (H$_2$O/MeCN/HCOOH). The product fraction was evaporated, extracted with DCM/satd. aq Na$_2$CO$_3$ solution, dried (MgSO$_4$), and concentrated to yield the title compound as a pink foam (124 mg, 17% yield). ^{1}H NMR (500 MHz, CDCl$_3$) δ 8.39 (dd, J = 4.9, 1.5 Hz, 1H), 7.43 (dd, J = 7.8, 1.6 Hz, 1H), 7.16–7.10 (m, 3H), 7.08 (dd, J = 7.7, 4.7 Hz, 1H), 3.45–3.32 (m, 2H), 2.92–2.74 (m, 4H), 2.50–2.42 (m, 1H), 2.40–2.26 (m, 5H), 1.60–1.50 (m, 1H), 0.47–0.35 (m, 4H). ^{13}C NMR (126 MHz, CDCl$_3$) δ 157.85, 146.75, 139.58, 139.35, 137.95, 137.30, 133.51, 132.69, 132.66, 131.01, 129.08, 126.10, 122.17, 55.16, 38.39, 31.97, 31.52, 31.00, 30.74, 6.09, one aliphatic signal overlapping or not visible. HRMS: C$_{22}$H$_{24}$ClN$_2$ (M + H)$^+$ calcd: 351.1623, found: 351.1610. LC–MS: t_R = 2.9 min, purity >98% (254 nm), m/z: 351.2 (M + H)$^+$.

8-Chloro-11-(1-isopropylpiperidin-4-ylidene)-6,11-dihydro-5Hbenzo[5,6]cyclohepta[1,2-b]pyridine (22)

A mixture of propan-2-one (49 mg, 0.84 mmol), desloratadine (218 mg, 0.70 mmol), and NaBH(OAc)$_3$ (238 mg, 1.12 mmol) in DCE (10 mL) was stirred at room temperature for 12 h. The resulting solution was diluted with water and extracted with DCM. The organic phase was washed with satd. aq NaHCO$_3$ solution. The organic layer was dried over Na$_2$SO$_4$, filtered, and concentrated under vacuum. The crude mixture was purified by column chromatography (cyclohexane/EtOAc/TEA = 40/58/2, v/v/v) to yield the title compound as a pink foam (101 mg, 41% yield). ^{1}H NMR (500 MHz, CDCl$_3$) δ 8.39 (dd, J = 4.8, 1.7 Hz, 1H), 7.43 (dd, J = 7.7, 1.7 Hz, 1H), 7.16−7.10 (m, 3H), 7.08 (dd, J = 7.6, 4.8 Hz, 1H), 3.45−3.32 (m, 2H), 2.87−2.69 (m, 5H), 2.55−2.47 (m, 1H), 2.46−2.22 (m, 5H), 1.04 (d, J = 6.6 Hz, 3H), 1.03 (d, J = 6.6 Hz, 3H). ^{13}C NMR (126 MHz, CDCl$_3$) δ 157.87, 146.76, 139.62, 137.93, 137.30, 133.55, 132.70, 132.43, 131.08, 129.08, 126.10, 122.17, 54.57, 50.34, 50.19, 32.01, 31.56, 31.40, 31.13, 18.60, 18.45, one aromatic signal overlapping or not visible. HRMS: C$_{22}$H$_{26}$ClN$_2$ (M + H)$^+$ calcd: 353.1779, found: 353.1770. LC−MS: t_R = 2.9 min, purity >95% (254 nm), m/z: 353.2 (M + H)$^+$.

8-Chloro-11-(1-ethylpiperidin-4-ylidene)-6,11-dihydro-5Hbenzo[5,6]cyclohepta[1,2-b]pyridine (23)

A mixture of acetaldehyde (37 mg, 0.84 mmol), desloratadine (218 mg, 0.70 mmol), and NaBH(OAc)$_3$ (238 mg, 1.12 mmol) in DCE (10 mL) was stirred at room temperature for 12 h. The resulting solution was diluted with water and extracted with DCM. The organic phase was washed with satd. aq NaHCO$_3$ solution. The organic layer was dried over Na$_2$SO$_4$, filtered, and concentrated under vacuum. The crude mixture was purified by column chromatography (cyclohexane/EtOAc/TEA = 40/58/2, v/v/v) to yield the title compound as a pink foam (65 mg, 27% yield). ^{1}H NMR (300 MHz, CDCl$_3$) δ 8.40 (dd, J = 4.8, 1.6 Hz, 1H), 7.43 (dd, J = 7.7, 1.7 Hz, 1H), 7.19−7.11 (m, 3H), 7.08 (dd, J = 7.7, 4.8 Hz, 1H), 3.48−3.29 (m, 2H), 2.91−2.70 (m, 4H), 2.62−2.50 (m, 1H), 2.50−2.29 (m, 5H), 2.24−2.05 (m, 2H), 1.09 (t, J = 7.2 Hz, 3H). ^{13}C NMR (126 MHz, CDCl$_3$) δ 157.76, 146.78, 139.64, 139.14, 137.93, 137.36, 133.54, 132.75, 132.66, 131.01, 129.08, 126.13, 122.21, 54.65, 54.59, 52.31, 31.97, 31.57, 31.05, 30.79, 12.23. HRMS: C$_{21}$H$_{24}$ClN$_2$ (M + H)$^+$ calcd: 339.1623, found: 339.1608. LC−MS: t_R = 2.7 min, purity >97% (254 nm), m/z: 339.1 (M + H)$^+$.

8-Chloro-11-(1-methylpiperidin-4-ylidene)-6,11-dihydro-5Hbenzo[5,6]cyclohepta[1,2-b]pyridine fumarate (24).

To a solution of desloratadine (5.00 g, 16.1 mmol) in DCM (150 mL) were added MeOH (75 mL), aq formaldehyde solution (ca. 13.4 M, 2.40 mL, 32.2 mmol) and AcOH (1.29 mL, 22.5 mmol), and the resulting mixture was stirred at room temperature for 15 min. Subsequently, NaBH(OAc)$_3$ (5.11 g, 24.1 mmol) was added and the resulting mixture was stirred for 1.5 h at room temperature. The reaction mixture was diluted with 1 M aqueous NaOH (600 mL) and extracted with DCM (2 × 200 mL). The combined organic phases were washed with brine (200 mL), dried over Na$_2$SO$_4$, filtered, and concentrated in vacuo. Purification by flash column chromatography (DCM/MeOH/TEA 190:5:5) gave the free base (3.96 g), which was subsequently converted to the fumaric acid salt to obtain the title compound as a white solid (4.27 g, 60%). ^{1}H NMR (500 MHz, DMSO-d_6) δ 8.36–8.32 (m, 1H), 7.57 (d, J = 7.6 Hz, 1H), 7.31 (d, J = 2.0 Hz, 1H), 7.24–7.17 (m, 2H), 7.09 (d, J = 8.2 Hz, 1H), 6.55 (s, 2H), 3.37–3.24 (m, 2H), 2.89–2.77 (m, 4H), 2.48–2.38 (m, 4H), 2.36 (s, 3H), 2.31–2.22 (m, 2H). ^{13}C NMR (126 MHz, DMSO-d_6) δ 167.0, 156.7, 146.4, 140.2, 137.8, 137.5, 135.3, 134.6, 133.3, 133.2, 131.6, 130.7, 129.0, 125.7, 122.4, 55.1, 44.2, 30.9, 30.6, 29.2, 29.1. HRMS: C$_{20}$H$_{22}$ClN$_2$ (M + H)$^+$ calcd: 325.1466, found 325.1452. LC−MS: t_R = 2.9 min, purity >99% (254 nm), m/z: 324.9 (M + H)$^+$.

(4-Chlorophenyl)(4-iodophenyl)methanol (25)

(4-Chlorophenyl) magnesium bromide (1.0 M in Et$_2$O) (3.23 mL, 3.23 mmol) was added dropwise over 15 min to a stirred solution of 4-iodobenzaldehyde (500 mg, 2.16 mmol) in Et$_2$O (4 mL) at 0 °C under nitrogen. The mixture was allowed to warm to room temperature and stirred for a further 16 h. Satd. aq NH$_4$Cl (1 mL) was added carefully (CAUTION! Exotherm and vigorous bubbling). After bubbling had ceased, the mixture was partitioned between Et$_2$O (10 mL) and satd. aq NH$_4$Cl (5 mL). The organic phase was washed with brine (5 mL), dried (MgSO$_4$), filtered, and evaporated to give the title compound (655 mg, 88%) as a cream solid. ^{1}H NMR (400 MHz, CDCl$_3$) δ 7.59 (d, J = 8.62 Hz, 2H), 7.27– 7.13 (m, 4H), 7.02 (d, J = 8.36 Hz, 2H), 5.68 (s, 1H).

1-Chloro-4-(chloro(4-iodophenyl)methyl)benzene (26)

SOCl$_2$ (0.138 mL, 1.89 mmol) was added dropwise to a stirred solution of 25 (0.65 g, 1.89 mmol) in DCM (9.29 mL) at room temperature. After 20 h, the solvent was evaporated under vacuum to give the product (0.653 g, 1.799 mmol, 95%) as a purple solid. ^{1}H NMR (400 MHz, CDCl$_3$) δ 7.63–7.58 (m, 2H), 7.27–7.16 (m, 4H), 7.07–7.02 (m, 2H), 5.94 (s, 1H).

2-(4-((4-Chlorophenyl)(4-iodophenyl)methyl)piperazin-1-yl)-ethanol (27)

A solution of 2-(piperazin-1-yl)ethanol (0.206 g, 1.58 mmol) in toluene (1 mL) was added to 26 (0.637 g, 1.75 mmol) and the mixture was stirred at 80 °C under nitrogen for 20 h. The mixture was diluted with DCM and purified by ion-exchange chromatography (strong cation exchange) eluting with 1 M NH₃/MeOH. Fractions containing product were purified by flash silica chromatography (elution gradient 0–5% MeOH–NH₃ (3.5 M) in DCM) to afford the product (165 mg, 0.361 mmol, 21%) as a white solid. ^{1}H NMR (600 MHz, DMSO-d_6) 7.65 (d, J = 8.1 Hz, 2H), 7.39 (d, J = 8.4 Hz, 2H), 7.34 (d, J = 8.4 Hz, 2H), 7.20 (d, J = 8.2 Hz, 2H), 4.15 (s, 1H), 4.32 (s, 1H), 3.5–3.42 (m, 2H), 2.48–2.41 (m, 4H), 2.38 (t, J = 6.0 Hz, 2H), 2.33–2.24 (m, 4H). LC–MS (ESI) m/z 457.

(S)-2-(2-(4-((4-Chlorophenyl)(4-iodophenyl)methyl)piperazin-1-yl)ethoxy)acetic acid (28)

KOH (79 mg, 1.41 mmol) was added to a stirred solution of 27 (161 mg, 0.35 mmol) in DMF (641 µL) at 0 °C and the mixture was stirred for 90 min. Sodium 2-chloroacetate (82 mg, 0.70 mmol) was added and the mixture was stirred for 3 h. Water (3 mL) was added and the pH was adjusted to 9–10 with aq HCl (1 M). The mixture was washed with EtOAc (2 × 1 mL) and the pH was adjusted to 4–5 with aq HCl (1 M). The mixture was extracted with DCM (3 × 2 mL). The combined DCM phases were washed with brine (2 mL), dried (MgSO₄), filtered, and evaporated to give, after trituration with Et₂O, racemic product (103 mg, 0.200 mmol, 57%) as an off-white solid. ^{1}H NMR (600 MHz, DMSO-d_6) 7.69–7.65 (m, 2H), 7.44–7.4 (m, 2H), 7.38–7.34 (m, 2H), 7.22 (d, J = 8.4 Hz, 2H), 3.87 (s, 2H), 4.39 (s, 1H), 3.62 (t, J = 5.5 Hz, 2H), 2.85–2.63 (m, 6H), 2.46–2.27 (m, 4H). LC–MS (ESI) m/z 515. The stereoisomers were separated by chromatography using a Chiralpak OD column, 5 µm silica, 20 mm diameter, 250 mm length, eluting with 95/05/0.2/0.1 mixture of MeCN/MeOH/AcOH/TEA to give the desired isomer (first eluted) (S)-2-(2-(4-((4-chlorophenyl)(4-iodophenyl)methyl)piperazin-1-yl)ethoxy)acetic acid (S)-28 (7.8 mg).

(R)-5-(4-((4-Chlorophenyl)([4-3H]phenyl)methyl)piperazin-1-yl)-pentanoic acid ([³H]Levocetirizine)

Precursor (S)-28 (0.8 mg, 1.55 µmol), Pd (10% on carbon, 0.5 mg, 0.47 µmol), and Et₃N (5 µL, 0.04 mmol) were mixed in EtOH (200 µL). The flask was fitted to the tritium manifold. The mixture was freeze–pump–thaw degassed and was then stirred under tritium gas (63.5 GBq) at 162 mbar for 2.5 h. The reaction mixture was filtered through a poly(tetrafluoroethylene) filter (Whatman 0.45 µm) and washed thoroughly with more EtOH (5 mL). The solution was lyophilized to remove labile

tritium, more EtOH (5 mL) was addeAmyloid Inhbitorsd, and the mixture was again lyophilized. Purification by preparative HPLC (Waters Xbridge C18 column, 5 μm, 4.6 × 150 mm^2) using decreasingly polar mixtures of water (containing 0.1% TFA) and MeCN as eluents followed by further preparative HPLC (Waters XBridge C18 column, 5 μm, 4.6 × 150 mm^2), using decreasingly polar mixtures of water (containing 0.1% ammonia) and MeCN as eluents, afforded [^{3}H]levocetirizine (728 MBq), which was dissolved in EtOH (10 mL) for storage as a colorless solution. Radiochemical purity >98% by HPLC. Chiral purity 93% enantiomeric excess by HPLC (obtained on ethyl ester derivative by standing in ethanol with TFA for 3 days). LC−MS (ESI) m/z 391 [M + H]$^+$. ^{1}H NMR (640 MHz, DMSO-d_6) 7.20 (t, J = 7.8). Specific activity by mass spectrometry: 956 GBq mmol^{-1}.

Author contributions

R. Bosma and Z. Wang have contributed equally to this manuscript.

Acknowledgements

Abbreviations used

DCE, dichloroethane; DCM, dichloromethane; DMF, dimethylformamide; DMSO, dimethylsulfoxide; GPCR, G protein-coupled receptors; H$_1$R, histamine H$_1$ receptor; KRI, kinetic rate index; RecT, recovery time; SKR, structure-kinetics relationship; THF, tetrahydrofuran; TEA, trimethylamine; PSA, polar surface area.

References

1.   Swinney, D. C., Biochemical mechanisms of drug action: what does it take for success? *Nature Reviews Drug Discovery* **2004,** *3*, 801.
2.   Copeland, R. A.; Pompliano, D. L.; Meek, T. D., Drug–target residence time and its implications for lead optimization. *Nature Reviews Drug Discovery* **2006,** *5*, 730.
3.   Swinney, D. C., Biochemical mechanisms of new molecular entities (NMEs) approved by United States FDA during 2001-2004: mechanisms leading to optimal efficacy and safety. *Current Topics in Medicinal Chemistry* **2006,** *6* (5), 461-78.
4.   Swinney, D. C., Applications of binding kinetics to drug discovery. *Pharmaceutical Medicine* **2008,** *22* (1), 23-34.
5.   Copeland, R. A., The drug–target residence time model: a 10-year retrospective. *Nature Reviews Drug Discovery* **2015,** *15*, 87.

6.   Hoffmann, C.; Castro, M.; Rinken, A.; Leurs, R.; Hill, S. J.; Vischer, H. F., Ligand residence time at G-protein–coupled receptors—why we should take our time to study it. *Molecular Pharmacology* **2015,** *88* (3), 552-560.

7.   Guo, D.; Hillger, J. M.; IJzerman, A. P.; Heitman, L. H., Drug-target residence time—a case for G protein-coupled receptors. *Medicinal Research Reviews* **2014,** *34* (4), 856-892.

8.   Lu, H.; Tonge, P. J., Drug-target residence time: critical information for lead optimization. *Current Opinion in Chemical Biology* **2010,** *14* (4), 467-74.

9.   Vauquelin, G.; Charlton, S. J., Long-lasting target binding and rebinding as mechanisms to prolong in vivo drug action. *British Journal of Pharmacology* **2010,** *161* (3), 488-508.

10.   Folmer, R. H. A., Drug target residence time: a misleading concept. *Drug Discovery Today* **2018,** *23* (1), 12-16.

11.   Dahl, G.; Akerud, T., Pharmacokinetics and the drug-target residence time concept. *Drug Discovery Today* **2013,** *18* (15-16), 697-707.

12.   de Witte, W. E. A.; Danhof, M.; van der Graaf, P. H.; de Lange, E. C. M., In vivo target residence time and kinetic selectivity: The association rate constant as determinant. *Trends in Pharmacological Sciences* **2016,** *37* (10), 831-842.

13.   Vauquelin, G., Effects of target binding kinetics on in vivo drug efficacy: koff, kon and rebinding. *British Journal of Pharmacology* **2016,** *173* (15), 2319-2334.

14.   de Witte, W. E. A.; Vauquelin, G.; van der Graaf, P. H.; de Lange, E. C. M., The influence of drug distribution and drug-target binding on target occupancy: The rate-limiting step approximation. *European Journal of Pharmaceutical Sciences* **2017,** *109*, S83-S89.

15.   Louizos, C.; Yáñez, J. A.; Forrest, M. L.; Davies, N. M. Understanding the hysteresis loop conundrum in pharmacokinetic/pharmacodynamic relationships. *Journal of Pharmacy and Pharmaceutical Science* **2014**, *17*, 34–91.

16.   Santos, R.; Ursu, O.; Gaulton, A.; Bento, A. P.; Donadi, R. S.; Bologa, C. G.; Karlsson, A.; Al-Lazikani, B.; Hersey, A.; Oprea, T. I.; Overington, J. P., A comprehensive map of molecular drug targets. *Nature Reviews Drug Discovery* **2017,** *16* (1), 19-34.

17.   Simons, F. E. R.; Simons, K. J., Histamine and H1-antihistamines: Celebrating a century of progress. *Journal of Allergy and Clinical Immunology* **2011,** *128* (6), 1139-1150.e4.

18.   Gillard, M.; Van Der Perren, C.; Moguilevsky, N.; Massingham, R.; Chatelain, P., Binding characteristics of cetirizine and levocetirizine to human H1 histamine receptors: Contribution of Lys191 and Thr194. *Molecular Pharmacology* **2002,** *61* (2), 391-399.

19.   Schoepke, N.; Church, M.; Maurer, M. The inhibition by levocetirizine and fexofenadine of the histamine-induced wheal and flare response in healthy caucasian and Japanese volunteers. *Acta Dermato-Venereologica* **2013**, *93*, 286–293.

20.   Church, M. K., Comparative inhibition by bilastine and cetirizine of histamine-induced wheal and flare responses in humans. *Inflammation Research* **2011,** *60* (12), 1107-1112.

21.   Church, M. K., Efficacy and tolerability of rupatadine at four times the recommended dose against histamine- and platelet-activating factor-induced flare responses and ex vivo platelet aggregation in healthy males. *British Journal of Dermatology* **2010,** *163* (6), 1330-1332.

22.   Sun, C.; Li, Q.; Pan, L.; Liu, B.; Gu, P.; Zhang, J.; Ding, L.; Wu, C., Development of a highly sensitive LC–MS/MS method for simultaneous determination of rupatadine and its two active metabolites in human plasma: Application to a clinical pharmacokinetic study. *Journal of Pharmaceutical and Biomedical Analysis* **2015,** *111*, 163-168.

23.   Solans, A.; Izquierdo, I.; Donado, E.; Antonijoan, R.; Peña, J.; Nadal, T.; Carbó, M.-l.; Merlos, M.; Barbanoj, M., Pharmacokinetic and safety profile of rupatadine when coadministered with azithromycin at steady-state levels: a randomized, open-label, two-way, crossover, Phase I study. *Clinical Therapeutics* **2008,** *30* (9), 1639-1650.

24.   Anthes, J. C.; Gilchrest, H.; Richard, C.; Eckel, S.; Hesk, D.; West, R. E.; Williams, S. M.; Greenfeder, S.; Billah, M.; Kreutner, W.; Egan, R. W., Biochemical characterization of desloratadine, a potent antagonist of the human histamine H1 receptor. *European Journal of Pharmacology* **2002,** *449* (3), 229-237.

25.   Gillard, M.; Chatelain, P., Changes in pH differently affect the binding properties of histamine H1 receptor antagonists. *European Journal of Pharmacology* **2006,** *530* (3), 205-214.

26.   Bosma, R.; Moritani, R.; Leurs, R.; Vischer, H. F., BRET-based β-arrestin2 recruitment to the histamine H1 receptor for investigating antihistamine binding kinetics. *Pharmacological Research* **2016,** *111*, 679-687.

27.   Gillard, M.; Benedetti, M. S.; Chatelain, P.; Baltes, E., Histamine H1 receptor occupancy and pharmacodynamics of second generation H1-antihistamines. *Inflammation Research* **2005,** *54* (9), 367-369.

28.   Carceller, E.; Merlos, M.; Giral, M.; Balsa, D.; Almansa, C.; Bartroli, J.; Garcia-Rafanell, J.; Forn, J., [(3-Pyridylalkyl)piperidylidene]benzocycloheptapyridine derivatives as dual antagonists of PAF and histamine. *Journal of Medicinal Chemistry* **1994,** *37* (17), 2697-2703.

29.   Guo, D.; van Dorp, E. J. H.; Mulder-Krieger, T.; van Veldhoven, J. P. D.; Brussee, J.; IJzerman, A. P.; Heitman, L. H., Dual-point competition association assay:A fast and High-Throughput kinetic screening method for assessing ligand-receptor binding kinetics. *Journal of Biomolecular Screening* **2013,** *18* (3), 309-320.

30.   Motulsky, H. J.; Mahan, L. C., The kinetics of competitive radioligand binding predicted by the law of mass action. *Molecular Pharmacology* **1984,** *25* (1), 1-9.

31.   Bosma, R.; Stoddart, L. A.; Georgi, V.; Bouzo-Lorenzo, M.; Bushby, N.; Inkoom, L.; Waring, M. J.; Briddon, S. J.; Vischer, H. F.; Sheppard, R. J.; Fernández-Montalván, A.; Hill, S. J.; Leurs, R., Probe dependency in the determination of ligand binding kinetics at a prototypical G protein-coupled receptor. *Scientific Reports* **2019,** *9* (1), 7906.

32.   Piwinski, J. J.; Wong, J. K.; Green, M. J.; Ganguly, A. K.; Billah, M. M.; West, R. E.; Kreutner, W., Dual antagonists of platelet-activating factor and histamine. Identification of structural requirements for dual activity of N-acyl-4-(5,6-dihydro-11H-benzo[5,6]cyclohepta[1,2-b]pyridin-11-ylidene)piperidines. *Journal of Medicinal Chemistry* **1991,** *34* (1), 457-461.

33.   Zhong, D.; Blume, H., [HPLC-determination of loratadine and its active metabolite descarboethoxyloratadine in human plasma]. *Pharmazie* **1994,** *49* (10), 736-739.

34.   Tanoli, S. T.; Ramzan, M.; Hassan, A.; Sadiq, A.; Jan, M. S.; Khan, F. A.; Ullah, F.; Ahmad, H.; Bibi, M.; Mahmood, T.; Rashid, U., Design, synthesis and bioevaluation of tricyclic fused ring system as dual binding site acetylcholinesterase inhibitors. *Bioorganic Chemistry* **2019,** *83*, 336-347.

35.   Okada, M.; Hasumi, K.; Nishimoto, T.; Yoshida, M.; Ishitani, K.; Aotsuka, T.; Kanazawa, H. Heterocyclic compound and H1 receptor antagonist. US20130085127, 2013.

36.   Baumann, K.; Flohr, A.; Jolidon, S.; Knust, H.; Luebbers, T.; Nettekoven, M. Indol-amide compounds as Beta-amyloid inhibitors. WO2014060386, 2014.

37.   Zhang, M. Q.; Leurs, R.; Timmerman, H. Histamine H1- Receptor Antagonists. In *Burger's Medicinal Chemistry an Drug Discovery*, 5th ed.; Wolff, M. E., Ed.; Vrije Universiteit: Amsterdam, 1997; Vol. 5.

38.   Saxena, M.; Gaur, S.; Prathipati, P.; Saxena, A. K., Synthesis of some substituted pyrazinopyridoindoles and 3D QSAR studies along with related compounds: Piperazines, piperidines, pyrazinoisoquinolines, and diphenhydramine, and its semi-rigid analogs as antihistamines (H1). *Bioorganic & Medicinal Chemistry* **2006,** *14* (24), 8249-8258.

39.   Tautermann, C. S.; Seeliger, D.; Kriegl, J. M., What can we learn from molecular dynamics simulations for GPCR drug design? *Computational and Structural Biotechnology Journal* **2015,** *13*, 111-121.

40.   Schmidtke, P.; Luque, F. J.; Murray, J. B.; Barril, X., Shielded hydrogen bonds as structural determinants of binding kinetics: Application in drug design. *Journal of the American Chemical Society* **2011,** *133* (46), 18903-18910.

41.   Bortolato, A.; Deflorian, F.; Weiss, D. R.; Mason, J. S., Decoding the role of water dynamics in ligand–protein unbinding: CRF1R as a test case. *Journal of Chemical Information and Modeling* **2015,** *55* (9), 1857-1866.

42.   Kooistra, A. J.; Kuhne, S.; de Esch, I. J. P.; Leurs, R.; de Graaf, C., A structural chemogenomics analysis of aminergic GPCRs: lessons for histamine receptor ligand design. *British Journal of Pharmacology* **2013,** *170* (1), 101-126.

43.   Kuhne, S.; Kooistra, A. J.; Bosma, R.; Bortolato, A.; Wijtmans, M.; Vischer, H. F.; Mason, J. S.; de Graaf, C.; de Esch, I. J. P.; Leurs, R., Identification of ligand binding hot spots of the histamine H1 receptor following structure-based fragment optimization. *Journal of Medicinal Chemistry* **2016,** *59* (19), 9047-9061.

44.   Mocking T., Bosma, R., R. Leurs, H.F. Vischer (2017) Ligand-binding kinetics on histamine receptors, in Histamine receptors as drug targets (Tiligada E and Ennis Meds) 115-155. Histamine receptors as drug targets. Methods in pharmacology and Toxicology. Humana Press, New York

45.   Miller, D. C.; Lunn, G.; Jones, P.; Sabnis, Y.; Davies, N. L.; Driscoll, P., Investigation of the effect of molecular properties on the binding kinetics of a ligand to its biological target. *MedChemComm* **2012,** *3* (4), 449-452.

46.   Tresadern, G.; Bartolome, J. M.; Macdonald, G. J.; Langlois, X., Molecular properties affecting fast dissociation from the D2 receptor. *Bioorganic & Medicinal Chemistry* **2011,** *19* (7), 2231-2241.

47.   Bosma, R.; Witt, G.; Vaas, L. A. I.; Josimovic, I.; Gribbon, P.; Vischer, H. F.; Gul, S.; Leurs, R., The target residence time of antihistamines determines their antagonism of the G protein-coupled histamine H1 receptor. *Frontiers in Pharmacology* **2017,** *8* (667).

48.   Shimamura, T.; Shiroishi, M.; Weyand, S.; Tsujimoto, H.; Winter, G.; Katritch, V.; Abagyan, R.; Cherezov, V.; Liu, W.; Han, G. W.; Kobayashi, T.; Stevens, R. C.; Iwata, S., Structure of the human histamine H1 receptor complex with doxepin. *Nature* **2011,** *475*, 65.

49.   Korb, O.; Stützle, T.; Exner, T. E., Empirical scoring functions for advanced protein–ligand docking with PLANTS. *Journal of Chemical Information and Modeling* **2009,** *49* (1), 84-96.

50.   Church, M. K.; Church, D. S. Pharmacology of antihistamines*. Indian Journal of Dermatology Venereology & Leprology* **2013**, *58*, 219–224.

51.   Slack, R. J.; Russell, L. J.; Hall, D. A.; Luttmann, M. A.; Ford, A. J.; Saunders, K. A.; Hodgson, S. T.; Connor, H. E.; Browning, C.; Clark, K. L., Pharmacological characterization of GSK1004723, a novel, long-acting antagonist at histamine H(1) and H(3) receptors. *British Journal of Pharmacology* **2011,** *164* (6), 1627-1641.

52.   Pan, A. C.; Borhani, D. W.; Dror, R. O.; Shaw, D. E., Molecular determinants of drug–receptor binding kinetics. *Drug Discovery Today* **2013,** *18* (13), 667-673.

53.   Tautermann, C. S.; Kiechle, T.; Seeliger, D.; Diehl, S.; Wex, E.; Banholzer, R.; Gantner, F.; Pieper, M. P.; Casarosa, P., Molecular basis for the long duration of action and kinetic selectivity of tiotropium for the muscarinic M3 receptor. *Journal of Medicinal Chemistry* **2013,** *56* (21), 8746-8756.

54.   Dowling, M. R.; Charlton, S. J., Quantifying the association and dissociation rates of unlabelled antagonists at the muscarinic M3 receptor. *British Journal of Pharmacology* **2006,** *148* (7), 927-937.

55.   Baell, J. B.; Holloway, G. A., New substructure filters for removal of pan assay interference compounds (PAINS) from screening libraries and for their exclusion in bioassays. *Journal of Medicinal Chemistry* **2010,** *53* (7), 2719-2740.

56.   Xie, X.-Q. PAINS-Remover, 2019. www.cbligand.org/PAINS/(accessed Mar 10, 2019).

57.		Yung-Chi, C.; Prusoff, W. H., Relationship between the inhibition constant (KI) and the concentration of inhibitor which causes 50 per cent inhibition (I50) of an enzymatic reaction. *Biochemical Pharmacology* **1973,** *22* (23), 3099-3108.
58.		Marcou, G.; Rognan, D., Optimizing fragment and scaffold docking by use of molecular interaction fingerprints. *Journal of Chemical Information and Modeling* **2007,** *47* (1), 195-207.

Chapter 3

Exploring the effect of cyclization of histamine H_1 receptor antagonists on ligand binding kinetics

Zhiyong Wang, [#] Reggie Bosma, [#] Sebastiaan Kuhne, [#] Jelle van den Bor, Wrej Garabitian, Henry F. Vischer, Maikel Wijtmans, Rob Leurs and Iwan J.P. de Esch*

Amsterdam Institute of Molecular and Life Sciences (AIMMS), Division of Medicinal Chemistry, Faculty of Science, Vrije Universiteit Amsterdam, De Boelelaan 1108, 1081 HZ Amsterdam, The Netherlands.

[#]Equal contributions.

Chapter 3

Abstract

abstract
There is an increasing interest to guide hit optimization by considering the target binding kinetics of ligands. However, compared to conventional structure-activity relationships (SAR), structure-kinetics relationships (SKR) have not been as thoroughly explored, even for well-studied archetypical drug targets such as the histamine H_1 receptor (H_1R), a member of the family A G-protein coupled receptor. In this study it is shown that the binding kinetics of H_1R antagonists at the H_1R is dependent on the cyclicity of both the aromatic head group and the amine moiety of H_1R ligands, the chemotypes that are characteristic for the first-generation H_1R antagonists. Fusing the two aromatic rings of H_1R ligands into one tricyclic aromatic head group prolongs the H_1R RT for benchmark H_1R ligands as well as for tailored synthetic analogues. The effect of constraining the aromatic rings and the basic amines is systematically explored, leading to a coherent series and detailed discussions of structure-kinetics relationships. This study shows that cyclicity has a pronounced effect on the binding kinetics.

Introduction

The drug-target residence time (RT), defined as the reciprocal of the kinetic dissociation rate constant k_{off}, is increasingly acknowledged as an important metric for drug binding and is suggested to be linked to the *in vivo* efficacy of drugs.[1-4] In contrast, SAR-based hit and lead optimization programs often rely on the equilibrium dissociation constant (K_D) as a measure for the drug binding affinity. Often, the target binding kinetics of ligands are ignored, although there is not always a good correlation between the K_D and RT values of ligands for a drug target.[5, 6] There is therefore a growing interest in understanding the molecular features that govern binding kinetics.[7-10] A study that used a Pfizer database containing mostly GPCR and kinase ligands shows that there is a trend between ligand flexibility and RT.[9] For ligands with a similar molecular weight (300–500 Da), it was shown that ligands with ≤5 rotatable bonds more often have a shorter drug-target RT than ligands with more than 5 rotatable bonds.[9] Tresadern *et al.* determined the RT of more than 1800 ligands for their binding to the dopamine D_2 receptor, showing that ligands with a long RT have, on average, a higher number of ring structures.[11] These findings suggest that the number of rotatable bonds[12] and the number of rings can influence the drug-target RT. Other factors have also been correlated to RT, including the role of shielded hydrogen bonds between ligand and protein that result in longer RT.[13]
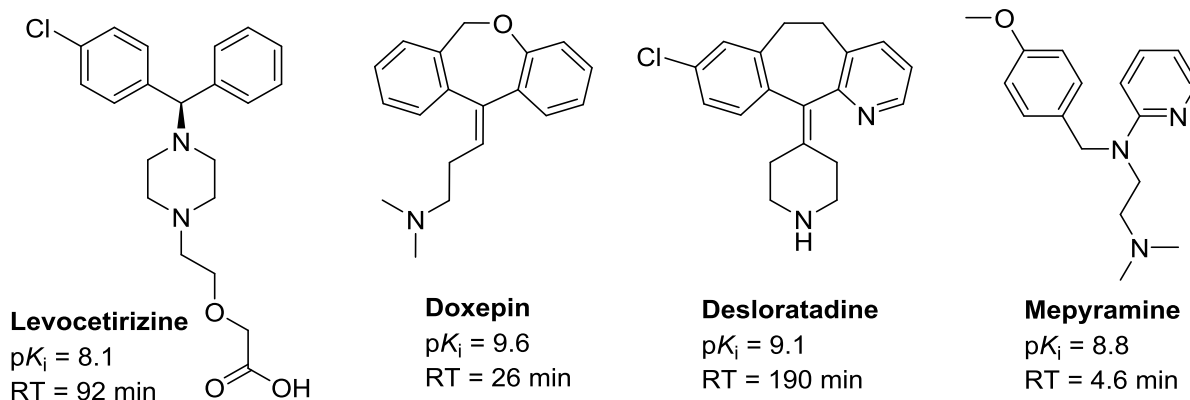
Figure 1. H$_1$R antagonist and their corresponding binding affinities (pK_i) and RT values.[14-18]

For ligands targeting the archetypical and therapeutically relevant H$_1$R, several structural features have so far been shown to play a role in the binding kinetics. For example, the role of a carboxylic acid group that is present in some of the second generation H$_1$R antagonists can slow down binding kinetics tremendously, as was shown amongst others for levocetirizine (Figure 1).[6, 15] Yet, the carboxylic acid moiety is necessarily not the only structural feature that plays an important role in the SKR of H$_1$R ligands. Also, for H$_1$R antagonists that lack this structural motif, major differences in binding kinetics have been observed. For example, it was shown that for some well-known tricyclic antihistamines like doxepin and desloratidine the RT is considerably longer when compared to *e.g.*, mepyramine (Figure 1).[14, 15] The aim of the current study is to explore in a more systematic manner how cyclic systems influence ligand RT at the H$_1$R.

Results

Selection of benchmark H$_1$R ligands

First, a set of known H$_1$R antagonists with similar size and a variety of ring systems was selected as benchmark ligands. The compounds all contain an aromatic head group and a basic amine, structural features that are characteristic for H$_1$R antihistamines.[19] Despite these similarities, *a priori* two groups of ligands can be distinguished, *i.e.*, the non-tricyclic ligands **1-4** and the tricyclic ligands **5-9** (Figure 2). These ligands result from different series and medicinal chemistry programs and have been optimized for affinity on a case to case basis, resulting amongst others in very specific substitution of the aromatic rings (*e.g.*, **2**, **3**, **7** and **8**) and the incorporation of heteroatoms in the aromatic rings (*e.g.*, pyridine rings in **2**, **3**, **6** and **7**).
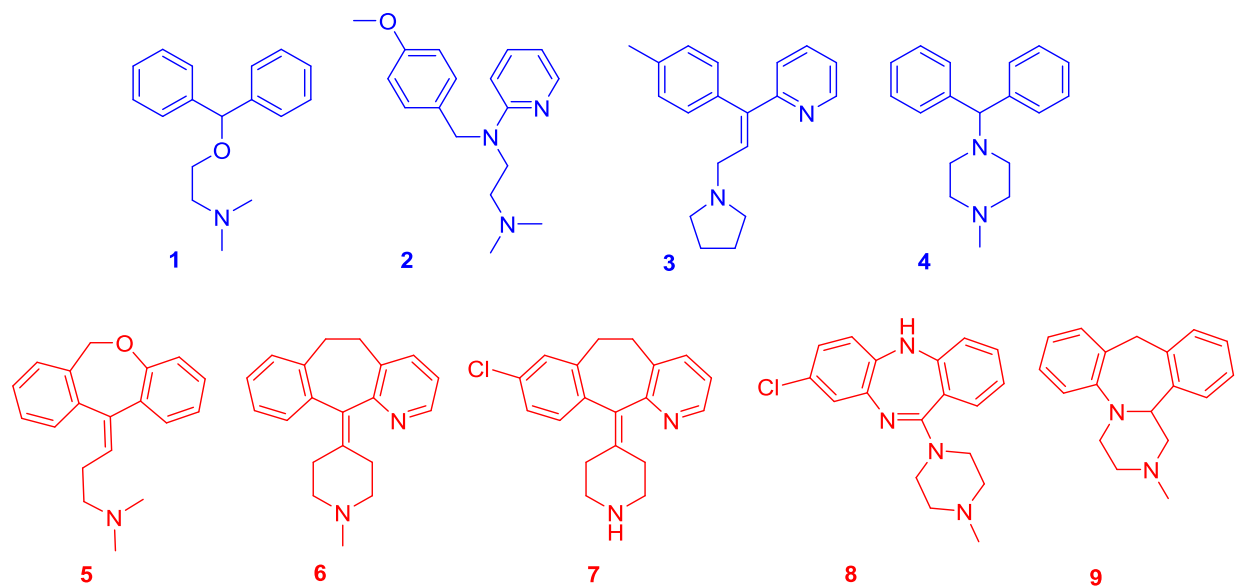
Figure 2. Structures of benchmark H₁R ligands with comparable molecular weight classified as non-tricyclic (1-4, blue) and tricyclic (5-9, red) molecules.

Selection and synthesis of a coherent set of tailored H₁R ligands

A series of tailored synthetic derivatives (**10**-**19**) was designed that allows the stepwise comparison of ligands with non-fused aromatic ring systems with ligands in which these rings are linked by an ethyl or ethylene bridge (see Table 2 for structures). The series also varies the constraints of the linker connecting the aromatic moieties to the amine portion. Diphenhydramine (**1**) was selected as the starting point as it contains the prototypical basic amine and two separate phenyl groups (Figure 2). These aromatic rings were captured in a fused tricyclic system by using an ethyl linker to afford **10** or an ethylene linker to afford **11**. These modifications of the aromatic head groups were systematically applied to analogous ligands that incorporate the amine group of **1** into a variety of ring systems (that is, starting from **4**, **17** and **12**). This includes replacing the sp³ hybridised O atom in **1** with an sp³ hybridised N (**4**) or C atom (**17**) or an sp² hybridised C atom (**12**). Bridging of the two aromatic rings in **4** and **17** and **12** as described for **1** affords three sets of analogs (**15**-**16, 18-19** and **13-14**, respectively). Except for **18**, compounds **10**-**19** and associated synthetic routes are known in the peer-review literature[20-25] with some of those having been used in a histamine-receptor context. Some target compounds were available *in-house* (i.e., **10**, **12**, **14**, **15** and **16**) from previous synthetic efforts. The remaining target compounds **11**, **13** and **17-19** were synthesized from commercially available 4-chloro-1-methylpiperidine and tricyclic alcohol 5H-dibenzo[a, d][7]annulen-5-ol (Scheme 1). The syntheses of **11** and **13** were prepared under similar conditions as described in reports.[20, 21]

However, for **17-19** the procedures applied were as follows. Compound **11** was made by addition of *N,N*-dimethylaminoethanol to 5H-dibenzo[a,d][7]annulen-5-ol,[26] while intermediate **21** was obtained via bromination of the alcohol.[27] The key Grignard reagent **22** was synthesized via the reaction of the corresponding alkyl chloride with Mg.[28] Next, **22** was subjected *in situ* to different electrophiles to deliver compounds **17-19** and intermediate **23**. All these reactions proceeded in extremely low isolated yield (1-16%). We attribute this to low reproducibility of the formation of **22** and of the required activation methods (such as I_2 and $BrCH_2CH_2Br$) as well as to very challenging purification of the product mixtures due to high crystallinity. Dehydration of **23** in HCOOH afforded **13** in 28% yield.
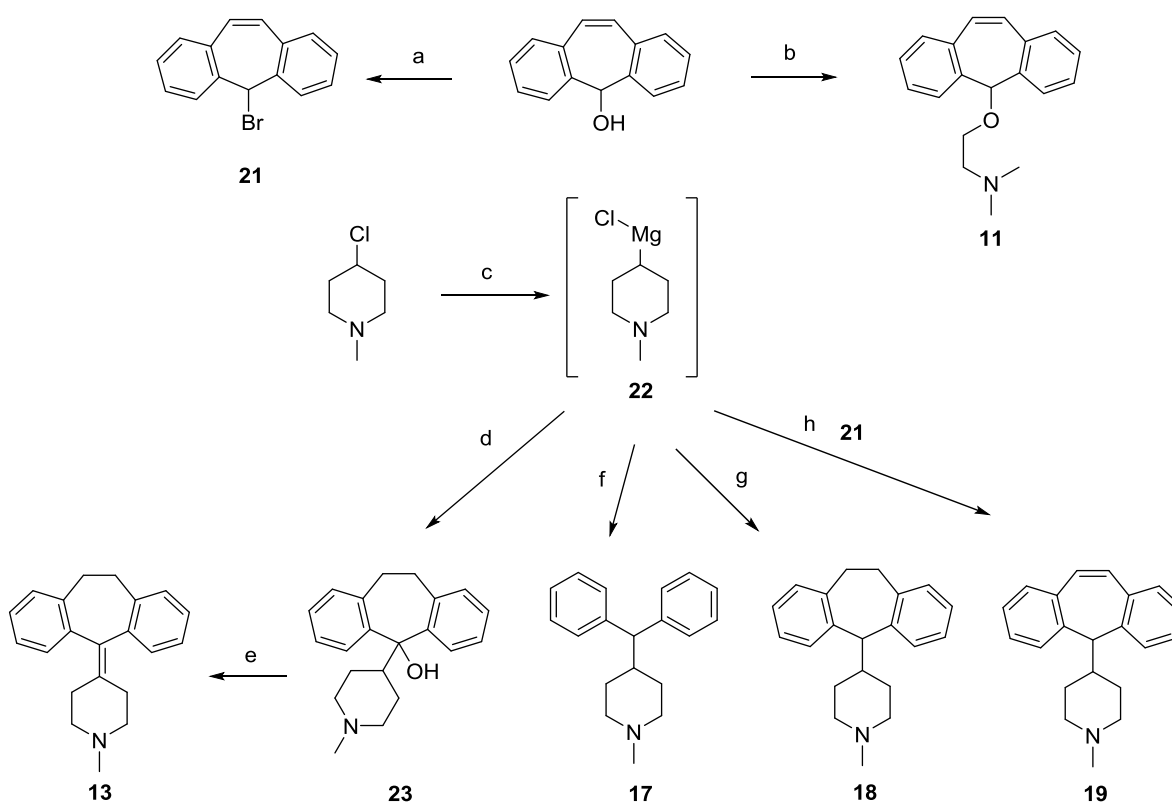
Scheme 1-Synthetic approach. (a) CH_3COBr, EtOAc, reflux, 2 h, 46%. (b) *N,N*-dimethylaminoethanol, KOH, DMSO, rt, 24 h, 8%. (c) Mg (I_2/1,2-dibromoethane), THF, reflux, 1-2 h. (d) 10,11-dihydro-5H-dibenzo[a,d][7]annulen-5-one, THF, rt, 15 h, reflux, 16% over two steps (incl. step c). (e) HCOOH, 100 °C, 2 h, 28%. (f) bromodiphenylmethane, THF, rt, 4 h, 2% over two steps (incl. step c). (g) 5-chloro-10,11-dihydro-5H-dibenzo[a,d][7]annulene, THF, 4 h, rt, 1% over two steps (incl. step c). (h) THF, rt, overnight, 2% over two steps (incl. step c).

Conformational analysis to assess flexibility

Conformational analysis was performed on all benchmark and tailored compounds to determine the number of conformers within 7 kcal/mol from the global energy minimum (Table 1 and Table 2) as a means to estimate the flexibility of the ligand. The stochastic search option within the Molecular Operating Environment (MOE) software package was used as this amongst others generates different conformations of the tricyclic ring systems.

Evaluation of the benchmark ligands

Binding affinity constants and kinetic parameters were determined using $[^3H]$mepyramine radioligand binding studies with a homogenate of HEK293T cells transiently expressing the human H_1R as described in the methods section. Table 1 shows the affinities and kinetic parameters for all benchmark ligands. It was found that the tricyclic ligands **5-9** generally have a higher binding affinity (pK_i and p$K_{D,calc}$) and longer RT than the non-tricyclic ligands **1-4**. Among the tricyclic compounds was desloratadine (**7**), for which we confirm its long RT (previously reported as 190 ± 40 min).[14-17] Table 1 also shows the results of the conformational analyses. In general, it is noted that the number of identified conformers of a particular compound is significantly influenced by the number of distinct conformations that are identified for the aromatic ring systems. Distinct conformations of tricyclic rings cannot easily interconvert during energy minimizations, whereas the unconstrained aromatic ring systems are always minimized in the same conformation during the energy minimization step of the conformational analysis, and there clearly is a difference between the number of identified low energy conformers and the number of conformations that can easily be obtained, especially by the unconstrained non-tricyclic ligands.

Table 1. Kinetic characterization of binding of benchmark ligands at the H_1R. All values represent mean ± SEM of N ≥ 3.

Non-tricyclic ligands	conformers[a] #	pK_i	$pK_{D,calc}$[b]	k_{on} $(10^6 \cdot M^{-1} \cdot min^{-1})$	k_{off} (min^{-1})	RT (min)[c]
1: diphenhydramine	52	8.0 ± 0.1	8.1 ± 0.2	300 ± 200	2.3 ± 0.2	0.43
2: mepyramine	20	8.8 ± 0.1	8.8 ± 0.1	150 ± 30	0.23 ± 0.03	4.4
3: triprolidine (Z)	26	8.3 ± 0.2	8.1 ± 0.1	40 ± 10	0.300 ± 0.035	3.1
4: cyclizine	13	8.2 ± 0.1	8.1 ± 0.0	53 ± 4	0.42 ± 0.06	2.4
Tricyclic ligands	conformers[a] #	pK_i	$pK_{D,calc}$[b]	k_{on} $(10^6 \cdot M^{-1} \cdot min^{-1})$	k_{off} (min^{-1})	RT (min)[c]
5: doxepin	40	9.6 ± 0.1	9.1 ± 0.1	70 ± 10	0.060 ± 0.016	23
6: azatadine	12	10.2 ± 0.1	9.6 ± 0.0	32.0 ± 0.3	0.0088 ± 0.0001	114
7: desloratadine	8	9.1 ± 0.1	9.5 ± 0.1	18 ± 3	0.006 ± 0.001	170
8: clozapine	10	9.2 ± 0.1	9.3 ± 0.0	14.3 ± 0.3	0.0068 ± 0.0004	148
9: mianserin	26	9.4 ± 0.1	9.4 ± 0.0	55 ± 1	0.022 ± 0.002	45

[a] Number of conformers within 7 kcal/mol from the global energy minimum. [b] Calculated as k_{off}/k_{on}.
[c] Calculated from the mean k_{off}: RT = $1/k_{off}$.

Exploration of the tricyclic ring system and linked amine

The set of tailored synthetic derivatives (**10-19**) together with **1** and **4** was inspected in detail thereafter (Table 2). Affinity for the H_1R was determined by [³H]mepyramine displacement as depicted in Figure 3A for an exemplary set of compounds (**13**, **17-19**). A 100-fold difference in affinity was observed between **13** and **17**, whereas **18-19** both have affinities similar to **13**. Subsequently, the kinetic binding rate constants for binding to H_1R were determined in [³H]mepyramine competitive association binding assays, as originally described by Motulsky and Mahan.[29] The binding of 1–5 nM [³H]mepyramine in competition with unlabeled ligand at a concentration amounting to approximately 10 times the K_i value of the latter was measured after different incubation times. Representative [³H]mepyramine association curves are shown in Figure 3B. In the presence and absence of **17**, [³H]mepyramine binding to the H_1R gradually increases over time, indicating that **17** has a relatively short residence time (*i.e.*, comparable or shorter than that of [³H]mepyramine.[18, 30] In the presence of **13**, **18** and **19**, however, initial overshoots are clearly observed (Figure 3B), indicating that these ligands have a longer RT as compared to [³H]mepyramine. Compounds **18** and **19** show a similar overshoot pattern, indicating that their k_{off} values are similar at the H_1R. In line with its high target-binding affinity, **13** shows the longest RT at the H_1R.
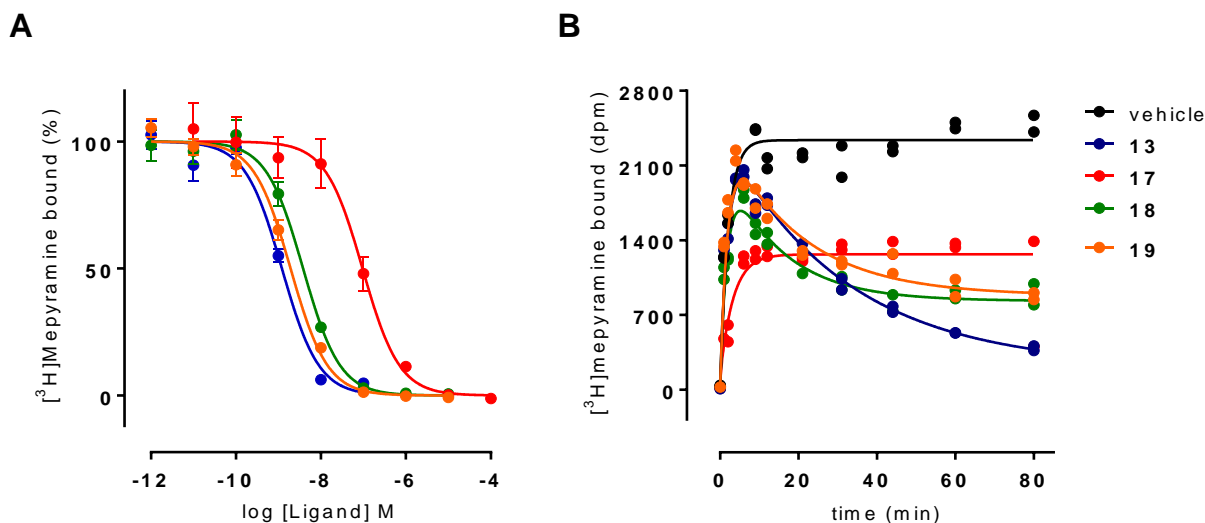
Figure 3. Radioligand binding in co-incubation with an exemplary set of compounds with varying rigidification elements. (A) [^{3}H]mepyramine was co-incubated with increasing concentrations of **13, 17-19** and the K_i value was determined from the resulting dose-dependent radioligand displacement by converting the observed IC$_{50}$ value using the Cheng-Prusoff equation. (B) [^{3}H]mepyramine binding was measured over time in the presence of a ±10·K_i concentration of **13, 17-19**. The kinetic association (k_{on}) and dissociation rate (k_{off}) constants were determined from the resulting radioligand binding kinetic traces. The shown representative graphs involve ≥ 3 experiments, depicting the mean and SEM of triplicate values (A) or the individual measurements with duplicate values per time point (B).

Table 2 shows the affinities and kinetic parameters as well as the results of the conformational analyses for all synthesized ligands. The conformational analyses afforded values in the same range as calculated for the benchmark ligands. For the biochemical assays levocetirizine (**20**) was used as a long-residence reference compounds, as it was in our earlier studies.[18, 31] For clarity, the cell background colors in Table 2 indicate a classification of four series of ligands with the same basic amine element but varying connectivity of the aromatic rings to give triplets (**1**, **10**, **11** / **4**, **15**, **16** / **17**, **18**, **19** / **12**, **13**, **14**). The color coding of the compound numbers indicates molecules with the same aromatic head group but with different amine elements (*e.g.*, red numbers for compounds **10**, **13**, **15**, **18** that all have a tricyclic ring with an ethyl linker).

Table 2 reveals that the systematic structural modifications have a pronounced effect on the binding kinetics. With the same unconstrained amine moiety, alteration of the aromatic rings by bridging **1** with an ethyl linker (to give **10**) results in a decrease of the dissociation rate constant (from 2.3 ± 0.2 to 0.129 ± 0.003 min^{-1}) and hence a 18-fold increase in RT at the H$_1$R. Replacing the ethyl linker of **10** with an ethylene linker causes an additional decrease in dissociation rate (k_{off} = 0.009 ± 0.002 min^{-1} for **11**), *i.e.*, a 14-fold increase in RT resulting in a long residence time of 110 min. Incorporating the aromatic rings in a tricyclic structure seems to lower the association rate constant, whereas the introduction of a double bond in the tricyclic ring does not seem to
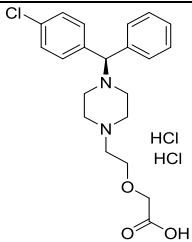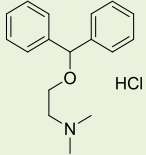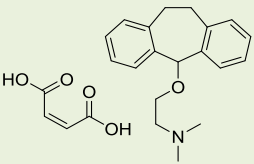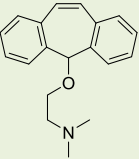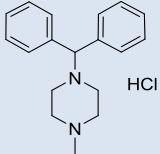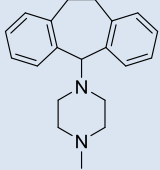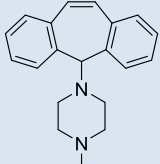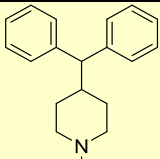
have a big additional effect (k_{on} = (300 ± 200) x $10^6 \cdot M^{-1} \cdot min^{-1}$, (66 ± 3) x $10^6 \cdot M^{-1} \cdot min^{-1}$ and (50 ± 20) x $10^6 \cdot M^{-1} \cdot min^{-1}$, for **1**, **10** and **11**, respectively). Within this triplet of **1**, **10** and **11**, the binding affinity increases gradually with **11** having a pK_i of 9.5.
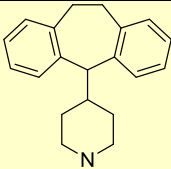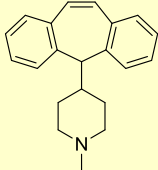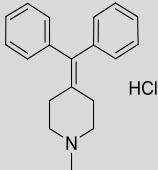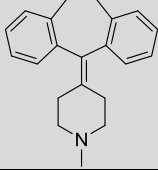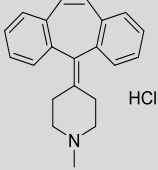
When bridging the two aromatic rings of the piperazine-containing structure of **4** with the ethyl and ethylene linker (leading to **15** and **16**, respectively), the residence time increases, although the differences are not as big as in the previous triplet (from 2.4 to 8 to 29 min, for compound **4**, **15** and **16**, respectively). The association rate constants gradually get smaller, (k_{on} = (53 ± 4) x $10^6 \cdot M^{-1} \cdot min^{-1}$, (34 ± 7) x $10^6 \cdot M^{-1} \cdot min^{-1}$ and (7 ± 1) x $10^6 \cdot M^{-1} \cdot min^{-1}$, for **4**, **15** and **16**, respectively), with the tricyclic piperazine **16** having the slowest association of the three. Within this triplet, the binding affinity does not increase substantially and remains at pK_i of 8.7 for both the tricyclic compounds **15** and **16**.

Within the piperidine-containing triplet **17**, **18** and **19**, a large 270-fold increase in RT is observed when connecting the aromatic rings of **17** (RT = 0.13 min) to the tricyclic **18** (RT = 35 min). Introducing a double bond in the linker (**19**) results in a similar increase in the RT (RT = 48 min). This latter modification does not seem to alter k_{on} ((43 ± 5) x $10^6 \cdot M^{-1} \cdot min^{-1}$ and (40 ± 7) x $10^6 \cdot M^{-1} \cdot min^{-1}$, for **18** and **19**, respectively).

Interestingly, when evaluating the triplet of constrained piperidines **12, 13** and **14**, the ethyl-bridged compound **13** has the longest RT within the triplet (RT = 200 min) and one of the longest RT values in this study, even compared to the benchmark compounds presented in Table 1. Introducing a double bond in the linker, leading to **14** (cyproheptadine) in this case affords a slightly shorter residence time (RT = 104 min). The association rate constants seem to gradually get smaller (k_{on} = (120 ± 20) x $10^6 \cdot M^{-1} \cdot min^{-1}$, (80 ± 20) x $10^6 \cdot M^{-1} \cdot min^{-1}$ and (60 ± 10) x $10^6 \cdot M^{-1} \cdot min^{-1}$, for **12**, **13** and **14**, respectively) and the binding affinity for **13** and **14** remains equally high (pK_i = 9.6 and pK_i = 9.5, respectively).

Table 2. Characterization of synthetic ligands binding at the H_1R. All values represent mean ± SEM of N ≥ 3.

#	Name	Structure	conformers #[a]	pK_i	$pK_{D.calc}$[b]	k_{on} ($10^6 \cdot M^{-1} \cdot min^{-1}$)	k_{off} (min^{-1})	RT[c] (min)
20	Levocetirizine		N.D.	8.3 ± 0.1	8.1 ± 0.0	1.4 ± 0.2	0.011 ± 0.001	91
1	Diphenhydramine		52	8.0 ± 0.1	8.1 ± 0.2	300 ± 200	2.3 ± 0.2	0.43
10	VUFH1607		26	8.9 ± 0.0	8.7 ± 0.0	66 ± 3	0.129 ± 0.003	7.8
11	VUF16417		51	9.5 ± 0.1	9.7 ± 0.2	50 ± 20	0.009 ± 0.002	110
4	Cyclizine		13	8.2 ± 0.1	8.1 ± 0.0	53 ± 4	0.42 ± 0.06	2.4
15	VUFH1896		20	8.7 ± 0.1	8.4 ± 0.0	34 ± 7	0.12 ± 0.02	8
16	BS7617		9	8.7 ± 0.1	8.3 ± 0.1	7 ± 1	0.035 ± 0.004	29
17	VUF16290		14	7.6 ± 0.0	7.4 ± 0.1	200 ± 50	8 ± 2	0.13

#	Name	Structure	Conf.a	pKi	pKD,calcb	kon	koff	RTc
18	VUF16416		28	9.2 ± 0.1	9.2 ± 0.0	43 ± 5	0.0285 ± 0.0004	35
19	VUF16327		5	9.3 ± 0.1	9.3 ± 0.0	40 ± 7	0.021 ± 0.003	48
12	VUF5577		11	8.5 ± 0.0	8.6 ± 0.0	120 ± 20	0.35 ± 0.06	2.9
13	VUF16217		12	9.6 ± 0.0	10.3 ± 0.1	80 ± 20	0.005 ± 0.002	200
14	Cyproheptadine		6	9.5 ± 0.1	9.8 ± 0.1	60 ± 10	0.010 ± 0.001	104

a Number of conformers within 7 kcal/mol from the global energy minimum. bCalculated as k_{off}/k_{on}. c Calculated from the mean k_{off}: RT = $1/k_{off}$.

It is noted that the binding affinities (pK_i) determined in equilibrium radioligand displacement experiments and the $pK_{D,calc}$ values derived from radioligand competitive association assays ($K_{D,calc} = k_{off}/k_{on}$) experiments correlate well (Figure 4A and 4B for the reference compounds and for the set of tailored H_1R ligands, respectively), giving confidence in the accuracy of the measured binding rate constants.
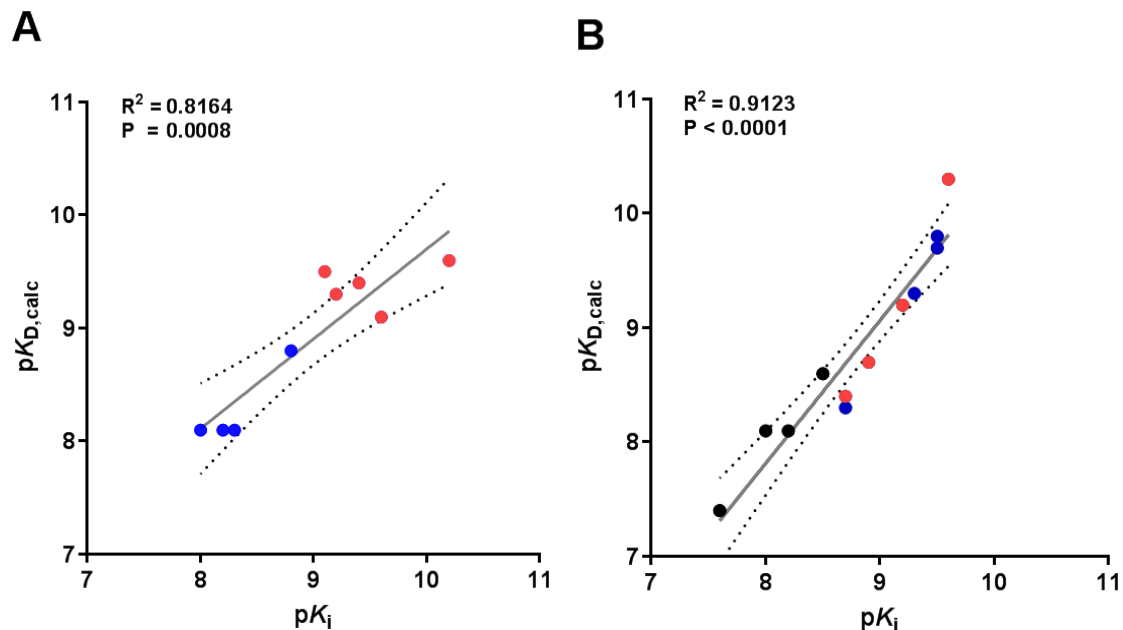
Figure 4. Affinity determined by radioligand displacement assay (pK_i) and the kinetic affinity (p$K_{D, calc}$). The lines represent linear regression of data. The two dashed lines indicate 95% confidence of the best-fit line. **(A)** data for the reference compounds (table 1) **(B)** data for the coherent set of tailored H_1R ligands (table 2).

Discussion

For several decades, H_1R antagonists have been successfully used in the clinic for treating symptoms of allergic diseases[32-34] and more recently they have also been applied to regulate sleep-wakefulness[35-37]. As such, structure-activity relationships of H_1R antagonists have been studied intensively. Hallmark features of H_1R ligands include aromatic rings arranged in a diphenyl or tricyclic structure. Another typical feature is the basic amine, that is either flexible or captured in an aliphatic heterocyclic ring. Other ligands are equipped with a carboxylic acid moiety to regulate pharmacokinetic properties and prevent brain penetration of the ligands. It has been shown by us and others[6] that these features also have a remarkable effect on binding kinetics. Here, we have focused on the structure-kinetic relationships associated with the aromatic rings and amine moiety.
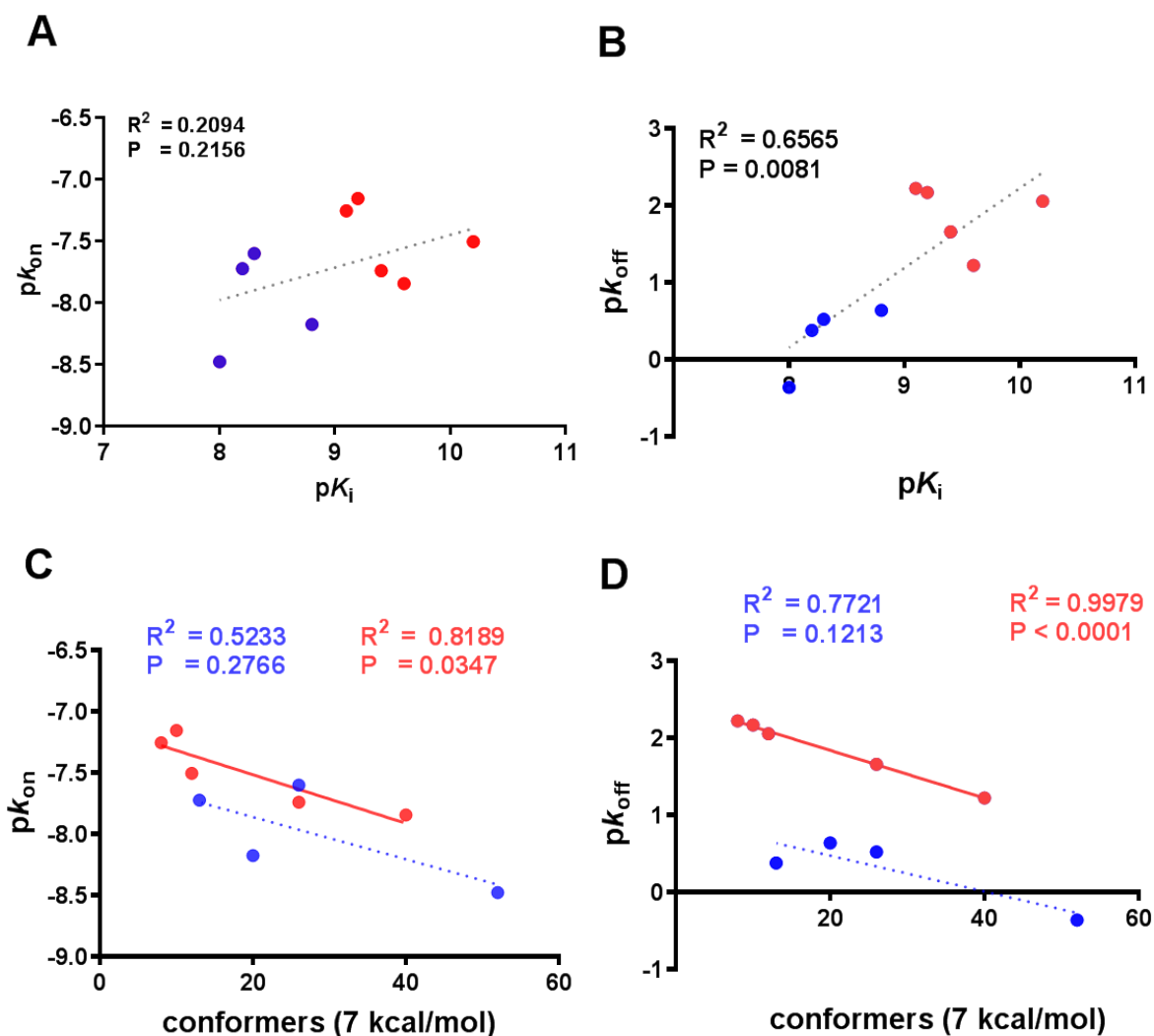
Figure 5. Exploring binding kinetics for the benchmark compounds. Blue dots represent the non-tricyclic compounds **1**-**4** and the red dots represent the tricyclic compounds **5**-**9**. The lines represent linear regression of data. Solid lines indicate trends with an $R^2 > 0.80$, whereas dashed lines represent less convincing trends with $R^2 < 0.80$. (A) Negative logarithm of k_{on} (pk_{on}) and of the affinity (pK_i). (B) Negative logarithm of k_{off} (pk_{off}) and of the affinity (pK_i). (C) Negative logarithm of k_{on} (pk_{on}) and the number of conformers within 7 kcal/mol from the global energy minimum. (D) Negative logarithm of k_{off} (pk_{off}) and the number of conformers within 7 kcal/mol from the global energy minimum.

For the selected benchmark compounds **1-9**, plotting pK_i against pk_{on} (Figure 5A) and pk_{off} (Figure 5B) indicates there is no clear trend between pK_i and the association rate constant, whereas there is a moderate, but significant correlation between the affinity and the dissociation rate constant. These results are in line with recent findings for adenosine A_3 receptor antagonists,[38] whereas a series of A_3 agonists showed a better correlation between the affinity and the association rate.[39] A recent study exploring the binding kinetics of histamine H_3R reference ligands showed a better correlation between the affinity and the association,[40] illustrating that the relationship between

97

affinity and binding kinetics is very receptor and compounds series dependent. For the compounds in Table 1, all tricyclic ligands have a lower dissociation rate k_{off} (longer RT) than the non-tricyclic ligands. The differences between non-tricyclic ligands **1**-**4** and tricyclic ligands **5**-**9** were further explored by conformational analysis. The number of conformers within an energy window of 7 kcal/mol from the global energy conformation was determined (Table 1). Figure 5 shows the number of conformations plotted against pk_{on} (Figure 5C) and pk_{off} (Figure 5D). While the number of compounds in this analysis is limited, a trend line across the non-tricyclic compounds (blue dots) appears significantly lower than a trend line across the tricyclic compounds (red dots), suggesting a correlation between residence times and number of conformers but also indicating an additional, unidentified feature (that is not captured by the conformational analysis) that distinguishes the non-tricyclic from the tricyclic compounds.

The series of tailored compounds (Table 2) that was synthesized to explore the SAR and SKR of the tricyclic ring systems and basic amines confirms the observations made for the benchmark H_1R antagonists (Table 1), namely that the ring systems have a pronounced effect on the binding kinetics. In all cases, linking the two aromatic rings into tricyclic systems leads to longer residence time and a higher affinity. Introducing a double bond in the linker that connects the aromatic rings (leading to compounds **11**, **16**, **19** and **14**) often results in the compounds with the longest residence time within the triplets. A notable exception to the latter is **14**, as in the triplet with the constrained piperidine moiety (i.e. **12**-**14**) it is the tricyclic compound with the ethyl linker (**13**) that has the longest RT. The residence time of **13** (RT = 200 min) is amongst the longest of the synthesized compounds (Table 2) and the studied benchmark compounds (Table 1).
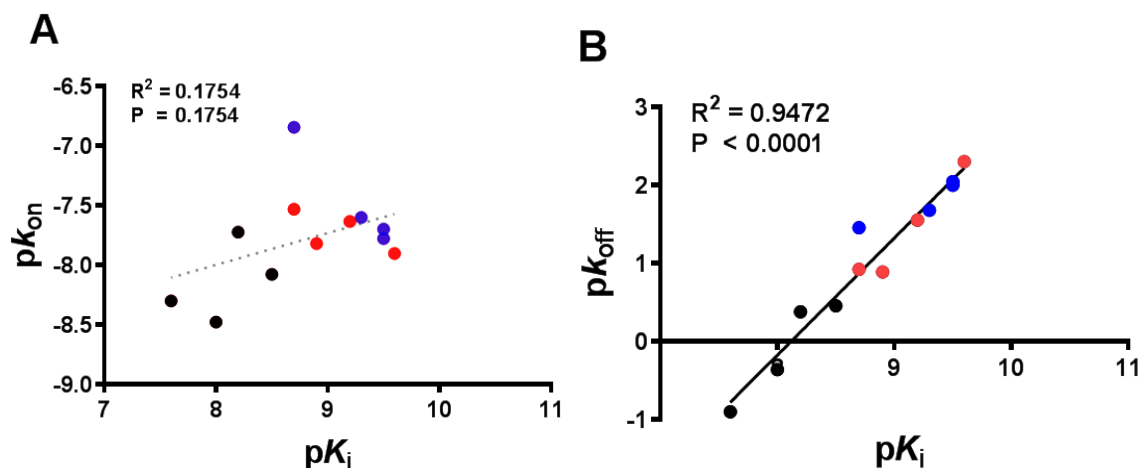
Figure 6. Exploring binding kinetics for the synthesized compounds. Molecules contain unconstrained diphenyl moieties (black dots), tricyclic structures with an ethyl linker (red dots) or tricyclic structures with an ethylene linker (blue dots), all combined with four different amines (Table 2). The lines represent linear regression of data. Solid lines indicate trends with an $R^2 > 0.80$, whereas dashed lines represent less convincing trends with $R^2 < 0.80$. (A) Negative logarithm of k_{on} (pk_{on}) and of the affinity (pK_i). (B) Negative logarithm of k_{off} (pk_{off}) and of the affinity (pK_i).

When plotting pK_i versus pk_{on} and pk_{off} (Figure 6A and 6B, respectively), it appears that the dissociation rate constants, but not the association rate constants, are correlated to the binding affinity, a finding that seems even more pronounced than observed for the benchmark compounds in Table 1 and Figure 5A and 5B. As shown in Figure 6B, compounds that contain two unconstrained aromatic rings (black dots; **1, 4, 17, 12**) have lower affinity and faster unbinding. The tricyclic compounds with an ethyl linker (red dots; **10, 15, 18, 13**) and the tricyclic compounds with an ethylene linker (blue dots; **11, 16, 19, 14**) have higher affinity and slower unbinding. A similar correlation cannot be observed for association rate constants (Figure 6A).

The compounds in Table 2 were also subjected to a conformational analysis. However, in contrast to the benchmark compounds listed in Table 1, no trends are observed between the number of conformers and the binding kinetics (Figure S1, Supporting Information). It is noted that the number of conformers is significantly influenced by the number of distinct conformations of the aromatic rings that are identified by the search algorithm. Bridging the aromatic rings leads to very different conformations of the tricyclic ring system that cannot easily interconvert, whereas the unconstrained aromatic rings of **1**, **4**, **17** and **12** are always minimized in the same relative conformation during the energy minimization step of the conformational analysis. Clearly, the non-tricyclic ligands can easily adjust the orientation of their unconstrained aromatic rings to adopt a slightly different binding conformation. The possibility that ligands can bind in an energy conformation that is somewhat higher than one of the identified conformers might be more

important for the series of tailored (unoptimized) compounds presented in Table 2 than for the optimized benchmark compounds represented in Table 1. The compounds from Table 2 are designed to allow pairwise comparisons of the tricyclic ring systems and different basic amines but are not fully optimized for binding to the H_1R, whereas the benchmark compounds of Table 1 represent the best compounds within highly optimized ligand series (the different decorations of the aromatic rings of the benchmark compounds illustrate this aspect).

The dataset represented in Table 2 allows for a careful deduction of SKRs, especially with respect to the effect of the structural elements in the compounds. As indicated earlier, capturing the unconstrained diphenyl rings into a tricyclic structure leads to lower association rate constants for every amine moiety explored (*i.e.*, flexible amine, piperazine, piperidine and piperidinylidene, see Figure 7A). In the case of the flexible amines (**1**, **10**, **11**), capturing the aromatic rings in a tricyclic system has a large effect on the association rate constants. In contrast, the differences in k_{on} are rather small if the constrained piperidinylidene is used as a basic moiety (**12**, **13**, **14**). In all cases, the tricyclic derivative with the ethylene linker has the lowest association rate constant within the triplet, but only for the derivative in the piperazine series (i.e., **16**, k_{on} = (7 ± 1) x $10^6 \cdot M^{-1} \cdot min^{-1}$) the association rate constant seems to be substantially lower than its analog with the ethyl linker (**15**, k_{on} = (34 ± 7) x $10^6 \cdot M^{-1} \cdot min^{-1}$).
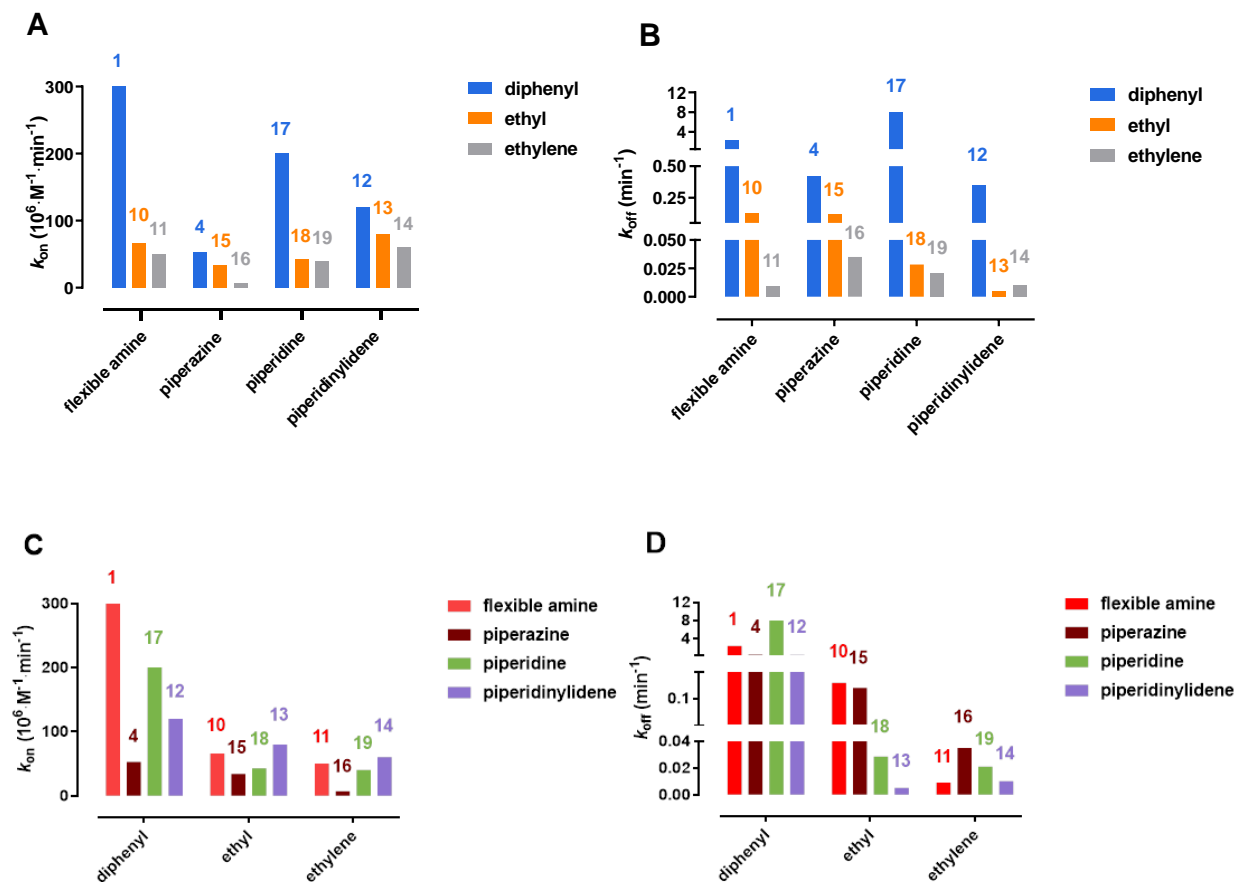
Figure 7. SKRs exploring the role of the different ring systems. (A) Association rate constants organized by aromatic ring systems. (B) Dissociation rate constants organized by aromatic ring systems. The same data can be rearranged to focus on basic amines: (C) Association rate constants organized by basic amines. (D) Dissociation rate constants organized by aromatic ring systems. The numbers above the bar correspond to the respective molecule numbers.

The influence on the dissociation rate constants (Figure 7B) is more pronounced, with the tricyclic compounds having a much smaller k_{off} value, i.e. longer residence time. For the flexible amines (**1**, **10**, **11**) and the piperazine-containing compounds (**4**, **15**, **16**), a clear difference is seen between the tricyclic compounds that contain an ethyl-linker and the ethylene-linker, the latter tricyclic ring system leading to the compounds with the slowest dissociation (longest RT). For the piperidine-containing compounds, there is no significant difference in dissociation rate constants for the two tricyclic compounds **18** and **19**. For the piperidinylidene-containing compounds, the tricyclic compounds also have very low dissociation rate constants (long RT), with the tricyclic compound with an ethyl-linker (i.e., **13**) having a remarkable slow dissociation ($k_{off} = 0.005$ min^{-1}).

Using the same data but focusing the SKR discussions on the different amine moieties (*i.e.*, flexible amine, piperazine, piperidine, piperidinylidene), it can be seen that the piperazine moiety consistently has the slowest association for the quartets that contain the same aromatic ring

systems (Figure 7C). Also, in this representation of the data, **16** is noted for having a particularly slow association. The effect of different amines on the dissociation rate constants (Figure 7D) is less pronounced than the effect of the aromatic ring systems (Figure 7A, B). No consistent pattern is observed for the different quartets, meaning that the effect of exchanging the basic moieties is difficult to predict. For the ethylene-linked tricyclic series, it is noted that the aforementioned piperazine **16** has the fastest unbinding.

Representing the same binding kinetic data of Table 2 in an isoaffinity kinetic plot (Figure 8) clearly illustrates that restraining the diphenyl moieties into tricyclic rings leads to higher affinity, an effect that is mainly caused by decreasing dissociation rate constants (consider the trend observed for squares **1**, **10**, **11,** diamonds **12**, **13**, **14** and inverted triangles **17**, **18**, **19**). For the piperazine-containing compounds (**4**, **15**, **16**), the changes in association and dissociation are more balanced, resulting in compounds with similar affinities ($pK_{D,calc}$ = 8.1, 8.4 and 8.3, respectively) as indicated in the plot by the three triangles that stay close to the same isoaffinity diagonal. The molecular reason for this is not clear. The amine moieties of all these ligands are expected to bind to the aspartic acid residue D3.32, a hallmark anchoring point in aminergic GPCRs that is known to bind the amine groups of the endogenous agonists and also to amine-containing ligands. As the piperazine ring contains a second basic nitrogen atom, it can be speculated that this feature facilitates the breaking of that key hydrogen-bonding as in an anchimeric assistance, resulting in a shorter residence time.
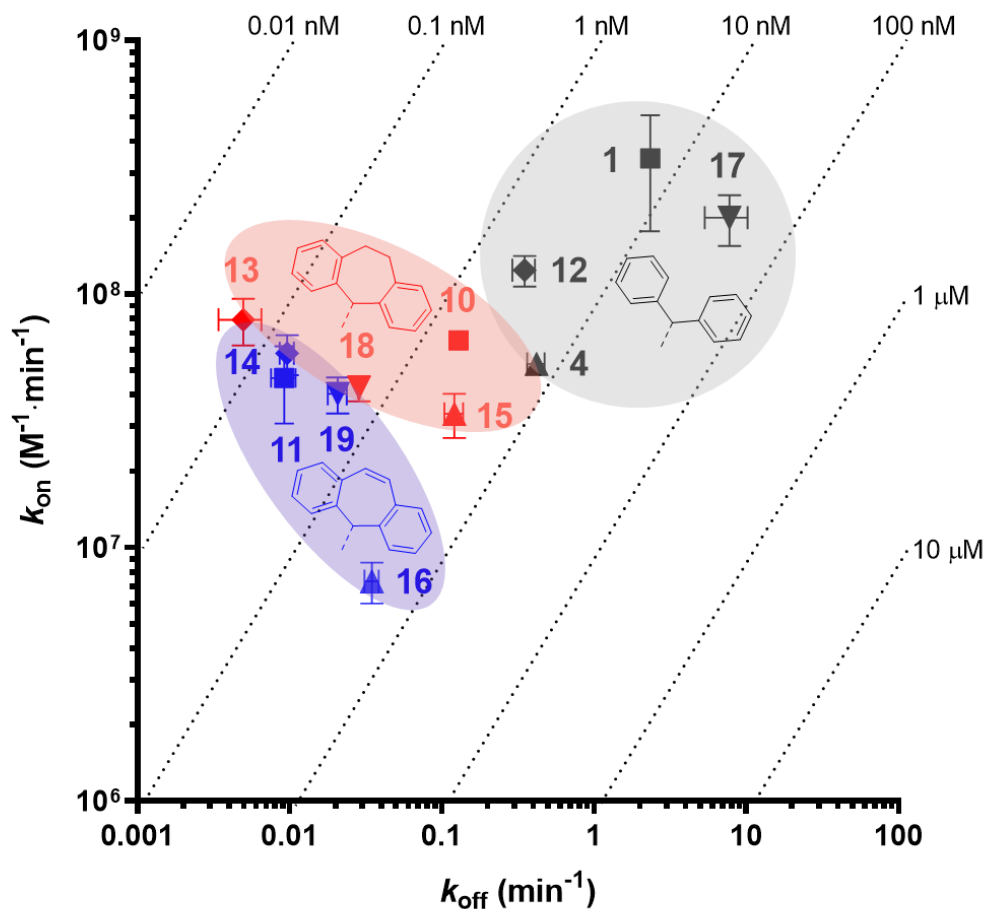
Figure 8. Two-dimensional isoaffinity kinetic plot indicating k_{on}, k_{off} values and $K_{D\text{-calc}}$ (diagonal lines). The colored molecule numbers, symbols and zones indicate the particular aromatic ring systems and correspond to the color coding used in the molecule numbers in Table 2 (black: no bridge, red: ethyl bridge, blue: ethylene bridge). Symbols correspond to ■ flexible amines ▲ piperazines ▼ piperidines ◆ piperidinylidenes.

In conclusion, it was shown in this study that a tricyclic ring system increases affinity and RT at the H_1R. The increase in affinity is mainly achieved by changes in dissociation rate constants. The influence of the basic amine moiety on the binding kinetics appears less pronounced, although for the piperazine-containing compounds the changes in dissociation and association rate constants are more balanced, resulting in compounds with similar affinity. While the effect of the tricyclic ring systems on the binding kinetics is very pronounced, analysis of well-studied benchmark compounds suggests that the effect of rigidification of the aromatic ring system on affinity and residence time can be further optimized by careful optimization of the tricyclic moiety, for example by decoration of the aromatic rings.

Experimental section

Pharmacology

Dulbecco's Modified Eagle's Medium was acquired from Sigma-Aldrich (St. Louis, MO, USA). Medium was supplemented with fetal bovine serum and penicillin/streptomycin from GE healthcare (Uppsala, Sweden). 25-kDa linear polyethylenimine was acquired from Polysciences (Warrington, PA, USA). HBSS, trypsin and the BCA protein assay were bought from Thermo Fischer scientific (Waltham, MA, USA). The Branson sonifier 250 homogenizer was bought from Emerson (St. Louis, MO, USA). GF/C plates, Microscint-O, [3H]mepyramine, the cell harvester and the Wallac Microbeta counter were all bought from Perkin Elmer (Waltham, MA, USA). Diphenhydramine hydrochloride was purchased from Sigma Aldrich. Mepyramine maleate was obtained from Research Biochemicals International. Triprolidine hydrochloride was purchased from Tocris. Azatadine dimaleate and desloratadine were purchased from HaiHang Industry Co., Ltd. Cyclizine hydrochloride was purchased from Toronto Research Chemicals (TRC).

Cell culture and radioligand binding. Production of cell homogenates expressing the HA-H_1R and the performed radioligand binding experiments conducted were previously described and adapted with minor changes.[14] In short, HEK293T cells were transiently transfected using 25kDa polyethylenimine with a pcDEF3 vector encoding the N-terminally HA tagged H_1R. Cells were collected and frozen two days post-transfection. Upon conducting a radioligand binding experiment, a frozen aliquot of cells was reconstituted in binding buffer [50mM Na_2HPO_4/KH_2PO_4, pH 7.4], homogenized and then co-incubated with [3H]mepyramine with or without an additional unlabeled ligand at 25°C under gentle agitation. Binding reactions were terminated by filtration and three rapid consecutive wash steps using ice-cold wash buffer [50mM Tris-HCl, pH 7.4]. Filter-bound radioactivity was quantified using scintillation counting using the Wallac Microbeta.

Competitive association assay. Previously it was determined for the radioligand [3H]mepyramine binding the H_1R, that the equilibrium dissociation constant (K_D) is 2.29 nM, the kinetic dissociation rate constant (k_{off}) is 0.22 min^{-1} and the kinetic association rate constant (k_{on}) is 1.1 x 10^8·min^{-1}·M^{-1}.[14] In radioligand displacement experiments, a single concentration 1–5 nM [3H]mepyramine was co-incubated with increasing concentrations (10^{-11} – 10^{-4} M) of unlabeled ligands for 4 h at 25 °C. K_i values could be determined from the displacement curves by converting the obtained IC_{50} values using Cheng-Prusoff equation.[41] For competitive association experiments a single concentration 1–5 nM [3H]mepyramine was co-incubated with a single concentration unlabeled ligand for increasing incubation times of 0 – 80 min at 25 °C. The concentration of the antagonist was chosen to be 10·K_i, or fine-tuned to have a similar level of radioligand displacement after 80 min (>40%). Kinetic binding rate constants of the unlabeled ligands were determined from the resulting radioligand binding over time by fitting the data to

the Motulsky and Mahan model using non-linear regression.[29] In this model the concentrations of both ligands and the k_{on} and k_{off} of [³H]mepyramine at the H_1R were constrained (see above). From the fitted kinetic binding rate constants, the equilibrium dissociation constant ($pK_{D,calc}$) and residence time (RT) could be calculated.

Calculations

SMILES for compounds **1-19** were obtained from ChemBioDraw Ultra (version 16.0.1.4) and protonated according to the protonate 3D module (default settings). Conformational analyses were performed in MOE2016.08 using a stochastic search algorithm. Under same energy windows of 7 kcal/mol, a stochastic search produces conformations by stochastically perturing structures. The rejection limit was increased to 1000 in order to find all possible conformers. Double bonds were allowed to rotate during sampling. The sp^3 stereocenters were allowed to invert in case of nitrogen atoms (e.g., mepyramine). Ring conformations other than chair were accepted. Unique conformations (within 0.25 RMSD limit) were stored and counted.

Chemistry

General remarks

Anhydrous THF, CH_2Cl_2, DMF and Et_2O were obtained by elution through an activated alumina column from Inert PureSolv MD5 before use. Diphenhydramine hydrochloride (**1**) was obtained from Sigma Aldrich, levocetirizine dihydrochloride (**20**) was obtained from Biotrend, and cyclizine hydrochloride (**4**) was obtained from Toronto Research Chemicals Inc. Compounds **10, 12, 15** and **16** as well as cyproheptadine hydrochloride (**14**) were gifts from Gist Brocades (The Netherlands). All other solvents and chemicals were acquired from commercial suppliers and were used without further purification. ChemDraw professional 16.0 was used to generate systematic names for all molecules. All reactions were performed under an inert atmosphere (N_2). Column purifications were performed automatically using Biotage equipment. NMR spectra were recorded on a Bruker 300 (300 MHz), Bruker 400 (400 MHz), Bruker 500 (500 MHz) or a Bruker 600 (600 MHz) spectrometer. Chemical shifts are reported in ppm (δ) and the residual solvent was used as internal standard (δ ^{1}H NMR: $CDCl_3$ 7.26; DMSO-d_6 2.50; CD_3OD 3.31; δ ^{13}C NMR: $CDCl_3$ 77.16; DMSO-d_6 39.52; CD_3OD 49.00). Data are reported as follows: chemical shift (integration, multiplicity (s = singlet, d = doublet, t = triplet, q = quartet, br = broad signal, m = multiplet, app = apparent), and coupling constants (Hz)). A Bruker microTOF-Q mass spectrometer using ESI in positive ion mode was used to obtain HRMS spectra. A Shimadzu HPLC/MS workstation equipped with an Xbridge C18 5 µM column (100 mm x 4.6 mm), LC-20AD pump system, SPD-M20A diode array detection and LCMS-2010 EV mass spectrometer was used to perform LC-MS analyses. Almost all compounds were measured in acidic mode: the solvents

that were used were the following: solvent B (acetonitrile with 0.1% formic acid) and solvent A (water with 0.1% formic acid), flow rate of 1.0 mL/min, start 5% B, linear gradient to 90% B in 4.5 min, then 1.5 min at 90% B, then linear gradient to 5% B in 0.5 min, then 1.5 min at 5% B; total run time of 8 min. For occasional measuring in basic mode, the mobile phase was a mixture of A = H_2O + 10% buffer and B = MeCN + 10% buffer. The buffer mentioned is a 0.4% (w/v) NH_4HCO_3 aq. soln., adjusted to pH 8.0 with aq. NH_4OH. The eluent program used is as follows: flow rate of 1.0 mL/min, start 5% B, linear gradient to 90% B in 4.5 min, then 1.5 min at 90% B, then linear gradient to 5% B in 0.5 min, then 1.5 min at 5% B, total run time of 8 min. Biotage Isolera One was used for normal phase column chromatography. Reverse-phase column chromatography purifications were performed using Buchi PrepChem C-700 equipment with a discharge deuterium lamp ranging from 200-600 nm to detect compounds using solvent B (acetonitrile with 0.1% formic acid), solvent A (water with 0.1% formic acid) and a flow rate of 15.0 mL/min. Unless specified otherwise, all compounds have a purity of ≥95%, calculated as the percentage peak area of the analyzed compound by UV detection at 230 nm. Samples for analytical LCMS analysis were prepared by dissolving 1 mg/mL in MeCN and injecting 1 µL. The compounds in Table 2 (**10-19**) pass the PAINS filter.[42]

2-((5H-dibenzo[a,d][7]annulen-5-yl)oxy)-N,N-dimethylethanamine (11)

This compound was prepared as reported.[20] A mixture of 5H-dibenzo[a,d][7]annulen-5-ol (1.0 g, 4.8 mmol) and KOH (2.7 g, 48 mmol) in DMSO (9.6 mL) was stirred at room temperature. To this mixture, 2-chloro-N,N-dimethylethanamine hydrochloride (1.4 g, 9.6 mmol) was added. The mixture was stirred for 24 hours at room temperature. A solution of 1.0 M aq. NaOH (13 mL) was added. The mixture was extracted with Et_2O (40 mL). The organic layer was dried over $MgSO_4$ and concentrated *in vacuo*. The crude product was purified using flash column chromatography (DCM/MeOH = 95:5, v/v) and reversed-phase column chromatography (H_2O/CH_3CN) to yield the title compound **11** as a yellow oil (0.10 g, 8%). High temperature NMR: ^{1}H NMR (400 MHz, DMSO-d_6, **373 K**) δ 7.62 (d, J = 7.6 Hz, 2H), 7.43 – 7.38 (m, 4H), 7.28 (t, J = 7.4 Hz, 2H), 7.12 (s, 2H), 4.99 (s, 1H), 3.51 (t, J = 5.0 Hz, 2H), 2.50 (app t, J = 7.2 Hz 2H), 2.18 (s, 6H). ^{13}C NMR (126 MHz, CDCl$_3$) δ 139.60, 132.74, 131.35, 128.73, 127.95, 126.42, 122.59, 79.26, 68.95, 59.28, 46.29. This ^{13}C spectrum at room temperature shows peaks for conformers, while the reported ^{1}H NMR spectrum at 373 K leads to coalescence. LC-MS (ESI): t_R = 3.38 min, 99% (area % @ 230 nm), m/z 280 [M + H]$^+$. HR-MS: $C_{19}H_{22}NO$ calc. for [M+H]$^+$ 280.1696, found 280.1687.

5-(1-methylpiperidin-4-yl)-10,11-dihydro-5H-dibenzo[a,d][7]annulen-5-ol (23)

To dry THF (3.0 mL), Mg turnings (0.20 g, 8.2 mmol) were added and the mixture was stirred at 50 °C. Two crystals of I_2 and a few drops of 1,2-dibromoethane were added. A vigorous reaction started, which subsided after a few minutes. To the reaction mixture was added 4-chloro-1-methylpiperidine (1.1 g, 8.2 mmol) in THF (7.0 mL) dropwise. The mixture was heated at reflux for 1 h to form Grignard reagent **22**. The mixture was cooled to room temperature. Then, 10,11-dihydro-5H-dibenzo[a,d][7]annulen-5-one (1.4 g, 6.6 mmol) in THF (3.0 mL) was added portion wise. The mixture was stirred at reflux overnight. The mixture was quenched with cold 10% aq. NH_4Cl solution, acidified with 5 M HCl (pH 3) and extracted with DCM. The aqueous phase was made alkaline with 1.0 M aq. NaOH (20 mL) and extracted with DCM. The organic layer was dried over Na_2SO_4, filtered and concentrated *in vacuo*. The crude product was purified using flash column chromatography (cyclohexane/ EtOAc/ TEA = 18:80:2, v/v/v) and recrystallized from DCM to yield the title compound as a white solid (0.40 g, 16%). ^{1}H NMR (500 MHz, $CDCl_3$) δ 7.19 – 7.03 (m, 8H), 3.57 – 3.36 (m, 3H), 3.01 – 2.87 (m, 2H), 2.81 (d, J = 11.1 Hz, 2H), 2.22 (s, 3H), 1.78 (app t, J = 11.5 Hz, 2H), 1.50 - 1.39 (m, 2H), 1.30 (app q, J = 12.4 Hz, 2H). LC-MS (ESI): t_R = 3.24 min, >99% (area % @ 230 nm), m/z 308 [M + H]+

4-(10,11-dihydro-5H-dibenzo[a,d][7]annulen-5-ylidene)-1-methylpiperidine (13)

This compound was prepared as reported.[21] A mixture of alcohol **23** (0.20 g, 0.65 mmol) and formic acid (1.0 mL, 26 mmol) was heated at 100 °C for 2 h. The mixture was cooled down to 0 °C, quenched with 2.0 M aq. NaOH (10 mL) and diluted with EtOAc. The organic phase was washed with water and brine, dried over Na_2SO_4, filtered and concentrated *in vacuo*. The crude product was purified by flash column chromatography (cyclohexane/EtOAc = 50:50, v/v) to obtain the title compound as a white solid (51 mg, 28%). ^{1}H NMR (500 MHz, $CDCl_3$) δ 7.18 – 7.02 (m, 8H), 3.49 – 3.32 (m, 2H), 2.88 – 2.76 (m, 2H), 2.67 – 2.57 (m, 2H), 2.48 – 2.34 (m, 4H), 2.27 (s, 3H), 2.17 – 2.07 (m, 2H). ^{13}C NMR (126 MHz, $CDCl_3$) δ 140.87, 138.10, 134.79, 133.81, 129.35, 128.98, 126.91, 125.55, 57.30, 46.30, 32.59, 31.08. LC-MS (ESI): t_R = 3.63 min, >99% (area % @ 230 nm), m/z 290 [M + H]+. HR-MS: $C_{21}H_{24}N$ calc. for [M+H]+ 290.1903, found 290.1899.

4-benzhydryl-1-methylpiperidine (17)[23]

To dry THF (3.0 mL), Mg turnings (0.30 g, 12 mmol) were added. The mixture was stirred at 50 °C for 10 min. One crystal of I_2 and 1,2-dibromoethane (0.37 g, 1.9 mmol) were added. A vigorous reaction started, which subsided after a few minutes. Then, 4-chloro-1-methylpiperidine (1.6 g,

12 mmol) in THF (4.0 mL) was added and the mixture was heated at reflux for 2 h to form Grignard reagent **22.** The mixture was cooled to room temperature and (bromomethylene)dibenzene (2.4 g, 9.7 mmol) in THF (5.0 mL) was added. The mixture was stirred for 4 h, quenched with water and extracted with toluene. The organic layer was washed with water, dried over Na_2SO_4, filtered and concentrated *in vacuo*. The crude product was purified using flash column chromatography (cyclohexane/EtOAc/TEA = 20:78:2, v/v/v) to yield the title compound as a white solid (50 mg, 2 %). ^{1}H NMR (500 MHz, $CDCl_3$) δ 7.32 – 7.26 (m, 8H), 7.19 – 7.14 (m, 2H), 3.50 (d, J = 11.0 Hz, 1H), 2.82 (app d, J = 11.8 Hz, 2H), 2.26 (s, 3H), 2.14 – 2.03 (m, 1H), 1.90 (app t, J = 11.9 Hz, 2H), 1.57 (app d, J = 13.4 Hz, 2H), 1.33 – 1.19 (m, 2H). ^{13}C NMR (126 MHz, $CDCl_3$) δ 143.95, 128.62, 128.16, 126.25, 59.04, 56.12, 46.54, 39.16, 31.59. LC-MS (ESI): t_R = 3.17 min, >99% (area % @ 230 nm), m/z 266 [M + H]$^+$. HR-MS: $C_{19}H_{24}N$ calc. for [M+H]$^+$ 266.1903, found 266.1893.

4-(10,11-dihydro-5H-dibenzo[a,d][7]annulen-5-yl)-1-methylpiperidine (18)

To dry THF (5.0 mL), Mg turnings (0.40 g, 16 mmol) were added and the mixture was stirred at 50 °C (10 min). One crystal of I_2 and 1,2-dibromoethane (0.37 g, 1.9 mmol) were added. A vigorous reaction started, which subsided after a few minutes. To the mixture was added 4-chloro-1-methylpiperidine (2.7 g, 20 mmol) in THF (4.0 mL). The mixture was heated at reflux for 1 h to form Grignard reagent **22**. The mixture was cooled to room temperature and 5-chloro-10,11-dihydro-5H-dibenzo[a,d][7]annulene (3.00 g, 13.12 mmol) in THF (5 mL) was added. The mixture was stirred for 4 h hours at room temperature. The mixture was diluted with toluene. The organic phase was washed with water (2 x), dried over Na_2SO_4, filtered and evaporated under reduced pressure. The crude product was purified using reversed-phase column chromatography ($H_2O/CH_3CN/HCOOH$). The product fractions were concentrated and extracted with DCM/satd. aq. Na_2CO_3 solution. The organic phase was dried ($MgSO_4$) and concentrated to obtain the title compound as a white solid (25 mg, 1 %). ^{1}H NMR (600 MHz, $CDCl_3$) δ 7.17 – 7.03 (m, 8H), 3.54 – 3.39 (m, 3H), 2.98 – 2.86 (m, 2H), 2.81 (d, J = 11.7 Hz, 2H), 2.23 (s, 3H), 2.15 – 2.04 (m, 1H), 1.79 (t, J = 11.3 Hz, 2H), 1.50–1.40 (m, 2H), 1.36 - 1.25 (m, 2H). ^{13}C NMR (151 MHz, $CDCl_3$) δ 140.46, 138.98, 131.89, 130.63, 126.78, 125.66, 61.84, 56.23, 46.42, 40.51, 33.07, 32.20. LC-MS (ESI): t_R = 3.82 min, >95% (area % @ 230 nm), m/z 292 [M + H]$^+$. HR-MS: $C_{21}H_{26}N$ calc. for [M+H]$^+$ 292.2060, found 292.2071.

5-bromo-5H-dibenzo[a,d][7]annulene (21)

A mixture of 5H-dibenzo[a,d][7]annulen-5-ol (3.0 g, 14 mmol) and CH_3COBr (5.8 g, 47 mmol) in EtOAc (3.0 mL) was heated at reflux for 2 h. The resulting mixture was concentrated *in vacuo*. The residue was recrystallized from cyclohexane to yield the title compound as yellow needles

(1.8 g, 46%). ^{1}H NMR (500 MHz, CDCl$_3$) δ 7.51 – 7.42 (m, 4H), 7.42 – 7.35 (m, 4H), 7.19 (s, 2H), 6.53 (s, 1H). LC-MS (ESI): t_R = 5.21 min, >78% (area % @ 230 nm), m/z 191 (benzylic cation).

4-(5H-dibenzo[a,d][7]annulen-5-yl)-1-methylpiperidine (19)[24]

To dry THF (4.0 ml), Mg turnings (0.20 g, 8.4 mmol) were added and the mixture was stirred at 50 °C (10 min). Two crystals of I$_2$ and 1,2-dibromoethane (0.081 g, 0.43 mmol) were added. A vigorous reaction started, which subsided after a few minutes. To the mixture was added 4-chloro-1-methylpiperidine (1.1 g, 8.4 mmol) in THF (5.2 ml) dropwise. The mixture was heated at reflux for 2 h to form Grignard reagent **22.** The mixture was cooled to room temperature. To the mixture was added bromide **21** (1.7 g, 6.3 mmol). The mixture was stirred at room temperature overnight. The mixture was quenched with water and extracted with toluene. The organic layer was washed with water, brine, dried over Na$_2$SO$_4$, filtered and concentrated *in vacuo*. The crude product was purified using flash column chromatography (cyclohexane/EtOAc = 60:40, v/v) to obtain the title compound as a white solid (40 mg, 2 %). ^{1}H NMR (500 MHz, CDCl$_3$) δ 7.32 – 7.27 (m, 4H), 7.25 – 7.20 (m, 4H), 6.88 (s, 2H), 3.56 (d, J =10.7 Hz, 1H), 2.70 (app d, J = 11.4 Hz, 2H), 2.18 (s, 3H), 2.02 – 1.91 (m, 1H), 1.67 (t, J = 11.8 Hz, 2H), 1.21– 1.08 (m, 2H), 1.03 – 0.96 (m, 2H). ^{13}C NMR (126 MHz, CDCl$_3$) δ 140.02, 133.93, 130.92, 130.73, 129.71, 128.54, 126.38, 61.42, 55.81, 46.37, 32.62, 31.61. LC-MS (ESI): t_R = 3.54 min, >99% (area % @ 230 nm), m/z 290 [M + H]$^+$. HR-MS: C$_{21}$H$_{24}$N calc. for [M+H]$^+$ 290.1903, found 290.1911.

2-((10,11-dihydro-5H-dibenzo[a,d][7]annulen-5-yl)oxy)-N,N-dimethylethan-1-amine maleate (10)[20]

Gift from Gist Brocades (The Netherlands). ^{1}H NMR (500 MHz, DMSO-d_6) δ 9.29 (br, 1H), 7.40 (dd, J = 7.2, 2.1 Hz, 2H), 7.27 – 7.22 (m, 2H), 7.21 – 7.12 (m, 4H), 6.02 (s, 2H), 5.55 (s, 1H), 3.62 (t, J = 5.1 Hz, 2H), 3.48 – 3.40 (m, 2H), 3.29 (t, J = 5.2 Hz, 2H), 3.01 – 2.91 (m, 2H), 2.74 (s, 6H). ^{13}C NMR (126 MHz, DMSO-d_6) δ 167.20, 139.14, 137.98, 136.17, 130.29, 128.74, 128.31, 125.90, 83.98 (confirmed by HSQC), 62.73, 55.94, 42.74, 31.45. LC-MS (ESI): t_R = 3.49 min, >99% (area % @ 230 nm), m/z 282 [M + H]$^+$. HR-MS: C$_{19}$H$_{24}$NO calc. for [M+H]$^+$. 282.1852, found 282.1845.

4-(diphenylmethylene)-1-methylpiperidine hydrochloride (12)[21]

Gift from Gist Brocades (The Netherlands). ^{1}H NMR (500 MHz, DMSO-d_6) δ 10.59 (s, 1H), 7.38 – 7.32 (m, 4H), 7.29 – 7.23 (m, 2H), 7.16 – 7.09 (m, 4H), 3.49 – 3.37 (m, 2H), 3.10 – 2.95 (m, 2H), 2.73 (s, 3H), 2.53 – 2.50 (m, 4H). ^{13}C NMR (126 MHz, DMSO-d_6) δ 141.2, 138.0, 129.2, 129.0, 128.4, 127.0, 53.9, 42.2, 28.1. LC-MS (ESI): t_R = 3.48 min, >99% (area % @ 230 nm), m/z 264 [M + H]$^+$ HR-MS: $C_{19}H_{22}N$ calc. for [M+H]$^+$. 264.1747, found 264.1758.

1-(10,11-dihydro-5H-dibenzo[a,d][7]annulen-5-yl)-4-methylpiperazine (15)[22]

Gift from Gist Brocades (The Netherlands). ^{1}H NMR (500 MHz, DMSO-d_6) δ 7.21 – 7.17 (m, 2H), 7.15 (dd, J = 7.3, 1.4 Hz, 2H), 7.13 – 7.10 (m, 2H), 7.09 – 7.04 (m, 2H), 4.00 (s, 1H), 3.95 – 3.83 (m, 2H), 2.78 – 2.68 (m, 2H), 2.51 (s, 3H), 2.44 – 1.78 (m, 8H). ^{13}C NMR (126 MHz, DMSO-d_6) δ 139.31, 139.00, 130.65, 130.43, 127.68, 125.52, 77.78, 54.99, 51.40, 45.71, 30.98. LC-MS (ESI): t_R = 3.48 min, >99% (area % @ 230 nm), m/z 293 [M + H]$^+$. HR-MS: $C_{20}H_{25}N_2$ calc. for [M+H]$^+$ 293.2012, found 293.2004.

1-(5H-dibenzo[a,d][7]annulen-5-yl)-4-methylpiperazine (16)[21]

Gift from Gist Brocades (The Netherlands). ^{1}H NMR (500 MHz, DMSO-d_6) δ 7.48 – 7.39 (m, 4H), 7.39 – 7.25 (m, 4H), 6.97 (s, 2H), 4.34 (s, 1H), 2.12 – 1.68 (br m, 11H). ^{13}C NMR (126 MHz, DMSO-d_6) δ 137.95, 134.08, 130.32, 129.92, 129.44, 128.09, 127.05, 76.68, 54.47, 51.05, 45.62. LC-MS (ESI): t_R = 5.49 min, >99% (area % @ 230 nm, basic mode), m/z 291 [M + H]$^+$. HR-MS: $C_{20}H_{23}N_2$ calc. for [M+H]$^+$ 291.1856, found 191.0879 (benzylic cation).

4-(5H-dibenzo[a,d][7]annulen-5-ylidene)-1-methylpiperidine hydrochloride (14)[25]

Gift from Gist Brocades (The Netherlands). ^{1}H NMR (400 MHz, DMSO-d6) δ 10.34 (br s, 1H), 7.46 – 7.38 (m, 4H), 7.36 – 7.29 (m, 2H), 7.29-7.23 (m, 2H), 7.00 (s, 2H), 3.35-3.20 (br, 4H), 2.68 (br s, 3H), 2.58-2.47 (br, 2H), 2.38-2.06 (br, 2H). ^{13}C NMR (126 MHz, CDCl$_3$) δ 137.59, 137.55, 137.44, 134.69, 134.44, 131.06, 130.98, 128.88, 128.50, 128.21, 128.15, 128.04, 127.23, 127.19, 127.11,

55.80, 55.39, 43.69, 42.95, 26.84, 26.59. All ^{13}C peaks for both conformers are listed. Conformers are known for this compound in NMR analysis in CDCl$_3$.[43] LC-MS (ESI): t_R = 3.65 min, >99% (area % @ 230 nm), m/z 288 [M + H]$^+$. HR-MS: C$_{21}$H$_{21}$N calc. for [M+H]$^+$ 288.1747, found 288.1749.

Acknowledgements

Abbreviations

THF, tetrahydrofuran; TEA, triethylamine; DCM, dichloromethane; DMSO, dimethylsulfoxide; GPCR, G protein-coupled receptors; H$_1$R, histamine H1 receptor; SAR, structure-affinity relationship; SKR, structure-kinetics relationship; RT, residence time.

References

1.	Hoffmann, C.; Castro, M.; Rinken, A.; Leurs, R.; Hill, S. J.; Vischer, H. F., Ligand residence time at GPCRs - why we should take our time to study it. *Molecular Pharmacology* **2015,** *88* (3), 552-560.
2.	Swinney, D. C., Biochemical mechanisms of drug action: what does it take for success? *Nature Reviews Drug Discovery* **2004,** *3*, 801.
3.	Copeland, R. A., The drug–target residence time model: a 10-year retrospective. *Nature Reviews Drug Discovery* **2015,** *15*, 87.
4.	Lu, H.; Tonge, P. J., Drug–target residence time: critical information for lead optimization. *Current Opinion in Chemical Biology* **2010,** *14* (4), 467-474.
5.	Dong, G.; Thea, M.-K.; P, I. A.; H, H. L., Functional efficacy of adenosine A2A receptor agonists is positively correlated to their receptor residence time. *British Journal of Pharmacology* **2012,** *166* (6), 1846-1859.
6.	Gillard, M.; Van Der Perren, C.; Moguilevsky, N.; Massingham, R.; Chatelain, P., Binding characteristics of cetirizine and levocetirizine to human H1 histamine receptors: contribution of Lys191 and Thr194. *Molecular Pharmacology* **2002,** *61* (2), 391-399.
7.	Guo, D.; IJzerman, A. P., Molecular basis of ligand dissociation from G protein-coupled receptors and predicting residence time. In *Computational Methods for GPCR Drug Discovery*, Heifetz, A., Ed. Springer New York: New York, NY, 2018; pp 197-206.
8.	Tautermann, C. S.; Kiechle, T.; Seeliger, D.; Diehl, S.; Wex, E.; Banholzer, R.; Gantner, F.; Pieper, M. P.; Casarosa, P., Molecular basis for the long duration of action and kinetic selectivity of tiotropium for the muscarinic M3 receptor. *Journal of Medicinal Chemistry* **2013,** *56* (21), 8746-8756.
9.	Miller, D. C.; Lunn, G.; Jones, P.; Sabnis, Y.; Davies, N. L.; Driscoll, P., Investigation of the effect of molecular properties on the binding kinetics of a ligand to its biological target. *MedChemComm* **2012,** *3* (4), 449-452.

10.   Pan, A. C.; Borhani, D. W.; Dror, R. O.; Shaw, D. E., Molecular determinants of drug–receptor binding kinetics. *Drug Discovery Today* **2013,** *18* (13), 667-673.

11.   Tresadern, G.; Bartolome, J. M.; Macdonald, G. J.; Langlois, X., Molecular properties affecting fast dissociation from the D2 receptor. *Bioorganic & Medicinal Chemistry* **2011,** *19* (7), 2231-2241.

12.   Veber, D. F.; Johnson, S. R.; Cheng, H.-Y.; Smith, B. R.; Ward, K. W.; Kopple, K. D., Molecular properties that influence the oral bioavailability of drug candidates. *Journal of Medicinal Chemistry* **2002,** *45* (12), 2615-2623.

13.   Schmidtke, P.; Luque, F. J.; Murray, J. B.; Barril, X., Shielded hydrogen bonds as structural determinants of binding kinetics: application in drug design. *Journal of the American Chemical Society* **2011,** *133* (46), 18903-18910.

14.   Bosma, R.; Moritani, R.; Leurs, R.; Vischer, H. F., BRET-based β-arrestin2 recruitment to the histamine H1 receptor for investigating antihistamine binding kinetics. *Pharmacological Research* **2016,** *111*, 679-687.

15.   Bosma, R.; Witt, G.; Vaas, L. A. I.; Josimovic, I.; Gribbon, P.; Vischer, H. F.; Gul, S.; Leurs, R., The target residence time of antihistamines determines their antagonism of the G protein-coupled histamine H1 receptor. *Frontiers in Pharmacology* **2017,** *8* (667).

16.   Anthes, J. C.; Gilchrest, H.; Richard, C.; Eckel, S.; Hesk, D.; West, R. E.; Williams, S. M.; Greenfeder, S.; Billah, M.; Kreutner, W.; Egan, R. W., Biochemical characterization of desloratadine, a potent antagonist of the human histamine H1 receptor. *European Journal of Pharmacology* **2002,** *449* (3), 229-237.

17.   Gillard, M.; Chatelain, P., Changes in pH differently affect the binding properties of histamine H1 receptor antagonists. *European Journal of Pharmacology* **2006,** *530* (3), 205-214.

18.   Bosma, R.; Stoddart, L. A.; Georgi, V.; Bouzo-Lorenzo, M.; Bushby, N.; Inkoom, L.; Waring, M. J.; Briddon, S. J.; Vischer, H. F.; Sheppard, R. J.; Fernández-Montalván, A.; Hill, S. J.; Leurs, R., Probe dependency in the determination of ligand binding kinetics at a prototypical G protein-coupled receptor. *Scientific Reports* **2019,** *9* (1), 7906.

19.   Kuhne, S.; Kooistra, A. J.; Bosma, R.; Bortolato, A.; Wijtmans, M.; Vischer, H. F.; Mason, J. S.; de Graaf, C.; de Esch, I. J. P.; Leurs, R., Identification of ligand binding hot spots of the histamine H1 receptor following structure-based fragment optimization. *Journal of Medicinal Chemistry* **2016,** *59* (19), 9047-9061.

20.   van Der Stelt, C.; Harms, A. F.; Nauta, W. T., The effect of alkyl-substitution in drugs--V. synthesis and chemical properties of some dibenzo [a,d]1,4-cycloheptadienyl ethers. *Journal of Medicinal Chemistry* **1961,** *4* (2), 335-349.

21.   Fujiwara, T.; Ohira, K.; Urushibara, K.; Ito, A.; Yoshida, M.; Kanai, M.; Tanatani, A.; Kagechika, H.; Hirano, T., Steric structure–activity relationship of cyproheptadine derivatives as inhibitors of histone methyltransferase Set7/9. *Bioorganic & Medicinal Chemistry* **2016,** *24* (18), 4318-4323.

22.   Naporra, F.; Gobleder, S.; Wittmann, H.-J.; Spindler, J.; Bodensteiner, M.; Bernhardt, G.; Hübner, H.; Gmeiner, P.; Elz, S.; Strasser, A., Dibenzo[b,f][1,4]oxazepines and dibenzo[b,e]oxepines: Influence of the chlorine substitution pattern on the pharmacology at the H1R, H4R, 5-HT2AR and other selected GPCRs. *Pharmacological Research* **2016,** *113*, 610-625.

23.   Ismaiel, A. M.; Arruda, K.; Teitler, M.; Glennon, R. A., Ketanserin analogs: The effect of structural modification on 5-HT2 serotonin receptor binding. *Journal of Medicinal Chemistry* **1995,** *38* (7), 1196-1202.

24.   Young, S. D.; Baldwin, J. J.; Cochran, D. W.; King, S. W.; Remy, D. C.; Springer, J. P., Conformational mobility of dibenzo[a,d]cycloheptene derivatives. Preparation and characterization of two intraconverting conformational isomers. *The Journal of Organic Chemistry* **1985,** *50* (3), 339-342.

25.   Wolf, C.; Schunack, W., Synthesis and pharmacology of combined histamine H1-/H2-receptor antagonists containing diphenhydramine and cyproheptadine derivatives. *Archiv der Pharmazie* **1996,** *329* (2), 87-94.

26.   Taylor, Buck. L. H.; Harris, Michael. R.; Jarvo, Elizabeth. R., Synthesis of enantioenriched triarylmethanes by stereospecific cross-coupling reactions. *Angewandte Chemie International Edition* **2012,** *51* (31), 7790-7793.

27.   Kawamura, Y.; Iwano, Y.; Watanabe, N.; Horie, T.; Tsukayama, M., Reactivity of methylenetriphenylphosphoranes having two phenyl groups constrained with ethano or etheno or bridge.. *Phosphorus, Sulfur, and Silicon and the Related Elements* **1998,** *132* (1), 167-181.

28.   Engelhardt, E. L.; Zell, H. C.; Saari, W. S.; Christy, M. E.; Colton, C. D.; Stone, C. A.; Stavorski, J. M.; Wenger, H. C.; Ludden, C. T., Structure-activity relationships in the cyproheptadine series. *Journal of Medicinal Chemistry* **1965,** *8* (6), 829-835.

29.   Motulsky, H. J.; Mahan, L. C., The kinetics of competitive radioligand binding predicted by the law of mass action. *Molecular Pharmacology* **1984,** *25* (1), 1-9.

30.   Bosma, R.; Mocking, T.; Leurs, R.; Vischer, H., Ligand-Binding Kinetics on Histamine Receptors (2017), in: Tiligada, E., Ennis, M. (Eds.), Histamine Receptors as Drug Targets. Springer New York, New York, NY, pp. 115–155.

31.   Bosma, R.; Wang, Z.; Kooistra, A. J.; Bushby, N.; Kuhne, S.; van den Bor, J.; Waring, M. J.; de Graaf, C.; de Esch, I. J.; Vischer, H. F.; Sheppard, R. J.; Wijtmans, M.; Leurs, R., Route to prolonged residence time at the histamine H1 receptor: Growing from desloratadine to rupatadine. *Journal of Medicinal Chemistry* **2019,** *62* (14), 6630-6644.

32.   Simons, F. E. R.; Simons, K. J., Histamine and H1-antihistamines: Celebrating a century of progress. *Journal of Allergy and Clinical Immunology* **2011,** *128* (6), 1139-1150.e4.

33.   Simons, F. E. R., Advances in H1-antihistamines. *New England Journal of Medicine* **2004,** *351* (21), 2203-2217.

34.   Parsons, M. E.; Ganellin, C. R., Histamine and its receptors. *British Journal of Pharmacology* **2006,** *147* (S1), S127-S135.

35.   Huang, Z.-L.; Mochizuki, T.; Qu, W.-M.; Hong, Z.-Y.; Watanabe, T.; Urade, Y.; Hayaishi, O., Altered sleep–wake characteristics and lack of arousal response to H3 receptor antagonist in histamine H1 receptor knockout mice. *Proceedings of the National Academy of Sciences* **2006,** *103* (12), 4687-4692.

36.   Ikeda-Sagara, M.; Ozaki, T.; Shahid, M.; Morioka, E.; Wada, K.; Honda, K.; Hori, A.; Matsuya, Y.; Toyooka, N.; Ikeda, M., Induction of prolonged, continuous slow-wave sleep by blocking cerebral H1 histamine receptors in rats. *British Journal of Pharmacology* **2012,** *165* (1), 167-182.

37.   Parmentier, R.; Zhao, Y.; Perier, M.; Akaoka, H.; Lintunen, M.; Hou, Y.; Panula, P.; Watanabe, T.; Franco, P.; Lin, J.-S., Role of histamine H1-receptor on behavioral states and wake maintenance during deficiency of a brain activating system: A study using a knockout mouse model. *Neuropharmacology* **2016,** *106*, 20-34.

38.   Xia, L.; Burger, W. A. C.; van Veldhoven, J. P. D.; Kuiper, B. J.; van Duijl, T. T.; Lenselink, E. B.; Paasman, E.; Heitman, L. H.; Ijzerman, A. P., Structure–affinity relationships and structure–kinetics relationships of pyrido[2,1-f]purine-2,4-dione derivatives as human adenosine A3 receptor antagonists. *Journal of Medicinal Chemistry* **2017,** *60* (17), 7555-7568.

39.   Xia, L.; Kyrizaki, A.; Tosh, D. K.; van Duijl, T. T.; Roorda, J. C.; Jacobson, K. A.; Ijzerman, A. P.; Heitman, L. H., A binding kinetics study of human adenosine A3 receptor agonists. *Biochemical Pharmacology* **2018,** *153*, 248-259.

40.   Mocking, T. A. M.; Verweij, E. W. E.; Vischer, H. F.; Leurs, R., Homogeneous, real-time nanoBRET binding assays for the histamine H3 and H4 receptors on living cells. *Molecular Pharmacology* **2018,** *94* (6), 1371-1381.

41.   Yung-Chi, C.; Prusoff, W. H., Relationship between the inhibition constant (KI) and the concentration of inhibitor which causes 50 per cent inhibition (I50) of an enzymatic reaction. *Biochemical Pharmacology* **1973,** *22* (23), 3099-3108.

42.   Baell, J. B.; Holloway, G. A., New substructure filters for removal of pan assay interference compounds (PAINS) from screening libraries and for their exclusion in bioassays. *Journal of Medicinal Chemistry* **2010,** *53* (7), 2719-2740.

43.   Sadek, M.; Craik, D. J.; Hall, J. G.; Andrews, P. R., Conformational analysis of cyproheptadine hydrochloride. *Journal of Medicinal Chemistry* **1990,** *33* (4), 1098-1107.

Chapter 4

Bioisosteric replacements of a carboxylic acid to explore binding kinetics on the histamine H$_1$ receptor

Zhiyong Wang, Sebastiaan Kuhne, Reggie Bosma, Daniel Da Costa Pereira, Philipp Fronik, Marc Stroet, Melanie van der Woude, Ivana Josimovic, Loretta Inkoom, Mounir Andaloussi, Henry F. Vischer, Iwan J. P. de Esch, Maikel Wijtmans and Rob Leurs

Abstract

Drug-target binding kinetics have gained increasing interest in predicting *in vivo* drug efficacy. Yet, structural ligand factors governing drug-target residence time are poorly understood and general insights for the design of small molecules with slow off-rate are therefore scarce. It has been hypothesised that the key ionic interaction between the carboxylic acid of histamine H_1R ligand levocetirizine and a lysine residue in phosphate pocket of the H_1R receptor can contribute to prolonged residence time. Here, we explored the effect of potential bioisosteric replacements in a carboxylic acid-containing ligand on H_1R binding kinetics. Common non-acidic and acidic isosteres as well as a tailored set of sulfonyl-containing ligands were designed and synthesized. Pharmacological evaluations showed that all isosteres have similar binding affinity but that acidic isosteres have longer RT than most non-acidic ones. The use of an acylphenylsulfonamide isostere was successfully demonstrated on the marketed H_1R drug levocetirizine. This work contributes to understanding structural factors underlying drug-target residence time of H_1R ligands.

Introduction

The binding affinity of a drug candidate to its target is an important metric for drug discovery to rank its potential. However, ligand-binding kinetics also play a key role in the drug discovery process.[1] Ligand binding kinetics are characterized by the association rate constant (k_{on}) and dissociation rate constant (k_{off}) that together determine the equilibrium dissociation constant K_d (k_{off}/k_{on}). A parameter that reflects how long the ligand-receptor complex persists is the residence time (RT), defined as the reciprocal of the k_{off} value. The kinetic binding parameters are increasingly thought to predict better the *in vivo* efficacy of a drug[2-5] and as such have gained interest in hit optimisation. Yet, the ligand factors that affect binding kinetics are not yet optimally understood. Over the years, several ligand features have been postulated to play a role in binding kinetics, for example, cyclization elements (Chapter 3), number of rotatable bonds and number of ring structures.[6, 7] Other molecular determinants which can govern the kinetics binding rate constants are, for instance, a shielded hydrogen bond,[8] a halogen bond,[9] and covalent binding.[10]

As the target of 30% of currently marketed drugs, G protein-coupled receptors (GPCRs) play a significant role in many physiological processes and are a very important class of proteins in drug discovery.[11-13] Conventional structure-activity relationships (SAR) have been widely explored in GPCR medicinal chemistry. In contrast, the study of structure-kinetics relationships (SKR) of ligands for GPCRs have been less widely investigated and reported.[14] The histamine H_1 receptor (H_1R) is an archetypical aminergic GPCR and SAR concerning H_1R has been extensively investigated for decades, leading to several blockbuster drugs.[15-17] The first-generation ligand

doxepin has been crystallized in H_1R.[18] The structure reveals that the amine moiety of doxepin interacts with the hallmark $D107^{3.32}$ residue of the receptor. The aromatic moieties of the ligand are accommodated by the aromatic residues in hydrophobic pockets that are formed by (mostly) aromatic residues. In the crystal structure, a phosphate ion was identified as binding between the orthosteric pocket and the extracellular vestibule containing the residues $K191^{5.39}$, $K179^{45.49}$, $H435^{7.35}$ and $Y431^{6.51}$. It has been proposed that some of the second-generation antihistamines occupy this 'phosphate pocket' with their anionic carboxylate group and thermodynamic studies addressing the roles of $K191^{5.39}$ and $K179^{45.49}$ in binding a select set of H_1R ligands have recently been disclosed.[15, 18, 19] The availability of the crystal structure combined with the wealth of available (clinical) small-molecule ligands renders H_1R a highly suitable benchmark GPCR for kinetic studies. For example, studies have shown that the second-generation antihistamine levocetirizine has a residence time longer than its methyl ester[20] and longer than other antihistamines, such as doxepin (Figure 1). One suggestion is that levocetirizine can modulate the binding kinetics via the ionic interaction between its carboxylic acid and the lysine $K191^{5.39}$ residue, which can slow down the dissciation.[20]

Doxepin
pK_i = 9.6
RT = 26 min

Levocetirizine
pK_i = 8.1
RT = 92 min

3
pK_i = 8.1
RT = 23 min
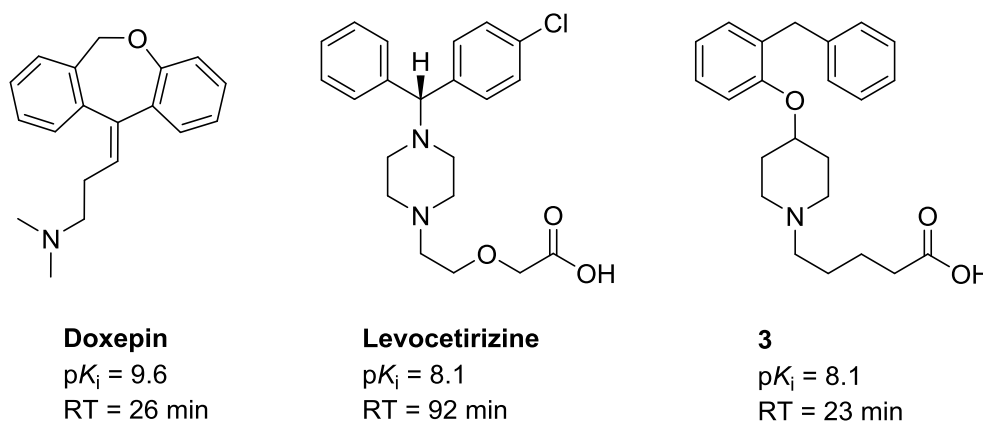
Figure 1. Selected H_1R antagonists and associated binding affinities (pK_i) and kinetic residence times (RT).[21, 22]

In general, the carboxylic acid moiety plays an important role in drug design[23] and more than 450 marketed drugs contain the carboxylic acid functional group.[24, 25] Nonetheless, medicinal chemists have explored various approaches to improve the physicochemical properties, metabolic stability and biological activities of carboxylic acid-containing ligands in drug discovery.[25, 26] The replacement of the carboxylic acid moiety with a suitable bioisostere, i.e. an alternative group that upon incorporation in the ligand gives rise to similar desired biological properties as the carboxylic acid parent compound, can be an effective strategy in medicinal chemistry. Various bioisosteric replacements for carboxylic acids have been reported to study SAR and affinity has often been the metric involved.[25, 26] However, the SKR of carboxylic acid

isosteric replacements has to our knowledge not been investigated in drug discovery. Predicting such a SKR outcome will be challenging as acidity, size, shape, charge distribution as well as lipophilicity, are all thought to play significant roles in the properties of the isostere.[26] Therefore, an experimental study addressing this will be of value to the field.

As part of our ongoing program in delineating factors governing the kinetic properties of H_1R ligands,[27-30] the aim of present study is to investigate the effect of bioisosteric replacements in a carboxylic acid-containing ligand on binding kinetics on H_1R. To this end, compound **3**[22] was selected as the starting compound (Figure 1 and 2), which has emerged after exploration of a carboxylic acid on a virtual screening hit **1**[31, 32] connected by different linker lengths and which has a longer residence time than the N-methyl analogue of **1** (i.e. **25**).[22] In the current study, putative targeting of the phosphate pocket by **3** using isosteric replacements with non-acidic and acidic moieties and exploration of the effect on binding kinetics were pursued.
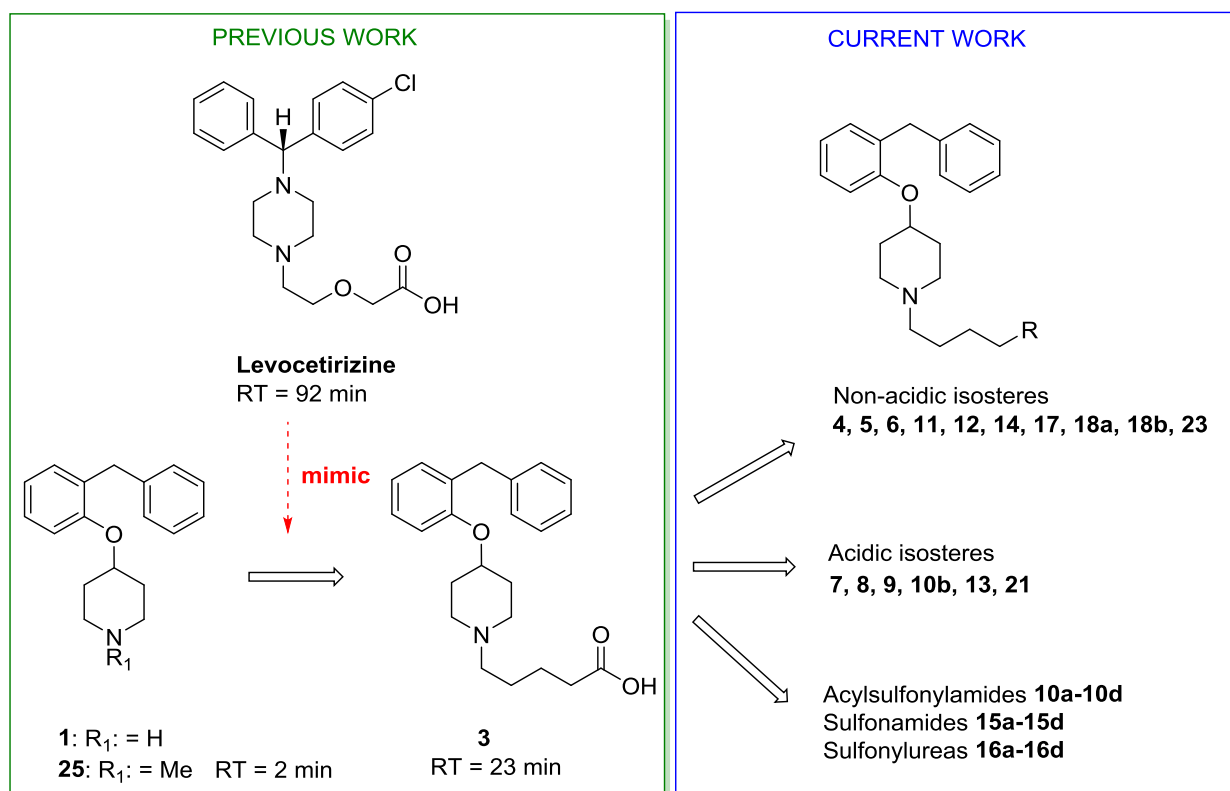

**Figure 2.** General strategy of the current study.[21, 22]

Results & Discussion

Design

Despite the longer residence time of **3** compared to **25**, the residence time of **3** (23 min) at the H_1R is still 4-fold shorter compared to levocetirizine (92 min). We designed a series of analogues of **3** with bioisosteric replacements (Figure 2). Throughout the manuscript, we chose to use the term 'acidic' for compounds having a calculated pK_a value < 7.4 for the acid bioisostere. These compounds are expected to display significant zwitter-ionic character at pH 7.4 owing to the tertiary amine present elsewhere in the molecule. We first explored a series of non-acidic moieties, although formally these may not fulfill the stricter definition of 'acid bioisostere'. This series includes an ester, an alcohol, a nitrile, a primary amide, a hydroxamic acid, a squaric acid/ester/amide and a boronic acid, with a ligand having a basic moiety (i.e. primary amine) serving as negative control. The second series comprised a selected set of acidic bioisosteres[25, 26], including a cyanamide, a tetrazole, a sulphonic acid, and three acylsulfonylamides. The final set of series focused on acylsulfonylamides and closely related sulfonyl moieties such as sulfonylureas and the less acidic sulfonamides. The compounds together with calculated pK_a values (ChemAxon) are shown in Tables 1-3.

Synthesis

The utilised syntheses are shown in scheme 1. Amine **1** was prepared as described by us.[31] Alkylation of **1** to ethyl ester **2** and subsequent hydrolysis afforded carboxylic acid **3**, which was treated with AcCl and MeOH to afford ester methyl ester **4**. A variety of amide coupling conditions with the appropriate nucleophiles were used to transform **3** to compounds **5-9** and **10a-d**. Fragment **1** was alkylated using 5-bromopentan-1-ol and 5-bromopentanenitrile to afford alcohol **11** and nitrile **12**, respectively. The latter was treated with NaN_3 and NH_4Cl to obtain tetrazole **13**, or reduced with $LiAlH_4$ and $AlCl_3$ to provide primary amine **14**.[33] In the presence of TEA, **14** was reacted with sulfonyl chlorides to yield sulfonamides **15a-d**.[34] Sulfonylureas **16a** and **16c-d** were obtained by reacting **14** with various sulfonylcarbamates **20**,[35] which were prepared from sulfonamides **19** and ethyl carbonochloridate,[36] while **16b** was obtained by reacting **14** and benzenesulfonyl isocyanate.[37] Reaction of **14** with 3,4-diethoxycyclobut-3-ene-1,2-dione gave **17**.[38] Hydrolysis of **17** afforded **18a**,[39] while treating **17** with $EtNH_2$ afforded **18b**.[40] Reaction of **1** with 1,2-oxathiane 2,2-dioxide afforded sulfonic acid **21**.[41] Alkylation of amine **1** by 4-bromobut-1-ene provided **22**, treatment of which with BCl_3 gave boronic acid **23**, which was purified by protection as its MIDA derivative and subsequent deprotection. Compound **24** was prepared by a HATU-coupling between phenylsulfonamide and levocetirizine.
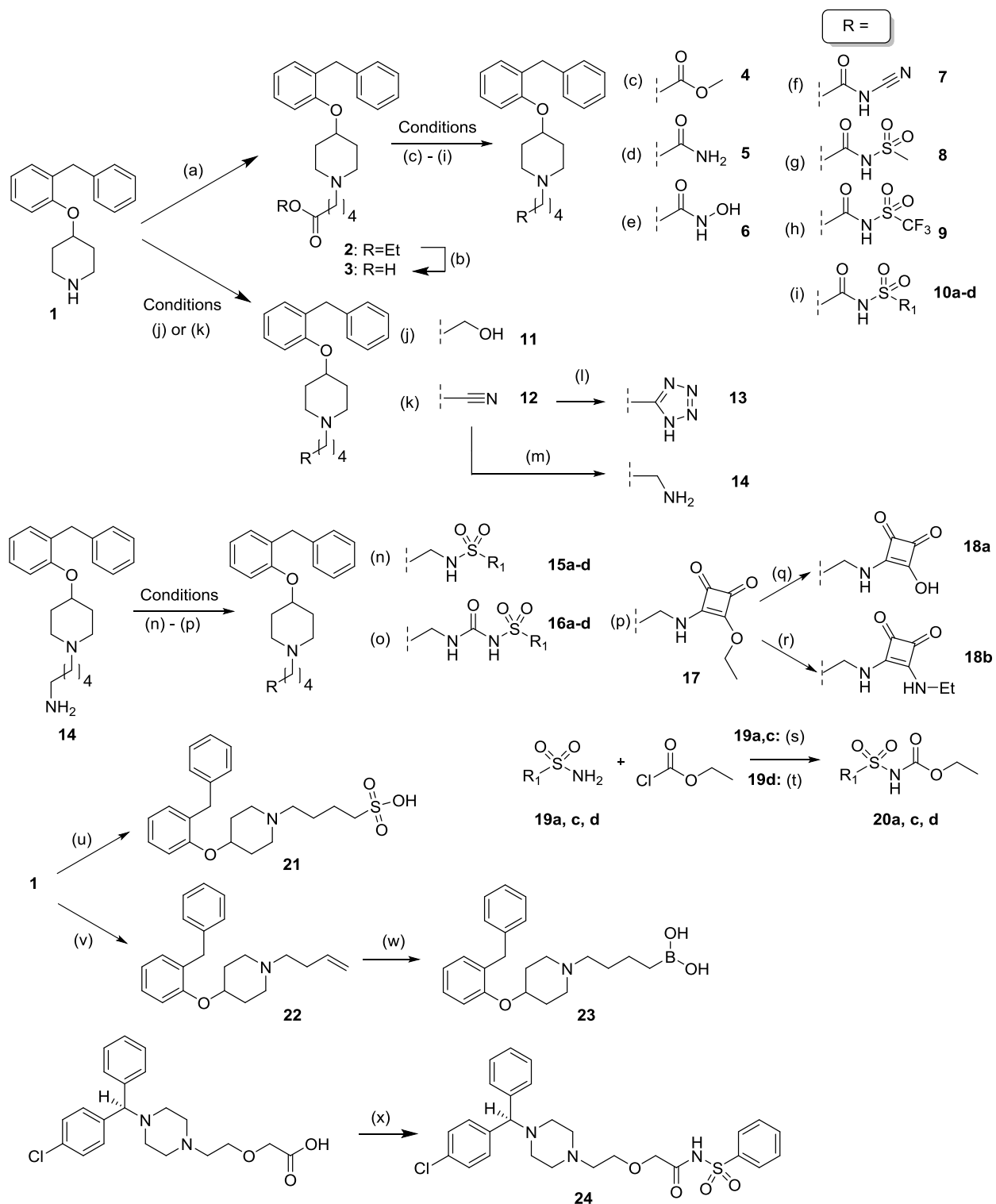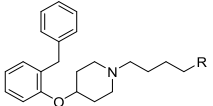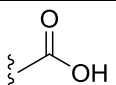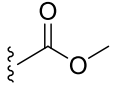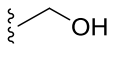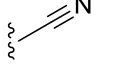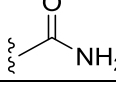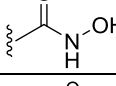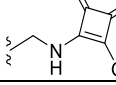
Scheme 1 Synthesis of ligands to target the phosphate pocket with carboxylic acid (bio)isosteres. Reagents and conditions: (a) Ethyl 5-bromopentanoate, K_2CO_3, DMF, 80 °C, 4 h, 82%. (b) 1.0 M NaOH, MeOH, reflux, 2.5 h, 91% as HCl salt. (c) AcCl, MeOH, rt, 30 min, 91%. (d) EDCI·HCl, HOBt, TEA, 1.0 M NH_3 in dioxane, DCM, rt, 16 h, 42%. (e) (1) EDCI·HCl, O-(*tert*-butyldimethylsilyl)-hydroxylamine, DCM, rt, 16 h, (2) TFA, DCM, 0 °C, 5 h; 64%. (f) EDCI·HCl, DMAP, DIPEA, NH_2CN, DCM, rt, 16 h, 29%. (g) EDCI·HCl, DMAP, DIPEA, $CH_3SO_2NH_2$, rt, 16 h, 39%. (h) EDCI·HCl, HOBt, DIPEA, $CF_3SO_2NH_2$, rt, 16 h, 27%. (i) **10a, 10c, 10d**: EDCI·HCl, sulfonamide, DMAP, rt, 8 h, 16-36%; **10b**: EDCI·HCl, HOBt, DIPEA, $PhSO_2NH_2$, rt, 16 h, 27%. (j) 5-bromopentan-1-ol, TEA, MeCN, 65 °C, 1 h, 72%. (k) 5-bromopentanenitrile, K_2CO_3, DMF, 85 °C, 2 h, 49%. (l) NaN_3, NH_4Cl, DMF, 100 °C, 72 h, 28%. (m) $AlCl_3$, $LiAlH_4$, THF, 6 h, rt, 43%. (n) sulfonyl chloride, TEA, DCM, rt, 24 h, 20-40%. (o) **16a, 16c, 16d**: substituted sulfonylcarbamate **20a,c,d**, MeCN, reflux, 18 h, 8-10%; **16b**: benzenesulfonyl isocyanate, TEA, MeCN, rt, 1 h, 26%. (p) 3,4-diethoxycyclobut-3-ene-1,2-dione, TEA, EtOH, 30 h, rt, 56%. (q) 4.0 N HCl in dioxane, THF, rt, 20 h, 70%. (r) TEA, $EtNH_2$.HCl, EtOH, 14 h, rt, 75%. (s) (1) TEA, DCM, 5 °C, 2 h, (2) rt, 4 h; 51-71%. (t) (1) K_2CO_3, acetone, rt, 3 h, (2) reflux, 18 h; 48%. (u) (1) 1,2-oxathiane 2,2-dioxide, MeCN, 48 h, reflux, (2) KO*t*Bu, reflux, 2 h; 49%. (v) 4-bromobut-1-ene, K_2CO_3, MeCN, 3 h, reflux, 65%. (w) (1) BCl_3 (1.0 M in DCM), Et_3SiH, DCM, 0 °C, 2 h, (2) 2,2'-(methylazanediyl)diacetic acid, DMF, 80 °C, 1 h, (3) 1.0 M NaOH, MeOH, rt, 12 h; 53%. (x) $PhSO_2NH_2$, HATU, DIPA, DMF, rt, 23 h, 62%.

Pharmacology

All synthesized compounds were evaluated for their equilibrium binding constant (K_i) on homogenates of HEK293T cells transiently expressing the human H_1R using [^3H]mepyramine as radioligand and levocetirizine as control. To evaluate binding kinetics, the Kinetic Rate Index (KRI) parameter was used.[42] We have used this parameter previously in a study on the binding kinetics of a series of rupatadine analogues.[27] While this parameter is not optimal for quantitative kinetic measurements, the experimental setup allows for efficient screening and ranking of compounds based on fast or slow dissociation. Tables 1-3 show the binding affinities and KRI data as well as the calculated pK_a (ChemAxon).
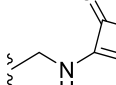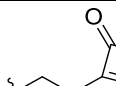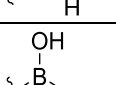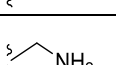
It was found that all compounds with non-acidic isosteres (Table 1) show good binding affinity (pK_i 7.4 to 8.5). Ligands with an ester (**4**), alcohol (**11**), nitrile (**12**), amide (**5**), hydroxamate (**6**), boronic acid (**23**) and amine (**14**) show KRI values between 1.2 and 1.6 and therefore appear to convey a slightly shorter residence time than the parent acid **3** (KRI = 2.3). It is evident that the number of potential H-bond acceptors and donors does not seem to have an effect in this subseries. On the other hand, ligands with a squaric acid (**18a**), squaric ester (**17**) and squaramide (**18b**) have a KRI value between 3.1 to 4.7, suggesting slower dissociation than the latter group of compounds. Since the predicted pK_a values suggest that the compounds in Table 1 contain no groups substantially ionized at pH 7.4, it is assumed none of these could make an ionic interaction with the lysine K191[5.39] in phosphate binding pocket. However, **18a**, **17** and **18b** harbour a distinct and relatively large group and the size and physicochemical properties of the squaric moiety will also contribute to the biological properties.

Table 1. Pharmacological characterization of non-acidic derivatives binding at the H_1R.
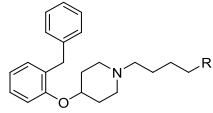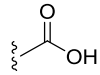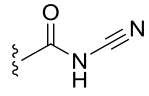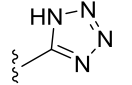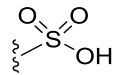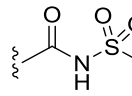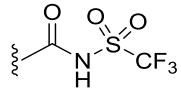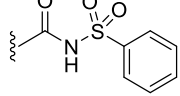
#	compound	R	p$K_{a, calc}$ [a]	p$K_i \pm$ SD	KRI $\pm$ SD
Levocetirizine		--	4.73	8.1 ± 0.1	4.0 ± 0.9
3	VUF14506		4.73	7.8 ± 0.1	2.3 ± 0.4
4	VUF15009		-[c]	8.0 ± 0.1	1.6 ± 0.3
11 [b]	VUF14901		-[c]	7.9 ± 0.1	1.2 ± 0.3
12 [b]	VUF14902		-[c]	7.9 ± 0.1	1.3 ± 0.5
5 [b]	VUF15010		-[c]	8.1 ± 0.2	1.2 ± 0.2
6 [b]	VUF15011		8.90	7.8 ± 0.0	1.2 ± 0.2
18a	VUF16335		8.17	7.4 ± 0.1	3.1 ± 0.2
17	VUF16336		-[c]	8.2 ± 0.2	4.7 ± 2.1
18b	VUF16414		-[c]	8.0 ± 0.1	4.4 ± 0.6
23	VUF16221		10.40 [d]	8.5 ± 0.1	1.2 ± 0.1
14	VUF16394		-[e]	7.6 ± 0.1	1.2 ± 0.1

[a]Calculated values using ChemAxon. [b]Tested as fumarate salt. [c] No ionizable or acidic group identified by ChemAxon. [d]Obtained for methylboronic acid from Babcock *et al.*[43] [e]This compound is basic.

The pharmacological properties of ligands with acidic isosteres (**21**, **7**-**9**, **13, 10b**) are collected in Table 2. The binding affinities (pK_i = 7.4 to 8.1) are similar to that of acid **3**. All KRI values are ⬜ 2.0, indicating slow dissociation. The acidic isosteres in Table 2 were also subjected to a pK_a analysis. Compounds **10b**, **7**, **8** and **13** have pK_a values similar that of the carboxylic acid, while compounds **9** (pK_a = 3.1) and especially the sulfonic acid **21** (pK_a = -0.79) are stronger acids than

3. However, there is no evident correlation between acidity of the isostere and the dissociation patterns. Collectively, based on the affinity and KRI values, **10b** attracted our attention for several reasons. First, it combines good affinity with slow dissociation (pK_i = 7.8, KRI = 5.9). Second, compared to other compounds with high KRI values (e.g. **17** and **18b**), **10b** offers a clear potential for growth vector owing to its sulfonamide substituent. Thus, **10b** was chosen for further exploration. A subseries of ligands differing in substituent size (cyclopropyl, phenyl, *tert*-butylphenyl, naphtyl) was designed and prepared (**10**). To also address roles for the atoms of the acidic moiety as potential pharmacophoric elements, two additional sulfonyl subseries (i.e. sulfonamides **15** and sulfonylureas **16**) with the same four substituents were designed and synthesized. It is of interest to point out that sulfonamides have been incorporated before in H_1R ligands, but not as a designed isostere for an acid and not in the context of binding kinetics.[44]
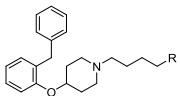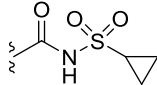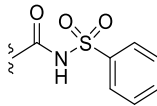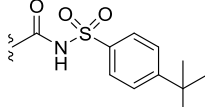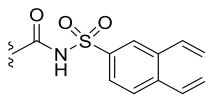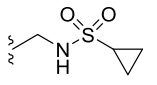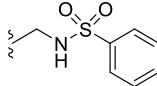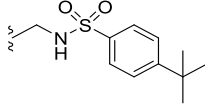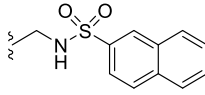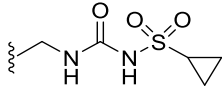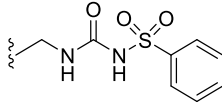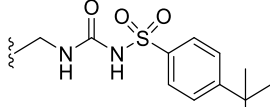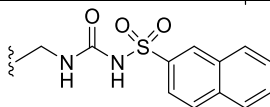
Table 2. Pharmacological characterization of acidic isosteres binding at the H_1R.

#	compound		$pK_{a, calc}$ [a]	$pK_i \pm SD$	KRI $\pm$ SD
Levocetirizine		--	4.73	8.1 ± 0.1	4.0 ± 0.9
3	VUF14506		4.73	7.8 ± 0.1	2.3 ± 0.4
7	VUF14991		4.52	7.5 ± 0.1	2.9 ± 1.0
13	VUF14989		5.08	8.1 ± 0.1	3.1 ± 0.5
21	VUF16317		-0.79	7.6 ± 0.0	2.7 ± 0.5
8	VUF14990		4.08	7.4 ± 0.1	2.0 ± 0.2
9	VUF15037		3.11	7.5 ± 0.0	2.5 ± 0.5
10b	VUF15290		4.28	7.8 ± 0.1	5.9 ± 0.7

[a] Calculated values using ChemAxon.

Table 3 shows pK_a, pK_i and KRI values for the three sulfonyl subseries. Acylsulfonamides with aromatic substitutions (**10b-d**) have slightly higher binding affinities (pK_i 7.7 to 7.8) than the cyclopropyl-substituted acylsulfonamide **10a** (pK_i = 7.3). Ligands **10a** and **10b** show a larger KRI value (KRI = 5.2 to 5.9) than that of compounds **10c** and **10d** with bigger substituents (KRI = 2.4 to 2.8). As expected since sulfonamides **15a-d** involve removal of the carbonyl moiety from the **10** subseries, **15a**-**d** have a much higher pK_a value than **10a-d** and are essentially non-acidic. Within this subseries, the phenyl-substituted sulfonamide (**15b**) has a slightly higher binding affinity (pK_i = 8.4) than the cyclopropyl-, *tert*-butylphenyl- and naphthyl-substituted compounds **15a,c,d** (pK_i = 7.8 to 8.1). Both **15a** (KRI = 4.9) as well as **15b-d** (KRI = 2.6 to 3.7) have large KRI values. Last, the sulfonylurea subseries **16** has similar pK_a values as **10**. Compounds in this subseries have acceptable binding affinities (pK_i = 7.6 to 8.1). Notably, **16c** shows a shorter KRI value (KRI = 1.9) than **16a,b,d** (KRI = 5.4 – 5.8), indicating that **16c** dissociates faster.

Table 3. Pharmacological characterization of acylsulfonamides, sulfonamides and sulfonylureas binding at the H_1R.

#	compound		$pK_{a,calc}$ [a]	$pK_i \pm$ SD	KRI $\pm$ SD
--	Levocetirizine	---	4.73	8.1 ± 0.1	4.0 ± 0.9
10a	VUF16329		4.06	7.3 ± 0.2	5.2 ± 1.2
10b	VUF15290		4.28	7.8 ± 0.1	5.9 ± 0.7
10c	VUF16330		4.28	7.8 ± 0.1	2.8 ± 0.3
10d	VUF16331		4.28	7.7 ± 0.2	2.4 ± 0.7
15a	VUF16328		11.87	8.1 ± 0.2	4.9 ± 0.5
15b	VUF16313		10.23	8.4 ± 0.2	2.6 ± 0.6
15c	VUF16314		10.38	7.8 ± 0.2	3.7 ± 1.8
15d	VUF16315		10.13	7.9 ± 0.1	2.8 ± 1.0
16a	VUF16372		4.10	7.6 ± 0.0	5.8 ± 0.8
16b	VUF16318		4.33	7.8 ± 0.2	5.7 ± 0.6
16c	VUF16332		4.33	8.1 ± 0.1	1.9 ± 0.3
16d	VUF16333		4.33	7.8 ± 0.3	5.4 ± 2.8

[a] Calculated values using ChemAxon.

The pK_i values were plotted per structural unit in two complementary ways (Figs. 4A-B). All compounds have acceptable affinities and all are comparable to the affinity of **3**, which further underscores the biaryl head of **25/1** as an efficient recognition element and the use of the explored sulfonyl moieties as isosteric elements. No evident trends can be identified within subseries. A few qualitative notes can be made about KRI values. Sulfonamides **15** have much higher pK_a values than acylsulfonamides **10** and sulfonylureas **16**. However, when comparing the KRI results of **15** versus **10**, the carbonyl moiety in **10** does not appear to play a decisive role through rendering the proton more acidic or by any other means (e.g. H-bond acceptor). Also, the subseries **16** does not deviate much from subseries **10** in pK_a values and in its pharmacological properties, once again underscoring that the chemical properties of the carbonyl moiety in **15** are not essential. Of note, however, is the relatively faster dissociation of *tert*-butyl-phenyl compound **16c**, a feature not observed in the analogues **15c** and **10c**.
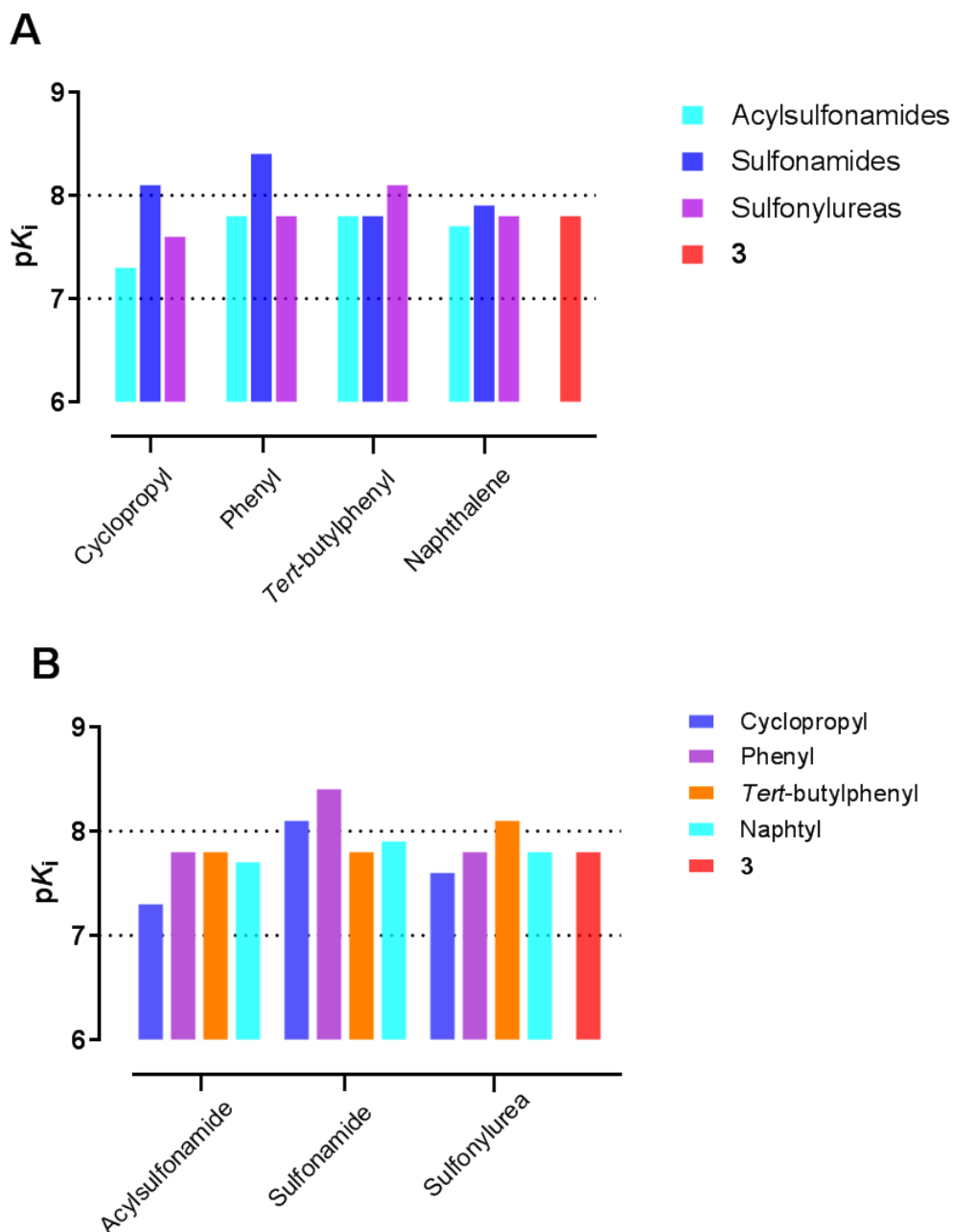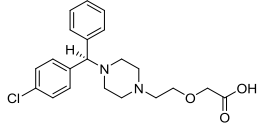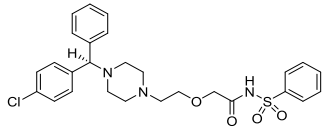
Figure 4. Exploring the role of different structural motives in affinity properties. Figure A contains the exact same data as Figure B but in a complementary setup. The pK_i = 7.0 and pK_i = 8.0 values are indicated by dotted lines for visual clarity.

The collective data on series **15**, **10** and **16** shows that virtually all compounds slowly dissociate, making a detailed SKR analysis challenging. Nonetheless, from our studies so far emerges the phenyl-substituted acylsulfonamide as an acid bioisostere that maintains affinity and slow dissociation kinetics in this series of H$_1$R ligands. For further proof of concept, we selected

carboxylic-acid containing clinical drug levocetirizine and prepared the isostere **24** (Table 7). Its pK_i and KRI values are 7.8 and 5.9, respectively, which upon comparison with levocetirizine confirms that also in this scaffold phenylsulfonamide is a bioisostere.

Table 7. Use of phenylsulfonamide as an isostere for the carboxylic acid in levocetirizine.

#	*compound*	Structure	$pK_{a,calc}$[a]	$pK_i \pm$ SD	KRI $\pm$ SD
	levocetirizine		4.73	8.1 ± 0.1	4.0 ± 0.9
24	VUF15665		4.28	7.8 ± 0.1	5.9 ± 1.1

[a] Calculated values using ChemAxon.

The effect of isosteric replacements on the kinetics of functional antagonism were finally characterized in a Ca^{2+} assay as previously disclosed by us.[27] In this assay, Hela cells, endogenously expressing the human H_1R are incubated overnight with the antagonists studied. The next day, the cells are rapidly washed, loaded with fluo-4 and challenged at specific time points with 10 µM histamine to measure the recovery of H_1R responsiveness over time. As can be seen in figure 5, the histamine responsiveness is rapidly reversed after washout of mepyramine, an H_1R with short residence time. In contrast, the recovery of H_1R responses after levocetirizine washout is slow and does not reach the 100 % level within the timeframe of the experiment. These data are in line with our earlier work on the recovery of second generation antihistamines[21, 45] and correlate with the known long residence time of levocetirizine.[27, 46] In line with the findings in Table 7, the isosteric replacement of the carboxylate group in **24** also results in a slow recovery of the histamine responsiveness in the calcium assay (Figure 5).
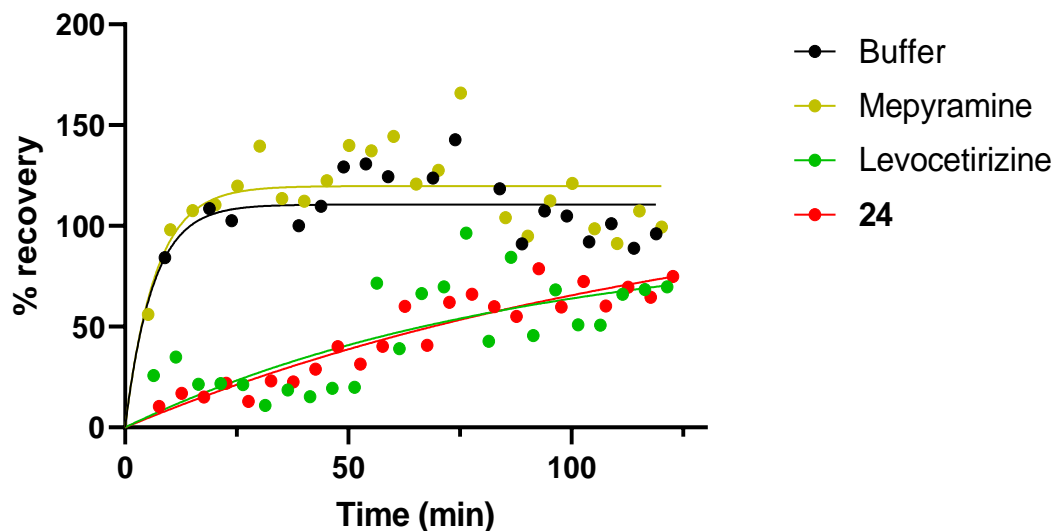
Figure 5. Recovery of histamine (10 µM) responsiveness, as measured as increase in calcium levels in fluo-4 loaded Hela cells, that have been incubated overnight with the indicated compounds (or buffer) and thoroughly washed before testing the histamine responses. Data shown are representative of at least 3 independent experiments.

Conclusion

The effect of acidity of a peripheral group in a common virtual screening hit scaffold on the kinetics of H_1R binding was investigated. Two series of potential isosteres (non-acidic and acidic) were designed and prepared in short synthetic sequences. All compounds have binding affinities at H_1R similar to that of parent acid **3**. In the non-acidic series, many ligands have a shorter RT (1.2 < KRI < 1.6) than **3**. However, introducing non-acidic squarate moieties results in long RT (3.1 < KRI < 4.7). All ligands containing acidic moieties show long RT (KRI > 2). Indeed, although acidity of the isostere generally leads to slower dissociation, no decisive trend could be obtained between the acidity of isosteres and dissociation patterns. Acylsulfonamide **10b** was designated a key compound as it has good affinity, slow dissociation (KRI = 5.9) and an evident growth factor, which was used to prepare three subseries of sulfonyl-containing derivatives. All of these have good binding affinities and can be considered as reasonable isosteres of parent **3**, but the high KRI values for almost all (indicating slow dissociation) prevent inspection of detailed trends. Qualitatively, the varying acidities within the three subseries do not seem to play a decisive role in binding kinetics. The bioisostere potential of the key phenyl-acylsulfonamide moiety was confirmed by application on levocetirizine (**24**). In all, using either an acidic or a non-acidic bioisosteric replacement for a carboxylic acid gives differential strategies to modulate binding kinetics in H_1R ligands.

Experimental section

Pharmacology

Cell culture and radioligand binding. Production of cell homogenates expressing the HA-H_1R and the performed radioligand binding experiments conducted were previously described with minor changes.[27, 47] In short, HEK293T cells were transiently transfected using 25kDa polyethylenimine with a pcDEF3 vector encoding the N-terminally HA tagged H_1R. Cells were collected and frozen two days post-transfection. Upon conducting a radioligand binding experiment, a frozen aliquot of cells was reconstituted in binding buffer [50mM Na_2HPO_4/KH_2PO_4, pH 7.4], homogenized and then co-incubated with [^{3}H]mepyramine with or without an additional unlabeled ligand at 25°C under gentle agitation. Binding reactions were terminated by filtration and three rapid consecutive wash steps using ice-cold wash buffer [50mM Tris-HCl, pH 7.4]. Filter- bound radioactivity was quantified using scintillation counting using the Wallac Microbeta.

Competitive binding assay. Previously it was determined for the radioligand [^{3}H]mepyramine binding the H_1R, that the equilibrium dissociation constant (K_D) is 2.29 nM. In radioligand displacement experiments, a single concentration [^{3}H]mepyramine (1–5 nM) was co-incubated with increasing concentrations unlabeled ligands (10^{-11} – 10^{-4} M) for 4 h at 25 °C. K_i values could be determined from the displacement curves by converting the obtained IC_{50} values using the binding affinity and concentration of [^{3}H]mepyramine.[48]

Competitive kinetic experiments. A single concentration [^{3}H]mepyramine (1–5 nM) was co-incubated with a single concentration unlabeled ligand for 6 min and 80 min at 25 °C. Concentration antagonists were chosen to be $10 \cdot K_i$, or fine-tuned to have a similar level of radioligand displacement after 80 min (>40%). To determine the non-specific radioligand binding, [^{3}H]mepyramine was additionally co-incubated with saturating concentrations mianserin (10^{-5}M). Specific binding was then determined by subtracting the measured radioligand binding by this non-specific binding. Finally, the kinetic rate index (KRI) of unlabeled ligands were determined by dividing the specific binding at the 6 min time point by the specific binding at the 80 min time point.

Functional assays. The functional recovery of the H_1R following antagonism was measured as described before.[45] In short, HeLa cells, endogenously expressing the H_1R, were seeded $2 \cdot 10^4$ cells/well in a clear bottom 96-well plate which were pre-incubated overnight with a concentration antagonist corresponding to 10 times the respective Ki at the H_1R (24 wells per antagonist). After 18-20 h, cells were labeled with the Fluo-4NW dye in the presence of the respective concentration antagonist for an hour. Both the excess dyesolution as well as the unbound antagonists were removed by washing the cells two times and cells were then reconstituted in HBSS buffer supplemented with probenecid (2.5 mM) (**t0**). Following the wash

step, cells were stimulated every 5 min by histamine injection, into a single well, using the NOVOstar plate reader (BMG Labtech, Ortenberg, Germany), while simultaneously detecting the calcium mediated Fluo4NW fluorescence (λexcitation 494 nm and λemission 516 nm). For each well stimulated with histamine, a consecutive triton-x100 injection after 65 sec was used to lyse the cells leading to saturation of the Fluo4 NW with calcium. The histamine-induced peak-response was then normalized to basal levels of fluorescence (prior to histamine injection; 0) and saturated Fluo4 NW fluorescence (following Triton X-100 injection; 1). This led to a reproducible histamine induced response over time for HeLa cells pretreated with vehicle condition, which was set to a 100%. Histamine-induced peakresponses were plotted against the difference in time between **t0** and the subsequent histamine injection. The recovery time (RecT) was determined for antagonists by non-linear regression using the one-phase association model in GraphPad Prism 7.03.

Chemistry

Anhydrous THF, DCM, DMF, and Et_2O were obtained by elution through an activated alumina column prior to use. All other solvents and chemicals were acquired from commercial suppliers and were used as received. ChemBioDraw Ultra 16.0.1.4 was used to generate systematic names for all molecules. All reactions were performed under an inert atmosphere (N_2), unless mentioned otherwise. TLC analyses were carried out with alumina silica plates (Merck F_{254}) using staining and/or UV visualization. Column purifications were performed manually using Silicycle Ultra Pure silica gel or automatically using Biotage equipment. NMR spectra (^{1}H, ^{13}C, and 2D) were recorded on a Bruker 300 (300 MHz), Bruker 500 (500 MHz) or a Bruker 600 (600 MHz) spectrometer. Chemical shifts are reported in ppm (δ) and the residual solvent was used as internal standard (δ ^{1}H NMR: $CDCl_3$ 7.26; DMSO-d6 2.50; CD_3OD 3.31; δ ^{13}C NMR: $CDCl_3$ 77.16; DMSO-d6 39.52; CD_3OD 49.00). Data are reported as follows: chemical shift (integration, multiplicity (s = singlet, d = doublet, t = triplet, q = quartet, br = broad signal, m = multiplet, app = apparent), and coupling constants (Hz)). A Bruker microTOF mass spectrometer using ESI in positive ion mode was used to record HRMS spectra. A Shimadzu LC-20AD liquid chromatograph pump system linked to a Shimadzu SPD-M20A diode array detector with MS detection using a Shimadzu LC-MS-2010EV mass spectrometer was used to perform LC-MS analyses. An Xbridge (C18) 5 μm column (50 mm, 4.6 mm) was used. The solvents that were used were the following: solvent B (MeCN with 0.1% formic acid) and solvent A (water with 0.1% formic acid), flow rate of 1.0 mL/min, start 5% B, linear gradient to 90% B in 4.5 min, then 1.5 min at 90% B, then linear gradient to 5% B in 0.5 min, then 1.5 min at 5% B; total run time of 8 min. All compounds have a purity of ≥95% (unless specified otherwise), calculated as the percentage peak area of the analyzed compound by UV detection at 254 nm (values are rounded). Reverse-phase column chromatography purifications were performed using Buchi PrepChem C-700 equipment with a discharge deuterium lamp ranging from 200-600 nm to detect compounds using solvent B (MeCN

with 0.1% formic acid), solvent A (water with 0.1% formic acid), flow rate of 15.0 mL/min and a gradient (start 95% A for 3.36 min, then linear gradient to 5% A in 30 min, then at 5% A for 3.36 min, then linear gradient to 95% A in 0.5 min, then 1.5 min at 95% A). The general procedure for making fumarate salts was as follows: (1) The free base was dissolved in iPrOH and fumaric acid (1.0 eq) was added; (2) The mixture was heated; (3) Generally a hot filtration was performed; (4) The formed solid was collected by filtration, washed and dried in $vacuo$.

Ethyl 5-(4-(2-benzylphenoxy)piperidin-1-yl)pentanoate (2)

To a solution of amine **1** (584 mg, 2.184 mmol) in DMF (10 mL) were added K_2CO_3 (906 mg, 6.55 mmol) and ethyl 5-bromopentanoate (0.691 mL, 4.37 mmol). The reaction mixture was stirred at 80°C for 4 h. The reaction mixture was diluted with water (50 mL) and extracted with EtOAc (3 x 25 mL). The combined organic layers were washed with brine, dried over Na_2SO_4, filtered and evaporated in $vacuo$. The crude product was purified by column chromatography (cyclohexane/EtOAc/TEA = 40/58/2, v/v/v) to yield the title compound as a colorless oil (712 mg, 82%). ^{1}H NMR (500 MHz, $CDCl_3$) δ 7.28 – 7.24 (m, 2H), 7.23 – 7.20 (m, 2H), 7.19 – 7.11 (m, 3H), 6.91 – 6.82 (m, 2H), 4.38 (app bs, 1H), 4.14 (q, J = 7.1 Hz, 2H), 3.98 (s, 2H), 2.56 (app bs, 2H), 2.38 – 2.26 (m, 6H), 2.01 – 1.92 (m, 2H), 1.85 – 1.77 (m, 2H), 1.69 – 1.60 (m, 2H), 1.57 – 1.48 (m, 2H), 1.27 (t, J = 7.1 Hz, 3H). LC-MS: t_R = 4.3 min, 96% (254 nm), m/z: 396.3 [M+H][+]

5-(4-(2-benzylphenoxy)piperidin-1-yl)pentanoic acid hydrochloride (3.HCl)

To a solution of ester **2** (500 mg, 1.26 mmol) in MeOH (10 mL) was added 1.0 M NaOH (0.948 mL, 1.90 mmol). The reaction mixture was stirred under reflux for 2.5 h. The volatiles were evaporated and the formed oil was dissolved in 1.0 M aq. HCl (20 mL). The mixture was stirred vigorously. A white/yellowish precipitate was formed and the mixture was evaporated to dryness. Subsequently, 1.0 M aq. HCl (20 mL) was added and the resulting mixture was stirred vigorously at room temperature for 30 min to give a suspension. The supernatant was decanted. The remaining wet solid was suspended in 1.0 M aq. HCl (10 mL). The solid was filtered and washed with 1.0 M aq. HCl. The white solid was dried in $vacuo$ to give the title compound (421 mg, 91%). ^{1}H NMR (500 MHz, $CDCl_3$) δ 11.28 (s, 1H), 7.33 – 7.26 (m, 4H), 7.19 (t, J = 7.3 Hz, 1H), 7.11 (d, J = 7.5 Hz, 2H), 6.99 (t, J = 7.4 Hz, 1H), 6.78 (d, J = 8.2 Hz, 1H), 4.67 (s, 1H), 4.00 (s, 2H), 3.13 – 3.01 (m, 2H), 2.54 – 2.43 (m, 4H), 2.40 (t, J = 7.0 Hz, 2H), 2.20 (t, J = 12.7 Hz, 2H), 2.02 (d, J = 14.8 Hz, 2H), 1.80 – 1.67 (m, 2H), 1.65 – 1.54 (m, 2H). ^{13}C NMR (126 MHz, $CDCl_3$) δ 175.8, 153.9, 142.4, 132.6, 128.7, 128.6, 128.4, 128.1, 126.2, 121.1, 111.5, 65.2, 56.8, 47.4, 37.5, 33.1, 26.6, 23.1, 22.0. LC-MS: t_R = 3.7 min, 99% (254 nm), m/z: 368.2 [M+H][+].

Methyl 5-(4-(2-benzylphenoxy)piperidin-1-yl)pentanoate (4, VUF15009)

To a solution of carboxylic acid **3.HCl** (157 mg, 0.39 mmol) in MeOH (10 mL) was added dropwise AcCl (0.116 mL, 1.63 mmol). The resulting mixture was stirred for 30 min at rt. The resulting mixture was diluted with aq. satd. $NaHCO_3$ (50 mL) and extracted with EtOAc (3 × 30 mL). The combined organic phases were washed with brine (50 mL), dried over Na_2SO_4, filtered and evaporated *in vacuo*. Purification by flash column chromatography EtOAc:TEA:MeOH 90:5:5 gave the title compound as a slightly yellow oil (135 mg, 91%). ^{1}H NMR (500 MHz, DMSO-d_6) δ 7.28–7.10 (m, 7H), 6.96 (d, J = 8.0 Hz, 1H), 6.83 (t, J = 7.2 Hz, 1H), 4.44–4.32 (m, 1H), 3.88 (s, 2H), 3.58 (s, 3H), 2.56–2.45 (m, 2H), 2.31 (t, J = 7.4 Hz, 2H), 2.27–2.12 (m, 4H), 1.90–1.78 (m, 2H), 1.65–1.47 (m, 4H), 1.44–1.33 (m, 2H). ^{13}C NMR (126 MHz, DMSO-d_6) δ 173.4, 154.6, 141.1, 130.5, 130.0, 128.6, 128.1, 127.4, 125.7, 120.1, 112.9, 71.6, 57.4, 51.2, 49.9, 35.7, 33.1, 30.5, 25.9, 22.5. HRMS: $C_{24}H_{32}NO_3^+$ [M+H]$^+$ calcd: 382.2377, found 382.2366. LC-MS: t_R = 3.7 min, 98% (254 nm), m/z: 382 [M+H]$^+$.

5-(4-(2-Benzylphenoxy)piperidin-1-yl)pentanamide fumarate (5, VUF15010)

A mixture of acid **3.HCl** (208 mg, 0.52 mmol), EDCI.HCl (148 mg, 0.77 mmol), HOBt.H_2O (87 mg, 0.57 mmol), 1 M NH_3 in dioxane, TEA (0.431 mL, 3.09 mmol) and DCM (5.5 mL) was stirred overnight at rt. The reaction mixture was diluted with DCM (50 mL) and water (50 mL). The phases were separated and the aqueous phase was extracted with DCM (2 × 50 mL). The combined organic phases were washed with brine (50 mL), dried over Na_2SO_4, filtered and evaporated *in vacuo*. Purification by flash column chromatography (EtOAc:MeOH:TEA 90:5:5) gave a colorless oil (163 mg, 86%). The oil was taken up in DCM (50 mL) and 1.0 M aq. NaOH (50 mL). The phases were separated and the aqueous phase was extracted with DCM (2 × 50 mL). The combined organic phases were dried over Na_2SO_4, filtered and evaporated *in vacuo*. Purification by reversed phase column chromatography (H_2O:MeCN 95:5 to 20:80) gave the free base (60 mg, 0.16 mmol), which was converted to a fumaric acid salt with the method described in the general procedure, to obtain the title compound as a white solid (33 mg, 42%). ^{1}H NMR (500 MHz, DMSO-d_6) δ 7.36–7.22 (m, 3H), 7.22–7.12 (m, 5H), 6.98 (d, J = 8.2 Hz, 1H), 6.86 (t, J = 7.4 Hz, 1H), 6.74 (bs, 1H), 6.55 (s, 2H), 4.54–4.43 (bs, 1H), 3.90 (s, 2H), 2.69–2.57 (m, 2H), 2.57–2.52 (m, 2H), 2.48–2.41 (m, 2H, overlaps with solvent signal), 2.08–2.02 (m, 2H), 1.97–1.85 (m, 2H), 1.75–1.62 (m, 2H), 1.51–1.40 (m, 4H). ^{13}C NMR (126 MHz, DMSO-d_6) δ 174.1, 166.9, 154.4, 141.2, 134.6, 130.8, 129.8, 128.6, 128.2, 127.6, 125.7, 120.3, 112.8, 56.7, 49.0, 35.8, 34.8, 29.1, 25.0, 22.8 (no ^{13}C resonance was observed for the OCH of the compound, but a HSQC signal was observed at 4.54 – 4.43 ppm (^{1}H) and 69.5 ppm (^{13}C)). HRMS: $C_{23}H_{31}N_2O_2^+$ [M+H]$^+$ calcd: 367.2380, found 367.2366. LC-MS: t_R = 3.5 min, 99% (254 nm), m/z: 367 [M+H]$^+$.

5-(4-(2-Benzylphenoxy)piperidin-1-yl)-N-hydroxypentanamide fumarate (6, VUF15011)

A mixture of acid **3.HCl** (207 mg, 0.51 mmol), EDCI.HCl (295 mg, 1.54 mmol), O-(*tert*-butyldimethylsilyl)hydroxylamine (242 mg, 1.64 mmol) and DCM (12 mL) was stirred overnight at rt. The reaction mixture was diluted with EtOAc (50 mL) and H_2O (50 mL). The phases were separated and the aqueous phase was extracted with DCM (3 × 50 mL). The combined organic phases were washed with brine (25 mL), dried over Na_2SO_4, filtered and evaporated *in vacuo*. The resulting mixture was diluted with DCM (5 mL) and cooled to 0 °C. TFA (2.18 mL, 28.2 mmol) was added and the resulting mixture was stirred for 5 h at 0 °C. The reaction mixture was diluted with DCM (50 mL) and 1.0 M aq. HCl (100 mL). The phases were separated and the aqueous phase was extracted with $CHCl_3$ (3 × 50 mL). The combined organic phases were dried over Na_2SO_4, filtered and evaporated *in vacuo*. Purification by reversed phase column chromatography (H_2O:MeCN 95:5 to 20:80) gave the free base (159 mg, 0.42 mmol). Conversion to a fumaric acid salt with the method described in the general procedure gave the title compound as a white solid (133 mg, 64%). ^1H NMR (500 MHz, DMSO-d_6) ^1H NMR (500 MHz, DMSO) δ 13.02 (bs, 1H), 10.42 (s, 1H), 8.74 (s, 1H), 7.31 − 7.25 (m, 2H), 7.24 − 7.14 (m, 5H), 7.01 (d, J = 8.0 Hz, 1H), 6.91 (t, J = 7.4 Hz, 1H), 6.62 (s, 3H), 4.66 (bs, 1H), 3.93 (s, 2H), 3.32 − 3.25 (bs, 2H), 3.22 − 3.06 (bs, 2H), 3.00 − 2.84 (bs, 2H), 2.15 − 1.93 (m, 4H), 1.92 − 1.75 (bs, 2H), 1.66 − 1.46 (m, 4H). ^{13}C NMR (126 MHz, DMSO-d_6) δ 168.6, 166.0, 154.0, 141.3, 134.0, 131.0, 129.6, 128.4, 128.3, 127.7, 125.8, 120.7, 112.6, 55.4, 35.8, 31.5, 23.2, 22.2 (no ^{13}C resonance was observed for the OCH of the compound, but a HSQC signal was observed at 4.66 ppm (^1H) and 65.3 ppm (^{13}C)). Two additional aliphatic ^{13}C signals could not be detected. HRMS: $C_{23}H_{31}N_2O_3^+$ [M+H]$^+$ calcd: 383.2329, found 383.2329. LC-MS: t_R = 3.4 min, >95% (254 nm), *m/z:* 383 [M+H]$^+$.

5-(4-(2-Benzylphenoxy)piperidin-1-yl)-*N*-cyanopentanamide (7, VUF14991)

A mixture of acid **3.HCl** (150 mg, 0.37 mmol), EDCI.HCl (100 mg, 0.52 mmol), DMAP (54 mg, 0.45 mmol), NH_2CN (31 mg, 0.74 mmol), DIPEA (0.195 mL, 1.11 mmol) and DCM (5 mL) was stirred overnight at rt. The volatiles were removed *in vacuo*. Purification by reversed phase column chromatography (H_2O:MeCN 95:5 to 5:95) gave the title compound as a white solid (42 mg, 29%). ^1H NMR (500 MHz, DMSO-d_6) δ 7.31–7.24 (m, 2H), 7.23–7.15 (m, 5H), 7.01 (d, J = 8.1 Hz, 1H), 6.90 (t, J = 7.4 Hz, 1H), 4.69–4.61 (m, 1H), 3.93 (s, 2H), 3.14–3.03 (m, 2H), 2.94–2.80 (m, 4H), 2.09–1.96 (m, 4H), 1.89–1.79 (m, 2H), 1.62–1.52 (m, 2H), 1.52–1.43 (m, 2H). ^{13}C NMR (126 MHz, DMSO-d_6) δ 181.3, 154.0, 141.2, 131.0, 129.6, 128.4, 128.3, 127.6, 125.8, 121.0, 120.6, 112.6, 67.5, 55.6, 48.2, 36.7, 35.8, 27.4, 23.4, 22.7. HRMS: $C_{24}H_{30}N_3O_2^+$ [M+H]$^+$ calcd: 392.2333, found 392.2326. LC-MS: t_R = 3.6 min, 99% (254 nm), *m/z:* 392 [M+H]$^+$.

5-(4-(2-Benzylphenoxy)piperidin-1-yl)-*N*-(methylsulfonyl)pentanamide (8, VUF14990)

A mixture of acid **3.HCl** (150 mg, 0.37 mmol), EDCI.HCl (100 mg, 0.52 mmol), DMAP (54 mg, 0.45 mmol), $CH_3SO_2NH_2$ (71 mg, 0.74 mmol), DIPEA (0.195 mL, 1.11 mmol) and DCM (5 mL) was stirred overnight at rt. The reaction mixture was diluted with DCM (100 mL) and 1.0 M aq. HCl (100 mL). The phases were separated and the aqueous phase was extracted with DCM (2 × 50 mL). The combined organic phases were washed with brine (50 mL), dried over Na_2SO_4, filtered and evaporated *in vacuo*. Purification by reversed phase column chromatography (H_2O:MeCN 95:5 to 5:95) gave the title compound as a white solid (64 mg, 39%). ^1H NMR (500 MHz, DMSO-d_6) δ 7.28–7.22 (m, 2H), 7.22–7.13 (m, 5H), 6.97 (d, *J* = 8.1 Hz, 1H), 6.86 (t, *J* = 7.4 Hz, 1H), 4.50–4.43 (bs, 1H), 3.90 (s, 2H), 3.07 (s, 3H), 2.68–2.54 (m, 2H), 2.50–2.44 (m, 2H, the signal overlaps with the solvent signal), 2.42 (t, *J* = 7.0 Hz, 2H), 2.19 (t, *J* = 7.0 Hz, 2H), 1.95–1.86 (m, 2H), 1.72–1.62 (m, 2H), 1.54–1.39 (m, 4H). ^{13}C NMR (126 MHz, DMSO-d_6) δ 174.2, 154.4, 141.2, 130.7, 129.9, 128.6, 128.2, 127.5, 125.7, 120.3, 112.8, 70.3, 56.8, 49.4, 40.8, 36.2, 35.8, 29.5, 25.1, 22.3. HRMS: $C_{24}H_{33}N_2O_4S^+$ [M+H]$^+$ calcd: 445.2156, found 445.2172. LC-MS: t_R = 3.6 min, 99% (254 nm), *m/z:* 445 [M+H]$^+$.

5-(4-(2-Benzylphenoxy)piperidin-1-yl)-N-((trifluoromethyl)sulfonyl)pentanamide (9, VUF15037)

A mixture of acid **3.HCl** (150 mg, 0.37 mmol), EDCI.HCl (100 mg, 0.52 mmol), HOBt.H_2O (68 mg, 0.45 mmol), $CF_3SO_2NH_2$ (111 mg, 0.74 mmol), DIPEA (0.195 mL, 1.11 mmol) and DCM (5 mL) was stirred for 16 h at rt. The reaction mixture was diluted with DCM (30 mL) and 1.0 M aq. HCl (100 mL). The phases were separated and the aqueous phase was extracted with DCM (3 × 30 mL). The combined organic phases were dried over Na_2SO_4, filtered and evaporated *in vacuo*. Purification by reversed phase column chromatography (H_2O:MeCN 95:5 to 5:95) gave the title compound as a white solid (50 mg, 27%). ^1H NMR (500 MHz, D_2O:DMSO-d_6, 2.75 mg compound:2.30 mg K_2CO_3) δ 7.21–7.03 (m, 7H), 6.90–6.78 (m, 2H), 4.37 (br, 1H), 3.81 (s, 2H), 2.27 (br, 4H), 2.18–2.02 (m, 4H), 1.80–1.67 (m, 2H), 1.67–1.54 (m, 2H), 1.44–1.24 (m, 4H). ^{13}C NMR (126 MHz, D_2O:DMSO:K_2CO_3) δ 183.6, 155.8, 142.7, 132.4, 131.6, 130.0, 129.8, 129.3, 127.4, 122.0, 121.5 (q, *J* = 325 Hz), 114.7, 58.8, 49.9, 40.3, 37.2, 30.6, 26.3, 25.0 (no ^{13}C resonance was observed for the O*C*H of the compound, but a HSQC signal was observed at 4.40 – 4.32 ppm (^1H) and 71.7 ppm (^{13}C)). HRMS: $C_{24}H_{30}N_2O_4F_3S^+$ [M+H]$^+$ calcd: 499.1873, found 499.1863. LC-MS: t_R = 4.2 min, 99% (254 nm), *m/z:* 507 [M+H]$^+$.

5-(4-(2-benzylphenoxy)piperidin-1-yl)-N-(cyclopropylsulfonyl)pentanamide (10a, VUF16329)

To a mixture of acid **3**.HCl (98 mg, 0.245 mmol) and cyclopropanesulfonamide (44 mg, 0.367 mmol) in DCM was added EDCI·HCl (57 mg, 0.299 mmol) followed by DMAP (14mg, 0.122 mmol). The reaction mixture was stirred 24 h at rt. The mixture was diluted with EtOAc (15 mL) and washed successively with 10% HCl (15 mL), H_2O and brine. The organic layer was dried (Na_2SO_4) and concentrated under reduced pressure. The residue was purified by reverse-phase column chromatography (H_2O:MeCN 100:0 to 0:100) to yield the title compound as a white solid (229 mg, 36% yield). ^{1}H NMR (500 MHz, CDCl$_3$) δ 7.26 – 7.22 (m, 4H), 7.17 (t, J = 7.3 Hz, 1H), 7.13 – 7.08 (m, 2H), 6.96 (t, J = 7.4 Hz, 1H), 6.77 (d, J = 8.1 Hz, 1H), 4.63 – 4.60 (m, 1H), 3.99 (s, 2H), 3.12 (d, J = 11.2 Hz, 2H), 2.68 (tt, J = 8.2, 4.9 Hz, 1H), 2.56 – 2.45 (m, 2H), 2.36 – 2.13 (m, 6H), 2.02 – 1.92 (m, 2H), 1.65 – 1.49 (m, 4H), 1.10 (dt, J = 6.6, 3.3 Hz, 2H), 0.91 – 0.79 (m, 2H). ^{13}C NMR (126 MHz, CDCl$_3$) δ 179.2, 154.0, 142.2, 132.3, 128.9, 128.6, 128.2, 126.1, 120.9, 111.5, 65.8, 56.7, 47.8, 37.7, 37.3, 31.0, 26.9, 23.5, 22.5, 5.1 (a peak at 128.2 ppm is not visible but is confirmed by HSQC). HRMS: $C_{26}H_{35}N_2O_4S^+$ [M+H]$^+$ calcd: 471.2312, found: 471.2320. LC-MS: t_R = 3.7 min, >97% (254 nm), m/z: 471.3 [M+H]$^+$.

5-(4-(2-Benzylphenoxy)piperidin-1-yl)-*N*-(phenylsulfonyl)pentanamide (10b, VUF15290)

A mixture of acid **3.HCl** (150 mg, 0.37 mmol), EDCI.HCl (100 mg, 0.52 mmol), HOBt.H_2O (68 mg, 0.45 mmol), PhSO$_2$NH$_2$ (117 mg, 0.74 mmol), DIPEA (0.195 mL, 1.11 mmol) and DCM (5 mL) was stirred for 36 h at rt. The reaction mixture was diluted with DCM (30 mL) and 1.0 M aq. HCl (100 mL). The phases were separated and the aqueous phase was extracted with DCM (3 × 30 mL). The combined organic phases were dried over Na_2SO_4, filtered and evaporated *in vacuo*. Purification by reversed phase column chromatography (H_2O:MeCN 10:0 to 3:7) gave the title compound as a white solid (50 mg, 27%). ^{1}H NMR (500 MHz, DMSO-d_6) δ 7.82–7.78 (m, 2H), 7.53–7.43 (m, 3H), 7.29–7.23 (m, 2H), 7.22–7.13 (m, 5H), 7.01–6.97 (m, 1H), 6.88 (td, J = 1.0, 7.4 Hz, 1H), 4.57–4.50 (m, 1H), 3.91 (s, 2H), 2.73–2.60 (m, 4H), 2.57–2.52 (m, 2H), 2.12–2.06 (m, 2H), 1.97–1.87 (m, 2H), 1.77–1.67 (m, 2H), 1.46–1.36 (m, 4H). ^{13}C NMR (126 MHz, DMSO-d_6) δ 175.0, 154.2, 143.6, 141.2, 131.2, 130.8, 129.8, 128.5, 128.2, 128.2, 127.6, 127.0, 125.8, 120.4, 112.7, 56.1, 48.8, 36.8, 35.8, 28.5, 24.3, 22.2 (no ^{13}C resonance was observed for the O*C*H of the compound, but a HSQC signal was observed at 4.57 – 4.50 ppm (^{1}H) and 68.6 ppm (^{13}C)). HRMS: $C_{29}H_{35}N_2O_4S^+$ [M+H]$^+$ calcd: 507.2312, found 507.2326. LC-MS: t_R = 3.8 min, 99% (254 nm), *m/z:* 507 [M+H]$^+$.

5-(4-(2-benzylphenoxy)piperidin-1-yl)-N-((4-(*tert*-butyl)phenyl)sulfonyl)pentanamide (10c, VUF16330)

To a mixture of acid **3**.HCl (153 mg, 0.381 mmol) and 4-(*tert*-butyl)benzenesulfonamide (81 mg, 0.381 mmol) in DCM was added EDCI·HCl (89 mg, 0.465 mmol) followed by DMAP (13 mg, 0.11 mmol). The reaction mixture was stirred 24 h at rt. The mixture was diluted with EtOAc (15 mL) and washed successively with 10% HCl (15 mL), H_2O and brine. The organic layer was dried (Na_2SO_4) and concentrated under reduced pressure. The residue was purified by reverse-phase column chromatography (H_2O:MeCN 100:0 to 0:100) to yield the title compound as a white solid (40 mg, 19% yield). ^{1}H NMR (600 MHz, $CDCl_3$) δ 7.88 (dt, J = 8.9, 2.4 Hz, 2H), 7.46 (dd, J = 8.7, 2.2 Hz, 2H), 7.22 – 7.16 (m, 4H), 7.12 – 7.07 (m, 1H), 7.05 – 6.99 (m, 2H), 6.94 – 6.88 (m, 1H), 6.73 (d, J = 8.0 Hz, 1H), 4.61 – 4.56 (m, 1H), 3.93 (s, 2H), 2.98 – 2.91 (m, 2H), 2.46 – 2.37 (m, 2H), 2.25 – 2.03 (m, 6H), 1.98 – 1.91 (m, 2H), 1.54 – 1.42 (m, 4H), 1.26 (s, 9H). ^{13}C NMR (151 MHz, $CDCl_3$) δ 171.7, 157.4, 153.8, 142.2, 136.3, 132.4, 128.7, 128.6, 128.2, 128.0, 127.9, 126.1, 125.9, 121.1, 111.4, 65.0, 56.2, 47.4, 37.2, 35.2, 34.9, 31.0, 26.6, 22.9, 21.0. HRMS: $C_{33}H_{43}N_2O_4S^+$ [M+H]$^+$ calcd: 563.2938, found: 563.2913. LC-MS: t_R = 4.3 min, >98% (254 nm), m/z: 563.4 [M+H]$^+$.

5-(4-(2-benzylphenoxy)piperidin-1-yl)-N-(naphthalen-2-ylsulfonyl)pentanamide (10d, VUF16331)

To a mixture of acid **3**.HCl (176 mg, 0.435 mmol) and naphthalene-2-sulfonamide (99 mg, 0.479 mmol) in DCM was added EDCI·HCl (102 mg, 0.531 mmol) followed by DMAP (15 mg, 0.122 mmol). The reaction mixture was stirred 24 h at rt. The mixture was diluted with EtOAc (15 mL) and washed successively with 10% HCl (15 mL), H_2O and brine. The organic layer was dried (Na_2SO_4) and concentrated under reduced pressure. The residue was purified by reverse-phase column chromatography (H_2O:MeCN 100:0 to 0:100) to yield the title compound as a white solid (38 mg, 16% yield). ^{1}H NMR (500 MHz, $CDCl_3$) δ 8.48 (s, 1H), 7.96 – 7.90 (m, 2H), 7.88 – 7.84 (m, 1H), 7.81 – 7.75 (m, 1H), 7.53 – 7.46 (m, 2H), 7.30 – 7.26 (m, 2H), 7.18 – 7.13 (m, 2H), 7.12 – 7.07 (m, 1H), 7.02 – 6.95 (m, 3H), 6.72 (d, J = 8.1 Hz, 1H), 4.58 – 4.52 (m, 1H), 3.93 (s, 2H), 2.99 (d, J = 11.4 Hz, 2H), 2.41 (t, J = 7.9 Hz, 2H), 2.31 (t, J = 6.1 Hz, 2H), 2.27 – 2.16 (m, 2H), 2.06 – 1.95 (m, 2H), 1.93 – 1.84 (m, 2H), 1.60 – 1.51 (m, 2H), 1.49 – 1.40 (m, 2H). ^{13}C NMR (126 MHz, $CDCl_3$) δ 179.0, 153.9, 142.1, 141.2, 134.3, 132.4, 132.3, 129.3, 128.8, 128.6, 128.5, 128.2, 128.1, 127.9, 127.7, 127.2, 127.0, 126.1, 123.5, 120.9, 111.4, 65.4, 56.7, 47.5, 37.4, 37.3, 26.7, 23.2, 22.5. HRMS: $C_{33}H_{37}N_2O_4S^+$ [M+H]$^+$ calcd: 557.2469, found: 557.2450. LC-MS: t_R = 4.2 min, >99% (254 nm), m/z: 557.3 [M+H]$^+$.

5-(4-(2-benzylphenoxy)piperidin-1-yl)pentan-1-ol fumarate (11, VUF14901)

A microwave vial was charged with amine **1** (300 mg, 1.12 mmol), TEA (0.610 mL, 4.38 mmol), 5-bromopentan-1-ol (0.258 mL, 2.13 mmol) and MeCN (5 mL). The resulting mixture was stirred for 1 h at 65 °C. The reaction mixture was diluted with EtOAc (200 mL) and washed with satd. aq. NaHCO$_3$ (100 mL) and brine (100 mL). The organic phase was dried over Na$_2$SO$_4$, filtered and evaporated *in vacuo*. Purification by flash column chromatography ((EtOAc:TEA):(EtOAc:TEA:MeOH) (99:1):0 to 0:(90:5:5) gave the free base (285 mg, 72%). The free base (280 mg, 0.79 mmol) was converted to a fumaric acid salt, with the method described in the general procedure, to obtain the title compound as a white solid (132 mg, 36%). ^{1}H NMR (500 MHz, DMSO-d_6) δ 7.28–7.22 (m, 2H), 7.21–7.12 (m, 5H), 6.98 (d, J = 8.2 Hz, 1H), 6.86 (t, J = 7.4 Hz, 1H), 6.55 (s, 2H), 4.54–4.47 (bs, 1H), 3.90 (s, 2H), 3.38 (t, J = 6.5 Hz, 2H), 2.76–2.52 (m, 4H), 2.49–2.42 (m, 2H), 1.99–1.88 (m, 2H), 1.76–1.64 (m, 2H), 1.53–1.35 (m, 4H), 1.32–1.23 (m, 2H). ^{13}C NMR (126 MHz, DMSO-d_6) δ 167.0, 154.4, 141.2, 134.6, 130.8, 129.8, 128.5, 128.2, 127.6, 125.7, 120.3, 112.8, 60.5, 56.9, 48.9, 35.8, 32.2, 29.0, 25.0, 23.2 (no ^{13}C resonance was observed for the OC*H* of the compound but a HSQC signal was observed at 4.54 − 4.47 ppm (^{1}H) and 69.3 ppm (^{13}C)). HRMS: C$_{23}$H$_{32}$NO$_2^+$ [M+H]$^+$ calcd: 354.2428, found 354.2422. LC-MS: t_R = 3.9 min, 99% (254 nm), *m/z:* 354 [M+H]$^+$).

5-(4-(2-benzylphenoxy)piperidin-1-yl)pentanenitrile fumarate (12, VUF14902)

A microwave vial was charged with amine **1** (2.00 g, 7.48 mmol), K$_2$CO$_3$ (1.16 g, 8.42 mmol), 5-bromopentanenitrile (0.95 mL, 8.2 mmol) and DMF (50 mL). The resulting mixture was stirred for 2 h at 85 °C. The reaction mixture was concentrated *in vacuo*, diluted with water (1.0 L) and extracted with EtOAc (300 mL). The organic phase was washed with brine (100 mL), dried over Na$_2$SO$_4$, filtered and evaporated *in vacuo*. Purification by flash column chromatography ((EtOAc:TEA):(EtOAc:TEA:MeOH) (99:1):0 to 0:(90:5:5) gave the free base (1.27 g, 49%). Part of the free base (120 mg, 0.34 mmol) was converted to a fumaric acid salt, with the method described in the general procedure, to obtain the title compound as a white solid (45 mg, 28%).^{1}H NMR (500 MHz, DMSO-d_6) δ 7.28–7.22 (m, 2H), 7.21–7.12 (m, 5H), 6.98 (d, J = 8.1 Hz, 1H), 6.88–6.83 (m, 1H), 6.57 (s, 2H), 4.51–4.44 (bs, 1H), 3.90 (s, 2H), 2.71–2.55 (m, 2H), 2.54–2.51 (m, 2H), 2.48–2.41 (m, 4H), 1.97–1.86 (m, 2H), 1.73–1.63 (m, 2H), 1.60–1.50 (m, 4H). ^{13}C NMR (126 MHz, DMSO-d_6) δ 166.7, 154.4, 141.2, 134.4, 130.7, 129.9, 128.6, 128.2, 127.5, 125.7, 120.7, 120.3, 112.8, 56.0, 49.2, 35.8, 29.4, 24.6, 22.7, 16.0 (no ^{13}C resonance was observed for the OC*H* of the compound, but a HSQC signal was observed at 4.51 − 4.44 ppm (^{1}H) and 69.9 ppm (^{13}C)). HRMS: C$_{23}$H$_{29}$N$_2$O$^+$ [M+H]$^+$ calcd: 349.2274, found 349.2271. LC-MS: t_R = 4.0 min, 99% (254 nm), *m/z:* 349 [M+H]$^+$.

1-(4-(1*H*-Tetrazol-5-yl)butyl)-4-(2-benzylphenoxy)piperidine (13, VUF14989)

A mixture of nitrile **12** (0.385 g, 1.11 mmol), NH_4Cl (0.355 g, 6.63 mmol), NaN_3 (0.431 g, 6.63 mmol) and DMF (15 mL) was stirred for 3 d at 100 °C. The reaction mixture was diluted with water (50 mL) and extracted with DCM (3 × 50 mL). The combined organic phases were dried over Na_2SO_4, filtered and evaporated *in vacuo*. Purification by reversed phase column chromatography (H_2O:MeCN 95:5 to 20:80) gave the title compound as a white solid (120 mg, 28%). ^1H NMR (500 MHz, DMSO-d_6) δ 7.27–7.22 (m, 2H), 7.22–7.11 (m, 5H), 6.97 (d, J = 8.0 Hz, 1H), 6.85 (t, J = 7.4 Hz, 1H), 4.49–4.40 (bs, 1H), 3.89 (s, 2H), 2.85 (t, J = 7.4 Hz, 2H), 2.65–2.53 (m, 2H), 2.43–2.30 (m, 4H), 1.95–1.83 (m, 2H), 1.74–1.58 (m, 4H), 1.51–1.42 (m, 2H). ^{13}C NMR (126 MHz, DMSO-d_6) δ 156.9, 154.5, 141.1, 130.6, 129.9, 128.6, 128.1, 127.5, 125.7, 120.2, 112.9, 70.8, 56.8, 49.5, 35.7, 29.8, 25.3, 25.1, 23.0. HRMS: $C_{23}H_{30}N_5O^+$ [M+H]$^+$ calcd: 392.2445, found 392.2443. LC-MS: t_R = 3.4 min, 99% (254 nm), *m/z:* 392 [M+H]$^+$.

5-(4-(2-benzylphenoxy)piperidin-1-yl)pentan-1-amine (14, VUF16394)

Nitrile **12** free base (821 mg, 2.356 mmol) was dissolved in THF (15 mL). This solution was added portion wise to a freshly prepared suspension of $AlCl_3$ (628 mg, 4.71 mmol) and $LiAlH_4$ (4.95 mL, 4.95 mmol) in THF (10 mL). The mixture was stirred for 6 h at rt. The mixture was **<u>cautiously</u>** quenched by slow addition of $Na_2SO_4·10H_2O$ and stirring at rt for several hours. The mixture was filtered and the filtrate was concentrated under reduced pressure. The residue was purified by reverse-phase column chromatography (H_2O:MeCN 100:0 to 0:100) to yield the title compound as a brown oil (361 mg, 43% yield). ^1H NMR (600 MHz, CDCl$_3$) δ 7.26 – 7.23 (m, 2H), 7.22 – 7.18 (m, 2H), 7.18 – 7.13 (m, 2H), 7.12 (dd, J = 7.5, 1.7 Hz, 1H), 6.89 – 6.81 (m, 2H), 4.41 – 4.31 (m, 1H), 3.97 (s, 2H), 2.70 (t, J = 7.1 Hz, 2H), 2.62 – 2.49 (m, 2H), 2.35 – 2.25 (m, 4H), 1.97 – 1.92 (m, 2H), 1.85 – 1.77 (m, 2H), 1.53 – 1.44 (m, 4H), 1.36 – 1.29 (m, 2H). ^{13}C NMR (151 MHz, CDCl$_3$) δ 155.2, 141.4, 131.0, 130.6, 129.0, 128.3, 127.4, 125.8, 120.4, 112.6, 58.8, 50.4, 42.2, 36.5, 33.6, 30.8, 27.0, 25.1. HRMS: $C_{23}H_{33}N_2O^+$ [M+H]$^+$ calcd: 353.2587, found: 353.2571. LC-MS: t_R = 3.1 min, >99% (254 nm), m/z: 353.2 [M+H]$^+$.

N-(5-(4-(2-benzylphenoxy)piperidin-1-yl)pentyl)cyclopropanesulfonamide (15a, VUF16328)

To a stirred solution of amine **14** (180 mg, 0.511 mmol) and TEA (0.214 mL, 1.532 mmol) in DCM (5 mL) was added cyclopropanesulfonyl chloride (71.8 mg, 0.511 mmol). The resulting mixture was stirred at rt for 24 h. The mixture was diluted with EtOAc (15 mL) and washed successively with 10% citric acid (15 mL), H_2O and brine. The organic layer was dried (Na_2SO_4) and concentrated under reduced pressure. The residue was purified by reverse-phase column chromatography (H_2O:MeCN 100:0 to 0:100) to yield the title compound as a brown oil (92 mg, 40% yield). ^{1}H NMR (500 MHz, CDCl$_3$) δ 7.26 – 7.11 (m, 7H), 6.89 – 6.81 (m, 2H), 4.65 (s, 1H), 4.43 – 4.33 (m, 1H), 3.97 (s, 2H), 3.16 (q, J = 6.4 Hz, 2H), 2.61 – 2.46 (m, 2H), 2.41 (td, J = 8.2, 4.0 Hz, 1H), 2.34 – 2.26 (m, 4H), 2.00 – 1.91 (m, 2H), 1.86 – 1.76 (m, 2H), 1.64 – 1.56 (m, 2H), 1.55 – 1.46 (m, 2H), 1.42 – 1.35 (m, 2H), 1.19 – 1.14 (m, 2H), 1.02 – 0.96 (m, 2H). ^{13}C NMR (126 MHz, CDCl$_3$) δ 155.0, 141.4, 131.0, 130.5, 129.0, 128.3, 127.4, 125.8, 120.3, 112.4, 58.4, 50.4, 43.4, 36.5, 30.6, 30.0, 29.8, 26.6, 24.5, 5.4 (a signal at 71.3 ppm is not visible but is confirmed by HSQC). HRMS: $C_{26}H_{37}N_2O_3S^+$ [M+H]$^+$ calcd: 457.2519, found: 457.2533. LC-MS: t_R = 3.7 min, >96% (254 nm), m/z: 457.2 [M+H]$^+$.

N-(5-(4-(2-benzylphenoxy)piperidin-1-yl)pentyl)benzenesulfonamide (15b, VUF16313)

To a stirred solution of amine **14** (200 mg, 0.567 mmol) and TEA (0.237 mL, 1.702 mmol) in DCM (5 mL) was added benzenesulfonyl-chloride (100 mg, 0.567 mmol). The resulting mixture was stirred at rt for 24 h. The mixture was diluted with EtOAc (15 mL) and washed successively with 10% citric acid (15 mL), H_2O and brine. The organic layer was dried (Na_2SO_4) and concentrated under reduced pressure. The residue was purified by reverse-phase column chromatography (H_2O:MeCN 100:0 to 0:100) to yield the title compound as a colorless foam (98 mg, 35% yield). ^{1}H NMR (500 MHz, CDCl$_3$) δ 7.89 – 7.83 (m, 2H), 7.60 – 7.55 (m, 1H), 7.54 – 7.48 (m, 2H), 7.26 – 7.08 (m, 7H), 6.89 – 6.80 (m, 2H), 4.83 (s, 1H), 4.37 (s, 1H), 3.97 (s, 2H), 2.97 (t, J = 6.9 Hz, 2H), 2.50 (s, 2H), 2.35 – 2.18 (m, 4H), 1.99 – 1.91 (m, 2H), 1.84 – 1.79 (m, 2H), 1.52 – 1.38 (m, 4H), 1.32 – 1.24 (m, 2H). ^{13}C NMR (126 MHz, CDCl$_3$) δ 155.1, 141.4, 140.2, 132.7, 131.0, 130.5, 129.2, 129.0, 128.3, 127.5, 127.1, 125.8, 120.4, 112.5, 58.2, 50.3, 43.3, 36.5, 30.6, 29.3, 26.4, 24.4 (a peak at 71.2 ppm is not visible but is confirmed by HSQC). HRMS: $C_{29}H_{37}N_2O_3S^+$ [M+H]$^+$ calcd: 493.2519, found: 493.2510. LC-MS: t_R = 3.9 min, >97% (254 nm), m/z: 493.3 [M+H]$^+$.

N-(5-(4-(2-benzylphenoxy)piperidin-1-yl)pentyl)-4-(*tert* butyl)benzenesulfonamide (15c, VUF16314)

To a stirred solution of amine **14** (200 mg, 0.567 mmol) and TEA (0.237 mL, 1.702 mmol) in DCM (5 mL) was added 4-(*tert*-butyl)benzene-sulfonyl chloride (92 mg, 0.700 mmol). The resulting mixture was stirred at rt for 24 h. The mixture was diluted with EtOAc (15 mL) and washed successively with 10% citric acid (15 mL), H_2O and brine. The organic layer was dried (Na_2SO_4) and concentrated under reduced pressure. The residue was purified by reverse-phase column chromatography (H_2O:MeCN 100:0 to 0:100) to yield the title compound as a brown foam (104 mg, 33% yield). ^{1}H NMR (500 MHz, $CDCl_3$) δ 7.80 – 7.75 (m, 2H), 7.54 – 7.49 (m, 2H), 7.25 – 7.08 (m, 7H), 6.88 – 6.80 (m, 2H), 4.71 (s, 1H), 4.37 (s, 1H), 3.97 (s, 2H), 3.00 – 2.91 (m, 2H), 2.57 – 2.43 (m, 2H), 2.33 – 2.18 (m, 4H), 1.99 – 1.90 (m, 2H), 1.84 – 1.78 (m, 2H), 1.53 – 1.39 (m, 4H), 1.34 (s, 9H), 1.32 – 1.27 (m, 2H). ^{13}C NMR (126 MHz, $CDCl_3$) δ 156.4, 155.1, 141.4, 137.0, 131.0, 130.6, 129.0, 128.3, 127.4, 127.0, 126.2, 125.8, 120.4, 112.6, 58.3, 50.4, 43.3, 36.5, 35.3, 31.2, 30.7, 29.4, 26.5, 24.5 (a peak at 71.6 ppm is not visible but is confirmed by HSQC). HRMS: $C_{33}H_{45}N_2O_3S^+$ $[M+H]^+$ calcd: 549.3145, found: 549.3172, LC-MS: t_R = 4.3 min, >99% (254 nm), m/z: 549.3 $[M+H]^+$.

N-(5-(4-(2-benzylphenoxy)piperidin-1-yl)pentyl)naphthalene-2-sulfonamide (15d, VUF16315)

To a stirred solution of amine **14** (200 mg, 0.567 mmol) and TEA (0.237 mL, 1.702 mmol) in DCM (5 mL) was added naphthalene-2-sulfonyl chloride (129 mg, 0.567 mmol). The resulting mixture was stirred at rt for 24 h. The mixture was diluted with EtOAc (15 mL) and washed successively with 10% citric acid (15 mL), H_2O and brine. The organic layer was dried (Na_2SO_4) and concentrated under reduced pressure. The residue was purified by reverse-phase column chromatography (H_2O:MeCN 100:0 to 0:100) to yield the title compound as a brown solid (62 mg, 20% yield). ^{1}H NMR (500 MHz, $CDCl_3$) δ 8.45 (d, *J* = 1.7 Hz, 1H), 7.97 (d, *J* = 8.3 Hz, 2H), 7.93 – 7.88 (m, 1H), 7.87 – 7.82 (m, 1H), 7.68 – 7.55 (m, 2H), 7.27 – 7.06 (m, 7H), 6.90 – 6.79 (m, 2H), 5.03 (s, 1H), 4.34 (s, 1H), 3.97 (s, 2H), 3.00 (t, *J* = 6.9 Hz, 2H), 2.55 – 2.37 (m, 2H), 2.29 – 2.11 (m, 4H), 1.96 – 1.88 (m, 2H), 1.82 – 1.71 (m, 2H), 1.53 – 1.44 (m, 2H), 1.42 – 1.34 (m, 2H), 1.30 – 1.22 (m, 2H). ^{13}C NMR (126 MHz, $CDCl_3$) δ 155.1, 141.4, 137.0, 134.9, 132.3, 130.9, 130.6, 129.6, 129.3, 129.0, 128.9, 128.5, 128.3, 128.0, 127.7, 127.4, 125.8, 122.4, 120.4, 112.6, 71.8, 58.3, 50.4, 43.3, 36.5, 30.7, 29.3, 26.4, 24.4. HRMS: $C_{33}H_{39}N_2O_3S^+$ $[M+H]^+$ calcd: 543.2676, found: 543.2649. LC-MS: t_R = 4.3 min, >97% (254 nm), m/z: 543.3 $[M+H]^+$.

N-((5-(4-(2-benzylphenoxy)piperidin-1-yl)pentyl)carbamoyl)cyclopropanesulfonamide (16a, VUF16372)

After complete dissolution of carbamate **20a** (152 mg, 0.789 mmol) in boiling MeCN (10 mL), amine **14** (278 mg, 0.789 mmol) was added portion wise. The mixture was heated at reflux for overnight and concentrated under reduced pressure. The residue was purified by reverse-phase column chromatography (H_2O:MeCN 100:0 to 0:100) to yield the title compound as a brown foam (30 mg, 8% yield). ^1H NMR (500 MHz, $CDCl_3$) δ 7.26 – 7.20 (m, 4H), 7.19 – 7.10 (m, 3H), 6.94 (t, J = 7.4 Hz, 1H), 6.79 (d, J = 8.2 Hz, 1H), 6.56 (s, 1H), 4.61 – 4.50 (m, 1H), 3.99 (s, 2H), 3.16 (q, J = 6.3 Hz, 2H), 3.04 – 2.84 (m, 2H), 2.64 (tt, J = 8.3, 4.8 Hz, 1H), 2.50 – 2.42 (m, 2H), 2.37 – 2.16 (m, 4H), 1.99 – 1.89 (m, 2H), 1.62 – 1.54 (m, 2H), 1.53 – 1.44 (m, 2H), 1.36 – 1.27 (m, 2H), 1.16 – 1.10 (m, 2H), 0.91 (q, J = 7.3 Hz, 2H). ^{13}C NMR (126 MHz, $CDCl_3$) δ 158.2, 154.2, 142.0, 132.1, 129.1, 128.6, 128.3, 128.1, 126.0, 120.8, 111.7, 57.4, 48.1, 40.0, 37.2, 31.6, 29.6, 27.6, 24.4, 24.1, 5.5 (a peak at 66.6 ppm is not visible but is confirmed by HSQC). HRMS: $C_{27}H_{38}N_3O_4S^+$ [M+H]$^+$ calcd: 500.2578, found: 500.2590. LC-MS: t_R = 3.5 min, >95% (254 nm), m/z: 500.3 [M+H]$^+$.

N-((5-(4-(2-benzylphenoxy)piperidin-1-yl)pentyl)carbamoyl)benzenesulfonamide (16b, VUF16318)

Amine **14** (200 mg, 0.567 mmol) was added to MeCN (10 mL) at rt. TEA (0.079 mL, 0.567 mmol) and benzenesulfonyl isocyanate (0.076 mL, 0.567 mmol) were added. After stirring for 1 h at rt, additional benzenesulfonyl isocyanate (0.091 mL, 0.68 mmol) was added and the mixture was stirred for 30 min at rt. The mixture was concentrated under reduced pressure. The residue was purified by reverse-phase column chromatography (H_2O:MeCN 100:0 to 0:100) to yield the title compound as a brown foam (80 mg, 26% yield). ^1H NMR (500 MHz, CD_3OD) δ 7.90 (dd, J = 7.6, 1.9 Hz, 2H), 7.47 – 7.39 (m, 3H), 7.24 – 7.20 (m, 2H), 7.19 – 7.10 (m, 5H), 6.92 (d, J = 8.2 Hz, 1H), 6.87 (t, J = 7.4 Hz, 1H), 4.52 – 4.44 (m, 1H), 3.96 (s, 2H), 3.08 – 2.98 (m, 2H), 2.62 – 2.42 (m, 4H), 2.38 – 2.28 (m, 2H), 1.98 – 1.87 (m, 2H), 1.84 – 1.74 (m, 2H), 1.52 – 1.38 (m, 4H), 1.31 – 1.20 (m, 2H). ^{13}C NMR (126 MHz, CD_3OD) δ 163.2, 156.1, 146.5, 143.0, 132.3, 131.7, 131.1, 129.6, 129.3, 129.2, 128.7, 127.8, 126.8, 121.5, 113.4, 59.3, 50.7, 40.7, 37.5, 31.0, 30.4, 26.6, 25.6 (a peak at 70.9 ppm is not visible but is confirmed by HSQC). HRMS: $C_{30}H_{38}N_3O_4S^+$ [M+H]$^+$ calcd: 536.2578, found: 536.2557. LC-MS: t_R = 3.7 min, >95% (254 nm), m/z: 536.3 [M+H]$^+$.

N-((5-(4-(2-benzylphenoxy)piperidin-1-yl)pentyl)carbamoyl)-4-(*tert*-butyl)benzenesulfonamide (16c, VUF16332)

After complete dissolution of carbamate **20c** (162 mg, 0.567 mmol) in boiling MeCN (10 mL), amine **14** (200 mg, 0.567 mmol) was added portion wise. The mixture was heated at reflux for overnight and concentrated under reduced pressure. The residue was purified by reverse-phase column chromatography (H_2O:MeCN 100:0 to 0:100) to yield the title compound as a white solid (32 mg, 10% yield). ^{1}H NMR (500 MHz, $CDCl_3$) δ 7.77 (d, J = 8.3 Hz, 2H), 7.42 (d, J = 8.4 Hz, 2H), 7.25 – 7.21 (m, 3H), 7.18 – 7.07 (m, 3H), 6.95 (t, J = 7.4 Hz, 1H), 6.77 (d, J = 8.5 Hz, 1H), 6.72 – 6.60 (m, 1H), 4.58 – 4.49 (m, 1H), 3.99 (s, 2H), 3.21 – 2.98 (m, 4H), 2.52 – 2.41 (m, 2H), 2.38 – 2.14 (m, 4H), 1.98 – 1.87 (m, 2H), 1.60 – 1.38 (m, 4H), 1.35 – 1.20 (m, 11H). ^{13}C NMR (126 MHz, $CDCl_3$) δ 158.4, 154.8, 154.3, 142.0, 141.4, 132.2, 129.2, 128.6, 128.3, 128.1, 126.1, 126.0, 125.7, 120.9, 111.7, 57.4, 48.0, 40.1, 37.2, 35.1, 31.3, 29.8, 27.5, 24.3, 24.0 (a peak at 66.6 ppm is not visible but is confirmed by HSQC). HRMS: $C_{34}H_{46}N_3O_4S^+$ [M+H]$^+$ calcd: 592.3204, found: 592.3174. LC-MS: t_R = 4.1 min, >98% (254 nm), m/z: 592.4 [M+H]$^+$.

N-((5-(4-(2-benzylphenoxy)piperidin-1-yl)pentyl)carbamoyl)naphthalene-2-sulfonamide (16d, VUF16333*)*

After complete dissolution of carbamate **20d** (158 mg, 0.567 mmol) in boiling MeCN (10 mL), amine **14** (200 mg, 0.567 mmol) was added portion wise. The mixture was heated at reflux for overnight and concentrated under reduced pressure. The residue was purified by reverse-phase column chromatography (H_2O:MeCN 100:0 to 0:100) to yield the title compound as a white solid (28 mg, 8% yield). ^{1}H NMR (600 MHz, $CDCl_3$) δ 8.41 (s, 1H), 7.93 – 7.84 (m, 4H), 7.55 (tt, J = 7.0, 5.3 Hz, 2H), 7.24 – 7.19 (m, 4H), 7.12 (t, J = 7.4 Hz, 1H), 7.10 – 7.06 (m, 2H), 6.98 – 6.92 (m, 1H), 6.74 – 6.68 (m, 2H), 4.53 – 4.48 (m, 1H), 3.97 (s, 2H), 3.17 – 2.98 (m, 4H), 2.45 – 2.36 (m, 2H), 2.33 – 2.18 (m, 4H), 1.96 – 1.86 (m, 2H), 1.53 – 1.44 (m, 2H), 1.44 – 1.35 (m, 2H), 1.20 – 1.11 (m, 2H). ^{13}C NMR (151 MHz, $CDCl_3$) δ 159.0, 154.2, 142.1, 141.5, 134.5, 132.4, 132.2, 129.2, 129.1, 128.9, 128.6, 128.3, 128.2, 128.0, 127.1, 126.6, 126.1, 122.8, 120.9, 111.7, 57.3, 47.9, 40.1, 37.2, 29.8, 27.3, 24.1, 23.8 (one carbon signal is not visible / a peak at 65.7 ppm is not visible but is confirmed by HSQC). HRMS: $C_{34}H_{40}N_3O_4S^+$ [M+H]$^+$ calcd: 586.2734, found: 586.2709. LC-MS: t_R = 4.2 min, >95% (254 nm), m/z: 586.3 [M+H]$^+$.

3-((5-(4-(2-benzylphenoxy)piperidin-1-yl)pentyl)amino)-4-ethoxycyclobut-3-ene-1,2-dione (17, VUF16336)

3,4-Diethoxycyclobut-3-ene-1,2-dione (72 mg, 0.426 mmol) was dissolved in EtOH (10 mL) containing TEA (0.119 mL, 0.851 mmol). Amine **14** (150 mg, 0.426 mmol) was added portion wise and the resulting mixture was stirred at rt for 30 h. The solvent was removed under reduced pressure. The residue was suspended in H_2O and filtered. The white precipitate was washed with H_2O and Et_2O and dried under vacuum. The compound was purified by reverse-phase column chromatography (H_2O:MeCN 100:0 to 0:100) to yield the title compound as a yellow foam (114 mg, 56% yield). NMR analysis indicates the presence of rotamers, resulting in e.g. more ^{13}C signals than expected. ^{1}H NMR (500 MHz, CD_3OD) δ 7.24 – 7.08 (m, 7H), 6.92 (d, J = 8.1 Hz, 1H), 6.86 (t, J = 7.4 Hz, 1H), 4.76-4.71 (m, 2H), 4.51 – 4.39 (m, 1H), 3.95 (s, 2H), 3.61 (t, J = 6.9 Hz, 1H), 3.43 (t, J = 6.9 Hz, 1H), 2.61 – 2.32 (m, 4H), 2.32 – 2.22 (m, 2H), 1.95 – 1.85 (m, 2H), 1.81 – 1.70 (m, 2H), 1.63 (app p, J = 7.1 Hz, 2H), 1.56 – 1.48 (m, 2H), 1.47 – 1.41 (m, 3H), 1.40 – 1.31 (m, 2H). ^{13}C NMR (126 MHz, CD_3OD) δ 189.9, 189.7, 184.7, 184.5, 178.0, 177.4, 174.8, 174.7, 156.2, 142.9, 132.2, 131.3, 129.7, 129.2, 128.6, 126.7, 121.4, 113.5, 70.7, 70.7, 59.5, 59.5, 50.8, 49.0, 45.4, 45.1, 37.5, 31.8, 31.4, 31.0, 27.1, 26.9, 25.5, 25.4, 16.2, 16.1 (a peak at 71.0 ppm is not visible but is confirmed by HSQC). HRMS: $C_{29}H_{37}N_2O_4^+$ [M+H]$^+$ calcd: 477.2748, found: 477.2747. LC-MS: t_R = 3.8 min, >99% (254 nm), m/z: 477.3 [M+H]$^+$.

3-((5-(4-(2-benzylphenoxy)piperidin-1-yl)pentyl)amino)-4-hydroxycyclobut-3-ene-1,2-dione (18a, VUF16335)

Ethyl ester **17** (108 mg, 0.22 mmol) was dissolved in THF (15 mL) and a solution of 4 N HCl in dioxane was added. The mixture was stirred at rt for 20 h and concentrated *in vacuo*. The solid material was dissolved in DCM and extracted four times with aq. $(NH_4)_2CO_3$ (0.3 M). The aqueous solution was lyophilized. The residue was purified by reverse-phase column chromatography (H_2O:MeCN 100:0 to 0:100) to yield the title compound as a white solid (69 mg, 70% yield). ^{1}H NMR (500 MHz, $CDCl_3$) δ 11.67 (s, 1H), 7.58 – 7.46 (m, 1H), 7.26 – 7.21 (m, 3H), 7.17 (t, J = 7.4 Hz, 1H), 7.11 (d, J = 7.5 Hz, 2H), 6.97 (t, J = 7.4 Hz, 1H), 6.76 (d, J = 8.1 Hz, 1H), 4.69 – 4.54 (m, 1H), 4.00 (s, 2H), 3.59 (app q, J = 6.4 Hz, 2H), 3.30 – 3.13 (m, 2H), 2.72 – 2.52 (m, 2H), 2.27 – 2.10 (m, 4H), 2.05 – 1.91 (m, 2H), 1.64 – 1.46 (m, 4H), 1.43 – 1.33 (m, 2H). ^{13}C NMR (126 MHz, $CDCl_3$) δ 195.9, 187.0, 182.1, 153.9, 142.3, 132.5, 128.7, 128.7, 128.3, 128.1, 126.1, 121.0, 111.4, 65.1, 56.8, 47.4, 42.9, 37.4, 30.1, 26.8, 23.3, 22.9, one carbon signal is not visible. HRMS: $C_{27}H_{33}N_2O_4^+$ [M+H]$^+$ calcd: 449.2435, found: 449.2433. LC-MS: t_R = 3.5 min, >99% (254 nm), m/z: 449.3 [M+H]$^+$.

3-((5-(4-(2-benzylphenoxy)piperidin-1-yl)pentyl)amino)-4-(ethylamino)cyclobut-3-ene-1,2-dione (18b, VUF16414)

A solution of ethyl ester **17** (190 mg, 0.399 mmol) in EtOH (10 mL) was treated with EtNH$_2$.HCl (17 mg, 0.399 mmol) and TEA (0.111 mL, 0.797 mmol). The resulting mixture was stirred for 14 h at rt and concentrated under vacuum. The residue was purified by reverse-phase column chromatography (H$_2$O:MeCN 100:0 to 0:100) to yield the title compound as a brown solid (142 mg, 75% yield). ^{1}H NMR (600 MHz, CD$_3$OD) δ 7.21 (t, J = 7.6 Hz, 2H), 7.18 – 7.09 (m, 5H), 6.92 (d, J = 8.2 Hz, 1H), 6.85 (t, J = 7.4 Hz, 1H), 4.46 – 4.40 (m, 1H), 3.95 (s, 2H), 3.70 – 3.54 (m, 4H), 2.58 – 2.43 (m, 2H), 2.40 – 2.32 (m, 2H), 2.31 – 2.26 (m, 2H), 1.95 – 1.87 (m, 2H), 1.78 – 1.71 (m, 2H), 1.65 (app p, J = 7.1 Hz, 2H), 1.56 – 1.49 (m, 2H), 1.38 (app p, J = 7.2 Hz, 2H), 1.26 (t, J = 7.2 Hz, 3H). ^{13}C NMR (151 MHz, CD$_3$OD) δ 183.6, 183.5, 169.5, 169.2, 156.3, 142.9, 132.1, 131.4, 129.7, 129.2, 128.6, 126.7, 121.4, 113.7, 59.5, 50.9, 45.1, 40.3, 37.4, 32.1, 31.2, 27.1, 25.4, 17.0. HRMS: C$_{29}$H$_{38}$N$_3$O$_3$$^+$ [M+H]$^+$ calcd: 476.2908, found: 476.2909. LC-MS: t_R = 3.7 min, >96% (254 nm), m/z: 476.3 [M+H]$^+$.

Ethyl (cyclopropylsulfonyl)carbamate (20a)

Cyclopropanesulfonamide **19a** (600 mg, 4.95 mmol), TEA (1.17 mL, 8.42 mmol) and DCM (10 mL) were mixed. The mixture was cooled to 0 °C. Ethyl carbonochloridate (0.566 mL, 5.94 mmol) was dissolved in DCM (10 mL). This solution was added drop wise to the solution of the sulfonamide while maintaining the temperature at 5 °C. The mixture was stirred at 5 °C for 2 h, then at rt for 4 h. H$_2$O and DCM were added and the pH of the mixture was adjusted to ca. 4 by addition of AcOH. The organic layer was separated, washed with H$_2$O and concentrated under pressure. The residue was purified by flash chromatography (cyclohexane/EtOAc=1:1, v/v) to yield the title compound as a white solid (680 mg, 71%). ^{1}H NMR (300 MHz, CDCl$_3$) δ 4.26 (q, J = 7.1 Hz, 2H), 2.95 – 2.83 (m, 1H), 1.41 – 1.36 (m, 2H), 1.32 (t, J = 7.1 Hz, 3H), 1.16 – 1.08 (m, 2H).

Ethyl ((4-(*tert*-butyl)phenyl)sulfonyl)carbamate (20c)

4-(*Tert*-butyl)benzenesulfonamide **19c** (100 mg, 0.469 mmol), TEA (0.111 mL, 0.797 mmol) and DCM (5 mL) were mixed. The mixture was cooled to 0 °C. Ethyl carbonochloridate (0.054 mL, 0.563 mmol) was dissolved in DCM (5 mL). This solution was added drop wise to the solution of the sulfonamide while maintaining the temperature at 5 °C. The mixture was stirred at 5 °C for 2 h, then stirred at rt for 4. H_2O and DCM were added. The pH of the mixture was adjusted to ca. 4 by addition of AcOH. The organic layer was separated, washed with H_2O and concentrated. The residue was purified by flash chromatography (cyclohexane/EtOAc=1:1, v/v) to yield the title compound as a white solid (68 mg, 51%). The crude product was used for further steps without purification. ^{1}H NMR (300 MHz, CDCl$_3$) δ 7.99 – 7.90 (m, 2H), 7.59 – 7.49 (m, 2H), 4.14 (q, *J* = 7.1 Hz, 2H), 1.34 (s, 9H), 1.21 (t, *J* = 6.9 Hz, 3H).

Ethyl (naphthalen-2-ylsulfonyl)carbamate (20d)

To a mixture of naphthalene-2-sulfonamide **19d** (250 mg, 1.206 mmol) and anhydrous K_2CO_3 (433 mg, 3.14 mmol), acetone (10 mL) was added. The resulting mixture was stirred for 3 h at rt. Ethyl carbonochloridate (0.152 mL, 1.592 mmol) was added. The mixture was stirred at reflux for 18 h. H_2O (5 mL) and DCM (5 mL) were added. The pH of the mixture was adjusted to ca. 4 by addition of AcOH. The organic layer was separated, washed with H_2O and concentrated under pressure. The crude product (163 mg, 48 %) was used for further steps without purification. ^{1}H NMR (300 MHz, CDCl$_3$) δ 8.67 – 8.61 (m, 1H), 8.13 (s, 1H), 8.04 – 7.95 (m, 2H), 7.94 – 7.88 (m, 1H), 7.72 – 7.56 (m, 2H), 4.11 (q, *J* = 7.1 Hz, 2H), 1.18 (t, *J* = 7.1 Hz, 3H).

4-(4-(2-benzylphenoxy)piperidin-1-yl)butane-1-sulfonic acid (21, VUF16317)

To a solution of amine **1** (300 mg, 1.12 mmol) in MeCN (10 mL) was added 1,2-oxathiane 2,2-dioxide (0.115 mL, 1.12 mmol) in portions within 30 min. The mixture was stirred at reflux for 48 h. KO*t*Bu (378 mg, 3.37 mmol) was added. The mixture was stirred at reflux for another 2 h and concentrated under reduced pressure. The residue was purified by reverse-phase column chromatography (H_2O:MeCN 100:0 to 0:100) to yield the title compound as a yellow solid (220 mg, 49% yield). ^{1}H NMR (600 MHz, CD$_3$OD) δ 7.25 (t, *J* = 7.5 Hz, 2H), 7.22 – 7.13 (m, 5H), 6.95 – 6.87 (m, 2H), 4.59 – 4.53 (m, 1H), 3.98 (s, 2H), 2.87 – 2.80 (m, 2H), 2.80 – 2.70 (m, 2H), 2.64 – 2.49 (m, 4H), 2.02 – 1.93 (m, 2H), 1.92 – 1.85 (m, 2H), 1.83 – 1.76 (m, 2H), 1.74 – 1.65 (m, 2H). ^{13}C NMR (151 MHz, CD$_3$OD) δ 155.8, 143.0, 132.5, 130.9, 129.5, 129.4, 128.8, 126.9, 121.7, 113.4, 58.4, 51.8, 50.2, 37.6, 29.7, 25.3, 23.7 (a peak at 69.3 ppm is not visible but is confirmed by HSQC).

HRMS: $C_{22}H_{30}NO_4S^+$ [M+H]$^+$ calcd: 404.1890, found: 404.1905. LC-MS: t_R = 3.5 min, >98% (254 nm), m/z: 404.1 [M+H]$^+$.

4-(2-benzylphenoxy)-1-(but-3-en-1-yl)piperidine (22)

To a solution of amine **1** (400 mg, 1.496 mmol) in MeCN (10 mL) were added K_2CO_3 (2068 mg, 14.96 mmol) and 4-bromobut-1-ene (0.759 mL, 7.48 mmol). The reaction mixture was stirred for 3 h under reflux. The reaction mixture was cooled to rt, diluted with EtOAc and washed with H_2O. The organic phase was dried over $MgSO_4$ and concentrated under reduced pressure. The crude mixture was purified by column chromatography (cyclohexane/EtOAc/TEA, 60:38:2) to yield the title compound as a colorless oil (312 mg, 65%). ^1H NMR (500 MHz, CDCl$_3$) δ 7.25 – 7.18 (m, 4H), 7.18 – 7.09 (m, 3H), 6.88 – 6.80 (m, 2H), 5.79 (ddt, J = 17.0, 10.3, 6.7 Hz, 1H), 5.11 – 4.94 (m, 2H), 4.38 (s, 1H), 3.97 (s, 2H), 2.64 – 2.47 (m, 2H), 2.41 – 2.28 (m, 4H), 2.28 – 2.19 (m, 2H), 2.00 – 1.91 (m, 2H), 1.87 – 1.74 (m, 2H). ^{13}C NMR (126 MHz, CDCl$_3$) δ 155.0, 141.4, 136.6, 131.0, 130.5, 129.0, 128.3, 127.4, 125.8, 120.3, 115.9, 112.4, 58.1, 50.2, 36.5, 31.7, 30.6 (one carbon signal for an aliphatic carbon is not visible). LC-MS: t_R = 3.8 min, >99% (254 nm), m/z: 322.2 [M+H]$^+$.

(4-(4-(2-benzylphenoxy)piperidin-1-yl)butyl)boronic acid (23, VUF16221)

A flask was charged with alkene **22** (700 mg, 2.18 mmol) and Et$_3$SiH (4.52 mL, 28.3 mmol) in DCM (10 mL). The mixture was cooled to 0 ºC and 1.0 M BCl$_3$ in DCM (3.01 mL, 30.5 mmol) was added. The mixture was stirred at 0 ºC for 100 min and warmed to rt over 1.5 h. The mixture was cooled to 0 ºC and Et$_2$O (10 mL) and H_2O (10 mL) were added. The mixture was extracted with Et$_2$O (3 x 10 mL). The combined organic layers were washed with brine, dried over Na$_2$SO$_4$, filtered, and concentrated to give the crude boronic acid (360 mg), which in previous trials could not be obtained pure by various methods and was therefore purified through MIDA protection and deprotection. It was used for the next step without purification. To a stirred solution of the intermediate (4-(4-(2-benzylphenoxy)piperidin-1-yl)butyl)boronic acid (360 mg) in DMF (5 mL) was added 2,2'-(methylazanediyl)diacetic acid (173 mg, 1.18 mmol) at rt. The reaction mixture was heated to 80 °C and stirred for 1 h. The mixture was concentrated under vacuum. The residue was purified by flash chromatography (MeOH/Et$_2$O 1.5/98.5, then THF 100% to elute product) to yield the intermediate MIDA-protected boronic acid as a white solid (229 mg). To a stirred solution of the intermediate MIDA-protected boronic acid (160 mg) in MeOH (5 mL), 1.0 M NaOH was added. The reaction mixture was stirred for 12 h at rt. The mixture was concentrated under reduced pressure. The residue was purified by reverse-phase column chromatography (H_2O:MeCN 100:0 to 0:100) to yield the title compound as a white solid (65 mg, 53% yield). ^1H

NMR (500 MHz, CD$_3$OD) δ 7.24 – 7.08 (m, 7H), 6.92 (d, J = 8.2 Hz, 1H), 6.86 (t, J = 7.4 Hz, 1H), 4.49 – 4.41 (m, 1H), 3.95 (s, 2H), 2.63 – 2.47 (m, 2H), 2.46 – 2.36 (m, 2H), 2.35 – 2.27 (m, 2H), 1.96 – 1.87 (m, 2H), 1.80 – 1.70 (m, 2H), 1.53 – 1.43 (m, 2H), 1.42 – 1.32 (m, 2H), 0.78 (t, J = 7.6 Hz, 2H). ^{13}C NMR (126 MHz, CD$_3$OD) δ 156.2, 142.9, 132.1, 131.3, 129.7, 129.2, 128.6, 126.7, 121.4, 113.6, 59.2, 50.6, 37.5, 30.7, 29.9, 23.1 (peaks at 71.6 ppm and 13.5 ppm are not visible but are confirmed by HSQC). HRMS: C$_{22}$H$_{31}$BNO$_3^+$ [M+H]$^+$ calcd : 368.2395, found: 368.2387. LC-MS: t_R = 3.4 min, >96% (254 nm), m/z: 368.2 [M+H]$^+$.

(*R*)-2-(2-(4-((4-chlorophenyl)(phenyl)methyl)piperazin-1-yl)ethoxy)-*N*-(phenylsulfonyl)acetamide (24, VUF15665)

To a solution of (*R*)-2-(2-(4-((4-chlorophenyl)(phenyl)methyl)piperazin-1-yl)ethoxy)acetic acid (1.00 g, 2.17 mmol), HATU (1.24 g, 3.25 mmol) and DIPEA (1.52 mL, 8.68 mmol) in DMF (10 mL), benzenesulfonamide (0.51 g, 3.25 mmol) in DMF (5 mL) was added. The mixture was stirred at rt for 23 h. The reaction mixture was diluted with water and acidified to pH = 4-5 with aq. HCl. The mixture was extracted with EtOAc (200 mL + 150 mL). The combined organic layers were washed with brine (2x) and water (2x), dried over Na$_2$SO$_4$, filtered and evaporated. The crude product was purified using silica gel (gradient 100% DCM ▢ 15% MeOH/85 % DCM) to give the product as a white solid (0.71 g, 62 %). ^{1}H NMR (500 MHz, DMSO-d6) δ 7.82 - 7.71 (m, 2H), 7.52 - 7.31 (m, 11H), 7.24 (t, J = 7.3 Hz, 1H), 4.46 (s, 1H), 3.77 (s, 2H), 3.74 - 3.67 (m, 2H), 3.33 - 3.10 (m, 6H), a CH$_2$ signal of the piperazine (counting for 4H) is overlapping with residual DMSO signal but can be identified from HSQC and COSY. ^{13}C NMR (126 MHz, DMSO-d6) δ 175.1, 144.9, 141.5, 141.1, 131.7, 130.5, 129.3, 128.9, 128.8, 127.9, 127.5, 127.4, 126.9, 73.1, 70.9, 65.1, 54.7, 51.1, 47.5. HRMS: C$_{27}$H$_{31}$ClN$_3$O$_4$S$^+$ [M+H]$^+$ calcd: 528.1718, found 528.1743. LC-MS: t_R = 4.3 min, >99% (254 nm), *m/z:* 528 [M+H]$^+$.

Acknowledgements

References

1.   Copeland, R. A., The drug–target residence time model: a 10-year retrospective. *Nature Reviews Drug Discovery* **2016,** *15* (2), 87-95.

2.   Guo, D.; Hillger, J. M.; IJzerman, A. P.; Heitman, L. H., Drug-target residence time—a case for G protein-coupled receptors. *Medicinal Research Reviews* **2014,** *34* (4), 856-892.

3.	David, C. S.; Brad, A. H.; Isabelle Van, L.; Georges, V., The role of binding kinetics in GPCR drug discovery. *Current Topics in Medicinal Chemistry* **2015,** *15* (24), 2504-2522.

4.	Vauquelin, G.; Charlton, S. J., Long-lasting target binding and rebinding as mechanisms to prolong in vivo drug action. *British Journal of Pharmacology* **2010,** *161* (3), 488-508.

5.	Hoffmann, C.; Castro, M.; Rinken, A.; Leurs, R.; Hill, S. J.; Vischer, H. F., Ligand residence time at G-protein–coupled receptors—why we should take our time to study it. *Molecular Pharmacology* **2015,** *88* (3), 552-560.

6.	Miller, D. C.; Lunn, G.; Jones, P.; Sabnis, Y.; Davies, N. L.; Driscoll, P., Investigation of the effect of molecular properties on the binding kinetics of a ligand to its biological target. *MedChemComm* **2012,** *3* (4), 449-452.

7.	Tresadern, G.; Bartolome, J. M.; Macdonald, G. J.; Langlois, X., Molecular properties affecting fast dissociation from the D2 receptor. *Bioorganic & Medicinal Chemistry* **2011,** *19* (7), 2231-2241.

8.	Schmidtke, P.; Luque, F. J.; Murray, J. B.; Barril, X., Shielded hydrogen bonds as structural determinants of binding kinetics: application in drug design. *Journal of the American Chemical Society* **2011,** *133* (46), 18903-18910.

9.	Heroven, C.; Georgi, V.; Ganotra, G. K.; Brennan, P.; Wolfreys, F.; Wade, R. C.; Fernández-Montalván, A. E.; Chaikuad, A.; Knapp, S., Halogen–aromatic π interactions modulate inhibitor residence times. *Angewandte Chemie International Edition* **2018,** *57* (24), 7220-7224.

10.	Bradshaw, J. M.; McFarland, J. M.; Paavilainen, V. O.; Bisconte, A.; Tam, D.; Phan, V. T.; Romanov, S.; Finkle, D.; Shu, J.; Patel, V.; Ton, T.; Li, X.; Loughhead, D. G.; Nunn, P. A.; Karr, D. E.; Gerritsen, M. E.; Funk, J. O.; Owens, T. D.; Verner, E.; Brameld, K. A.; Hill, R. J.; Goldstein, D. M.; Taunton, J., Prolonged and tunable residence time using reversible covalent kinase inhibitors. *Nature Chemical Biology* **2015,** *11* (7), 525-531.

11.	Garland, S. L., Are GPCRs still a source of new targets? *Journal of Biomolecular Screening* **2013,** *18* (9), 947-966.

12.	Overington, J. P.; Al-Lazikani, B.; Hopkins, A. L., How many drug targets are there? *Nature Reviews Drug Discovery* **2006,** *5* (12), 993-996.

13.	Santos, R.; Ursu, O.; Gaulton, A.; Bento, A. P.; Donadi, R. S.; Bologa, C. G.; Karlsson, A.; Al-Lazikani, B.; Hersey, A.; Oprea, T. I.; Overington, J. P., A comprehensive map of molecular drug targets. *Nature Reviews Drug Discovery* **2017,** *16* (1), 19-34.

14.	Sykes, D. A.; Stoddart, L. A.; Kilpatrick, L. E.; Hill, S. J., Binding kinetics of ligands acting at GPCRs. *Molecular and Cellular Endocrinology* **2019,** *485*, 9-19.

15.	Kooistra, A. J.; Kuhne, S.; de Esch, I. J. P.; Leurs, R.; de Graaf, C., A structural chemogenomics analysis of aminergic GPCRs: lessons for histamine receptor ligand design. *British Journal of Pharmacology* **2013,** *170* (1), 101-126.

16.	Zhang, M. Q.; Leurs, R.; Timmerman, H. Histamine H1- Receptor Antagonists. In *Burger's Medicinal Chemistry an Drug Discovery*, 5th ed.; Wolff, M. E., Ed.; Vrije Universiteit: Amsterdam, 1997; Vol. 5.

17.	Walter, M.; Stark, H., Histamine receptor subtypes: a century of rational drug design. *Frontiers in Bioscience (Scholar edition)* **2012,** *4*, 461-88.

18.	Shimamura, T.; Shiroishi, M.; Weyand, S.; Tsujimoto, H.; Winter, G.; Katritch, V.; Abagyan, R.; Cherezov, V.; Liu, W.; Han, G. W.; Kobayashi, T.; Stevens, R. C.; Iwata, S., Structure of the human histamine H1 receptor complex with doxepin. *Nature* **2011,** *475* (7354), 65-70.

19.	Kobayashi, C.; Tanaka, A.; Yasuda, T.; Hishinuma, S., Roles of Lys191 and Lys179 in regulating thermodynamic binding forces of ligands to determine their binding affinity for human histamine H1 receptors. *Biochemical Pharmacology* **2020,** *180*, 114185.

20.	Gillard, M.; Van Der Perren, C.; Moguilevsky, N.; Massingham, R.; Chatelain, P., Binding characteristics of cetirizine and levocetirizine to human H1 histamine receptors: contribution of Lys191and Thr194. *Molecular Pharmacology* **2002,** *61* (2), 391-399.

21.   Bosma, R.; Stoddart, L. A.; Georgi, V.; Bouzo-Lorenzo, M.; Bushby, N.; Inkoom, L.; Waring, M. J.; Briddon, S. J.; Vischer, H. F.; Sheppard, R. J.; Fernández-Montalván, A.; Hill, S. J.; Leurs, R., Probe dependency in the determination of ligand binding kinetics at a prototypical G protein-coupled receptor. *Scientific Reports* **2019,** *9* (1), 7906.

22.   Kuhne, S. Design and synthesis of tool compounds to probe GPCRs (doctoral dissertation), Vrije Universiteit Amsterdam, **2018**.

23.   Ertl, P.; Altmann, E.; McKenna, J. M., The most common functional groups in bioactive molecules and how their popularity has evolved over time. *Journal of Medicinal Chemistry* **2020,** *63* (15), 8408-8418.

24.   Kalgutkar, A. S.; Scott Daniels, J., Carboxylic acids and their bioisosteres. In *Metabolism, Pharmacokinetics and Toxicity of Functional Groups: Impact of Chemical Building Blocks on ADMET*, The Royal Society of Chemistry: 2010; pp 99-167.

25.   Lassalas, P.; Gay, B.; Lasfargeas, C.; James, M. J.; Tran, V.; Vijayendran, K. G.; Brunden, K. R.; Kozlowski, M. C.; Thomas, C. J.; Smith, A. B.; Huryn, D. M.; Ballatore, C., Structure property relationships of carboxylic acid isosteres. *Journal of Medicinal Chemistry* **2016,** *59* (7), 3183-3203.

26.   Ballatore, C.; Huryn, D. M.; Smith III, A. B., Carboxylic acid (bio)Isosteres in drug design. *ChemMedChem* **2013,** *8* (3), 385-395.

27.   Bosma, R.; Wang, Z.; Kooistra, A. J.; Bushby, N.; Kuhne, S.; van den Bor, J.; Waring, M. J.; de Graaf, C.; de Esch, I. J.; Vischer, H. F.; Sheppard, R. J.; Wijtmans, M.; Leurs, R., Route to prolonged residence time at the histamine H1 receptor: growing from desloratadine to rupatadine. *Journal of Medicinal Chemistry* **2019,** *62* (14), 6630-6644.

28.   Bosma, R.; van den Bor, J.; Vischer, H. F.; Labeaga, L.; Leurs, R., The long duration of action of the second generation antihistamine bilastine coincides with its long residence time at the histamine H1 receptor. *European Journal of Pharmacology* **2018,** *838*, 107-111.

29.   Bosma, R.; Moritani, R.; Leurs, R.; Vischer, H. F., BRET-based β-arrestin2 recruitment to the histamine H1 receptor for investigating antihistamine binding kinetics. *Pharmacological Research* **2016,** *111*, 679-687.

30.   Bosma, R.; Stoddart, L. A.; Georgi, V.; Bouzo-Lorenzo, M.; Bushby, N.; Inkoom, L.; Waring, M. J.; Briddon, S. J.; Vischer, H. F.; Sheppard, R. J.; Fernández-Montalván, A.; Hill, S. J.; Leurs, R., Probe dependency in the determination of ligand binding kinetics at a prototypical G protein-coupled receptor. *Scientific Reports* **2019,** *9* (1), 7906.

31.   Kuhne, S.; Kooistra, A. J.; Bosma, R.; Bortolato, A.; Wijtmans, M.; Vischer, H. F.; Mason, J. S.; de Graaf, C.; de Esch, I. J. P.; Leurs, R., Identification of ligand binding hot spots of the histamine H1 receptor following structure-based fragment optimization. *Journal of Medicinal Chemistry* **2016,** *59* (19), 9047-9061.

32.   de Graaf, C.; Kooistra, A. J.; Vischer, H. F.; Katritch, V.; Kuijer, M.; Shiroishi, M.; Iwata, S.; Shimamura, T.; Stevens, R. C.; de Esch, I. J. P.; Leurs, R., Crystal structure-based virtual screening for fragment-like ligands of the human histamine H1 receptor. *Journal of Medicinal Chemistry* **2011,** *54* (23), 8195-8206.

33.   Vermeulen, E. S.; van Smeden, M.; Schmidt, A. W.; Sprouse, J. S.; Wikström, H. V.; Grol, C. J., Novel 5-HT7 receptor inverse agonists. synthesis and molecular modeling of arylpiperazine- and 1,2,3,4-tetrahydroisoquinoline-based arylsulfonamides. *Journal of Medicinal Chemistry* **2004,** *47* (22), 5451-5466.

34.   Falgueyret, J.-P.; Oballa, R. M.; Okamoto, O.; Wesolowski, G.; Aubin, Y.; Rydzewski, R. M.; Prasit, P.; Riendeau, D.; Rodan, S. B.; Percival, M. D., Novel, nonpeptidic cyanamides as potent and reversible inhibitors of human cathepsins K and L. *Journal of Medicinal Chemistry* **2001,** *44* (1), 94-104.

35.   Rathish, I. G.; Javed, K.; Bano, S.; Ahmad, S.; Alam, M. S.; Pillai, K. K., Synthesis and blood glucose lowering effect of novel pyridazinone substituted benzenesulfonylurea derivatives. *European Journal of Medicinal Chemistry* **2009,** *44* (6), 2673-2678.

36.   Marshall, F.; Sigal, J. M., Notes - Some N-arylculfonyl-N '-alkylureas. *The Journal of Organic Chemistry* **1958,** *23* (6), 927-929.

37.   Walker, J. D.; Madalengoitia, J. S., Optimization of methods for the generation of carbodiimides for zwitterionic 1,3-diaza-Claisen rearrangements. *Tetrahedron Letters* **2015,** *56* (24), 3786-3789.

38.   Mejuch, T.; Garivet, G.; Hofer, W.; Kaiser, N.; Fansa, E. K.; Ehrt, C.; Koch, O.; Baumann, M.; Ziegler, S.; Wittinghofer, A.; Waldmann, H., Small-molecule inhibition of the UNC119–cargo interaction. *Angewandte Chemie International Edition* **2017,** *56* (22), 6181-6186.

39.   Smet, C.; Duckert, J.-F.; Wieruszeski, J.-M.; Landrieu, I.; Buée, L.; Lippens, G.; Déprez, B., Control of protein–protein interactions: structure-based discovery of low molecular weight inhibitors of the interactions between Pin1 WW domain and phosphopeptides. *Journal of Medicinal Chemistry* **2005,** *48* (15), 4815-4823.

40.   Kinney, W. A.; Lee, N. E.; Garrison, D. T.; Podlesny, E. J.; Simmonds, J. T.; Bramlett, D.; Notvest, R. R.; Kowal, D. M.; Tasse, R. P., Bioisosteric replacement of the .alpha.-amino carboxylic acid functionality in 2-amino-5-phosphonopentanoic acid yields unique 3,4-diamino-3-cyclobutene-1,2-dione containing NMDA antagonists. *Journal of Medicinal Chemistry* **1992,** *35* (25), 4720-4726.

41.   Chen, Z.; Bi, J.; Su, W., Synthesis and antitumor activity of novel coumarin derivatives via a three-component reaction in water. *Chinese Journal of Chemistry* **2013,** *31* (4), 507-514.

42.   Guo, D.; van Dorp, E. J. H.; Mulder-Krieger, T.; van Veldhoven, J. P. D.; Brussee, J.; IJzerman, A. P.; Heitman, L. H., Dual-point competition association assay:a fast and high-throughput kinetic screening method for assessing ligand-receptor binding kinetics. *Journal of Biomolecular Screening* **2013,** *18* (3), 309-320.

43.   Babcock, L.; Pizer, R., Dynamics of boron acid complexation reactions. Formation of 1:1 boron acid-ligand complexes. *Inorganic Chemistry* **1980,** *19* (1), 56-61.

44.   Procopiou, P. A.; Ford, A. J.; Gore, P. M.; Hancock, A. P.; Hodgson, S. T.; Holmes, D. S.; Looker, B. E.; Vile, S.; Clark, K. L.; Saunders, K. A.; Slack, R. J.; Watts, C. J., Identification of selective 8-(piperidin-4-yloxy)quinoline sulfone and sulfonamide histamine H1 receptor antagonists for use in allergic rhinitis. *Bioorganic & Medicinal Chemistry Letters* **2017,** *27* (21), 4914-4919.

45.   Bosma, R.; Witt, G.; Vaas, L. A. I.; Josimovic, I.; Gribbon, P.; Vischer, H. F.; Gul, S.; Leurs, R., The target residence time of antihistamines determines their antagonism of the G protein-coupled histamine H1 receptor. *Frontiers in Pharmacology* **2017,** *8* (667).

46.   Gillard, M.; Chatelain, P., Changes in pH differently affect the binding properties of histamine H1 receptor antagonists. *European Journal of Pharmacology* **2006,** *530* (3), 205-214.

47.   Bosma, R.; Moritani, R.; Leurs, R.; Vischer, H. F., BRET-based β-arrestin2 recruitment to the histamine H1 receptor for investigating antihistamine binding kinetics. *Pharmacological Research* **2016,** *111*, 679-687.

48.   Yung-Chi, C.; Prusoff, W. H., Relationship between the inhibition constant (KI) and the concentration of inhibitor which causes 50 per cent inhibition (I50) of an enzymatic reaction. *Biochemical Pharmacology* **1973,** *22* (23), 3099-3108.

Chapter 5

Exploring ligand-binding kinetics at the histamine H_1 receptor: a pilot study with boron-containing ligands

Zhiyong Wang, Reggie Bosma, Marta Arimont, Melanie van der Woude, Daniel Da Costa Pereira, Henry F. Vischer, Iwan J. P. de Esch, Maikel Wijtmans and Rob Leurs

Abstract

Drugs with prolonged drug-target residence times are speculated to give a higher chance of better drug efficacy. The general trends underlying the design of small molecules with prolonged residence time are nonetheless poorly understood. One method to slow dissociation is the utilization of covalent ligands. Here, we explore the hypothesis that the unique chemical properties of boron can be a means to affect ligand binding kinetics on a GPCR via reversible covalent binding with the protein. We report two series of boron-containing ligands that were designed and synthesized to engage key lysine residue K191$^{5.39}$ in the histamine H_1 receptor (H_1R). Equilibrium and kinetic binding properties were systematically analysed. The currently available data shows that kinetic properties can be modulated modestly by an α-aminoboronic acid, but our current pilot data does not substantiate the hypothesis of reversible covalent binding to the H_1R.

Introduction

Whereas classical pharmacology has primarily focused on equilibrium binding affinity of a ligand to a specific biochemical target as the means to determine ligand efficacy, it has more recently become apparent that other parameters, i.e., ligand residence time, are particularly important to determine efficacy.[1-6] Many drug candidates fail to meet the criteria in clinical trials, and toxicity and/or lack of drug efficacy is often a major problem. Successfully approved drugs show good efficacy and toxicity profiles which may be (partially) ascribed to long drug target residence time.[5] Indeed, it was found that the drug residence time (RT), a measure for the time that a drug occupies its molecular target and defined as the reciprocal value of the dissociation rate constant k_{off}, can improve drug safety and reduce off-target toxicity.[7] Recently, several structural factors of the ligand have been postulated to correlate to RT, such as shielded hydrogen bonds[8], rings[9] as well as rotatable bonds[10]. It has also been found that the RT can be prolonged by covalent binding to the targets.[11-14] Whereas typical small-molecule drugs bind to their targets reversibly with non-covalent interactions,[15] covalent binders also undergo such reversible molecular recognition but in a second step form a covalent bond with a nearby nucleophilic residue of the target.[16] The formed covalent ligand-protein complex is often characterized by slower or absent dissociation rate of the ligand from the complex.

The most common residue to be targeted by covalent ligands is cysteine by virtue of its high nucleophilicity.[17] However, in some cases it may be preferred to target a lysine. The nucleophilicity of lysine depends on its basicity, typically expressed by the pK_a value of the corresponding ammonium cation. It has previously been found that the pK_a value of a lysine residue depends on its location in the protein.[18] For example, lysine residues which are located on the protein surface typically have a higher pK_a value which can reach >10, whereas the pK_a

values of residues located in the binding pocket can be much lower. Covalent targeting of a lysine residue is known to be challenging, because at pH 7.4 many lysine residues are predominantly in their protonated and therefore non-nucleophilic state. Nonetheless, several warheads have been developed to target lysine and a few examples are listed here. An NHS-ester was identified by Chen *et al.* to selectively label lysine.[19] A vinyl sulfone warhead was reported to covalently bind to lysine by Anscombe *et al*.[20] Matos *et al.* reported that a sulfonylated acrylate can modify a single lysine residue chemo- and regioselectively.[21]

Interestingly, it has also been reported that boronic acids can be used to covalently target lysine.[21] In 2016, Akçay *et al*. reported a novel covalent inhibitor to treat Myeloid cell leukemia 1 (Mcl-1) (**1**, Figure 1A). This reversible boronic acid inhibitor showed an increased potency compared to non-covalent analogues, which was further confirmed by mutation studies.[22] Indeed, the chemical properties of boron have more generally been of interest to medicinal chemists. Such properties include the capacity to form (reversible) covalent bonds with nitrogen and oxygen atoms, giving the potential of forming tricoordinated sp^2 or tetracoordinated sp^3 configurations.[23] It has become evident that the affinity and other pharmacological properties of ligands can be improved by including boron.[24-28] However, a systematic study on the use of boron moieties in molecules to modulate ligand-binding kinetics has received relatively little attention in previous work.

A

B

Covalent Mcl-1 inhibitor
1

Doxepin

Levocetirizine

2

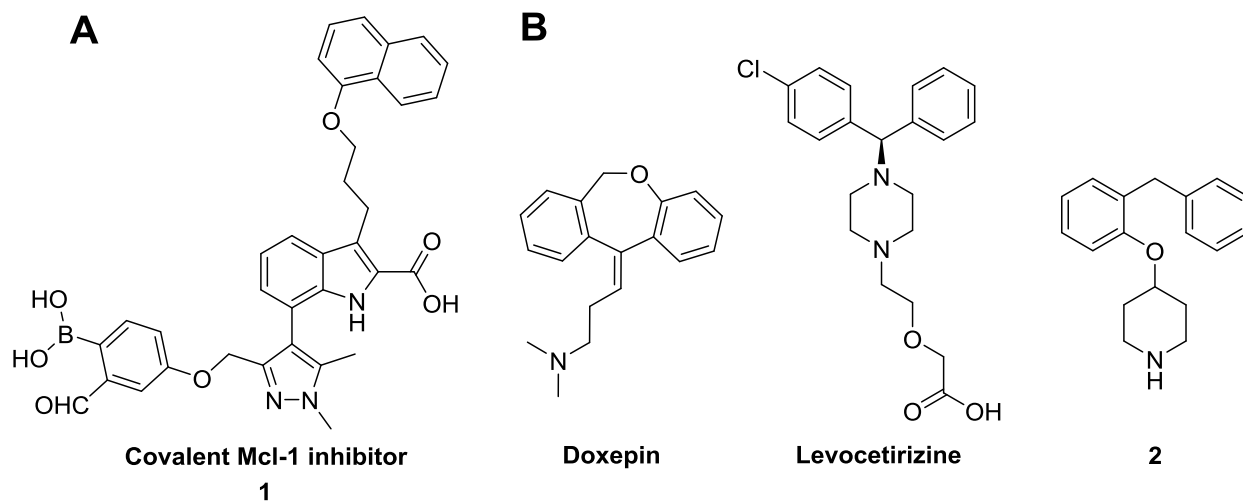**Figure 1.** (A) Structure of a boron-containing reversible covalent inhibitor for Mcl-1; (B) Structures of some antagonists for H_1R.

We focus our attention on the binding kinetics of ligands for G protein-coupled receptors (GPCRs), the therapeutically largest and most relevant protein family. New ways to modulate the binding kinetics of GPCR ligands are in demand. We use a therapeutically highly successful GPCR, namely

the histamine H_1 receptor (H_1R). It has been reported to play an important role in many physiological processes, such as itch, allergy and sleep-wake cycles.[29-35] In 2011, the co-crystal structure of H_1R with doxepin (Figure 1B) was published,[36] which opened up new opportunities in studying key pharmacological parameters, such as drug residence time, at a more detailed level. Indeed, while considerable research has been performed to explore the SAR of H_1R ligands,[37-39] detailed structure–kinetics relationships (SKRs) of H_1R ligands have only recently be addressed. Factors studied include, amongst others, steric hindrance in the binding pocket[40] and the level of rigidity of the typical aromatic head group of H_1R ligands (Chapter 3). It has also been postulated that the ionic interaction between the carboxylate group of the antihistamine levocetirizine (Figure 1B) and $K191^{5.39}$ in H_1R contributes significantly to its long residence time.[41] Last, the effect of bioisosteres of the carboxylic acid on the residence time has been explored (Chapter 4).

Here, we evaluate the possibility of engaging $K191^{5.39}$ with boron-containing ligands as a means to modulate binding kinetics. To this end, we report the synthesis and evaluation of two series of boron-containing ligands. These compounds are hybrids between a hit scaffold **2** (Figure 1B) reported by Kuhne *et al*[42] and different warheads, i.e. an aldehyde boronic acid and an α-aminoboronic acid. Through the synthesis and pharmacological evaluation of these boron-containing compounds and appropriate control ligands, we investigate if a boron atom in the ligands can affect binding kinetics of GPCR ligands.

Results and discussion

Design

To investigate the binding kinetics of boron-containing ligands and the $K191^{5.39}$ residue, the hit scaffold **2** was selected as starting point. Fragment **2** was previously identified from a structure-based virtual fragment screening campaign.[43] We have since successfully used it in the exploration of binding kinetics as the core of ligands with acid moieties[44] and acid isosteres to engage $K191^{5.39}$ (Chapter 4). Using the X-ray crystal structure of the H_1R,[36] we determined for the current work that the accessibility of $K191^{5.39}$ offered the best opportunity for covalent bonds with a boron moiety if the scaffold **2** was decorated with a four atom linker (four carbon atoms or three carbon atoms and an oxygen atom) to which the warhead was appended.

In series A, an aromatic aldehyde boronic acid was the warhead for the lysine, as based on previous work by others.[22, 45] It has been postulated that the boron atom activates the carbonyl group toward nucleophilic attack from the lysine nitrogen atom, which after expulsion of water is followed by imine formation (Figure 2A).[45] The imine nitrogen atom coordinates to the boron atom. Thus, the Lewis acidity of boron is used to significantly lower the energy barrier to form the iminoboronate[18, 46] and may contribute to the stability of the final complex. As such, it may

prolong the process of the reversible reaction, i.e. imine hydrolysis, thus increasing residence time of the ligand. The benzaldehyde boronic acid **10** and the corresponding aromatic reference compounds **5** and **6** having none or just one of the two required components of the benzaldehyde boronic acid warhead, were designed and synthesized. It should be noted that an isolated boronic acid (as in reference compound **6**) can potentially give reversible covalent bonds to a lysine in its own right through formation of dative complexes[47], but that the combination with the aldehyde function (Fig. 2A) should give an especially powerful warhead. Docking of compound **10** in the available H_1R x-ray structure indicates that the aldehyde group can be positioned within 3 angstrom distance of the target residue K191[5.39] (Figure 3).

In Series B, an α-aminoboronic acid warhead (**13**) and a control amide (**12**) were incorporated into the VS hit scaffold. Bock *et al* have shown that an α-amidoboronic acid forms a five-membered ring by coordination of the amide carbonyl and the boron atom (Fig. 2B).[48, 49] We hypothesise that this complex as a result of the dative bond has increased electrophilicity at the carbonyl group and if geometrically positioned appropriately can be attacked by a lysine residue (Fig. 2B). The formed complex would lose a molecule of water to provide an amidine complex. The amidine nitrogen atom can coordinate to the boron to form the final complex. Also here, the presumed stability of this reversible complex is hypothesized to lead to slower dissociation of the ligand.

Figure 2. The proposed mechanism of two series of boron-containing compounds designed to covalently bind with a lysine residue. (A) Use of a benzaldehyde boronic acid.[22, 45] (B) Hypothesised use of an α-aminoboronic acid.[48, 49] Lys=lysine.
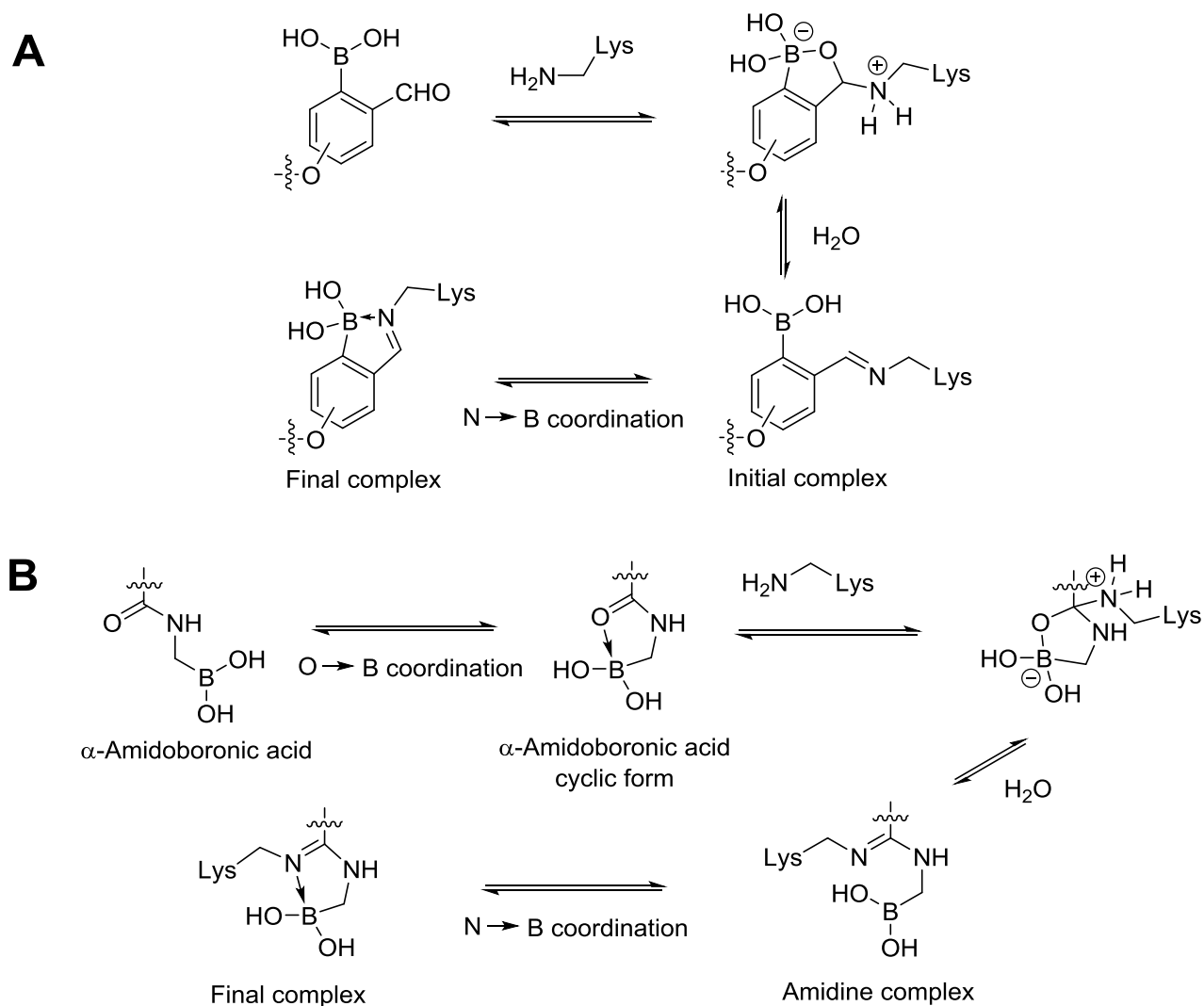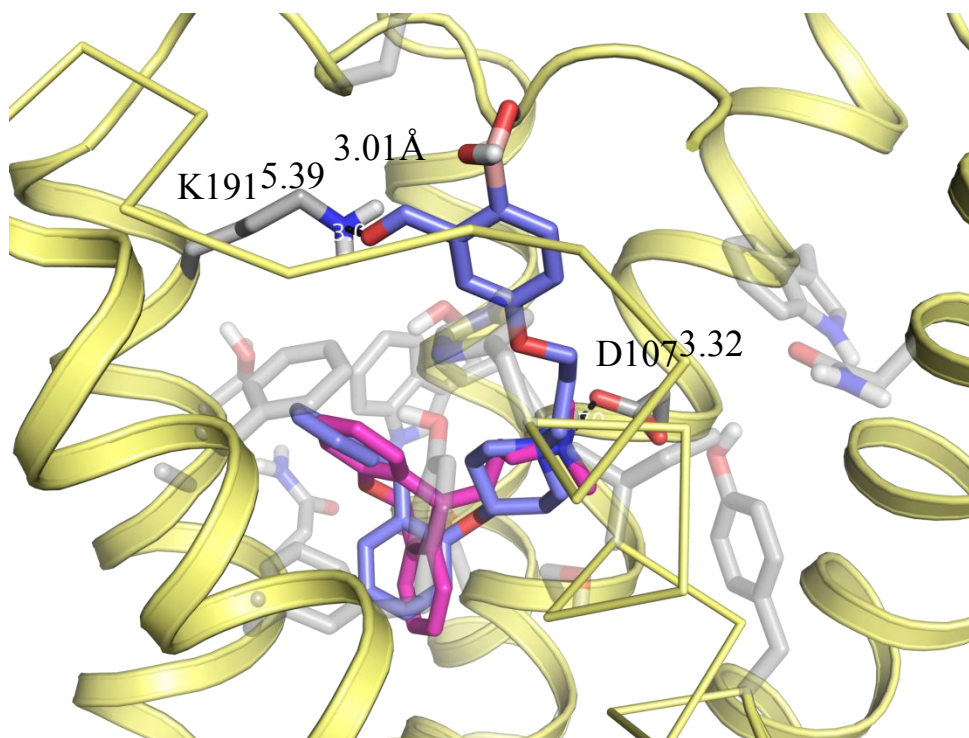
Figure 3. Proposed binding mode of **10** into the crystal structure (PDB-code 3RZE37) of H$_1$R. Doxepin (magenta carbon atoms) and **10** (blue carbon atoms) are depicted as overlay, both interacting with D107$^{3.52}$, whereas **10** is directed also towards the target lysine residue K191$^{5.39}$.

Synthesis

Alkylation of commercially available phenol **3** with 1-bromo-3-chloropropane afforded **4**.[50] Amine **2** was synthesized according to Kuhne *et al*.[42] Nucleophilic substitution on **4** with **2** afforded **5**. Boronic acid **6** was prepared in a two-step sequence starting with the boronic-acid containing phenol **3b** but without purification of the potentially unstable boronic-acid containing alkyl bromide intermediate. Alkylation of commercially available **7** provided bromide **8** and subsequent nucleophilic substitution yielded intermediate **9**. Boronic acid **10** was prepared using a Miyaura borylation coupling of **9** and *in situ* hydrolysis. Coupling reactions with carboxylic acid **11** yielded compounds **12** (Chapter 4) and **13**.[48]
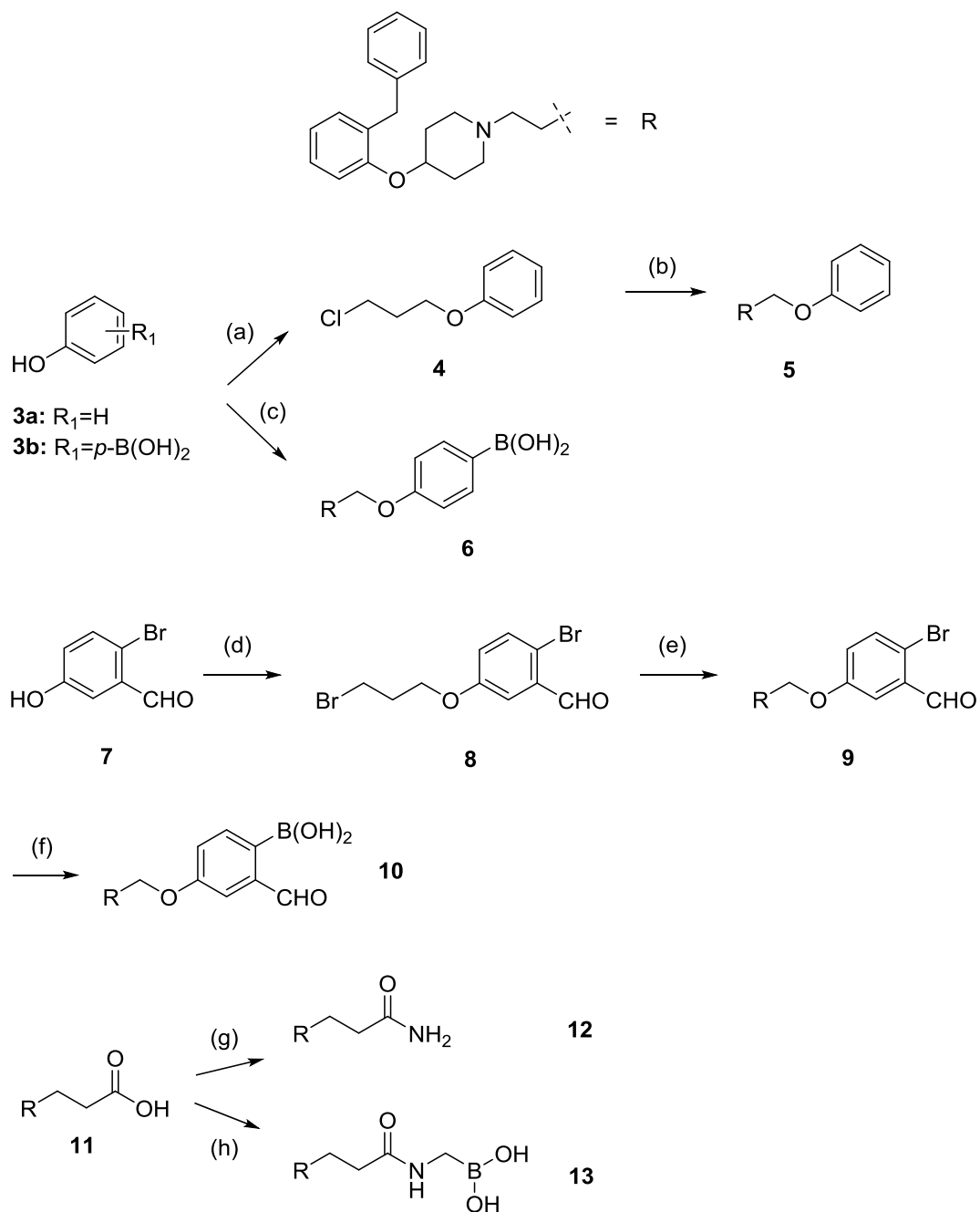
Scheme 1. Synthesis of boron-containing ligands. *Reagents and conditions:* (a) 1-Bromo-3-chloropropane, acetone, K_2CO_3, reflux, 16 h, 60%; (b) **2**, NaHCO$_3$, NaI, MeCN, 1 h, 130 °C, microwave, 43%; (c) (1) 1,3-Dibromopropane, K_2CO_3, DMF, 60-80 °C, 2-24 h; (2) **2**, K_2CO_3, MeCN, 3 h, reflux, 47% over two steps; (d) 1,3-Dibromopropane, K_2CO_3, DMF, 60-80 °C, 2-24 h, 53 %; (e) **2**, K_2CO_3, MeCN, 3 h, reflux, 46%; (f) 4,4,4',4',5,5,5',5'-octamethyl-2,2'-bi(1,3,2-dioxaborolane), KOAc, PdCl$_2$(dppf)CH$_2$Cl$_2$, 1,4-dioxane, reflux, 30 min, 29%; (g) HOBt·H$_2$O, EDCl·HCl, TEA, 1.0 M NH$_3$ in dioxane, DCM, rt, 16 h, 42% as fumarate; (h) HATU, DIPEA, (4,4,5,5-tetramethyl-1,3,2-dioxaborolan 2-yl)methanamine hydrochloride, DCM, rt, 16 h, 17%.

Pharmacological evaluation

Competition binding values (K_i) and association/dissociation rate constants (k_{on}/k_{off}) of ligands for the human H_1R were determined using [^{3}H]mepyramine and H_1R transiently expressed in homogenates of HEK293T cells a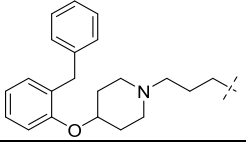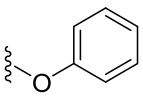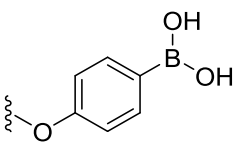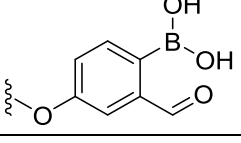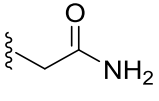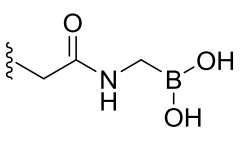s described previously.[51] Dissociation equilibrium constants (K_d) were calculated from the k_{on}/k_{off} values and in general matched reasonably with K_i values. Table 1 shows the binding affinities for all synthesized ligands and kinetic data for the majority of those. All synthesized ligands show high binding affinity (pK_i values range from 8.1 to 8.9). This indicates that, per our design, the molecular recognition induced by the scaffold of **2** is sufficiently efficient.

Within series A (**5**, **6** and **10**), the unsubstituted phenyl analogue **5** has the highest binding affinity (pK_i = 8.9). This indicates that the variety of substitution patterns in the other two compounds induces a modest steric and/or electronic mismatch in the molecular recognition event. No effect on RT from the introduction of a boronic acid group on the aromatic ring (**6**) was found which shows, compared to **5**, similar k_{on} and k_{off} values. The latter does not support the hypothesis that the boronic acid affects RT by giving any substantial formation of a dative complex with a lysine in this particular molecule (*vide supra*). Moreover, the kinetic properties of the fully equipped benzaldehyde boronic acid **10** were also not very different from the unsubstituted **5** or the boronic acid **6**. Compared to its boronic acid control **6**, ligand **10** has a similar association rate (k_{on} (10^6) = 4.2 (**6**), 2.2 (**10**)) and similar dissociation rate (k_{off} = 0.04 (**6**), 0.04 (**10**)). Unfortunately, the currently available dataset on series A cannot support the hypothesized formation of covalent complexes. Perhaps, the chosen linker length was not optimal as a result of which the warhead was not able to achieve a suitable proximity to a lysine. Future experiments should aim to optimize the linker length and/or position of the boronic acid.

In Series B, α-aminoboronic acid **13** shows a slightly lower binding affinity (pK_i = 8.1) compared to amide **12** (pK_i = 8.5). The k_{on} value is substantially lowered by appending the boronic acid (k_{on} (10^6) = 58.4 (**12**), 3.8 (**13**)), while the k_{off} value is also significantly lowered (k_{off} = 0.20 (**12**), 0.05 (**13**)) resulting in a 4-fold increase in RT for **13**. The obseverd RT value for **13**, however, does not suggest an efficient covalent binding process as the RT of compound **13** is not very long in comparison with non-covalent slow kinetic binders such as desloratadine, rupatadine or levocetirizine (see chapters 2 and 4). Indeed, neither the pK_a value of the targeted lysine in H_1R nor its nucleophilicity are known. It is conceivable that even though complexation of the boron atom to the carbonyl oxygen atom can increase the electrophilicity of the latter, subsequent nucleophilic attack from the lysine amine nitrogen may not occur. The current data shows that the α-aminoboronic acid was only moderately able to modulate binding kinetics compared to the corresponding amide, but whether this happens through formation of a reversible covalent complex or even through mere coordination with a lysine residue is questionable.

Table 1. Pharmacological characterization of ligand binding at the H_1R. Equilibrium binding affinity constants (K_i) and binding rate constants (k_{on}, k_{off}) were determined from competitive binding assay using [^{3}H] mepyramine as radioligand. H_1R was transiently expressed on HEK293T cell. All values represent mean ± SD of N ≥ 3. N.D.=Not determined.

#	VUF		pK_i	k_{on} ($10^6 \cdot M^{-1} \cdot min^{-1}$)	k_{off} (min^{-1})	$pK_{d, calc}$[a]	RT (min)[b]
5	VUF16590		8.9 ± 0.02	7.5 ± 5.0	0.031 ± 0.005	8.3 ± 0.4	32.1
6	VUF16548		8.7 ± 0.07	4.2 ± 2.0	0.04 ± 0.01	8.0 ± 0.3	25.0
10	VUF16550		8.4 ± 0.06	2.2 ± 1.1	0.04 ± 0.02	7.7 ± 0.3	24.7
12[c]	VUF15010		8.5 ± 0.11	58.4 ± 7.7	0.20 ± 0.01	8.5 ± 0.0	5.0
13	VUF16552		8.1 ± 0.03	3.8 ± 1.8	0.05 ± 0.01	7.9 ± 0.1	19.7

[a] Calculated as k_{off}/k_{on}. [b] Calculated from the mean k_{off}: RT = $1/k_{off}$. [c] Tested as fumarate salt.

Conclusion

Two series of boron-containing ligands were designed to explore the potential effect boron may have in modulating binding kinetics of small molecules at the histamine H_1R. Series A capitalized on a recently published benzaldehyde boronic acid for lysines,[22, 45] whereas series B used an α-aminoboronic unit which was hypothesized to be able to form a complex with lysines. Compounds from both series were synthesized through multi-step synthetic sequences. Equilibrium and kinetic binding parameters for H_1R were explored. Based on the currently available compounds and data set, it is shown that some structural features might be able to modestly modulate binding kinetics, e.g. the introduction of a boronic acid moiety on an amide (compare **12** to **13**). The introduction of a boronic acid alone or in combination with an aldehyde (**5**, **6** and **10**) provides two scenarios that deliver warheads with varying theoretical capacity to

bind lysines. However, the currently available kinetic data within that set of compounds does not allow us to confirm the hypothesis of increasing RT by covalent lysine engagement. For further studying of covalent modification in binding kinetics, more compounds in combination with crystal structure-based design, mass spectrometry and mutagenesis will be needed.

Experimental section

Pharmacology

Cell culture and radioligand binding. Production of cell homogenates expressing the HA-H_1R and the performed radioligand binding experiments conducted were previously described with minor changes.[51] In short, HEK293T cells were transiently transfected using 25kDa polyethylenimine with a pcDEF3 vector encoding the N-terminally HA tagged H_1R. Cells were collected and frozen two days post-transfection. Upon conducting a radioligand binding experiment, a frozen aliquot of cells was reconstituted in binding buffer [50mM Na_2HPO_4/KH_2PO_4, pH 7.4], homogenized and then co-incubated with [^{3}H]mepyramine with or without an additional unlabeled ligand at 25 °C under gentle agitation. Binding reactions were terminated by filtration and three rapid consecutive wash steps using ice-cold wash buffer [50mM Tris-HCl, pH 7.4]. Filter-bound radioactivity was quantified by scintillation counting using the Wallac Microbeta.

Competitive association assay. Previously it was determined for [^{3}H]mepyramine binding the H_1R, that the equilibrium dissociation constant (K_D) is 2.29 nM[42], the kinetic dissociation rate constant (k_{off}) is 0.22 min^{-1} and the kinetic association rate constant (k_{on}) is 1.1·10^8 M^{-1}·min^{-1}.[52] In radioligand displacement experiments single concentration 1–5 nM [^{3}H]mepyramine was co-incubated with increasing concentrations (10^{-11} – 10^{-4} M) unlabeled ligands for 4 h at 25 °C. K_i values could be determined from the displacement curves by converting the obtained IC$_{50}$ values using the binding affinity and concentration of [^{3}H]mepyramine.[53] For competitive association experiments a single concentration 1–5 nM [^{3}H]mepyramine was co-incubated with a single concentration unlabeled ligand for increasing incubation times of 0 – 80 min at 25 °C. Concentration antagonist was chosen to be 10·K_i, or fine-tuned in order to have a similar level of radioligand displacement after 80 min (>40%). Kinetic binding rate constants of the unlabeled ligands were determined from the resulting radioligand binding over time by fitting the data to the Motulsky and Mahan model using non-linear regression.[54] In this model the concentrations of both ligands and the k_{on} and k_{off} of [^{3}H]mepyramine at the H_1R were constrained. From the fitted kinetic binding rate constants, the equilibrium dissociation constant (p$K_{D,calc}$) and residence time (RT) could be calculated.

Chemistry

Anhydrous THF, DCM, DMF, and Et_2O were obtained by elution through an activated alumina column prior to use. All other solvents and chemicals were acquired from commercial suppliers and were used as received. ChemBioDraw Ultra 16.0.1.4 was used to generate systematic names for all molecules. All reactions were performed under an inert atmosphere (N_2), unless mentioned otherwise. TLC analyses were carried out with alumina silica plates (Merck F_{254}) using staining and/or UV visualization. Column purifications were performed manually using Silicycle Ultra Pure silica gel or automatically using Biotage equipment. NMR spectra (^1H, ^{13}C, and 2D) were recorded on a Bruker 300 (300 MHz), Bruker 500 (500 MHz) or a Bruker 600 (600 MHz) spectrometer. Chemical shifts are reported in ppm (δ) and the residual solvent was used as internal standard (δ ^1H NMR: $CDCl_3$ 7.26; DMSO-d6 2.50; CD_3OD 3.31; δ ^{13}C NMR: $CDCl_3$ 77.16; DMSO-d6 39.52; CD_3OD 49.00). Data are reported as follows: chemical shift (integration, multiplicity (s = singlet, d = doublet, t = triplet, q = quartet, br = broad signal, m = multiplet, app = apparent), and coupling constants (Hz)). A Bruker microTOF mass spectrometer using ESI in positive ion mode was used to record HRMS spectra. A Shimadzu LC-20AD liquid chromatograph pump system linked to a Shimadzu SPD-M20A diode array detector with MS detection using a Shimadzu LC-MS-2010EV mass spectrometer was used to perform LC-MS analyses. An Xbridge (C18) 5 μm column (50 mm, 4.6 mm) was used. The solvents that were used were the following: solvent B (MeCN with 0.1% formic acid) and solvent A (water with 0.1% formic acid), flow rate of 1.0 mL/min, start 5% B, linear gradient to 90% B in 4.5 min, then 1.5 min at 90% B, then linear gradient to 5% B in 0.5 min, then 1.5 min at 5% B; total run time of 8 min. All compounds have a purity of ≥95% (unless specified otherwise), calculated as the percentage peak area of the analyzed compound by UV detection at 254 nm (values are rounded). Reverse-phase column chromatography purifications were performed using Buchi PrepChem C-700 equipment with a discharge deuterium lamp ranging from 200-600 nm to detect compounds using solvent B (MeCN with 0.1% formic acid), solvent A (water with 0.1% formic acid), flow rate of 15.0 mL/min and a gradient (start 95% A for 3.36 min, then linear gradient to 5% A in 30 min, then at 5% A for 3.36 min, then linear gradient to 95% A in 0.5 min, then 1.5 min at 95% A). The general procedure for making fumarate salts was as follows: (1) The free base was dissolved in *i*PrOH and fumaric acid (1.0 eq) was added; (2) The mixture was heated; (3) Generally a hot filtration was performed; (4) The formed solid was collected by filtration, washed and dried *in vacuo*.

Experimental procedures

(3-chloropropoxy)benzene (4)

To a solution of phenol **3a** (600 mg, 12.28 mmol) in acetone (10 mL) were added K_2CO_3 (4406 mg, 31.9 mmol) and 1-bromo-3-chloropropane (1.89 mL, 19.1 mmol). The reaction mixture was stirred overnight under reflux. The reaction mixture was cooled to rt and filtered. The filtrate was concentrated under reduced pressure. The crude mixture was purified by column chromatography (cyclohexane/EtOAc, 10:1) to yield the title compound as a colorless oil (1252 mg, 60%). ^{1}H NMR (300 MHz, CDCl$_3$) δ 7.34 – 7.27 (m, 2H), 7.01 – 6.89 (m, 3H), 4.13 (t, *J* = 5.8 Hz, 2H), 3.77 (t, *J* = 6.3 Hz, 2H), 2.25 (app p, *J* = 6.1 Hz, 2H). LC-MS: t_R = 4.9 min, >99% (254 nm), *m/z*: no signal because of lack of ionization in MS.

4-(2-benzylphenoxy)-1-(3-phenoxypropyl)piperidine (5, VUF16590)

To a solution of amine **2** (564 mg, 2.11 mmol) in MeCN (8 mL) in a microwave vial were added NaHCO$_3$ (295 mg, 3.52 mmol), NaI (527 mg, 3.52 mmol) and chloride **4** (300 mg, 1.76 mmol). The reaction mixture was stirred at 130 °C under microwave irradiation for 1 h. The reaction mixture was washed with 1.0 M aq. NaOH (50 mL) and EtOAc (2 x 25 mL). The combined organic phases were dried over Na$_2$SO$_4$, filtered and concentrated under vacuum. The crude product was purified by column chromatography (EtOAc/MeOH/TEA = 90/5/5, v/v/v) to yield the title compound as a colorless oil (300 mg, 43%). ^{1}H NMR (600 MHz, CDCl$_3$) δ 7.32 – 7.23 (m, 4H), 7.23 – 7.12 (m, 5H), 6.97 – 6.93 (m, 1H), 6.93 – 6.90 (m, 2H), 6.89 – 6.86 (m, 1H), 6.85 (d, *J* = 8.2 Hz, 1H), 4.43 – 4.36 (m, 1H), 4.02 (t, *J* = 6.3 Hz, 2H), 3.99 (s, 2H), 2.64 – 2.54 (m, 2H), 2.54 – 2.49 (m, 2H), 2.43 – 2.31 (m, 2H), 2.03 – 1.95 (m, 4H), 1.86 – 1.78 (m, 2H). ^{13}C NMR (151 MHz, CDCl$_3$) δ 159.1, 155.1, 141.5, 131.1, 130.5, 129.6, 129.0, 128.4, 127.5, 125.9, 120.8, 120.5, 114.6, 112.6, 66.2, 55.4, 50.3, 36.6, 30.6, 27.0. A signal at 71.5 ppm is not visible but is confirmed by HSQC. HRMS: C$_{27}$H$_{32}$NO$_2$ [M+H]$^+$ calcd: 402.2428, found: 402.2439. LC-MS: t_R = 4.5 min, >97% (254 nm), *m/z*: 402.2 [M+H]$^+$.

(4-(3-(4-(2-benzylphenoxy)piperidin-1-yl)propoxy)phenyl)boronic acid (6, VUF16548)

A flask was charged with phenol **3b** (300 mg, 2.18 mmol) and DMF (12 mL). K_2CO_3 (361 mg, 2.61 mmol) and 1,3-dibromopropane (0.221 mL, 2.18 mmol) were added. The reaction mixture was stirred at 60 °C for 24 h. The reaction mixture was treated with 5% aq. HCl (75 mL) and extracted with EtOAc (2 x 15 mL). The combined organic phases were dried over Na$_2$SO$_4$ and concentrated

under reduced pressure to give 305 mg of crude intermediate, which was not pure and used for the next step without purification. To a solution of crude intermediate (300 mg) and amine **2** (449 mg, 1.68 mmol) in MeCN (10 mL) in a microwave vial were added $NaHCO_3$ (235 mg, 2.80 mmol) and NaI (419 mg, 2.80 mmol). The reaction mixture was stirred at 130 °C under microwave irradiation for 1 h. The reaction mixture was washed with 1.0 M NaOH (50 mL) and EtOAc (2 x 25 mL). The combined organic phases were dried over Na_2SO_4, filtered and concentrated under vacuum. The crude mixture was purified by column chromatography (THF/MeOH = 2/1, v/v) to yield the title compound as an off-white solid (461 mg, 47% over two steps). ^{1}H NMR (300 MHz, CD_3OD) δ 7.75 – 7.50 (m, 2H), 7.29 – 7.05 (m, 7H), 6.96 – 6.80 (m, 4H), 4.52 – 4.41 (m, 1H), 4.03 (t, J = 6.0 Hz, 2H), 3.96 (s, 2H), 2.64 – 2.37 (m, 6H), 2.03 – 1.86 (m, 4H), 1.85 – 1.69 (m, 2H). ^{13}C NMR (151 MHz, CD_3OD) δ 156.3, 142.9, 136.5, 132.2, 131.3, 129.7, 129.2, 128.6, 126.7, 121.4, 114.6, 113.7, 66.9, 56.4, 50.9, 37.5, 31.0, 27.5. Two aromatic carbon signals are not visible / a signal at 71.9 ppm is not visible but is confirmed by HSQC. HRMS: $C_{27}H_{33}BNO_4$ [M+H]$^+$ calcd: 446.2502, found: 446.2509. LC-MS: t_R = 3.6 min, >97% (254 nm), m/z: 446.2 [M+H]$^+$.

2-bromo-5-(3-bromopropoxy)benzaldehyde (8)

To a solution of phenol **7** (500 mg, 2.49 mmol) in DMF (10 mL), 1,3-dibromopropane (0.252 mL, 2.49 mmol) and K_2CO_3 (688 mg, 4.97 mmol) were added. The reaction mixture was stirred at 60 °C for 4 h. The mixture was diluted with EtOAc (30 mL) and washed with H_2O (2 x 15 mL) and brine. The organic phase was dried over Na_2SO_4, filtered, and concentrated under reduced pressure. The crude mixture was purified by column chromatography (cyclohexane/EtOAc, 3:1) to yield the title compound as a white powder (423 mg, 53%). ^{1}H NMR (300 MHz, $CDCl_3$) δ 10.31 (s, 1H), 7.57 – 7.48 (m, 1H), 7.42 (d, J = 3.2 Hz, 1H), 7.10 – 6.98 (m, 1H), 4.14 (t, J = 5.8 Hz, 2H), 3.59 (t, J = 6.4 Hz, 2H), 2.39 – 2.25 (m, 2H). LC-MS: t_R = 5.6 min, >98% (254 nm), m/z: no signal because of lack of ionization in MS.

5-(3-(4-(2-benzylphenoxy)piperidin-1-yl)propoxy)-2-bromobenzaldehyde (9)

To a solution of amine **2** (498 mg, 1.86 mmol) in MeCN (10 mL) were added K_2CO_3 (429 mg, 3.11 mmol) and bromide **8** (500 mg, 1.55 mmol). The reaction mixture was stirred under reflux for 3 h. The reaction mixture was diluted with EtOAc (50 mL) and washed with H_2O (2 x 25 mL). The organic phase was dried over $MgSO_4$ and concentrated under reduced pressure. The crude mixture was purified by column chromatography (cyclohexane/EtOAc, 50:50) to yield the title compound as a colorless oil (359 mg, 46%). ^{1}H NMR (600 MHz, $CDCl_3$) δ 10.32 (s, 1H), 7.52 (d, J = 8.7 Hz, 1H), 7.42 (d, J = 3.2 Hz, 1H), 7.24 (d, J = 7.4 Hz, 2H), 7.22 – 7.19 (m, 2H), 7.18 – 7.11 (m,

3H), 7.04 (dd, J = 8.8, 3.2 Hz, 1H), 6.91 – 6.79 (m, 2H), 4.42 – 4.33 (m, 1H), 4.05 (t, J = 6.3 Hz, 2H), 3.98 (s, 2H), 2.63 – 2.52 (m, 2H), 2.48 (t, J = 7.3 Hz, 2H), 2.39 – 2.28 (m, 2H), 2.01 – 1.90 (m, 4H), 1.86 – 1.76 (m, 2H). ^{13}C NMR (151 MHz, CDCl$_3$) δ 192.0, 158.8, 155.1, 141.4, 134.7, 134.1, 131.1, 130.6, 129.0, 128.3, 127.5, 125.9, 123.6, 120.4, 118.0, 113.6, 112.6, 67.0, 55.1, 50.4, 36.6, 30.7, 26.9, the carbon signal for the OCH moiety is not visible. LC-MS: t_R = 4.7 min, >99% (254 nm), m/z: 508.2, 510.2 [M+H]$^+$.

(4-(3-(4-(2-benzylphenoxy)piperidin-1-yl)propoxy)-2-formylphenyl)boronic acid (10, VUF16550)

To a mixture of bromide **9** (480 mg, 0.944 mmol), 4,4,4',4',5,5,5',5'-octamethyl-2,2'-bi(1,3,2-dioxaborolane) (479 mg, 1.89 mmol) and KOAc (463 mg, 4.72 mmol) in 1,4-dioxane (10 mL) was added PdCl$_2$(dppf)CH$_2$Cl$_2$ (79.5 mg, 0.094 mmol). The reaction mixture was stirred under reflux for 30 min. The reaction mixture was diluted with EtOAc (2 x 25 mL) and washed with H$_2$O (2 x 25 mL). The combined organic phases were dried over MgSO$_4$, filtered and concentrated under reduced pressure. The crude mixture was purified by reverse-phase chromatography (H$_2$O:MeCN 100:0 to 0:100 + 0.1 % TFA) to yield the title compound as a white powder (130 mg, 29%). ^{1}H NMR (600 MHz, CDCl$_3$) δ 12.12 (s, 1H), 9.94 (s, 1H), 8.22 (d, J = 8.3 Hz, 1H), 7.44 (d, J = 2.6 Hz, 1H), 7.32 – 7.26 (m, 4H), 7.20 – 7.10 (m, 4H), 7.03 – 6.97 (m, 1H), 6.80 (d, J = 8.1 Hz, 1H), 4.73 – 4.68 (m, 1H), 4.17 (t, J = 5.6 Hz, 2H), 4.03 (s, 2H), 3.14 – 3.04 (m, 2H), 2.80 – 2.69 (m, 2H), 2.62 – 2.48 (m, 2H), 2.34 – 2.23 (m, 4H), 2.09 – 2.00 (m, 2H). ^{13}C NMR (151 MHz, CDCl$_3$) δ 198.0, 160.6, 153.9, 142.6, 142.0, 140.7, 132.6, 128.7, 128.6, 128.5, 128.2, 126.2, 123.4, 121.3, 119.2, 111.5, 65.5, 65.2, 54.8, 47.6, 37.6, 26.7, 23.8, one aromatic signal is not visible. HRMS: C$_{28}$H$_{33}$BNO$_5$ [M+H]$^+$ calcd: 474.2451, found: 474.2429. LC-MS: t_R = 3.9 min, >99% (254 nm), m/z: 474.3 [M+H]$^+$.

5-(4-(2-benzylphenoxy)piperidin-1-yl)pentanamide fumarate (12, VUF15010)

A mixture of acid **11·HCl** (Chapter 4) (208 mg, 0.515 mmol), EDCI·HCl (148 mg, 0.77 mmol), HOBt·H$_2$O (87 mg, 0.566 mmol), 1.0 M NH$_3$ in dioxane, TEA (0.431 mL, 3.09 mmol) and DCM (5.5 mL) was stirred overnight at rt. The reaction mixture was diluted with DCM (50 mL) and water (50 mL). The phases were separated and the aqueous phase was extracted with DCM (2 × 50 mL). The combined organic phases were washed with brine (50 mL), dried over Na$_2$SO$_4$, filtered and evaporated *in vacuo*. Purification by flash column chromatography (EtOAc:MeOH:TEA 90:5:5) gave a colorless oil (163 mg). The oil was taken up in DCM (50 mL) and 1.0 M aq. NaOH (50 mL). The phases were separated and the aqueous phase was extracted with DCM (2 × 50 mL). The combined organic phases were dried over Na$_2$SO$_4$, filtered and evaporated *in vacuo*. Purification

by reversed phase column chromatography (H$_2$O:MeCN 95:5 to 20:80) gave the free base (60 mg), which was converted to a fumaric acid salt with the method described in the general procedure. This afforded the title compound as a white solid (33 mg, 42%). ^{1}H NMR (500 MHz, DMSO-d_6) δ 7.36–7.22 (m, 3H), 7.22–7.12 (m, 5H), 6.98 (d, J = 8.2 Hz, 1H), 6.86 (t, J = 7.4 Hz, 1H), 6.74 (app bs, 1H), 6.55 (s, 2H), 4.54–4.43 (app bs, 1H), 3.90 (s, 2H), 2.69–2.57 (m, 2H), 2.57–2.52 (m, 2H), 2.48–2.41 (m, 2H, overlaps with solvent signal), 2.08–2.02 (m, 2H), 1.97–1.85 (m, 2H), 1.75–1.62 (m, 2H), 1.51–1.40 (m, 4H). ^{13}C NMR (126 MHz, DMSO-d_6) δ 174.1, 166.9, 154.4, 141.2, 134.6, 130.8, 129.8, 128.6, 128.2, 127.6, 125.7, 120.3, 112.8, 56.7, 49.0, 35.8, 34.8, 29.1, 25.0, 22.8 (no ^{13}C resonance was observed for the OCH of the compound, but a HSQC signal was observed at 4.54 – 4.43 ppm (^{1}H) and 69.5 ppm (^{13}C)). HRMS: C$_{23}$H$_{31}$N$_2$O$_2^+$ [M+H]$^+$ calcd: 367.2380, found 367.2366. LC-MS: t_R = 3.5 min, 99% (254 nm), m/z: 367 [M+H]$^+$

((5-(4-(2-benzylphenoxy)piperidin-1-yl)pentanamido)methyl)boronic acid (13, VUF16552)

A mixture of acid **11·HCl** (Chapter 4) (100 mg, 0.272 mmol), (4,4,5,5-tetramethyl-1,3,2-dioxaborolan-2-yl)methanamine hydrochloride (51.3 mg, 0.327 mmol), HATU (124 mg, 0.327 mmol), DIPEA (0.119 mL, 0.680 mmol) and DCM (10 mL) was stirred at rt overnight. Volatiles were removed under reduced pressure and the residue was diluted with EtOAc (20 mL). The mixture was washed with aq. KHSO$_4$ (0.1 M, 3 x 15 mL), aq. NaHCO$_3$ (5%, 3 x 10 mL), and brine (3 x 10 mL). The organic layer was dried over MgSO$_4$, filtered and concentrated under vacuum. The crude compound was purified by preparative TLC (MeOH: THF = 1:1) to yield the title compound as a colorless oil (20 mg, 17%). ^{1}H NMR (600 MHz, CD$_3$OD) δ 7.29 – 7.20 (m, 4H), 7.19 – 7.10 (m, 3H), 6.98 – 6.91 (m, 2H), 4.70 – 4.63 (m, 1H), 4.00 (s, 2H), 3.09 – 2.93 (m, 2H), 2.81 – 2.57 (m, 4H), 2.50 (t, J = 6.9 Hz, 2H), 2.31 (s, 2H), 2.11 – 2.02 (m, 2H), 2.01 – 1.89 (m, 2H), 1.75 – 1.62 (m, 4H). ^{13}C NMR (151 MHz, CD$_3$OD) δ 180.3, 155.7, 143.3, 132.8, 130.8, 129.5, 129.5, 129.0, 127.0, 121.9, 113.3, 57.7, 49.9, 37.7, 30.9, 28.9, 24.9, 23.4. Signals at 67.8 ppm and 33.1 ppm are not visible but are confirmed by HSQC. HRMS: C$_{24}$H$_{34}$BN$_2$O$_4$ [M+H]$^+$ calcd: 425.2610, found: 425.2609. LC-MS: t_R = 3.6 min, >92% (254 nm), m/z: 425.3 [M+H]$^+$.

Acknowledgements

References

1.   David, C. S.; Brad, A. H.; Isabelle Van, L.; Georges, V., The role of binding kinetics in GPCR drug discovery. *Current Topics in Medicinal Chemistry* **2015,** *15* (24), 2504-2522.

2.   Copeland, R. A., The drug–target residence time model: a 10-year retrospective. *Nature Reviews Drug Discovery* **2016,** *15* (2), 87-95.

3.   Vauquelin, G.; Charlton, S. J., Long-lasting target binding and rebinding as mechanisms to prolong in vivo drug action. *British Journal of Pharmacology* **2010,** *161* (3), 488-508.

4.   Hoffmann, C.; Castro, M.; Rinken, A.; Leurs, R.; Hill, S. J.; Vischer, H. F., Ligand residence time at G-protein–coupled receptors—why we should take our time to study it. *Molecular Pharmacology* **2015,** *88* (3), 552-560.

5.   Guo, D.; Hillger, J. M.; IJzerman, A. P.; Heitman, L. H., Drug-target residence time—a case for G protein-coupled receptors. *Medicinal Research Reviews* **2014,** *34* (4), 856-892.

6.   Bosma, R.; Witt, G.; Vaas, L. A. I.; Josimovic, I.; Gribbon, P.; Vischer, H. F.; Gul, S.; Leurs, R., The target residence time of antihistamines determines their antagonism of the G protein-coupled histamine H1 receptor. *Frontiers in Pharmacology* **2017,** *8* (667).

7.   Copeland, R. A.; Pompliano, D. L.; Meek, T. D., Drug–target residence time and its implications for lead optimization. *Nature Reviews Drug Discovery* **2006,** *5* (9), 730-739.

8.   Schmidtke, P.; Luque, F. J.; Murray, J. B.; Barril, X., Shielded hydrogen bonds as structural determinants of binding kinetics: application in drug design. *Journal of the American Chemical Society* **2011,** *133* (46), 18903-18910.

9.   Tresadern, G.; Bartolome, J. M.; Macdonald, G. J.; Langlois, X., Molecular properties affecting fast dissociation from the D2 receptor. *Bioorganic & Medicinal Chemistry* **2011,** *19* (7), 2231-2241.

10.   Miller, D. C.; Lunn, G.; Jones, P.; Sabnis, Y.; Davies, N. L.; Driscoll, P., Investigation of the effect of molecular properties on the binding kinetics of a ligand to its biological target. *MedChemComm* **2012,** *3* (4), 449-452.

11.   Bradshaw, J. M.; McFarland, J. M.; Paavilainen, V. O.; Bisconte, A.; Tam, D.; Phan, V. T.; Romanov, S.; Finkle, D.; Shu, J.; Patel, V.; Ton, T.; Li, X.; Loughhead, D. G.; Nunn, P. A.; Karr, D. E.; Gerritsen, M. E.; Funk, J. O.; Owens, T. D.; Verner, E.; Brameld, K. A.; Hill, R. J.; Goldstein, D. M.; Taunton, J., Prolonged and tunable residence time using reversible covalent kinase inhibitors. *Nature Chemical Biology* **2015,** *11* (7), 525-531.

12.   Singh, J.; Petter, R. C.; Baillie, T. A.; Whitty, A., The resurgence of covalent drugs. *Nature Reviews Drug Discovery* **2011,** *10* (4), 307-317.

13.   Serafimova, I. M.; Pufall, M. A.; Krishnan, S.; Duda, K.; Cohen, M. S.; Maglathlin, R. L.; McFarland, J. M.; Miller, R. M.; Frödin, M.; Taunton, J., Reversible targeting of noncatalytic cysteines with chemically tuned electrophiles. *Nature Chemical Biology* **2012,** *8* (5), 471-476.

14.   Miller, R. M.; Paavilainen, V. O.; Krishnan, S.; Serafimova, I. M.; Taunton, J., Electrophilic fragment-based design of reversible covalent kinase inhibitors. *Journal of the American Chemical Society* **2013,** *135* (14), 5298-5301.

15.   Bauer, R. A., Covalent inhibitors in drug discovery: from accidental discoveries to avoided liabilities and designed therapies. *Drug Discovery Today* **2015,** *20* (9), 1061-1073.

16.   Baillie, T. A., Targeted covalent inhibitors for drug design. *Angewandte Chemie International Edition* **2016,** *55* (43), 13408-13421.

17.   Ábrányi-Balogh, P.; Petri, L.; Imre, T.; Szijj, P.; Scarpino, A.; Hrast, M.; Mitrović, A.; Fonovič, U. P.; Németh, K.; Barreteau, H.; Roper, D. I.; Horváti, K.; Ferenczy, G. G.; Kos, J.; Ilaš, J.; Gobec, S.; Keserű, G. M., A road map for prioritizing warheads for cysteine targeting covalent inhibitors. *European Journal of Medicinal Chemistry* **2018,** *160*, 94-107.

18.   Pettinger, J.; Jones, K.; Cheeseman, M. D., Lysine-targeting covalent inhibitors. *Angewandte Chemie International Edition* **2017,** *56* (48), 15200-15209.

19.   Chen, X.; Muthoosamy, K.; Pfisterer, A.; Neumann, B.; Weil, T., Site-selective lysine modification of native proteins and peptides via kinetically controlled labeling. *Bioconjugate Chemistry* **2012,** *23* (3), 500-508.

20.   Anscombe, E.; Meschini, E.; Mora-Vidal, R.; Martin, Mathew P.; Staunton, D.; Geitmann, M.; Danielson, U. H.; Stanley, Will A.; Wang, Lan Z.; Reuillon, T.; Golding, Bernard T.; Cano, C.; Newell, David R.; Noble, Martin E. M.; Wedge, Stephen R.; Endicott, Jane A.; Griffin, Roger J., Identification and characterization of an irreversible inhibitor of CDK2. *Chemistry & Biology* **2015,** *22* (9), 1159-1164.

21.   Matos, M. J.; Oliveira, B. L.; Martínez-Sáez, N.; Guerreiro, A.; Cal, P. M. S. D.; Bertoldo, J.; Maneiro, M.; Perkins, E.; Howard, J.; Deery, M. J.; Chalker, J. M.; Corzana, F.; Jiménez-Osés, G.; Bernardes, G. J. L., Chemo- and regioselective lysine modification on native proteins. *Journal of the American Chemical Society* **2018,** *140* (11), 4004-4017.

22.   Akçay, G.; Belmonte, M. A.; Aquila, B.; Chuaqui, C.; Hird, A. W.; Lamb, M. L.; Rawlins, P. B.; Su, N.; Tentarelli, S.; Grimster, N. P.; Su, Q., Inhibition of Mcl-1 through covalent modification of a noncatalytic lysine side chain. *Nature Chemical Biology* **2016,** *12* (11), 931-936.

23.   Soriano-Ursúa, M. A.; Das, B. C.; Trujillo-Ferrara, J. G., Boron-containing compounds: chemico-biological properties and expanding medicinal potential in prevention, diagnosis and therapy. *Expert Opinion on Therapeutic Patents* **2014,** *24* (5), 485-500.

24.   Hunter, P., Not boring at all. *EMBO Reports* **2009,** *10* (2), 125-128.

25.   Soriano-Ursúa, M. A.; Mancilla-Percino, T.; Correa-Basurto, J.; Querejeta, E.; Trujillo-Ferrara, J. G., Give boron a chance: boron containing compounds reach ionotropic and metabotropic transmembrane receptors. *Mini Reviews in Medicinal Chemistry* **2011,** *11* (12), 1031-8.

26.   Baker, S. J.; Ding, C. Z.; Akama, T.; Zhang, Y. K.; Hernandez, V.; Xia, Y., Therapeutic potential of boron-containing compounds. *Future Medicinal Chemistry* **2009,** *1* (7), 1275-88.

27.   Ciani, L.; Ristori, S., Boron as a platform for new drug design. *Expert Opinion on Drug Discovery* **2012,** *7* (11), 1017-27.

28.   Das, B. C.; Thapa, P.; Karki, R.; Schinke, C.; Das, S.; Kambhampati, S.; Banerjee, S. K.; Van Veldhuizen, P.; Verma, A.; Weiss, L. M.; Evans, T., Boron chemicals in diagnosis and therapeutics. *Future Medicinal Chemistry* **2013,** *5* (6), 653-76.

29.   Schneider, E. H.; Seifert, R., Pharmacological characterization of human histamine receptors and histamine receptor mutants in the Sf9 cell expression system. *Handbook of Experimental Pharmacology* **2017,** *241*, 63-118.

30.   Simons, F. E.; Simons, K. J., Histamine and H1-antihistamines: celebrating a century of progress. *The Journal of Allergy and Clinical Immunology* **2011,** *128* (6), 1139-1150.e4.

31.   Simons, F. E., Advances in H1-antihistamines. *The New England Journal of Medicine* **2004,** *351* (21), 2203-17.

32.   Parsons, M. E.; Ganellin, C. R., Histamine and its receptors. *British Journal of Pharmacology* **2006,** *147* (S1), S127-S135.

33.   Huang, Z. L.; Mochizuki, T.; Qu, W. M.; Hong, Z. Y.; Watanabe, T.; Urade, Y.; Hayaishi, O., Altered sleep-wake characteristics and lack of arousal response to H3 receptor antagonist in histamine H1 receptor knockout mice. *Proceedings of the National Academy of Sciences* **2006,** *103* (12), 4687-92.

34.   Ikeda-Sagara, M.; Ozaki, T.; Shahid, M.; Morioka, E.; Wada, K.; Honda, K.; Hori, A.; Matsuya, Y.; Toyooka, N.; Ikeda, M., Induction of prolonged, continuous slow-wave sleep by blocking cerebral H_1 histamine receptors in rats. *British Journal of Pharmacology* **2012,** *165* (1), 167-82.

35.   Parmentier, R.; Zhao, Y.; Perier, M.; Akaoka, H.; Lintunen, M.; Hou, Y.; Panula, P.; Watanabe, T.; Franco, P.; Lin, J. S., Role of histamine H1-receptor on behavioral states and wake maintenance during

deficiency of a brain activating system: A study using a knockout mouse model. *Neuropharmacology* **2016,** *106*, 20-34.

36.   Shimamura, T.; Shiroishi, M.; Weyand, S.; Tsujimoto, H.; Winter, G.; Katritch, V.; Abagyan, R.; Cherezov, V.; Liu, W.; Han, G. W.; Kobayashi, T.; Stevens, R. C.; Iwata, S., Structure of the human histamine H1 receptor complex with doxepin. *Nature* **2011,** *475* (7354), 65-70.

37.   Walter, M.; Stark, H., Histamine receptor subtypes: a century of rational drug design. *Frontiers in Bioscience (Scholar edition)* **2012,** *4*, 461-88.

38.   Zhang, M. Q.; Leurs, R.; Timmerman, H. Histamine H1- receptor antagonists. In *Burger's Medicinal Chemistry an Drug Discovery*, 5th ed.; Wolff, M. E., Ed.; Vrije Universiteit: Amsterdam, 1997; Vol. 5.

39.   Kooistra, A. J.; Kuhne, S.; de Esch, I. J. P.; Leurs, R.; de Graaf, C., A structural chemogenomics analysis of aminergic GPCRs: lessons for histamine receptor ligand design. *British Journal of Pharmacology* **2013,** *170* (1), 101-126.

40.   Bosma, R.; Wang, Z.; Kooistra, A. J.; Bushby, N.; Kuhne, S.; van den Bor, J.; Waring, M. J.; de Graaf, C.; de Esch, I. J.; Vischer, H. F.; Sheppard, R. J.; Wijtmans, M.; Leurs, R., Route to prolonged residence time at the histamine H1 receptor: growing from desloratadine to rupatadine. *Journal of Medicinal Chemistry* **2019,** *62* (14), 6630-6644.

41.   Gillard, M.; Van Der Perren, C.; Moguilevsky, N.; Massingham, R.; Chatelain, P., Binding characteristics of cetirizine and levocetirizine to human H1 histamine receptors: contribution of Lys191 and Thr194. *Molecular Pharmacology* **2002,** *61* (2), 391-399.

42.   Kuhne, S.; Kooistra, A. J.; Bosma, R.; Bortolato, A.; Wijtmans, M.; Vischer, H. F.; Mason, J. S.; de Graaf, C.; de Esch, I. J. P.; Leurs, R., Identification of ligand binding hot spots of the histamine H1 receptor following structure-based fragment optimization. *Journal of Medicinal Chemistry* **2016,** *59* (19), 9047-9061.

43.   de Graaf, C.; Kooistra, A. J.; Vischer, H. F.; Katritch, V.; Kuijer, M.; Shiroishi, M.; Iwata, S.; Shimamura, T.; Stevens, R. C.; de Esch, I. J. P.; Leurs, R., Crystal structure-based virtual screening for fragment-like ligands of the human histamine H1 receptor. *Journal of Medicinal Chemistry* **2011,** *54* (23), 8195-8206.

44.   Kuhne, S. Design and synthesis of tool compounds to probe GPCRs (doctoral dissertation), Vrije Universiteit Amsterdam, **2018**.

45.   Cal, P. M. S. D.; Vicente, J. B.; Pires, E.; Coelho, A. V.; Veiros, L. s. F.; Cordeiro, C.; Gois, P. M. P., Iminoboronates: a new strategy for reversible protein modification. *Journal of the American Chemical Society* **2012,** *134* (24), 10299-10305.

46.   Diaz, D. B.; Yudin, A. K., The versatility of boron in biological target engagement. *Nature Chemistry* **2017,** *9* (8), 731-742.

47.   Whyte, G. F.; Vilar, R.; Woscholski, R., Molecular recognition with boronic acids—applications in chemical biology. *Journal of Chemical Biology* **2013,** *6* (4), 161-174.

48.   Lai, J.; Liu, Y.; Wu, W.; Zhou, Y.; Maw, H.; Bachovchin, W.; Bhat, K.; Bock, C., Synthesis and structural investigation of internally coordinated α-amidoboronic acids. *The Journal of Organic Chemistry* **2006,** *71*, 512-9.

49.   Bhat, K. L.; Braz, V.; Laverty, E.; Bock, C. W., The effectiveness of a primary aliphatic amino group as an internal Lewis base on the formation of a boron–oxygen–carbon linkage: a computational study. *Journal of Molecular Structure: THEOCHEM* **2004,** *712* (1), 9-19.

50.   Ono, F.; Hirata, O.; Ichimaru, K.; Saruhashi, K.; Watanabe, H.; Shinkai, S., Mild one-step synthesis of 4,6-Benzylideneglycopyranosides from aromatic aldehydes and gelation abilities of the glucose derivatives. *European Journal of Organic Chemistry* **2015,** *2015* (29), 6439-6447.

51.   Bosma, R.; Moritani, R.; Leurs, R.; Vischer, H. F., BRET-based β-arrestin2 recruitment to the histamine H1 receptor for investigating antihistamine binding kinetics. *Pharmacological Research* **2016,** *111*, 679-687.

52.   Bosma, R.; Stoddart, L. A.; Georgi, V.; Bouzo-Lorenzo, M.; Bushby, N.; Inkoom, L.; Waring, M. J.; Briddon, S. J.; Vischer, H. F.; Sheppard, R. J.; Fernández-Montalván, A.; Hill, S. J.; Leurs, R., Probe dependency in the determination of ligand binding kinetics at a prototypical G protein-coupled receptor. *Scientific Reports* **2019,** *9* (1), 7906.

53.   Yung-Chi, C.; Prusoff, W. H., Relationship between the inhibition constant (KI) and the concentration of inhibitor which causes 50 per cent inhibition (I50) of an enzymatic reaction. *Biochemical Pharmacology* **1973,** *22* (23), 3099-3108.

54.   Motulsky, H. J.; Mahan, L. C., The kinetics of competitive radioligand binding predicted by the law of mass action. *Molecular Pharmacology* **1984,** *25* (1), 1-9.

Chapter 6

Design and synthesis of photocaged H_1 receptor antagonists for GPCR photopharmacology

Zhiyong Wang, Ivana Josimovic, Tiffany K van der Meer, Hans Custers, Andrea van de Stolpe, Karan Pultoo, Henry F. Vischer, Iwan J. P. de Esch, Maikel Wijtmans and Rob Leurs

Abstract

Temporal and spatial regulation of biological processes is one of the new challenges for medicinal chemistry. Here, we present a coumarin-based photocaging strategy to control the pharmacology of the histamine H_1 receptor (H_1R), a prototypic family A G-protein coupled receptor. Three different potent H_1 antagonist scaffolds were caged with a photolabile coumarin group with the ultimate aim to strongly reduce H_1R affinity. Substitution on the clinically used antagonist desloratadine with the photo-removable coumarin moiety ultimately resulted in the photocaged desloratadine analog **10** (VUF25245), that has a 100-fold lower affinity for the human H_1R than desloratidine. Photo-uncaging at 400 nm results in the release of the parent compound desloratadine. Thus, the presented coumarin-based photocaging of desloratadine offers a powerful approach for the optical control of H_1R function and presents a new tool for successful H_1R photopharmacology.

Introduction

The emerging field of photopharmacology aims to accurately control biological activity with light. With this approach, real-time and spatially restricted activation or inactivation of cellular responses can be studied.[1-5] Ultimately, photopharmacology is expected to result in the development of new therapeutic modalities for the local treatment of disease.[3, 6, 7] There are two medicinal chemistry strategies to deliver tools for photopharmacology. The first approach is based on the incorporation of photoswitchable moieties (e.g. an azobenzene group) in bioactive ligands that results in ligands that can be reversibly switched to different isomers with distinct biological activities upon illumination at appropriate wavelengths.[3, 6-8] Such a "photoswitching approach" has been successfully demonstrated to result in new tools for e.g. a number of G protein-coupled receptors (GPCRs)[9-14] and ion channels[15-17].

A second photopharmacology strategy achieves optical control of bioactive molecules by the light-induced release of bioactive molecules from inactive ligands. The general concept of this approach is depicted in Figure 1 and shows a photoactive protecting group (PPG) that is incorporated in a ligand and prevents its interaction with the intended target. Upon illumination, the PPG is irreversibly removed and the bioactive molecule is released *in situ*[4, 5] (Figure 1). The term "caging" was introduced in 1978 by Kaplan *et al.* upon the successful synthesis of PPG-protected ATP, that could be released upon illumination.[18] A number of photoremovable protecting groups have been developed over the years, i.e. *ortho*-nitrobenzyl group[19, 20], BODIPY[21] and coumarin[22]. Coumarin-based compounds have received attention as photo-uncaging can be achieved at biocompatible wavelengths of light (>400 nm)[23] and because of the relative low toxicity of the co-released coumarin.[24] To date, the "photocage approach" has been applied to a number of biological targets, including GPCRs.[25-28] Photocaging of e.g. a number of

important neurotransmitters acting at GPCRs, like dopamine[29], glutamate[30] and histamine[29, 31], has proven to be successful.
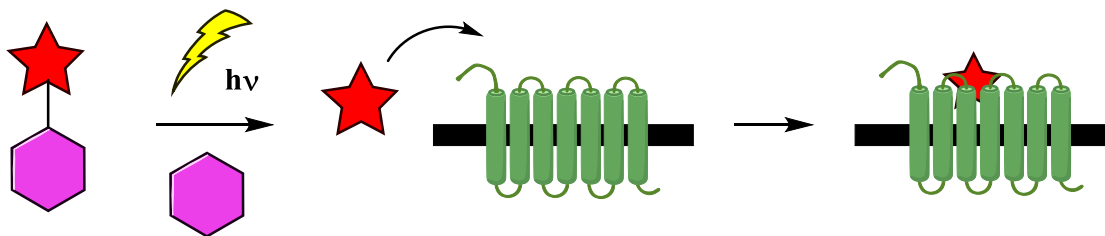

Figure 1. General scheme of the photocleavable approach on a GPCR protein. Image adapted from Fuchter[6].

Histamine is one of the important aminergic neurotransmitters and is relevant in a large number of pathophysiological processes, such as allergic conditions, cardiovascular regulation, sleep-wakefulness, memory and learning processes.[32] Histamine exerts its function via four distinct GPCRs, $H_1R – H_4R$, which have all their therapeutic use (H_1R-H_3R) or promise (H_4R).[32] Whereas the medicinal chemistry of these receptors is in general well developed, the recent field of photopharmacology is clearly underdeveloped for the histamine receptors. Only very recently this field has been opened up for the histamine H_3R with the development of both agonist and antagonist photoswitchable ligands[33, 34], whereas initial attempts towards potent photoswitchable H_1R antagonists have also been reported[35].

The human H_1 receptor (H_1R) is an archetypical GPCR, belonging to the large A subfamily.[32] The H_1R is expressed throughout the human body, including the brain, lung, blood vessels, immune cells, etc.[32] The H_1R plays a role in important physiological processes, i.e. sleep, food intake and allergic reactions, including itch.[36] In the past few decades, histamine H_1 antagonists, like desloratadine, levocetirizine and olopatadine (Figure 2) have been successfully developed and used clinically.[32, 37] As especially allergic conditions often only require local treatment, the H_1R system offers a prime target for the development of photopharmacology approaches. Moreover, the carboxylate functional group, present in a number of successful second-generation H_1R antagonists (Figure 2), is also often used for photocage approaches.[23, 38] In this work, we present new photocaged tools for the precision control of H_1R antagonism activity. One of the designed photocleavable analogs shows reduced H_1R binding affinity *in vitro* and results in the release of the active H_1R antagonist upon illumination.
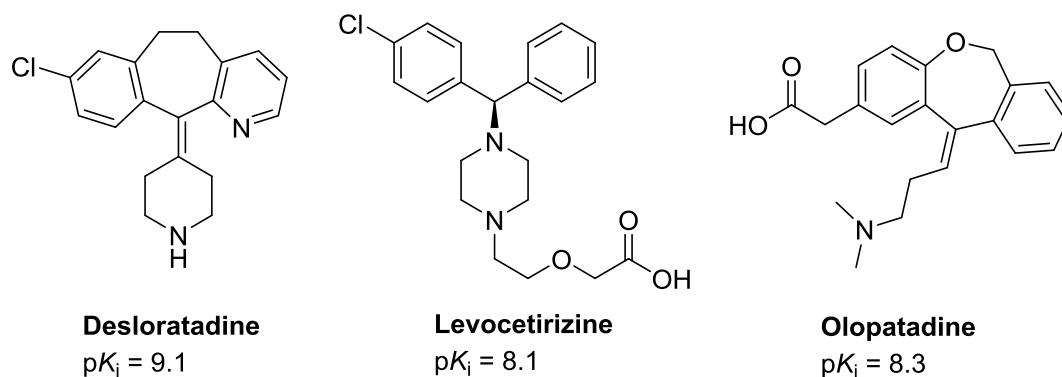
Desloratadine
$pK_i = 9.1$

Levocetirizine
$pK_i = 8.1$

Olopatadine
$pK_i = 8.3$

Figure 2. Exemplary antihistamines and their corresponding binding affinities (pK_i).[39, 40]

Results and discussion

Design of the caged H₁R antagonists

Following the successful co-crystallization of the human H_1R protein with the classical H_1R antagonist doxepin (PDB: 3RZE) (Fig. 3A) by Shimamura *et al.*[41], three main sub-pockets can be identified in the H_1R binding pocket: one pocket accommodating the positively charged amine and a lower and upper aromatic subpocket that will each bind one of the 2 aromatic rings of H_1R antagonists (Fig. 3B). In the design of the currently presented coumarin-based photocaged H_1R antagonists, we considered photocaging of carboxylate and amine functional groups most appropriate as such functionalities are key elements in important clinically used H_1R antagonists, like olopatadine, levocetirizine or desloratadine (Fig. 1). Moreover, SAR studies have previously shown that typical structural elements that can be photocaged (hydroxyl, amine, carboxylate, thiol groups) are not well tolerated in the lower aromatic H_1R subpocket.[42, 43] Consequently, our efforts have focused on the modulation of the binding of ligands to the amine binding pocket and to the upper aromatic H_1R subpocket.

The carboxylate group in olopatadine is attached to the phenyl moiety that is accommodated in the upper aromatic H_1R subpocket. We have therefore chosen this carboxylate as one of our first targets for coumarin photocaging (Fig. 4A). The PPG is envisioned to result in a bulky, caged olopatadine analog, that will sterically clash with the transmembrane helixes in the pocket.
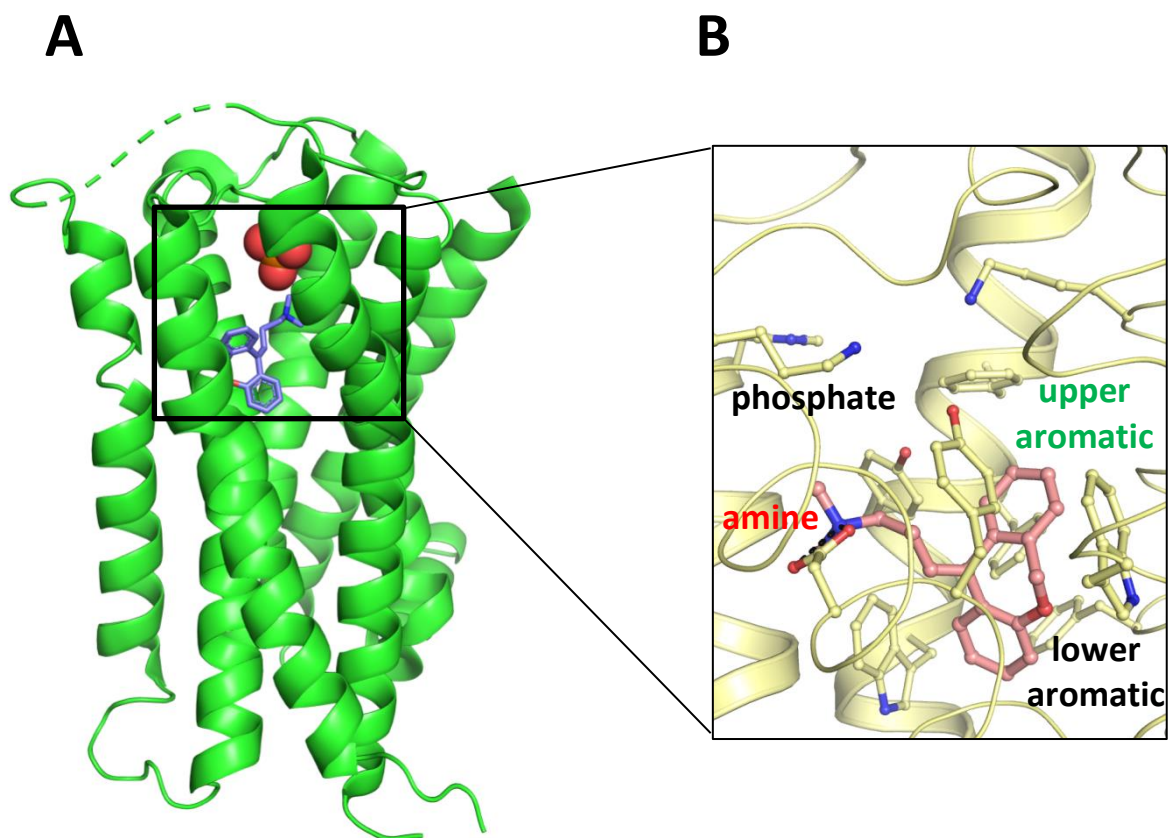
Figure 3. (A) X-ray structure of H$_1$R co-crystallized with doxepin, as taken from Shimamura *et al*. [41]; (B) Binding pocket of H$_1$R with doxepin (pink carbon atoms) and different binding regions.
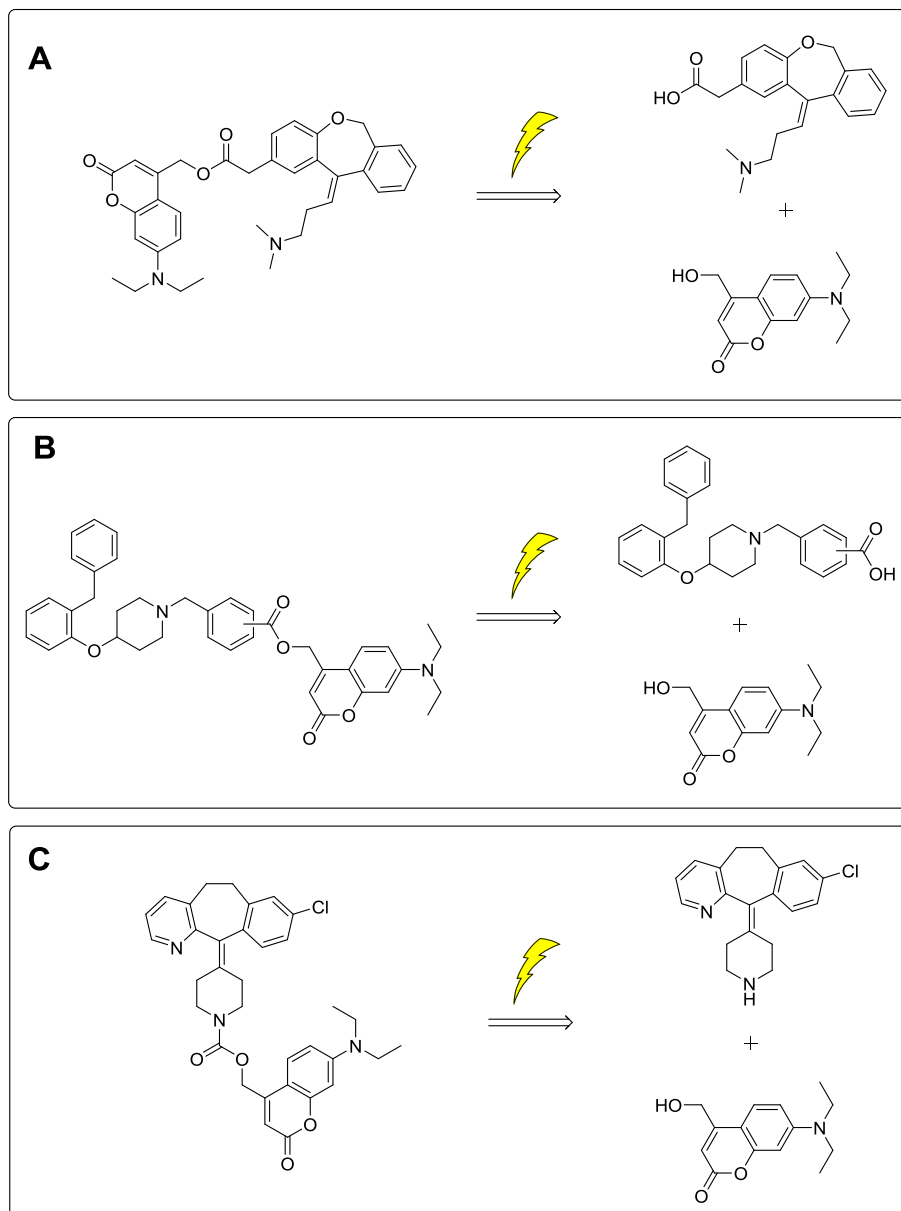
Figure 4. Design of coumarin-based photocaged H$_1$R antagonists, which upon uncaging will liberate olopatadine (A), **6a-c** (B) or desloratadine (C).

Next, we focused our attention to the amine binding pocket. The residues D107[3.32], W428[6.48], Y431[6.54], I454[7.39] in the amine binding region can fit small substituents up to a benzyl group.[39] We envisioned that, due to the relatively small space in the amine-binding region, the incorporation of a large PPG connected through a benzyl linker would result in a ligand that would not fit easily the H$_1$R binding pocket. To probe this hypothesis, we synthesized *ortho*, *meta* and *para*-substituted carboxybenzyl analogs (**6a-6c**) of VUF14544 (**4**), which was previously shown to

effectively bind in the doxepin binding site.[44] These presumed H_1R antagonists were thereafter converted into coumarin-based photocaged analogs (Fig. 4B) that presumably would be sterically hindered.

Lastly, we focused our attention to the clinically used antagonist desloratadine. For H_1R antagonists the ionic interaction between the positively charged amine and $D107^{3.32}$ is essential.[41, 45] The installation of a coumarin PPG directly on the piperidine nitrogen of desloratadine (Fig. 4C) through a carbamate connection will reduce the basicity of the amine and might in addition result in a steric clash with nearby residues, in all most likely affecting the H_1R affinity. For example, H_1R ligand loratadine, in which the N atom of desloratadine is substituted by an ethylcarbamate, has ca. 100 times lower affinity than desloratadine.[46]

Synthesis of the caged analogs

Commercially available coumarin **1** was reacted with SeO_2 to afford aldehyde **2**.[23] Subsequent reduction provided alcohols **3**. Amine **4** was synthesized according to Kuhne *et al*.[47] Nucleophilic substitution with the corresponding bromo esters provided **5a-b**, which were hydrolysed to afford carboxylic acids **6a-b**. The *ortho* counterpart **6c** was obtained by reductive amination of 2-formylbenzoic acid with **4**. Esterification of carboxylic acids **6a-b** by **3** yielded caged compounds **7a-b** in very low yield after purification.[23] Caged olopatadine analogue **8** was obtained via a coupling reaction of olopatadine and **3** in very low yield after purification. Alcohol **3** was reacted with 4-nitrophenyl chloroformate in the presence of pyridine to afford activated intermediate **9** in excellent yield,[48] which was used for a substitution reaction with desloratadine to provide **10** in low yield.

Scheme 1. Synthesis of photocaged ligands targeting H$_1$R.
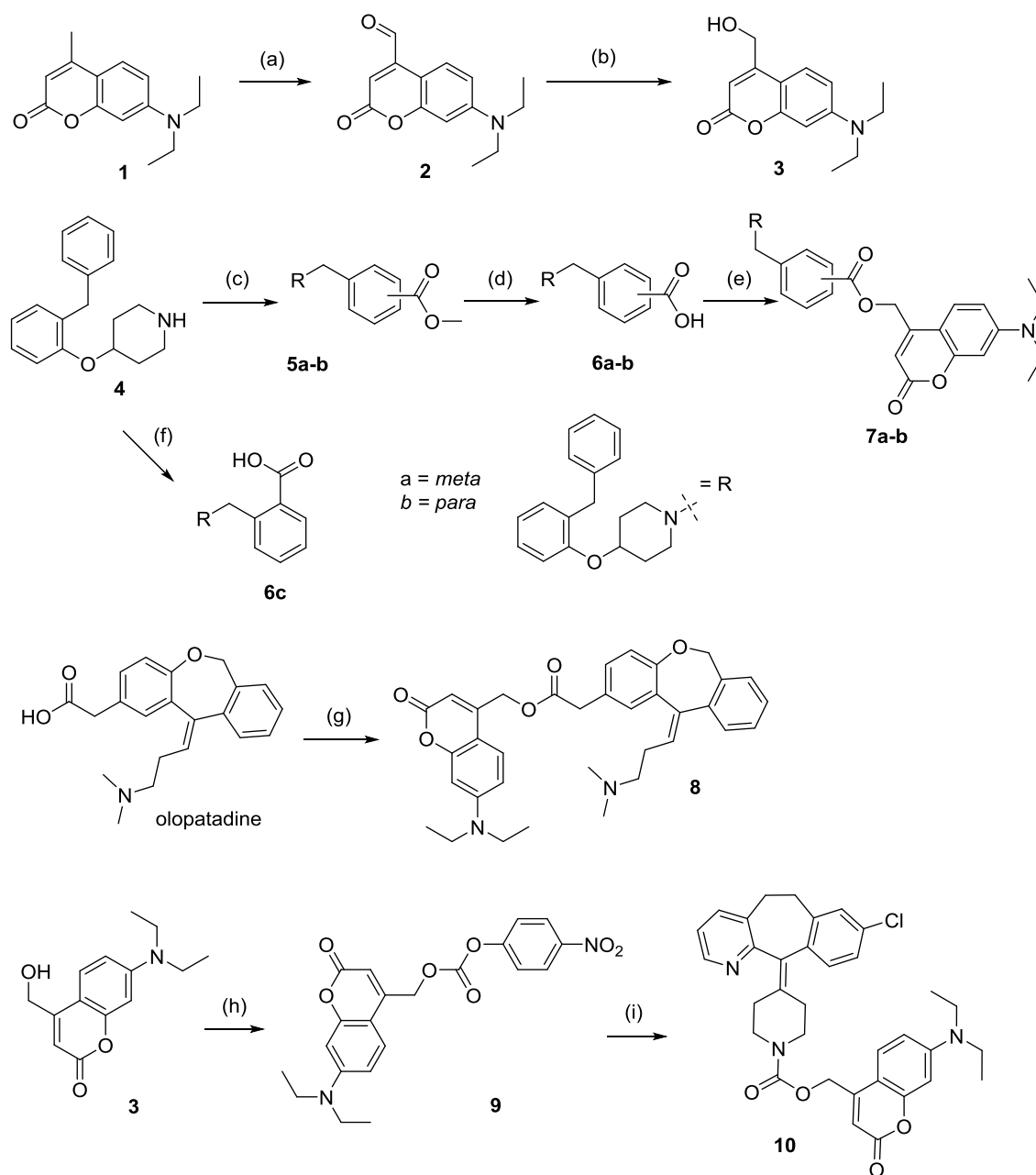
Reagents and conditions: (a) SeO$_2$, *p*-xylene, 150 °C, 16 h, dark, 42%; (b) NaBH$_4$, EtOH, 8 h, rt, 34%; (c) BrCH$_2$PhCOOMe, TEA, DCM, rt, 12 h, 71-77%; (d) 2.0 M NaOH, EtOH/THF, rt, 18 h, 69-70%; (e) **3**, DMAP, EDC·HCl, DCM, 0 °C to rt, 16 h, 3-5%; (f) 2-CHOPhCOOH, Na(CH$_3$COO)$_3$BH, DCE, rt, 24 h, 53%; (g) **3**, DMAP, EDC·HCl, DIPEA, DCM, 0 °C to rt, 16 h, 5%. (h) 4-NO$_2$PhOCOCl, pyridine, rt, 30 min, 45%; (i) desloratadine, DIPEA, pyridine, 35 °C, 1 h, 22%.
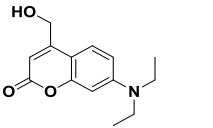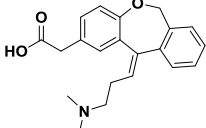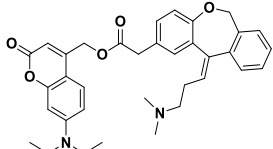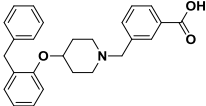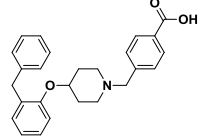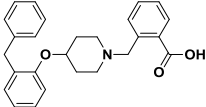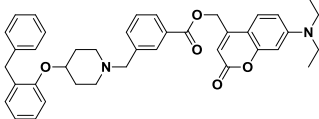
Evaluation of H₁R binding affinity

Competition binding values (K_i) of all newly synthesized compounds, either illuminated using 400 nm (60 min) or kept in the dark, were determined for human H₁R using competitive [³H]mepyramine radioligand-binding studies. The human H₁R was transiently expressed in HEK293T cells and cell homogenates for radioligand binding studies were prepared as described previously.[49]
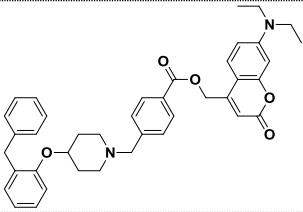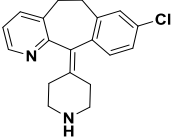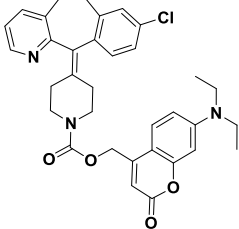
First, we determined that the coumarin analog **3**, used as PPG, does not affect the H₁R. Indeed, the affinity of **3** for the H₁R turned out to be lower than 5 (Table 1), substantiating the use of **3** as a non-interfering PPG for H₁R antagonists. Yet, photocaging of the carboxylate group of olopatadine, as in **8**, did not result in the expected reduction in affinity in comparison with olopatadine (Table 1). In contrast, **8** shows a nanomolar affinity for H₁R (Table 1), indicating that the coumarin moiety can be accommodated efficiently by the H₁R, probably by binding to part of the extracellular vestibular region of the H₁R. Moreover, these data also indicate that the negative charge of the carboxylate is not an essential feature for the high affinity of olopatadine analogs.

Next, we moved our attention to the other important subpocket in the H₁R, the amine-binding pocket. Compounds **6a-c** were designed as potent H₁R antagonists with a carboxylate moiety, that could easily be photocaged with coumarin. *Meta-* and *para*-substituted carboxylic acid ligands (**6a-b**) indeed show good binding affinity for the H₁R, as indicated by their pK_i values of 8.5 and 8.0, respectively (Table 1). Yet, the *ortho*-substituted benzoic acid **6c** is more than 10-fold less active as H₁R antagonist with a pK_i value of 7.0 (Table 1). This compound was therefore considered to be unsuitable for the foreseen photocaging strategy. Photocaging compounds **6a-b** with coumarin **3** resulted in **7a-b**. Unfortunately, also these photocaged analogs still turned out to be potent H₁R antagonists with pK_i values of 7.9 and 8.1 (Table 1) and no or very small differences in affinity compared to the parent compounds **6a-b**. Similar to the olopatadine-derivative **8**, we speculate that the coumarin moieties in **7a-b** are properly accommodated by the extracellular vestibule of the H₁R, resulting in active H₁R antagonists.

Finally, we redirected our photocaging strategy by not just aiming for a spatial misfit of photocaged ligands, but by simultaneously modifying the basicity of the amine function. It is known that a protonated amine function is crucial for H₁R antagonist binding[50-52] and by lowering the basicity of the amine in the clinically used desloratadine we hypothesized a considerable effect on their H₁R affinity. Desloratadine is potent H₁R antagonist (Table 1) and allows a direct appending of the coumarin moiety on the amine function, leading to the photocaged compound **10**. Indeed, caged desloratadine (**10**) shows a large loss in H₁R affinity. Compound **10** has a pK_i value of 6.6, which is much lower than the active ligand desloratadine (pK_i = 9.0) (Table 1).

Table 1. Histamine H_1R binding affinity of photocaged and uncaged H_1R ligands.

#	Compound	Structure	$pK_i \pm SD^a$	LC area % (irradiation time, min)[b]	Minimum concentration of aggregation[c]
3	VUF25165		< 5	N/A	> $10^{-5.5}$ M
---	olopatadine		8.3 ± 0.2	N/A	> $10^{-4.0}$ M
8	VUF25163		8.6 ± 0.1	36 (90)	> $10^{-6.0}$ M
6a	VUF16875		8.5 ± 0.1	N/A	> $10^{-5.0}$ M
6b	VUF16876		8.0 ± 0.1	N/A	> $10^{-4.0}$ M
6c	VUF16874		7.0 ± 0.1	N/A	> $10^{-4.0}$ M
7a	VUF25247		7.9 ± 0.5	25 (55)	> $10^{-6.0}$ M

7b	**VUF25248**		8.1 ± 0.1	25 (45)	$> 10^{-6.5}$ M
---	**Desloratadine**		9.0 ± 0.1	N/A	$> 10^{-4.5}$ M
10	**VUF25245**		6.6 ± 0.1	37 (90)	$> 10^{-6.5}$ M

[a]Determined by competitive [^{3}H]mepyramine radioligand displacement on human H_1R (n=3). [b]Caged ligand (500 µM) in phosphate buffer/5% DMSO was illuminated under 400 nm light at room temperature for the indicated time. The conversion was monitored by LC (λ = 254 nm) and the area % of uncaged compound is listed. N/A: Not applicable, as this compound is not a caged compound. [c]The highest concentration at which no scattering was observed in nephelometry analysis.

Nephelometry measurement

Nephelometry measurements were employed for all compounds to check for any aggregation of the ligands in assay buffer. It is noted that considerable differences were observed between some parent and caged compounds. For instance, no aggregation was observed for the parent compound desloratadine. However, aggregation of **10** significantly increased at concentrations higher than 0.32 µM (Fig. 5). The nephelometry data for all parent and caged compounds are summarized in Table 1.

187
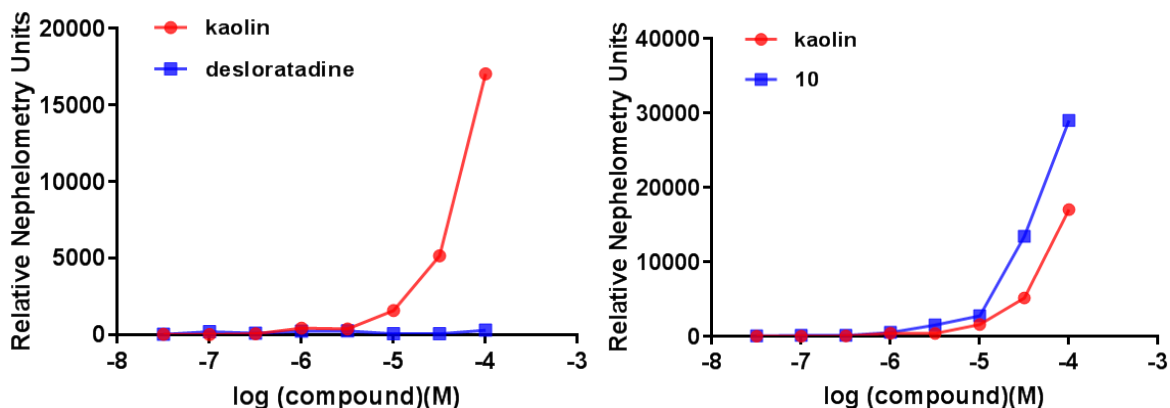
Figure 5. Representative plots for nephelometry measurements at different concentrations of parent compound desloratadine and **10** in the dark. A kaolin dispersion was used as a positive control. Experiments were performed in duplicate in 50 mM phosphate buffer (pH 7.4)/1 % DMSO.

Photochemical properties of the caged ligands

Next, the photochemical properties of the caged ligands were investigated. In phosphate buffer, the absorption maximum of the compound amounted to 392 nm (Figure 6). After 45-90 min continuous illumination at 500 µM in phosphate buffer with λ = 400 ± 5 nm light the active ligand could be obtained for compounds (Table 1). For instance, in LC analysis, only **10** was observed in the dark at 254 nm, whereas 37 % (LC peak area) of desloratadine was detected after 400 nm illumination for 90 min. Under these conditions 9 area % of **10** was still present. The uncaging conditions were further improved for **10.** On average, 53 ± 5 area % (n=4) of the active compound desloratadine (LC area at 254 nm) with 8 ± 5 area % of **10** remaining was obtained after illumination of 40 µM caged ligand for 60 min in 50 mM phosphate buffer with 1% DMSO. A representative example of a LC chromatogram is shown in Figure 7.
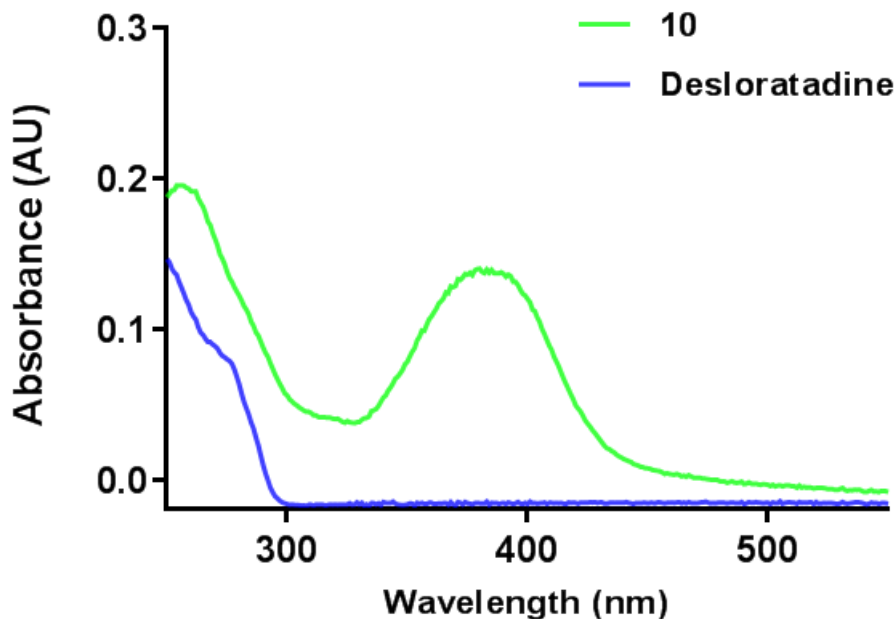
Figure 6. UV–vis spectra of **10** (25 µM) and desloratadine (25 µM) in 50 mM phosphate (pH 7.4)/1% DMSO.
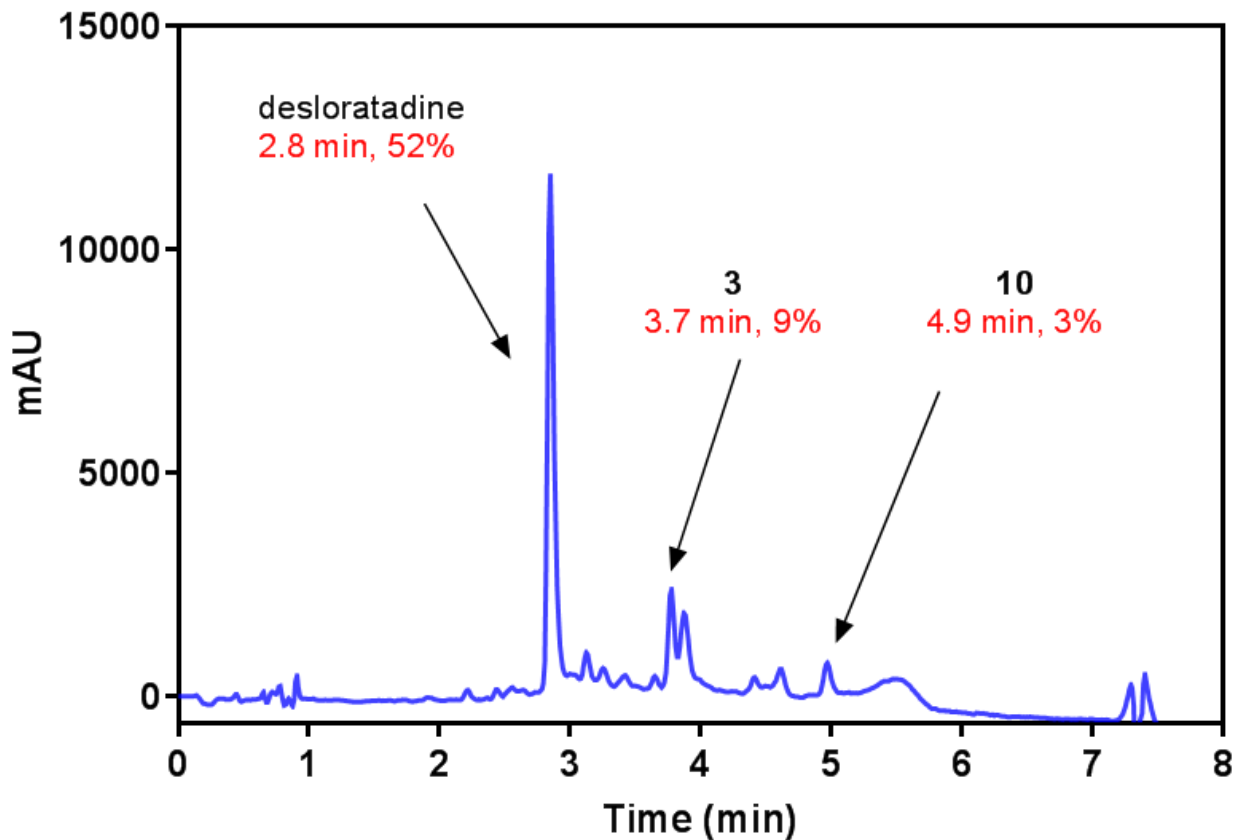
Figure 7. Representative full LC chromatogram for uncaging of **10** (40 µM) in 50 mM phosphate buffer (pH 7.4)/1% DMSO upon illumination at 400 nm at room temperature for 60 min. The progress was analysed by LC (λ = 254 nm) and area percentages are provided.

It is evident, most notably from LC analysis, that the uncaging is not perfectly clean. In addition to the two peaks expected in an ideal scenario, i.e. desloratadine and alcohol **3**, several impurities were detected as well. It has been proposed that photochemical cleavage of coumarin PPGs proceeds through carbocations.[53] While this cation is ideally trapped by H_2O, we speculate that in our case it follows additional pathways too. For example, LCMS evidence suggests a reaction of the cation with desloratadine. In line with such interfering bimolecular reactions is the concentration dependence of the uncaging profile, since at higher concentrations (1-10 mM) more complex uncaging profiles were observed by us (*data not shown*) than at lower μM concentrations.

Finally, we focused our attention specifically on the photocaged desloratadine (**10**), as this coumarin-based compound is the best tool compound arising from this work. The purity of **10** remained over 90% after 24 h in the dark at room temperature in phosphate buffer (Figure 8A), indicating sufficient aqueous stability of most notably the carbamate moiety. Faster degradation under light was observed for **10**, with the purity of **10** being less than 90% within 1 h under daylight at room temperature in phosphate buffer (Figure 8B).
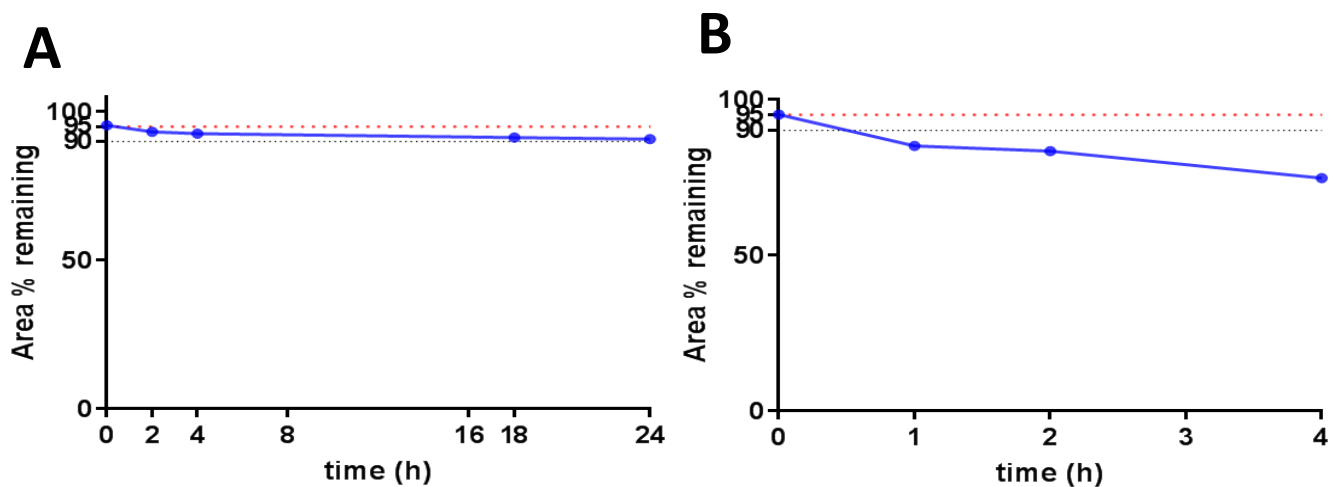
Figure 8. Chemical stability of **10** under dark (A) and daylight (B) conditions in 50 mM phosphate buffer/5% DMSO. Compound **10** (50 μM) was incubated in 50 mM phosphate buffer (pH 7.4)/5% DMSO at room temperature and analysis by LC (λ = 254 nm, area % of **10** versus total area of all present signals shown) was performed at different time points.

Uncaging of **10** was also analysed using real time ^{1}H NMR spectroscopy by illuminating 1 mM of **10** in DMSO-d_6 and monitoring indicative proton signals. The coumarin signals for the CH_2 group to the oxygen atom in **10** and **3** gave a clear pattern for distinction. Only a carbamate CH_2 signal (5.3 ppm) was observed in the dark, whereas this decreased and an alcohol CH_2 signal (4.7 ppm) increased gradually during 400 nm illumination (Figure 9A). Corresponding signal sets for the aromatic protons of **10** and desloratidine are less well resolved. However, upon illumination, the

appearance of the designated aromatic doublet signal at 7.1 ppm of desloratadine can be observed (Figure 9B), while the adjacent corresponding doublet signal from **10** decreased gradually.
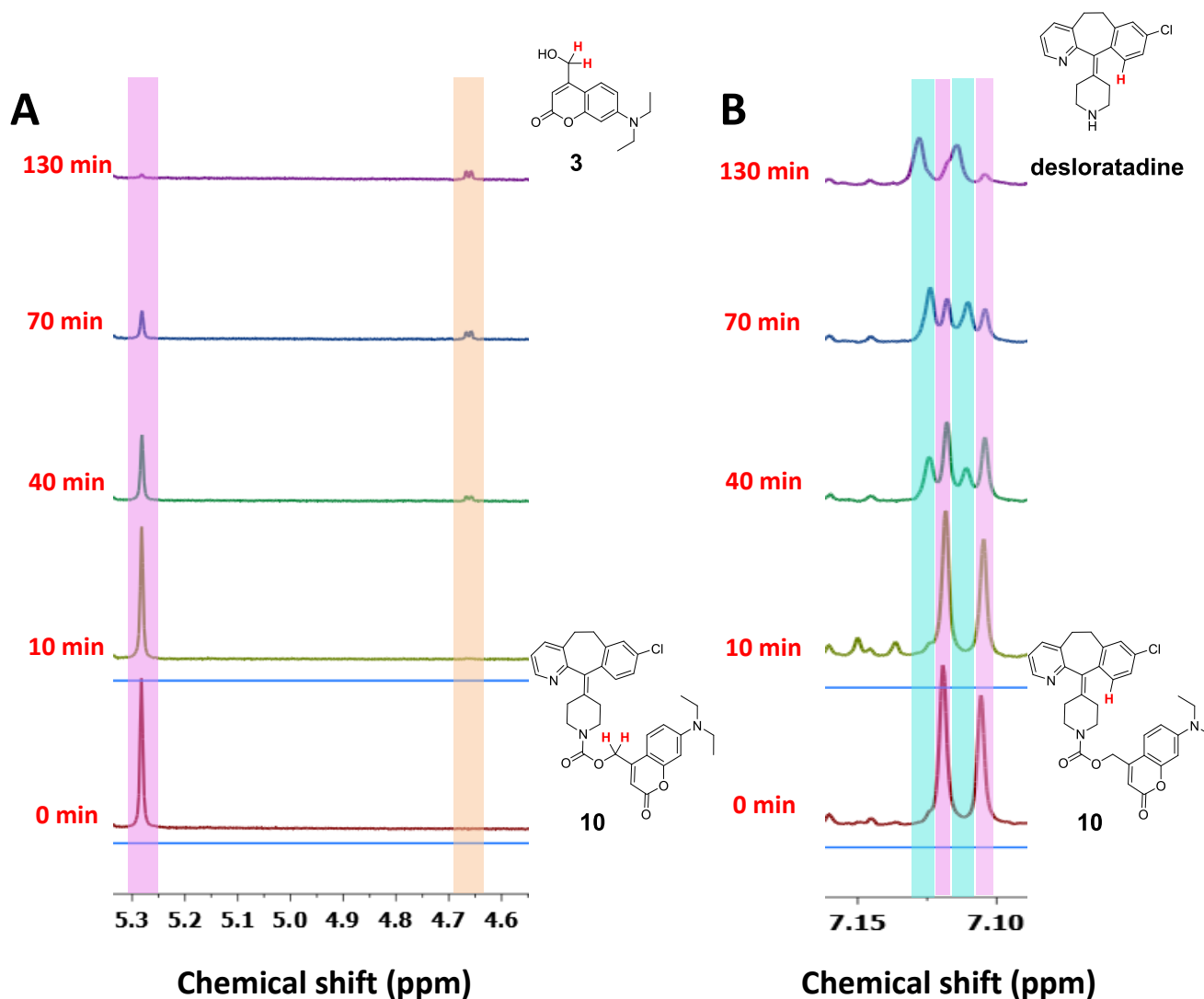
Figure 9. Representative parts of ^{1}H NMR spectra at different time points of uncaging of **10** (1.0 mM) by illumination at 400 nm in DMSO-d_6 at at room temperature. (A) The proton atoms indicated in bold (in **10** and in coumarin **3**) are analysed; (B) The proton atoms shown in red and bold (in **10** and desloratadine) are analysed.

Pharmacological evaluation of caged desloratadine 10

Since the largest shift in H_1R affinity was observed between caged desloratadine (**10**) and desloratadine, **10** was selected for further exploration in comparison to its parent compound desloratadine. Pre-illumination of **10** and desloratadine (40 µM with 1% DMSO in phosphate

buffer) was performed at room temperature for 60 min at 400 nm. Subsequently, non-illuminated and illuminated samples were tested in the dark for H_1R affinity by [^{3}H]mepyramine displacement studies. As can be seen in Figure 10 and Table 2, photouncaging of **10** results in a pK_i value of 8.4, which is close to the value of the parent compound desloratadine (Table 2). Moreover, 400 nm illumination of desloratadine does not affect the resulting affinity for the H_1R (Table 2).

A **B**
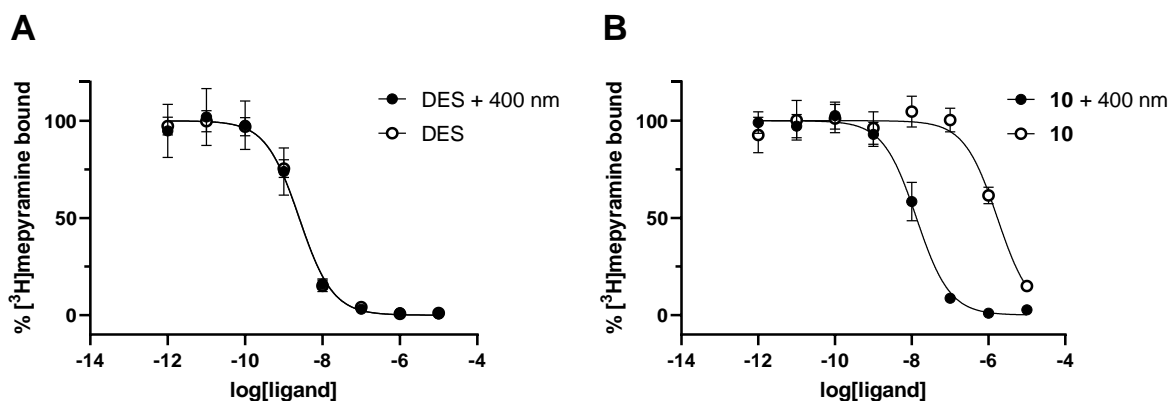
Figure 10. (A) Representative displacement curves of desloratadine with and without illumination at 400 nm. (B) Representative displacement curves of caged compound **10** with and without illumination at 400 nm.

Table 2. Pharmacological evaluation ([^{3}H]mepyramine competition binding to H_1R) of desloratadine and caged desloratadine before and after illumination.

Compound	Condition	pK_i ± SD	N
10	Dark[a]	6.2 ± 0.1	3
10	Illuminated[b]	8.4 ± 0.1	3
Desloratadine	Dark[a]	9.1 ± 0.1	3
Desloratadine	Illuminated[b]	9.1 ± 0.1	3

[a]Dark conditions: 40 µM compound with 1% DMSO in phosphate buffer in the dark at room temperature for 60 min.
[b]Illumination conditions: 40 µM compound with 1% DMSO in phosphate buffer under 400 nm illumination at room temperature for 60 min.

Next to radioligand binding displacement studies, **10** and parent compound desloratadine were also evaluated in a functional assay. To this end, we used the H_1R-mediated activation of NFAT, as measured in a luciferase-based reporter gene assay in transfected HEK293 cells, recombinantly expressing the human H_1R as well. In this assay system, histamine effectively activates NFAT-mediated luciferase transcription with a pEC_{50} of 6.8 ± 0.2 (n = 3). As can be seen in Figure 11A,

the histamine induced response can be fully blocked by increasing concentrations of desloratadine, leading to a pK_B value of 8.8 ± 0.1 (n = 3). This value corresponds well to the affinity value obtained in the radioligand binding studies (Table 2). In this cellular model system, we observed some antagonistic effect for **10** (pK_B = 6.4 ± 0.1, n = 3). As seen in the binding studies, uncaging of **10** with 400 nm light results in a promising leftward-shift of the dose-response curve (Figure 11B) and a pK_B value of 7.8 ± 0.2 (n = 3). This value is in line with a partial uncaging of **10** and the observed binding data under the same conditions.
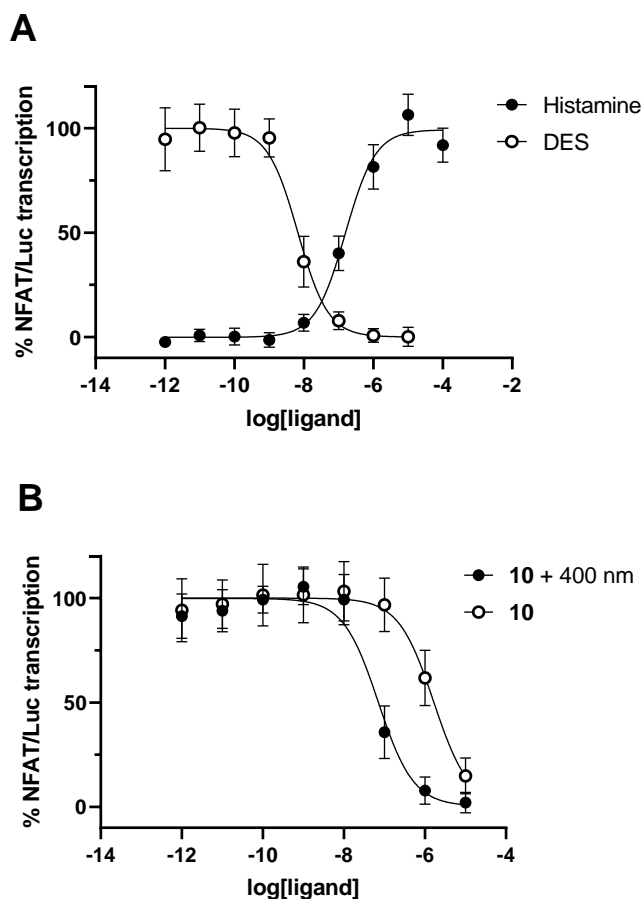
Figure 11. (A) Representative dose response curves of histamine and desloratadine in the presence of 1.5 µM histamine. Receptor activation is measured as NFAT-mediated transcription of luciferase in co-transfected HEK293T cells (B) Representative dose response curves of caged compound **10** with and without illumination at 400 nm in the presence of 1.5 µM histamine. Receptor activation is measured as NFAT-mediated transcription of luciferase in co-transfected HEK293T cells.

Conclusion

A coumarin-based photocaging strategy to modulate the pharmacology of the histamine H_1 receptor (H_1R) was successfully developed. Three antagonist scaffolds were selected to initialize

the exploration. Photocaged analogs **7a**-**b** show no loss of binding affinities compared to parent compounds **6a**-**b**, whereas photocaged olopatadine analog (**8**) has slightly better binding affinity than olopatadine. However, photocaging desloratadine leads to **10** (VUF25245) which shows 100-fold lower affinity than desloratadine. This key compound, together with its efficient uncaging and other presented photochemical properties, enabled us to further assess it in a functional assay. Compound **10** was also less active in antagonizing histamine induced NFAT activation, as measured in a NFAT-based reporter gene assay. Uncaging of **10** with 400 nm resulted in potent inhibition of the H_1R response in this cell-based assay. Our data show that photocaging is a powerful approach able to modulate H_1R pharmacology. Successful utilization of the photocaging strategy on prototypic family A G-protein coupled receptors paves the way for future GPCR photopharmacology efforts.

Experimental section

Pharmacology

Materials: Human embryo kidney cells transformed with large T-antigen (HEK293T) cells were acquired from ATCC, linear polyethyleneimine (PEI) from Polyscience (Washington, PA 18976, USA), Dulbecco's modified eagle's medium (DMEM) from Life Technologies Limited (3 Fountain Drive, Paisley, PA4 9RF, UK), Peniciline/Streptomycine (Pen Strep) from Gibco, Life Technologies (Grand Island, NY 14072, USA), Fetal bovine serum (FBS) from Bodinco BV (Hodijkstraat 2, 1814 EC, Alkmaar, Netherlands). $Na_2PO_4 \cdot 7H_2O$ (Dibasic, Heptahydrate) was bought from Melford (Ipswich, UK). KH_2PO_4, dimethyl sulfoxide (DMSO) and poly-L-Lysine from Sigma Aldrich (St. Louis, MO 63103, USA) phosphate buffer consisting of 40 mM Na_2PO_4 and 10 mM KH_2PO_4, pH 7.4 at 22 °C, was made in house. Histamine·2HCl was purchased from TCI Chemicals, Tokyo, Japan and desloratadine·2HCl from Haihang Industry Co., Ltd. (No.100 South Gongye Road, Jinan City, China. PC.250100). White sterile 96 well plate Cellstar was acquired from Greiner Bio one, Germany. Luciferin reaction agent (LAR) consisting of 43.2 % (v/v) glycerol, 2.9 % (v/v) Triton-X, 1 mM DTT, 0.26 mg/ml d-Luciferine, 0.9 mM ATP, 21 mM $MgCl_2$, 86.1 µM $Na_2H_2P_2O_7$, was made in house.

Constructs: The reporter gene construct pNFAT-luc was obtained from Agilent Technologies (Santa Clara, CA, USA). N-terminal HA-tagged hH_1R construct expressed in the mammalian expression vector pcDEF3 was previously described.[49]

Cell culture: HEK293T cells were cultured in DMEM, supplemented with FBS to 10% and Pen Strep to 1% of complete culture medium and kept in an incubator on 37 °C and 5 % CO_2.

Cell culture and radioligand binding: Production of homogenates of HEK293T cells expressing the human H_1R and the performed [^{3}H]mepyramine radioligand binding experiments were previously described.[49] In short, HEK293T cells were transiently transfected using 25kDa

polyethylenimine with a pcDEF3-based expression vector encoding for the N-terminally HA tagged H_1R. Transfected cells were collected and frozen two days post-transfection. For a radioligand binding experiment, a frozen aliquot of cells was reconstituted in icecold binding buffer [50 mM Na_2HPO_4/KH_2PO_4, pH 7.4], homogenized and then co-incubated for 60 min with [^3H]mepyramine with or without an unlabeled ligand at 25 °C under gentle agitation (600 rpm). Incubations were terminated by filtration through GF/C filter plates and three rapid consecutive wash steps using ice-cold wash buffer [50 mM Tris-HCl, pH 7.4]. Filter-bound radioactivity was quantified using scintillation counting using the Wallac Microbeta.

NFAT reporter gene assay to measure H_1R signaling: Transfection protocol was performed as described[49], with minor changes. $2 \cdot 10^6$ HEK293T cells were seeded in a 10 cm culture dish and transfected the next day with 1 µg HA- hH_1R/pcDEF3, 2.5 µg pNFAT-Luc, 1.5 µg $pcDEF_3$, and 20 µg linear PEI (1 mg/mL water). The transfection mix was incubated for 20 minutes on 22 °C before being added to the adherent cells. One day post-transfection, $5 \cdot 10^4$ cells/well were seeded in a poly-L-Lysine coated white 96 well plate. The plate was coated with 10 times diluted poly-L-Lysine, washed twice with 150 µL sterile water, and left to dry at least 30 minutes prior to cell-plating. The plated cells were incubated at 37 °C, 5% CO_2 for a day before being exposed to ligands. Compound handling was conducted under red light to maintain integrity of light sensitive compounds. Cells were exposed in the dark to irradiated and non-irradiated compounds in a concentration range from 10 µM to 1 pM in a solution of 1:3 phosphate buffer:DMEM with a final concentration of 0.25% DMSO. NFAT induced luciferase transcription was stimulated by adding 1.5 µM histamine to the cells. The cells were incubated with ligands for 6 hours at 37 °C, 5% CO_2. After 6 hours of incubation, the medium was aspirated and cells were lysed by a 30 min incubation with 25 µL/well of LAR at 22 °C. Luminescence was measured with a PHERAstar (BMG) plate reader. Inhibitory potency (IC_{50}) of compounds were determined in GraphPad Prism (Version 8.4.0) via non-linear regression, using the Dose-response-Inhibition (three parameters) model.

Nephelometry

In transparent flat-bottom 96-well plates, compounds under dark conditions were placed at different concentrations in duplicate (10^{-4} M, $10^{-4.5}$ M, 10^{-5} M, $10^{-5.5}$ M, 10^{-6} M, $10^{-6.5}$ M, 10^{-7} M, $10^{-7.5}$ M and a blank) in phosphate buffer with 1% DMSO at least 1 h before the measurement. A kaolin dispersion was used as a positive control in each plate at different concentrations (10^{-4} M, $10^{-4.5}$ M, 10^{-5} M, $10^{-5.5}$ M, 10^{-6} M, $10^{-6.5}$, 10^{-7} M and $10^{-7.5}$ M) under the same conditions as compounds.[54] Nephelometry measurements were performed with a NEPHELO star Plus (BMG Labtech, Germany) with the following settings: 4 cycles, measurement start time 0.1 s, measurement interval time 0.1 s, laser intensity 80%, beam focus 2.0 mm, and orbital shaking mode at 200 rpm with an additional shaking time of 10 s before each cycle. Results were analysed

using GraphPad Prism 8 software, plotting all available data points and plotting mean and standard deviation values in a line chart compared to kaolin control. The linear fit (R^2) of the kaolin control was above 0.99 in all cases.

Photochemistry

UV-Vis spectra were obtained using a Thermo-scientific Evolution 201 PC spectrophotometer. Fits of UV-Vis spectroscopy data were generated using GraphPad Prism 8 software. Illumination was executed using a Sutter instruments Lambda LS with a 300 Watt full-spectrum lamp connected to a Sutter instruments Lambda 10-3 optical filter changer equipped with 400 ± 5 nm filter. The light intensity is 0.22 mW/mm^2 using the 400 ± 5 nm filter as measured using a Thorlabs PM16-401 power meter.

For the determination of UV-Vis spectra, illuminations were analysed in Hellma Suprasil™ quartz 114-QS cuvettes with a 400 ± 5 nm filter. Samples were 25 µM in 50 mM phosphate buffer (pH = 7.4) + 1% DMSO.

Illuminations for NMR spectroscopy experiments were performed in an NMR tube with a 1.0 mM sample in DMSO-d_6 at a volume of 0.5 mL during 7800 seconds with 400 nm irradiation.

Illuminations for binding and functional pharmacological experiments were performed at rt in cylindrical clear glass vials with a volume of 500 or 1200 ⁇L during 60 min with a 400 nm filter. Samples were 40 ⁇M in phosphate buffer/1% DMSO. The uncaging was monitored by LCMS for all the samples. The typical distance between light source and vial or cuvette was 5 cm. Samples were regularly manually shaken.

(Photo)chemical stability assay: Experiments addressing aqueous stability and room light stability were performed in transparent glass vials with 50 µM samples in 50 mM phosphate buffer + 5% DMSO at rt. Samples for aqueous stability experiments were kept in the dark and monitored by LC (λ = 254 nm) at 0 h, 2 h, 4 h, 18 h and 24 h. Samples for room light stability experiments were kept under room light and monitored by LC (λ = 254 nm) at 0 h, 1 h, 2 h, 4 h, 6 h and 8 h.

Chemistry

Anhydrous THF, DCM, DMF, and Et$_2$O were obtained by elution through an activated alumina column prior to use. All other solvents and chemicals were acquired from commercial suppliers and were used as received. ChemBioDraw Ultra 16.0.1.4 was used to generate systematic names for all molecules. All reactions were performed under an inert atmosphere (N$_2$), unless mentioned otherwise. TLC analyses were carried out with alumina silica plates (Merck F$_{254}$) using staining and/or UV visualization. Column purifications were performed manually using Silicycle Ultra Pure silica gel or automatically using Biotage equipment. NMR spectra (^{1}H, ^{13}C, and 2D)

were recorded on a Bruker 300 (300 MHz), Bruker 500 (500 MHz) or a Bruker 600 (600 MHz) spectrometer. Chemical shifts are reported in ppm (δ) and the residual solvent was used as internal standard (δ ^{1}H NMR: CDCl$_3$ 7.26; DMSO-d_6 2.50; CD$_3$OD 3.31; δ ^{13}C NMR: CDCl$_3$ 77.16; DMSO-d_6 39.52; CD$_3$OD 49.00). Data are reported as follows: chemical shift (integration, multiplicity (s = singlet, d = doublet, t = triplet, q = quartet, br = broad signal, m = multiplet, app = apparent), and coupling constants (Hz)). A Bruker microTOF mass spectrometer using ESI in positive ion mode was used to record HRMS spectra. A Shimadzu LC-20AD liquid chromatograph pump system linked to a Shimadzu SPD-M20A diode array detector with MS detection using a Shimadzu LC-MS-2010EV mass spectrometer was used to perform LC-MS analyses. An Xbridge (C18) 5 μm column (50 mm, 4.6 mm) was used. The solvents that were used were the following: solvent B (MeCN with 0.1% formic acid) and solvent A (water with 0.1% formic acid), flow rate of 1.0 mL/min, start 5% B, linear gradient to 90% B in 4.5 min, then 1.5 min at 90% B, then linear gradient to 5% B in 0.5 min, then 1.5 min at 5% B; total run time of 8 min. Basic mode LC condition: solvent B (MeCN with 10% ammonium carbonate buffer, pH 8.0) and solvent A (water with 10% ammonium carbonate buffer, pH 8.0), flow rate of 1.0 mL/min, start 5% B, linear gradient to 90% B in 4.5 min, then 7.5 min at 90% B, then linear gradient to 5% B in 0.5 min, then 2.5 min at 5% B; total run time of 15 min. All compounds have a purity of ≥95% (unless specified otherwise), calculated as the percentage peak area of the analyzed compound by UV detection at 254 nm (values are rounded). Reverse-phase column chromatography purifications were performed using Buchi PrepChem C-700 equipment with a discharge deuterium lamp ranging from 200-600 nm to detect compounds using solvent B (MeCN with 0.1% formic acid), solvent A (water with 0.1% formic acid), flow rate of 15.0 mL/min and a gradient (start 95% A for 3.36 min, then linear gradient to 5% A in 30 min, then at 5% A for 3.36 min, then linear gradient to 95% A in 0.5 min, then 1.5 min at 95% A).

7-(diethylamino)-2-oxo-2H-chromene-4-carbaldehyde (2)

To a solution of coumarin **1** (500 mg, 2.16 mmol) in *p*-xylene (20 mL) was added SeO$_2$ (480 mg, 4.32 mmol). The reaction mixture was stirred at 150 °C for 16 h in the dark. The reaction mixture was filtered while hot and concentrated *in vacuo*. The crude product was purified by flash column chromatography (DCM) to yield the title product as an orange viscous oil (223 mg, 42%). ^{1}H NMR (300 MHz, CDCl$_3$) δ 10.03 (s, 1H), 8.32 (d, *J* = 9.2 Hz, 1H), 6.64 (dd, *J* = 9.2, 2.6 Hz, 1H), 6.54 (d, *J* = 2.6 Hz, 1H), 6.46 (s, 1H), 3.43 (q, *J* = 7.1 Hz, 4H), 1.22 (t, *J* = 7.1 Hz, 6H). ^{13}C NMR (151 MHz, CDCl$_3$) δ 192.7, 192.7, 162.0, 157.5, 151.1, 144.0, 127.2, 117.5, 109.7, 103.9, 97.8, 45.0, 12.6. Two apparent aldehyde signals are visible. The compound decomposes under the used LC conditions.

7-(diethylamino)-4-(hydroxymethyl)-2H-chromen-2-one (3, VUF25165)

To a solution of aldehyde **2** (3.00 g, 12.2 mmol) in EtOH (200 mL) was added $NaBH_4$ (925 mg, 24.5 mmol). The reaction mixture was stirred for 8 h at rt. H_2O (50 mL) and 1.0 M HCl (25 mL) were added to the reaction mixture. The reaction mixture was extracted with DCM (50 mL). The organic layer was washed with satd. aq $NaHCO_3$ and brine. The organic phase was dried over Na_2SO_4, filtered and concentrated *in vacuo*. The crude product was purified by column chromatography (DCM/MeOH, 99:1) to yield as a light yellow solid (1.02 g, 34%). ^1H NMR (500 MHz, $CDCl_3$) δ 7.30 (d, *J* = 9.0 Hz, 1H), 6.55 (dd, *J* = 9.0, 2.6 Hz, 1H), 6.47 (d, *J* = 2.6 Hz, 1H), 6.26 (t, *J* = 1.4, 1H), 4.82 (s, 2H), 3.39 (q, *J* = 7.1 Hz, 4H), 1.19 (t, *J* = 7.1 Hz, 6H). ^{13}C NMR (126 MHz, $CDCl_3$) δ 163.0, 156.2, 155.1, 150.6, 124.5, 108.7, 106.4, 105.4, 97.8, 61.0, 44.8, 12.6. HRMS: $C_{14}H_{18}NO_3$ $[M+H]^+$ calcd: 248.1281, found: 248.1271. LC-MS: t_R = 3.7 min, >96% (254 nm), *m/z*: 248.6 $[M+H]^+$.

methyl 3-((4-(2-benzylphenoxy)piperidin-1-yl)methyl)benzoate (5a)

To a solution of amine **4** (400 mg, 1.50 mmol) and TEA (0.417 mL, 2.99 mmol) in DCM (10 mL), methyl 3-(bromomethyl)benzoate (514 mg, 2.24 mmol) was added. The reaction mixture was stirred at rt for 12 h. The reaction mixture was extracted with EtOAc (15 mL) and H_2O (15 mL). The organic layer was washed with brine (10 mL), dried over Na_2SO_4, filtered and concentrated under reduced pressure. The crude product was purified by flash column chromatography (cyclohexane/EtOAc, 3:1) to yield the title compound as a colorless oil (296 mg, 71 %). ^1H NMR (600 MHz, $CDCl_3$) δ 8.00 (t, *J* = 1.8 Hz, 1H), 7.98 – 7.93 (m, 1H), 7.58 – 7.53 (m, 1H), 7.43 – 7.39 (m, 1H), 7.31 – 7.27 (m, 2H), 7.25 – 7.12 (m, 5H), 6.91 – 6.83 (m, 2H), 4.43 – 4.35 (m, 1H), 4.00 (s, 2H), 3.94 (s, 3H), 3.51 (s, 2H), 2.61 – 2.54 (m, 2H), 2.37 – 2.27 (m, 2H), 1.97 – 1.91 (m, 2H), 1.86 – 1.78 (m, 2H). ^{13}C NMR (151 MHz, $CDCl_3$) δ 167.3, 155.1, 141.4, 139.1, 133.7, 131.0, 130.6, 130.3, 130.2, 129.0, 128.4, 128.4, 128.3, 127.4, 125.8, 120.3, 112.6, 71.8, 62.7, 52.2, 50.2, 36.5, 30.8. LC-MS: t_R = 4.4 min, >98% (254 nm), *m/z*: 416.2 $[M+H]^+$.

methyl 4-((4-(2-benzylphenoxy)piperidin-1-yl)methyl)benzoate (5b)

To a solution of amine **4** (400 mg, 1.50 mmol) and TEA (0.417 mL, 2.99 mmol) in DCM (10 mL), methyl 4-(bromomethyl)benzoate (514 mg, 2.24 mmol) was added. The reaction mixture was stirred at rt for 12 h. The reaction mixture was extracted with EtOAc (15 mL) and H_2O (15 mL). The organic layer was washed with brine (10 mL), dried over Na_2SO_4, filtered and concentrated under reduced pressure. The crude product was purified by flash column chromatography

(cyclohexane/EtOAc, 3:1) to yield the title compound as a colorless oil (480 mg, 77 %). ^{1}H NMR (600 MHz, CDCl$_3$) δ 8.03 – 8.00 (m, 2H), 7.43 – 7.39 (m, 2H), 7.30 – 7.26 (m, 2H), 7.24 – 7.21 (m, 2H), 7.21 – 7.15 (m, 2H), 7.13 (dd, J = 7.5, 1.7 Hz, 1H), 6.90 – 6.83 (m, 2H), 4.43 – 4.34 (m, 1H), 4.00 (s, 2H), 3.92 (s, 3H), 3.51 (s, 2H), 2.60 – 2.53 (m, 2H), 2.36 – 2.28 (m, 2H), 1.98 – 1.90 (m, 2H), 1.86 – 1.78 (m, 2H). ^{13}C NMR (151 MHz, CDCl$_3$) δ 167.1, 155.1, 144.2, 141.4, 131.0, 130.6, 129.7, 129.0, 129.0, 128.3, 127.4, 125.8, 120.4, 112.6, 71.7, 62.8, 52.1, 50.3, 36.5, 30.8. One signal in the >100 pm region is not visible. LC-MS: t_R = 4.4 min, >97% (254 nm), m/z: 416.2 [M+H]$^+$.

3-((4-(2-benzylphenoxy)piperidin-1-yl)methyl)benzoic acid (6a, VUF16875)

A mixture of ester **5a** (280 mg, 0.674 mmol) and aq. 2.0 M NaOH (0.337 mL, 0.674 mmol) in THF (3 mL) and EtOH (3 mL) was stirred for 18 h at rt. The volatiles were evaporated. The mixture was acidified with AcOH to pH = 6.0. After addition of H$_2$O (10 mL) the precipitate was filtered. The residue was purified by reverse-phase column chromatography (H$_2$O:MeCN 100:0 to 0:100) to yield the title compound as a white solid (190 mg, 70% yield). ^{1}H NMR (600 MHz, DMSO-d_6) δ 7.78 (s, 1H), 7.75 – 7.71 (m, 1H), 7.27 – 7.21 (m, 4H), 7.20 – 7.17 (m, 2H), 7.17 – 7.11 (m, 3H), 6.94 (d, J = 8.2 Hz, 1H), 6.86 – 6.80 (m, 1H), 4.43 – 4.36 (m, 1H), 3.87 (s, 2H), 3.41 (s, 2H), 2.49 – 2.44 (m, 2H), 2.27 – 2.17 (m, 2H), 1.87 – 1.80 (m, 2H), 1.65 – 1.54 (m, 2H). ^{13}C NMR (151 MHz, DMSO-d_6) δ 169.7, 154.8, 141.3, 139.5, 137.4, 130.8, 130.2, 130.0, 129.9, 128.8, 128.4, 127.9, 127.7, 127.3, 125.9, 120.3, 113.2, 62.5, 49.8, 35.9, 30.5. A signal at 71.8 ppm is not visible but is confirmed by HSQC. HRMS: C$_{26}$H$_{38}$NO$_3$ [M+H]$^+$ calcd: 402.2064, found: 402.2070. LC-MS: t_R = 3.7 min, >98% (254 nm), m/z: 402.1 [M+H]$^+$.

4-((4-(2-benzylphenoxy)piperidin-1-yl)methyl)benzoic acid (6b, VUF16876)

A mixture of ester **5b** (270 mg, 0.650 mmol) and aq. 2.0 M NaOH (0.325 mL, 0.650 mmol) in THF (3 mL) and EtOH (3 mL) was stirred at rt for 18 h. The volatiles were evaporated. The mixture was acidified with AcOH to pH = 6.0. After addition of H$_2$O (10 mL) the precipitate was filtered to give the crude product. The residue was purified by reverse-phase column chromatography (H$_2$O:MeCN 100:0 to 0:100) to yield the title compound as a white solid (180 mg, 69%). ^{1}H NMR (500 MHz, DMSO-d_6) δ 12.87 (s, 1H), 7.89 (d, J = 8.0 Hz, 2H), 7.41 (d, J = 7.9 Hz, 2H), 7.26 (t, J = 7.5 Hz, 2H), 7.22 – 7.08 (m, 5H), 6.96 (d, J = 8.1 Hz, 1H), 6.84 (t, J = 7.4 Hz, 1H), 4.47 – 4.39 (m, 1H), 3.88 (s, 2H), 3.50 (s, 2H), 2.31 – 2.19 (m, 2H), 1.90 – 1.79 (m, 2H), 1.67 – 1.55 (m, 2H). A CH$_2$ signal of the piperidine (counting for 2H) is overlapping with residual DMSO signal but can be identified from HSQC and COSY. ^{13}C NMR (126 MHz, DMSO-d_6) δ 167.3, 154.6, 143.8, 141.2, 130.6, 129.9, 129.3, 128.7, 128.7, 128.2, 127.5, 125.7, 120.1, 113.0, 61.6, 49.7, 35.7, 30.4. A signal at

71.2 ppm is not visible but is confirmed by HSQC. One signal in the >100 pm region is not visible. HRMS: $C_{26}H_{28}NO_3$ [M+H]+ calcd: 402.2064, found: 402.2061. LC-MS: t_R = 3.8 min, >97% (254 nm), *m/z*: 402.2 [M+H]+.

2-((4-(2-benzylphenoxy)piperidin-1-yl)methyl)benzoic acid (6c, VUF16874)

A mixture of 2-CHOPhCOOH (270 mg, 1.795 mmol), amine **4** (400 mg, 1.50 mmol), and Na(CH₃COO)₃BH (507 mg, 2.39 mmol) in DCE (10 mL) was stirred at rt for 24 h. The reaction mixture was poured into H_2O (30 mL) and extracted with EtOAc (2 x 15 mL). The combined organic layers were washed with brine (10 mL). The organic layer was dried with Na_2SO_4, filtered and concentrated under reduced pressure. The crude product was purified by reverse-phase column chromatography (H_2O:MeCN 100:0 to 0:100) to yield the title compound as a white solid (321 mg, 53% yield). ¹H NMR (600 MHz, DMSO-d_6) δ 7.85 (dd, *J* = 7.6, 1.6 Hz, 1H), 7.48 – 7.39 (m, 2H), 7.35 – 7.27 (m, 3H), 7.23 – 7.16 (m, 5H), 6.99 (d, *J* = 8.2 Hz, 1H), 6.91 – 6.84 (m, 1H), 4.65 – 4.56 (m, 1H), 3.93 (s, 2H), 3.87 (s, 2H), 2.71 – 2.54 (m, 4H), 1.93 – 1.81 (m, 2H), 1.79 – 1.68 (m, 2H). ¹³C NMR (151 MHz, DMSO-d_6) δ 169.5, 154.2, 141.3, 137.1, 132.4, 131.8, 131.2, 130.9, 130.5, 129.7, 128.5, 128.3, 127.6, 125.8, 120.4, 112.7, 59.1, 46.6, 35.9, 28.3. A signal at 68.2 ppm is not visible but is confirmed by HSQC. One signal in the >100 pm region is not visible. HRMS: $C_{26}H_{28}NO_3$ [M+H]+ calcd: 402.2064, found: 402.2056. LC-MS: t_R = 4.1 min, >99% (254 nm), m/z: 402.2 [M+H]+.

(7-(diethylamino)-2-oxo-2H-chromen-4-yl)methyl   3-((4-(2-benzylphenoxy)piperidin-1-yl)methyl)benzoate (7a, VUF25247)

To a solution of acid **6a** (187 mg, 0.467 mmol) and alcohol **3** (105 mg, 0.425 mmol) in DCM (5 mL) was added EDC·HCl (169 mg, 0.881 mmol) and DMAP (25 mg, 0.205 mmol) at 0 °C. The reaction mixture was allowed to warm to rt and stirred for 16h. The reaction mixture was diluted with DCM (10 mL) and washed with 0.5 M aq. HCl (3 x 10 mL), sat. aq. $NaHCO_3$ (2 x 10 mL) and brine (10 mL). The organic layer was dried with $MgSO_4$, filtered and concentrated under reduced pressure. The crude product was purified by reverse-phase column chromatography (H_2O:MeCN 100:0 to 0:100) to yield the product as a bright yellow solid (8.0 mg, 3 %). ¹H NMR (500 MHz, CDCl₃) δ 8.06 (t, *J* = 1.7 Hz, 1H), 8.02 (dt, *J* = 7.8, 1.5 Hz, 1H), 7.63 (d, *J* = 7.6 Hz, 1H), 7.45 (t, *J* = 7.7 Hz, 1H), 7.40 – 7.35 (m, 1H), 7.30 – 7.26 (m, 1H), 7.24 – 7.12 (m, 6H), 6.89 – 6.83 (m, 2H), 6.61 (dd, *J* = 9.0, 2.6 Hz, 1H), 6.54 (d, *J* = 2.6 Hz, 1H), 6.26 (t, *J* = 1.1 Hz, 1H), 5.48 (d, *J* = 1.4 Hz, 2H), 4.44 – 4.37 (m, 1H), 3.99 (s, 2H), 3.53 (s, 2H), 3.42 (q, *J* = 7.1 Hz, 4H), 2.61 – 2.48 (m, 2H), 2.37 – 2.30 (m, 2H), 2.00 – 1.91 (m, 2H), 1.85 – 1.78 (m, 2H), 1.22 (t, *J* = 7.1 Hz, 6H). ¹³C NMR (126 MHz, CDCl₃) δ 166.6, 165.9, 162.0, 156.3, 155.0, 150.7, 149.7, 141.4, 139.3, 134.4, 131.0, 130.4, 129.3,

129.2, 128.9, 128.7, 128.3, 127.4, 125.8, 124.5, 120.3, 112.5, 108.8, 106.3, 106.0, 97.8, 71.5, 62.5, 61.8, 50.1, 44.8, 36.5, 30.6, 12.5. HRMS: $C_{40}H_{43}N_2O_5$ [M+H]$^+$ calcd: 631.3166, found: 631.3188. LC-MS (15 min, basic mode): t_R = 9.1 min, >97% (254 nm), *m/z*: 631.4 [M+H]$^+$.

(7-(diethylamino)-2-oxo-2H-chromen-4-yl)methyl 4-((4-(2-benzylphenoxy)piperidin-1-yl)methyl)benzoate (7b, VUF25248)

To a solution of acid **6b** (98.2 mg, 0.245 mmol) and alcohol **3** (55 mg, 0.222 mmol) in DCM (5 mL) was added EDC·HCl (46.5 mg, 0.243 mmol) and DMAP (6.0 mg, 0.049 mmol) at 0 °C. The reaction mixture was allowed to warm to rt and stirred for 16 h. The reaction mixture was diluted with DCM (10 mL) and washed with 0.5 M aq. HCl (3 x 10 mL), sat. aq. NaHCO$_3$ (2 x 10 mL) and brine (10 mL). The organic layer was dried with MgSO$_4$, filtered and concentrated under reduced pressure. The crude product was purified by reverse-phase column chromatography (H$_2$O:MeCN 100:0 to 0:100) to yield the product as a bright yellow solid (8.0 mg, 5 %). ^{1}H NMR (600 MHz, CDCl$_3$) δ 8.07 (d, *J* = 8.1 Hz, 2H), 7.50 – 7.41 (m, 2H), 7.37 (d, *J* = 9.0 Hz, 1H), 7.30 – 7.27 (m, 1H), 7.23 – 7.10 (m, 6H), 6.87 (t, *J* = 7.4 Hz, 1H), 6.83 (d, *J* = 8.2 Hz, 1H), 6.60 (dd, *J* = 9.0, 2.6 Hz, 1H), 6.54 (d, *J* = 2.6 Hz, 1H), 6.24 (t, *J* = 1.3 Hz, 1H), 5.46 (d, *J* = 1.3 Hz, 2H), 4.45 – 4.34 (m, 1H), 3.98 (s, 2H), 3.53 (s, 2H), 3.42 (q, *J* = 7.1 Hz, 4H), 2.58 – 2.45 (m, 2H), 2.40 – 2.27 (m, 2H), 2.00 – 1.88 (m, 2H), 1.86 – 1.76 (m, 2H), 1.22 (t, *J* = 7.1 Hz, 6H). ^{13}C NMR (151 MHz, CDCl$_3$) δ 165.9, 162.1, 156.4, 155.1, 150.9, 149.8, 145.4, 141.5, 138.4, 131.1, 130.0, 129.3, 129.0, 128.4, 127.5, 125.9, 124.6, 120.5, 112.6, 108.9, 106.6, 106.2, 98.0, 62.7, 61.9, 50.4, 44.9, 36.6, 30.6, 12.6. A signal at 71.9 ppm is not visible but is confirmed by HSQC. One signal in the >100 pm region is not visible. HRMS: $C_{40}H_{43}N_2O_5$ [M+H]$^+$ calcd: 631.3166, found: 631.3194. LC-MS (15 min, basic mode): t_R = 9.2 min, >97% (254 nm), *m/z*: 631.4 [M+H]$^+$.

(7-(diethylamino)-2-oxo-2H-chromen-4-yl)methyl (Z)-2-(11-(3-(dimethylamino)propylidene)-6,11-dihydrodibenzo[b,e]oxepin-2-yl)acetate (8, VUF25163)

To a solution of olopatadine (166 mg, 0.445 mmol), DIPEA (0.085 mL, 0.485 mmol) and alcohol **3** (100 mg, 0.404 mmol) in DCM (8 mL) was added EDC·HCl (85.3 mg, 0.445 mmol) and DMAP (11.6 mg, 0.095 mmol) at 0 °C. The reaction mixture was allowed to warm to room temperature and stirred for 16 h. The reaction mixture was diluted with DCM (15 mL) and washed with 0.5 M aq. HCl (2 x 15 mL), sat. aq. NaHCO$_3$ (2 x 15 mL) and brine (35 mL). The organic layer was dried (MgSO$_4$), filtered and concentrated under reduced pressure. The crude product was purified by

reverse-phase column chromatography (H$_2$O:MeCN 100:0 to 0:100) to yield the product as a bright yellow solid (12 mg, 5%). ^{1}H NMR (600 MHz, CDCl$_3$) δ 7.32 – 7.28 (m, 2H), 7.27 – 7.23 (m, 4H), 7.22 (d, *J* = 8.9 Hz, 1H), 7.11 (d, *J* = 2.3 Hz, 1H), 7.08 (dd, *J* = 8.3, 2.4 Hz, 1H), 6.82 (d, *J* = 8.3 Hz, 1H), 6.53 (dd, *J* = 9.0, 2.6 Hz, 1H), 6.51 – 6.49 (m, 1H), 6.09 (t, *J* = 1.3 Hz, 1H), 5.71 (t, *J* = 7.3 Hz, 1H), 5.20 (d, *J* = 1.3 Hz, 2H), 3.65 (s, 2H), 3.40 (q, *J* = 7.1 Hz, 4H), 2.64 – 2.58 (m, 2H), 2.52 – 2.42 (m, 2H), 2.28 – 2.18 (m, 6H), 1.20 (t, *J* = 7.1 Hz, 6H). ^{13}C NMR (151 MHz, CDCl$_3$) δ 171.2, 161.9, 156.4, 155.0, 150.8, 149.4, 133.7, 132.2, 130.2, 129.3, 127.7, 127.6, 126.5, 125.1, 124.6, 124.1, 120.1, 108.8, 106.7, 106.1, 98.0, 70.6, 62.0, 59.4, 45.3, 44.9, 40.3, 12.6. Two signals at 139.8 and 145.5 ppm are not visible but are confirmed by HMBC. One other signal in the >100 pm region is not visible. A signal at 28.2 ppm is not visible but is confirmed by HSQC. HRMS: C$_{35}$H$_{39}$N$_2$O$_5$ [M+H]$^+$ calcd: 567.2853, found: 567.2827. LC-MS (15 min, basic mode): t_R = 5.1 min, >96% (254 nm), *m/z*: 567.3 [M+H]$^+$.

(7-(diethylamino)-2-oxo-2H-chromen-4-yl)methyl (4-nitrophenyl) carbonate (9)

To a solution of alcohol **3** (200 mg, 0.81 mmol) in pyridine (5 mL) was added 4-nitrophenyl chloroformate (489 mg, 2.42 mmol). The reaction mixture was stirred at rt for 30 min. The reaction mixture was poured into H$_2$O (20 mL) and extracted with EtOAc (2 x 15 mL). The combined organic layers were dried over Na$_2$SO$_4$, filtered and concentrated *in vacuo*. The crude product was purified by flash column chromatography (EtOAc/cyclohexane, 2:5) to yield the title compound as white solid (150 mg, 45 %). ^{1}H NMR (600 MHz, CDCl$_3$) δ 8.33 – 8.28 (m, 2H), 7.45 – 7.40 (m, 2H), 7.34 (d, *J* = 9.0 Hz, 1H), 6.69 (d, *J* = 8.0 Hz, 1H), 6.60 (d, *J* = 2.5 Hz, 1H), 6.25 (s, 1H), 5.41 (d, *J* = 1.2 Hz, 2H), 3.43 (q, *J* = 7.1 Hz, 4H), 1.22 (t, *J* = 7.1 Hz, 6H). ^{13}C NMR (151 MHz, CDCl$_3$) δ 161.5, 156.4, 155.4, 152.3, 147.7, 145.8, 125.6, 124.5, 121.9, 109.6, 107.6, 98.8, 65.9, 45.5, 12.5. Two signals at 150.9 ppm and 106.3 ppm are not visible but are confirmed by HMBC. The compound is not stable during LC analysis.

(7-(diethylamino)-2-oxo-2H-chromen-4-yl)methyl 4-(8-chloro-5,6-dihydro-11H-benzo[5,6]cyclohepta[1,2-b]pyridin-11-ylidene)piperidine-1-carboxylate (10, VUF25245)

A mixture of desloratadine (60 mg, 0.193 mmol), formate **9** (159 mg, 0.386 mmol), DIPEA (1.7 mL, 9.65 mmol) and pyridine (5 mL) was stirred at 35 ˚C for 1 h. The reaction mixture was diluted with H$_2$O (10 mL) and extracted with DCM (2 x 10 mL). The combined organic layers were dried over Na$_2$SO$_4$, filtered and concentrated *in vacuo*. The crude product was purified by reverse-phase column chromatography (H$_2$O:MeCN 100:0 to 0:100) to yield the title compound as a white solid

(25 mg, 22 %). ^1H NMR (500 MHz, CDCl$_3$) δ 8.41 (dd, J = 4.8, 1.7 Hz, 1H), 7.45 (dd, J = 7.7, 1.7 Hz, 1H), 7.30 (d, J = 9.0 Hz, 1H), 7.19 – 7.17 (m, 1H), 7.17 – 7.09 (m, 3H), 6.56 (dd, J = 9.0, 2.6 Hz, 1H), 6.50 (d, J = 2.5 Hz, 1H), 6.07 (s, 1H), 5.35 – 5.15 (m, 2H), 3.92 – 3.79 (m, 2H), 3.45 – 3.18 (m, 8H), 2.91 – 2.76 (m, 2H), 2.59 – 2.49 (m, 1H), 2.46 – 2.31 (m, 3H), 1.20 (t, J = 7.1 Hz, 6H). ^{13}C NMR (151 MHz, CDCl$_3$) δ 162.2, 157.0, 156.4, 154.4, 150.8, 150.6, 146.8, 139.7, 137.8, 137.7, 137.0, 134.7, 133.5, 133.2, 130.6, 129.2, 126.4, 124.5, 122.5, 108.8, 106.2, 106.1, 97.9, 62.5, 45.3, 45.2, 44.9, 31.8, 31.6, 30.7, 30.5, 12.6. HRMS: C$_{34}$H$_{35}$ClN$_3$O$_4$ [M+H]$^+$ calcd: 584.2311, found: 584.2308. LC-MS: t_R = 4.9 min, >95% (254 nm), m/z: 584.2 [M+H]$^+$.

Acknowledgements

References

1.   Broichhagen, J.; Frank, J. A.; Trauner, D., A roadmap to success in photopharmacology. *Accounts of Chemical Research* **2015,** *48* (7), 1947-1960.

2.   Szobota, S.; Isacoff, E. Y., Optical control of neuronal activity. *Annual Review of Biophysics* **2010,** *39* (1), 329-348.

3.   Velema, W. A.; Szymanski, W.; Feringa, B. L., Photopharmacology: beyond proof of principle. *Journal of the American Chemical Society* **2014,** *136* (6), 2178-2191.

4.   Silva, J. M.; Silva, E.; Reis, R. L., Light-triggered release of photocaged therapeutics - Where are we now? *Journal of Controlled Release* **2019,** *298*, 154-176.

5.   Klán, P.; Šolomek, T.; Bochet, C. G.; Blanc, A.; Givens, R.; Rubina, M.; Popik, V.; Kostikov, A.; Wirz, J., Photoremovable protecting groups in chemistry and biology: reaction mechanisms and efficacy. *Chemical Reviews* **2013,** *113* (1), 119-191.

6.   Fuchter, M. J., On the promise of photopharmacology using photoswitches: a medicinal chemist's perspective. *Journal of Medicinal Chemistry* **2020**.

7.   Hüll, K.; Morstein, J.; Trauner, D., In vivo photopharmacology. *Chemical Reviews* **2018,** *118* (21), 10710-10747.

8.   Szymański, W.; Beierle, J. M.; Kistemaker, H. A. V.; Velema, W. A.; Feringa, B. L., Reversible photocontrol of biological systems by the incorporation of molecular photoswitches. *Chemical Reviews* **2013,** *113* (8), 6114-6178.

9.   Pittolo, S.; Gómez-Santacana, X.; Eckelt, K.; Rovira, X.; Dalton, J.; Goudet, C.; Pin, J.-P.; Llobet, A.; Giraldo, J.; Llebaria, A.; Gorostiza, P., An allosteric modulator to control endogenous G protein-coupled receptors with light. *Nature Chemical Biology* **2014,** *10* (10), 813-815.

10.   Schönberger, M.; Trauner, D., A photochromic agonist for μ-opioid receptors. *Angewandte Chemie International Edition* **2014,** *53* (12), 3264-3267.

11.   Bahamonde, M. I.; Taura, J.; Paoletta, S.; Gakh, A. A.; Chakraborty, S.; Hernando, J.; Fernández-Dueñas, V.; Jacobson, K. A.; Gorostiza, P.; Ciruela, F., Photomodulation of G protein-coupled adenosine receptors by a novel light-switchable ligand. *Bioconjugate Chemistry* **2014,** *25* (10), 1847-1854.

12.   Broichhagen, J.; Johnston, N. R.; von Ohlen, Y.; Meyer-Berg, H.; Jones, B. J.; Bloom, S. R.; Rutter, G. A.; Trauner, D.; Hodson, D. J., Allosteric optical control of a class B G-protein-coupled receptor. *Angewandte Chemie International Edition* **2016,** *55* (19), 5865-5868.

13.   Westphal, M. V.; Schafroth, M. A.; Sarott, R. C.; Imhof, M. A.; Bold, C. P.; Leippe, P.; Dhopeshwarkar, A.; Grandner, J. M.; Katritch, V.; Mackie, K.; Trauner, D.; Carreira, E. M.; Frank, J. A., Synthesis of photoswitchable Δ9-tetrahydrocannabinol derivatives enables optical control of cannabinoid receptor 1 signaling. *Journal of the American Chemical Society* **2017,** *139* (50), 18206-18212.

14.   Gómez-Santacana, X.; de Munnik, S. M.; Vijayachandran, P.; Da Costa Pereira, D.; Bebelman, J. P. M.; de Esch, I. J. P.; Vischer, H. F.; Wijtmans, M.; Leurs, R., Photoswitching the efficacy of a small-molecule ligand for a peptidergic GPCR: from antagonism to agonism. *Angewandte Chemie International Edition* **2018,** *57* (36), 11608-11612.

15.   Stein, M.; Middendorp, S. J.; Carta, V.; Pejo, E.; Raines, D. E.; Forman, S. A.; Sigel, E.; Trauner, D., Azo-propofols: photochromic potentiators of GABAA receptors. *Angewandte Chemie International Edition* **2012,** *51* (42), 10500-10504.

16.   Frank, J. A.; Moroni, M.; Moshourab, R.; Sumser, M.; Lewin, G. R.; Trauner, D., Photoswitchable fatty acids enable optical control of TRPV1. *Nature Communications* **2015,** *6* (1), 7118.

17.   Broichhagen, J.; Schönberger, M.; Cork, S. C.; Frank, J. A.; Marchetti, P.; Bugliani, M.; Shapiro, A. M. J.; Trapp, S.; Rutter, G. A.; Hodson, D. J.; Trauner, D., Optical control of insulin release using a photoswitchable sulfonylurea. *Nature Communications* **2014,** *5* (1), 5116.

18.   Kaplan, J. H.; Forbush, B.; Hoffman, J. F., Rapid photolytic release of adenosine 5'-triphosphate from a protected analog: utilization by the sodium:potassium pump of human red blood cell ghosts. *Biochemistry* **1978,** *17* (10), 1929-1935.

19.   Kolarski, D.; Sugiyama, A.; Breton, G.; Rakers, C.; Ono, D.; Schulte, A.; Tama, F.; Itami, K.; Szymanski, W.; Hirota, T.; Feringa, B. L., Controlling the circadian clock with high temporal resolution through photodosing. *Journal of the American Chemical Society* **2019,** *141* (40), 15784-15791.

20.   Xue, G.; Wang, K.; Zhou, D.; Zhong, H.; Pan, Z., Light-induced protein degradation with photocaged PROTACs. *Journal of the American Chemical Society* **2019,** *141* (46), 18370-18374.

21.   Goswami, P. P.; Syed, A.; Beck, C. L.; Albright, T. R.; Mahoney, K. M.; Unash, R.; Smith, E. A.; Winter, A. H., BODIPY-derived photoremovable protecting groups unmasked with green light. *Journal of the American Chemical Society* **2015,** *137* (11), 3783-3786.

22.   Furuta, T.; Wang, S. S.-H.; Dantzker, J. L.; Dore, T. M.; Bybee, W. J.; Callaway, E. M.; Denk, W.; Tsien, R. Y., Brominated 7-hydroxycoumarin-4-ylmethyls: photolabile protecting groups with biologically useful cross-sections for two photon photolysis. *Proceedings of the National Academy of Sciences* **1999,** *96* (4), 1193-1200.

23.   Hansen, M. J.; Feringa, F. M.; Kobauri, P.; Szymanski, W.; Medema, R. H.; Feringa, B. L., Photoactivation of MDM2 inhibitors: controlling protein–protein interaction with light. *Journal of the American Chemical Society* **2018,** *140* (41), 13136-13141.

24.   Peng, X.-M.; L.V. Damu, G.; He Zhou, C., Current developments of coumarin compounds in medicinal chemistry. *Current Pharmaceutical Design* **2013,** *19* (21), 3884-3930.

25.   Banghart, Matthew R.; Sabatini, Bernardo L., Photoactivatable neuropeptides for spatiotemporally precise delivery of opioids in neural tissue. *Neuron* **2012,** *73* (2), 249-259.

26.   Gaur, P.; Kucherak, O. A.; Ermakova, Y. G.; Shvadchak, V. V.; Yushchenko, D. A., Nitrobenzyl-based fluorescent photocages for spatial and temporal control of signalling lipids in cells. *Chemical Communications* **2019,** *55* (82), 12288-12291.

27.   Banghart, M. R.; Williams, J. T.; Shah, R. C.; Lavis, L. D.; Sabatini, B. L., Caged naloxone reveals opioid signaling deactivation kinetics. *Molecular Pharmacology* **2013,** *84* (5), 687-695.

28.   Kramer, R. H.; Mourot, A.; Adesnik, H., Optogenetic pharmacology for control of native neuronal signaling proteins. *Nature Neuroscience* **2013,** *16* (7), 816-823.

29.   Kand, D.; Liu, P.; Navarro, M. X.; Fischer, L. J.; Rousso-Noori, L.; Friedmann-Morvinski, D.; Winter, A. H.; Miller, E. W.; Weinstain, R., Water-soluble BODIPY photocages with tunable cellular localization. *Journal of the American Chemical Society* **2020,** *142* (11), 4970-4974.

30.   Ellis-Davies, G. C. R., Caged compounds: photorelease technology for control of cellular chemistry and physiology. *Nature Methods* **2007,** *4* (8), 619-628.

31.   Umeda, N.; Takahashi, H.; Kamiya, M.; Ueno, T.; Komatsu, T.; Terai, T.; Hanaoka, K.; Nagano, T.; Urano, Y., Boron dipyrromethene as a fluorescent caging group for single-photon uncaging with long-wavelength visible light. *ACS Chemical Biology* **2014,** *9* (10), 2242-2246.

32.   Panula, P.; Chazot, P. L.; Cowart, M.; Gutzmer, R.; Leurs, R.; Liu, W. L. S.; Stark, H.; Thurmond, R. L.; Haas, H. L., International union of basic and clinical pharmacology. XCVIII. histamine receptors. *Pharmacological Reviews* **2015,** *67* (3), 601-655.

33.   Hauwert, N. J.; Mocking, T. A. M.; Da Costa Pereira, D.; Lion, K.; Huppelschoten, Y.; Vischer, H. F.; De Esch, I. J. P.; Wijtmans, M.; Leurs, R., A photoswitchable agonist for the histamine H3 receptor, a prototypic family a G-protein-coupled receptor. *Angewandte Chemie International Edition* **2019,** *58* (14), 4531-4535.

34.   Hauwert, N. J.; Mocking, T. A. M.; Da Costa Pereira, D.; Kooistra, A. J.; Wijnen, L. M.; Vreeker, G. C. M.; Verweij, E. W. E.; De Boer, A. H.; Smit, M. J.; De Graaf, C.; Vischer, H. F.; de Esch, I. J. P.; Wijtmans, M.; Leurs, R., Synthesis and characterization of a bidirectional photoswitchable antagonist toolbox for real-time GPCR photopharmacology. *Journal of the American Chemical Society* **2018,** *140* (12), 4232-4243.

35.   Rustler, K.; Pockes, S.; König, B., Light-switchable antagonists for the histamine H1 receptor at the isolated guinea pig ileum. *ChemMedChem* **2019,** *14* (6), 636-644.

36.   Kay, G. G., The effects of antihistamines on cognition and performance. *The Journal of Allergy and Clinical Immunology* **2000,** *105* (6 Pt 2), S622-7.

37.   Simons, F. E. R.; Simons, K. J., Histamine and H1-antihistamines: celebrating a century of progress. *Journal of Allergy and Clinical Immunology* **2011,** *128* (6), 1139-1150.e4.

38.   Li, Z.; Su, K.; Jiang, Z.; Yu, Y.; You, Q.; Zhang, X., Photoactivatable prolyl hydroxylase 2 inhibitors for stabilizing the hypoxia-inducible factor with light. *Journal of Medicinal Chemistry* **2019,** *62* (16), 7583-7588.

39.   Bosma, R.; Wang, Z.; Kooistra, A. J.; Bushby, N.; Kuhne, S.; van den Bor, J.; Waring, M. J.; de Graaf, C.; de Esch, I. J.; Vischer, H. F.; Sheppard, R. J.; Wijtmans, M.; Leurs, R., Route to prolonged residence time at the histamine H1 receptor: growing from desloratadine to rupatadine. *Journal of Medicinal Chemistry* **2019,** *62* (14), 6630-6644.

40.   Bosma, R.; Stoddart, L. A.; Georgi, V.; Bouzo-Lorenzo, M.; Bushby, N.; Inkoom, L.; Waring, M. J.; Briddon, S. J.; Vischer, H. F.; Sheppard, R. J.; Fernández-Montalván, A.; Hill, S. J.; Leurs, R., Probe dependency in the determination of ligand binding kinetics at a prototypical G protein-coupled receptor. *Scientific Reports* **2019,** *9* (1), 7906.

41.   Shimamura, T.; Shiroishi, M.; Weyand, S.; Tsujimoto, H.; Winter, G.; Katritch, V.; Abagyan, R.; Cherezov, V.; Liu, W.; Han, G. W.; Kobayashi, T.; Stevens, R. C.; Iwata, S., Structure of the human histamine H1 receptor complex with doxepin. *Nature* **2011,** *475* (7354), 65-70.

42.   Zhang, M. Q.; Leurs, R.; Timmerman, H. Histamine H1- receptor antagonists. In *Burger's Medicinal Chemistry an Drug Discovery*, 5th ed.; Wolff, M. E., Ed.; Vrije Universiteit: Amsterdam, 1997; Vol. 5.

43.   Walter, M.; Stark, H., Histamine receptor subtypes: a century of rational drug design. *Frontiers in Bioscience (Scholar edition)* **2012,** *4*, 461-88.

44.   de Graaf, C.; Kooistra, A. J.; Vischer, H. F.; Katritch, V.; Kuijer, M.; Shiroishi, M.; Iwata, S.; Shimamura, T.; Stevens, R. C.; de Esch, I. J. P.; Leurs, R., Crystal structure-based virtual screening for fragment-like ligands of the human histamine H1 receptor. *Journal of Medicinal Chemistry* **2011,** *54* (23), 8195-8206.

45.   Kooistra, A. J.; Kuhne, S.; de Esch, I. J. P.; Leurs, R.; de Graaf, C., A structural chemogenomics analysis of aminergic GPCRs: lessons for histamine receptor ligand design. *British Journal of Pharmacology* **2013,** *170* (1), 101-126.

46.   Kobayashi, C.; Tanaka, A.; Yasuda, T.; Hishinuma, S., Roles of lys191 and lys179 in regulating thermodynamic binding forces of ligands to determine their binding affinity for human histamine H1 receptors. *Biochemical Pharmacology* **2020,** *180*, 114185.

47.   Kuhne, S.; Kooistra, A. J.; Bosma, R.; Bortolato, A.; Wijtmans, M.; Vischer, H. F.; Mason, J. S.; de Graaf, C.; de Esch, I. J. P.; Leurs, R., Identification of ligand binding hot spots of the histamine H1 receptor following structure-based fragment optimization. *Journal of Medicinal Chemistry* **2016,** *59* (19), 9047-9061.

48.   Xu, Z.; Gao, Z.; Shao, X., Light-triggered release of insecticidally active spirotetramat-enol. *Chinese Chemical Letters* **2018,** *29* (11), 1648-1650.

49.   Bosma, R.; Moritani, R.; Leurs, R.; Vischer, H. F., BRET-based β-arrestin2 recruitment to the histamine H1 receptor for investigating antihistamine binding kinetics. *Pharmacological Research* **2016,** *111*, 679-687.

50.   Kristiansen, K.; Dahl, S. G., Molecular modeling of serotonin, ketanserin, ritanserin and their 5-HT2C receptor interactions. *European Journal of Pharmacology* **1996,** *306* (1), 195-210.

51.   Kristiansen, K.; Kroeze, W. K.; Willins, D. L.; Gelber, E. I.; Savage, J. E.; Glennon, R. A.; Roth, B. L., A highly conserved aspartic acid (Asp-155) anchors the terminal amine moiety of tryptamines and is involved in membrane targeting of the 5-HT2A serotonin receptor but does not participate in activation via a "salt-bridge disruption" mechanism. *Journal of Pharmacology and Experimental Therapeutics* **2000,** *293* (3), 735-746.

52.   Booth, R. G.; Fang, L.; Wilczynski, A.; Sivendren, S.; Sun, Z.; Travers, S.; Bruysters, M.; Sansuk, K.; Leurs, R., Molecular determinants of ligand-directed signaling for the histamine H1 receptor. *Inflammation Research* **2008,** *57* (1), 43-44.

53.   Schmidt, R.; Geissler, D.; Hagen, V.; Bendig, J., Mechanism of photocleavage of (coumarin-4-yl)methyl esters. *The Journal of Physical Chemistry A* **2007,** *111* (26), 5768-5774.

54.   Roessler, W. G.; Brewer, C. R., Permanent turbidity standards. *Journal of Applied Microbiology* **1967,** *15* (5), 1114-11

Chapter 7

Discussion

Molecular determinants that underly the design of small molecules with desired properties play an important role in modern Medicinal Chemistry. An important theme of this thesis has been the understanding of molecular determinants that govern ligand-target residence time (RT) at a prototypic GPCR. Structural ligand features governing RT are poorly understood, which leads to generally scarce insights for the design of small molecules with desired association and dissociation rates. Several studies have suggested some structural features key in modulating binding kinetics. For example, a study using a Pfizer database which contains mostly GPCR and kinase ligands suggests a trend between ligand flexibility and RT. For ligands with molecular weight of 300–500 Da, ligands with less rotatable bonds (≤5) more often have a shorter drug-target RT than ligands with more rotatable bonds.[1] In a different study, the RT of more than 1800 ligands for the dopamine D_2 receptor was determined by Tresadern *et al*, showing that ligands with a long RT have, on average, a higher number of ring structures.[2] Others factors that have been found to be correlated to RT are shielded hydrogen bonds[3] and the number of rotatable bonds.[4]

Detailed studies on structure-kinetics relationships (SKRs) of ligand series will help to better understand the importance of ligand residence time in drug action. Therefore, in this thesis the histamine H_1 receptor H_1R (a prototypic class A GPCR) was used as an ideal "work horse" to study GPCR modulation by small-molecule ligands by means of binding kinetics. Although a few studies have explored H_1R ligand-binding kinetics[5-13], detailed structure-kinetics relationship of series of H_1R ligands have been not thoroughly studied. In the current work, several sets of tools compounds have been designed, synthesized and pharmacologically characterized in order to reach this objective.

Investigating H_1R binding kinetics - the effect of substitution in rupatadine and desloratadine analogues

In **chapter 2**, the structure-kinetics relationship of the rupatadine/desloratadine scaffold is presented. Rupatadine, a marketed drug for H_1R, was found to have an at least ten times longer residence time than its analog desloratadine (Figure 1).
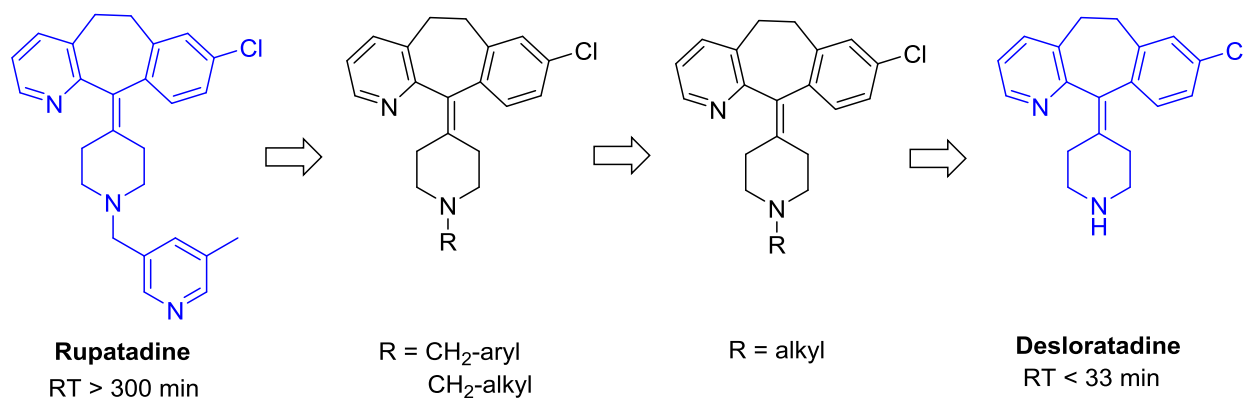
Figure 1. Stepwise deconstruction of the (5-methylpyridin-3-yl)methyl substituent of rupatadine to desloratadine. RT data shown was determined using [^{3}H]levocetirizine.

A proper radiolabel compound is very important to characterize the differences in kinetic binding profiles within a set of compounds. The prototypical H_1R radioligand [^{3}H]mepyramine has a short residence time (RT = 4.6 min),[7, 14] which may not allow a sufficiently resolved analysis of binding kinetics for a set of analogs. Levocetirizine is known to have a much longer residence time at H_1R than mepyramine.[7] Thus, [^{3}H]levocetirizine was prepared for the study of the binding kinetics of ligands with a much longer residence time. It was used in the subsequent probing of the structural elements that affect the kinetic binding profile of the common scaffold of both antihistamines rupatadine and desloratadine. To this end, 22 analogs embodying a stepwise deconstruction of the (5-methylpyridin-3-yl)methyl substituent of rupatadine were designed and synthesized (Figure 1). The binding kinetics were characterized for these analogs. All the analogs have good binding affinity (pK_i = 7.7 − 9.4) and this can be the result of the privileged desloratadine-like core scaffold that all analogues have. Analogs with large cycloaliphatic or aromatic substituents and/or an additional CH_2 spacer on the piperidine have a long residence time at H_1R as measured by the Kinetic Rate Index (KRI). In contrast, analogs with cycloaliphatic substituents without CH_2 spacer on the piperidine have a relatively short residence time at H_1R (Figure 2). Studies on the kinetics of functional H_1R antagonism show that exemplary compounds having cycloaliphatic N-substituents with a CH_2 spacer (e.g. **14**, **16**) completely inhibit the functional response of H_1R after washing off unbound ligands, which is in line with their higher KRI value. In contrast, analogs with the same cycloaliphatic groups but without a CH_2 spacer (**19**, **20**) show a clear recovery of functional response in the same assay. Modeling studies indicate that such differences in kinetic profile probably result from steric hindrance in the ligand-H_1R complex. Less steric clash between ligands with a CH_2 spacer and residues near the amine-binding region results in a better fit in the binding pocket, which may prevent ligand dissociation. Analogs such as **19** and **20** without the spacer are less well accommodated in the H_1R binding pocket, which is caused by steric clash between the cycloaliphatic group and I454[7.39] and Y458[7.43].
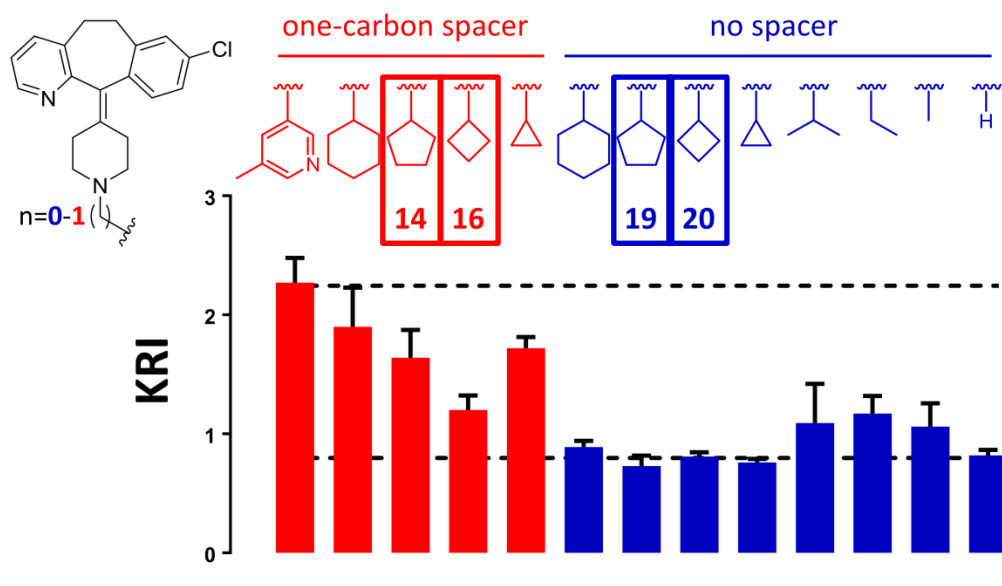
Figure 2. Differential binding kinetics of analogs with aliphatic *N*-substituents at H_1R.

The combination of an appropriate long-residence radiolabel and structure-kinetics relationship of a tailored set of compounds helps the better understanding of ligand protein interaction as well as molecular factors that modulate binding kinetics on H_1R. The study shows that subtle changes in substitution pattern can affect the kinetic properties of the ligands substantially and provides a rationale for the observed difference in kinetic behavior between rupatadine and desloratadine.

Investigating H_1R binding kinetics - the effect of cyclization of H_1R antagonists

In **chapter 3**, structure-kinetics relationships of H_1R ligands are described focusing on two hallmark features of H_1R antagonists: the aromatic head group and the basic amine moiety. Gradual constraining of these elements was key in the approach.

Figure 3. Cyclization of H_1R antagonists and exploring structure-kinetics relationships.

For the aromatic head, it was found that this pharmacophoric element has an impact on binding kinetics. For example, fusing the two aromatic rings of clinically used H_1R ligands into one tricyclic aromatic head group increases binding affinity and prolongs the RT at H_1R. However, this set of clinically used ligands has some specific substitut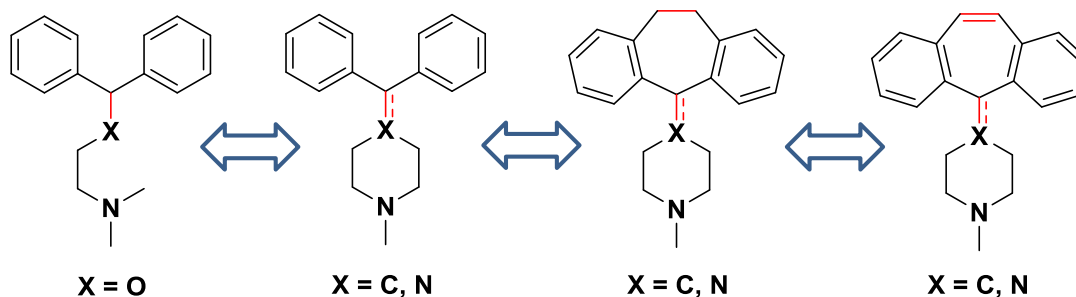ion of the aromatic rings or involves the incorporation of heteroatoms in the aromatic rings. To allow a more accurate understanding of the structure-kinetics relationships, a series of tailored analogues that provides a systematic exploration of the effect of constraining the aromatic rings was designed and synthesized (Figure 3). A second hallmark feature of H_1R antagonists, i.e. the basic amine moiety, was also taken into consideration in this synthetic effort. The detailed study of the structure-kinetics relationship of the resulting 12 compounds shows that cyclization has a pronounced effect on the RT. In general, tricyclic analogues show higher binding affinities and a longer RT than non-fused ligands. The effect of constraining the basic amine moiety on the binding kinetics is less pronounced. Detailed trend analyses were undertaken on this series of tailored synthetic derivatives. The overall isoaffinity plot (Figure 4) shows that constraining is a valid approach to modulate affinity as well as association and dissociation rates, but an overall unifying trend for this particular scaffold proves challenging to formulate.

Kinetic K_D
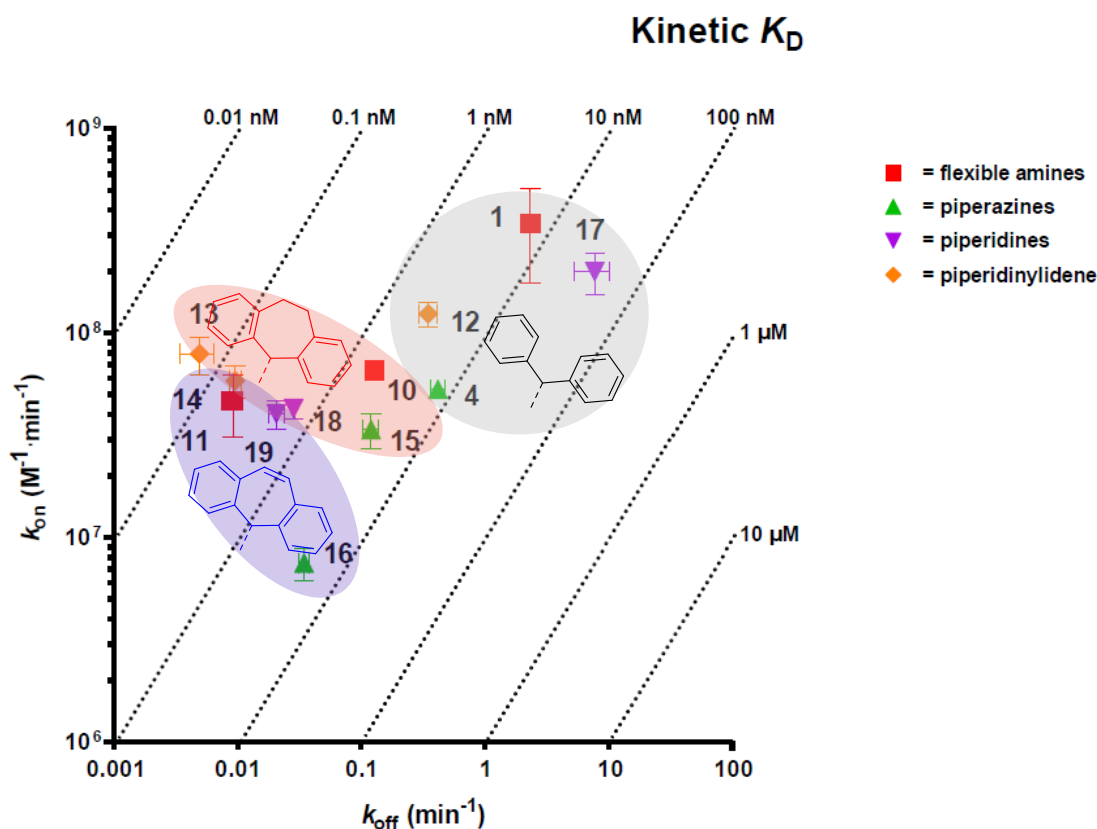
Figure 4. Isoaffinity map indicating k_{on}, k_{off} and $K_{D, calc}$ values for tailored compounds. The color-coded dots represent different amine moieties that are present in the compounds. The color-coded zones cover compounds having the same aromatic ring system.

Investigating H_1R binding kinetics - the effect of isosteric replacement of the carboxylic acid in H_1R antagonists

The work in this thesis has suggested some structural features that can modulate binding kinetics, for instance the effect of steric hindrance (**chapter 2**) and cyclization (**chapter 3**). In **chapter 4**, the aim was to explore the effect of bioisosteric replacements in a carboxylic acid-containing ligand on H_1R binding kinetics. A carboxylic acid (VUF14506) was selected as a starting point. Functional groups studied (Figure 5) include potential non-acidic isosteres, classical acidic isosteres and a tailored set of potential sulfonyl-containing isosteres (both non-acidic and acidic). All functional groups afford compounds with similar binding affinity and as such these groups can formally be considered as reasonable isosteres of the parent carboxylic acid. Kinetic studies show

that acidic isosteres in general have longer RT than most non-acidic ones. The data cannot clearly substantiate that the difference in RT between acidic and non-acidic isosteres results from a presumed ionic interaction between the ligands and a targeted lysine residue.

Interestingly, within the non-acidic isosteres, ligands containing squaric moieties appear to show longer RT than non-acidic isosteres (Figure 5 & 6). The size of the this relatively large group may contribute to its kinetics binding profile. The distinct squaric moieties may also possess specific physicochemical properties which contribute to the biological properties. However, a suitable growth vector on the squaric moieties for further SKR is not evident. Moreover, the stability of squaric esters can be a problem. In contrast, acylsulfonamide VUF15290 has good affinity, slow dissociation and an evident growth factor on its aromatic moiety. It was therefore chosen as a key compound to further explore the kinetic binding profile for a tailored set of potential sulfonyl-containing isosteres, consisting of acylsulfonamides, sulfonamides and sulfonylureas. No decisive trend could be observed between the acidity of these sulfonyl-isosteres and dissociation patterns. The observed differences in KRI values (Fig. 6) need to be interpreted with caution, since a KRI value over ca. 2.0 (indicating slow dissociation) prevents further inspection of detailed trends. The acylsulfonamide moiety of VUF15290 was also used as an isostere for the carboxylic acid in levocetirizine and the resulting compound also displays slow unbinding. This was further substantiated in a functional assay in which pre-treatment of H_1R with this acylsulfonamide gave only a slow recovery of the histamine-induced calcium response.

When looking at the role of the acidity for all compounds from Figure 5, it can be noted that no clear trend is observed when plotting KRI against p$K_{a,calc}$ for all compounds (Figure 7A). Similarly, plotting pK_i against p$K_{a,calc}$ (Figure 7B) indicates there is no correlation between binding affinities and acidity.

A single report on the replacement of the carboxylic acid in quinoline-containing H_1R ligands by sulfones and sulfonamides has been disclosed,[15] leading to compounds with longer duration of action. However, the study did not measure binding kinetics and did not pursue the analysis of a broad range of potential isosteres. The work presented in this chapter suggests that the sulfonyl moiety group may contribute substantially to binding kinetics as almost all sulfonyl-containing compounds show high KRI value (KRI > 2.4).

Non-acidic non-squaric isosteres	1.2 < KRI < 1.6	
Non-acidic squaric isosteres	3.1 < KRI < 4.7	
Acidic isosteres	KRI > 2.0	
Acylsulfonamides	2.4 < KRI < 5.9	
Sulfonamides	2.6 < KRI < 4.9	
Sulfonylureas	1.9 < KRI < 5.8	

VUF14506
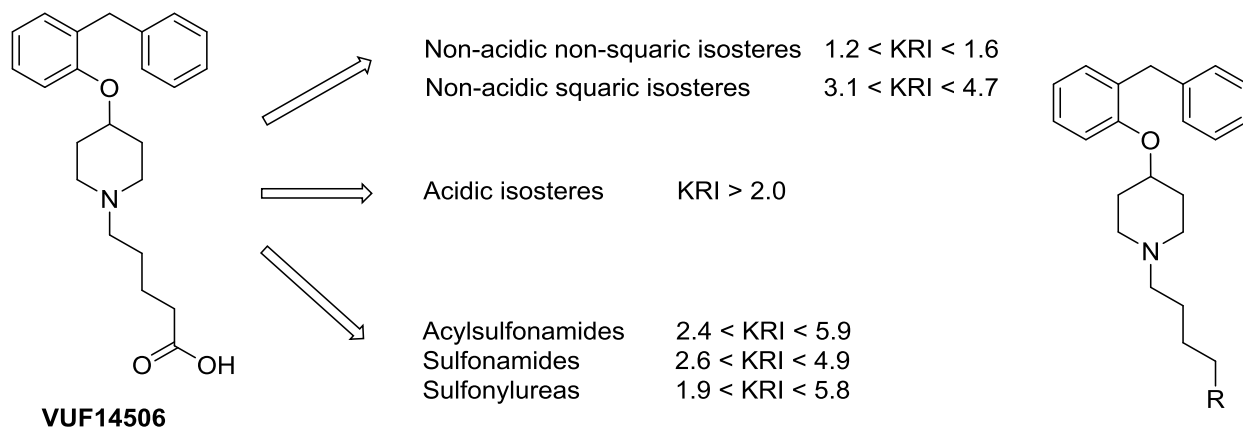
Figure 5. The general strategy for isosteric replacements of the carboxylic acid in a H$_1$R ligand.
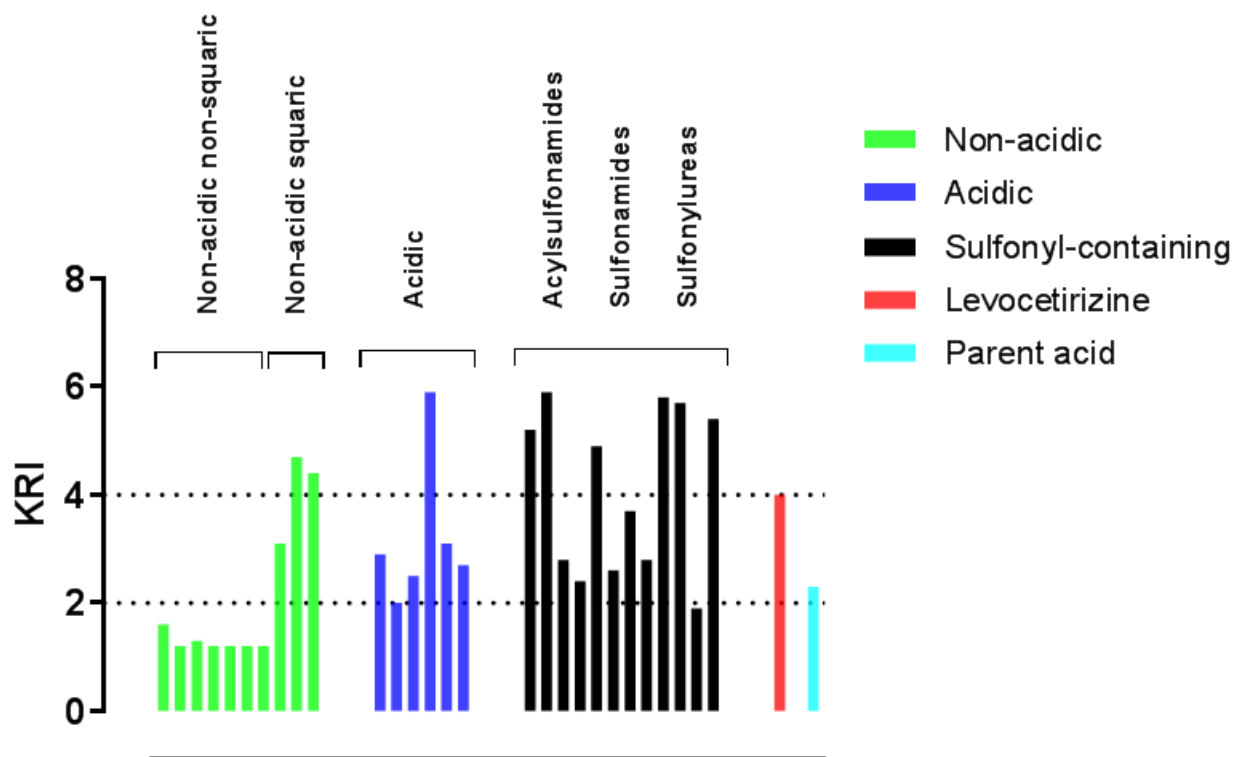
Figure 6. Overview of the binding kinetics of H$_1$R ligands with potential acid isosteres.
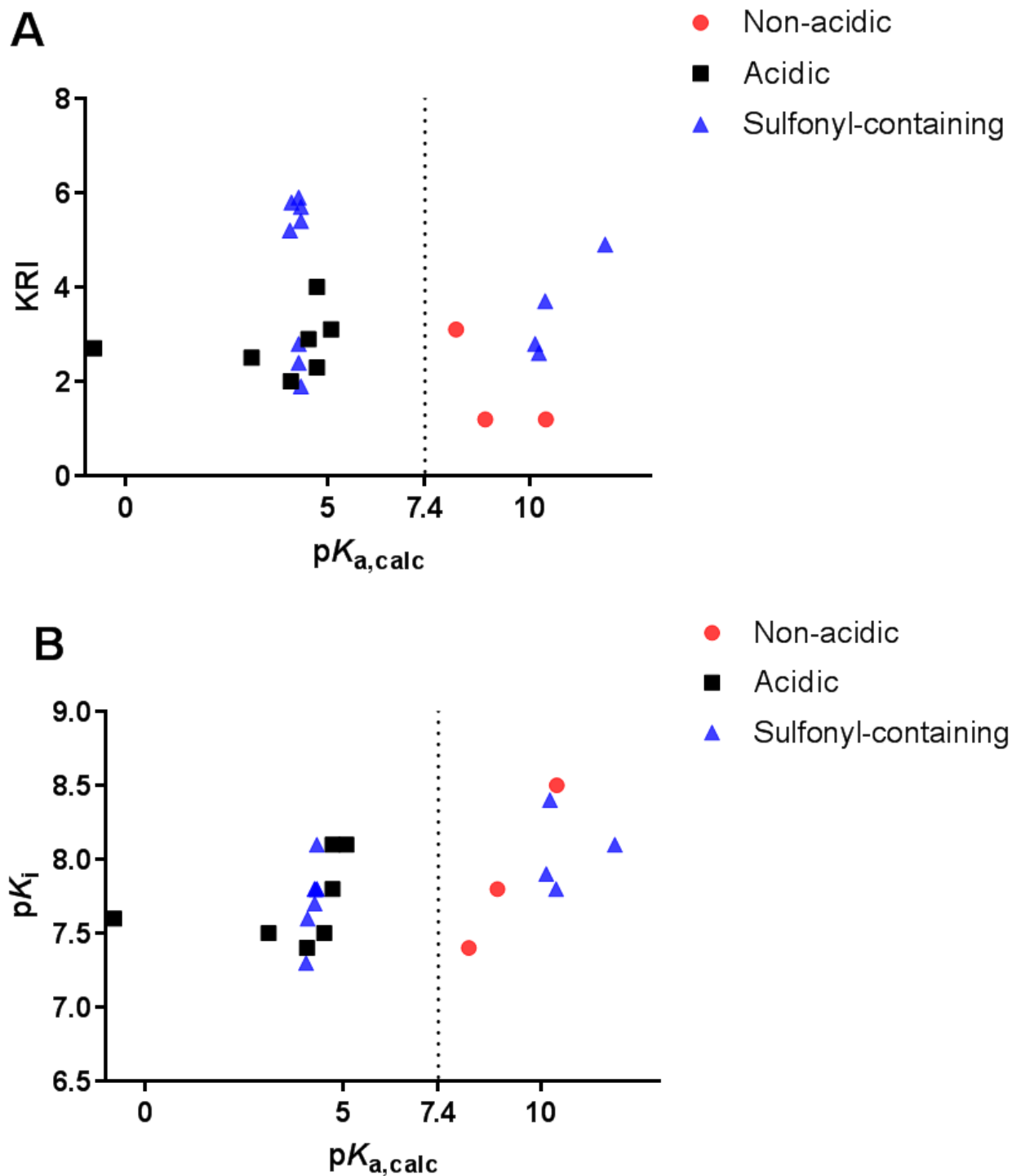
Figure 7. Exploring binding kinetics for the synthesized sets of isosteres. (A) KRI value versus calculated acidity ($pK_{a,calc}$). (B) Binding affinity (pK_i) versus calculated acidity ($pK_{a,calc}$). Compounds for which no pK_a value could be calculated have been omitted.

Investigating H$_1$R binding kinetics – the influence of a boron atom in H$_1$R ligands

In **chapter 5**, boron-containing ligands were probed for their potential to give slow dissociation. The utilization of boron-containing ligands was hypothesized to be a means to modulate ligand binding kinetics via formation of a reversible covalent complex with the protein. Specifically, the effect of engagement of the boron atom with key lysine residue K191$^{5.39}$ in H$_1$R on binding kinetics was explored. Two series of boron-containing ligands were designed and synthesized. Series A used a recently published benzaldehyde boronic acid trap for lysines (Figure 8A), whereas series B used an α-aminoboronic acid unit which was hypothesized to be able to form a complex with lysine (Figure 8B).[16, 17]

All ligands have good binding affinity similar to that of the parent compound hit. Results on kinetic studies should be interpreted with caution. Based on the available compounds and the current data set, there is no evident data able to show that covalent engagement takes place between the designed ligands and target protein and that RT is consistently and substantially increased. However, it was found that some structural features are able to modestly modulate binding kinetics, e.g. the introduction of a boronic acid moiety on an amide. Previous studies have shown that the introduction of either an aldehyde or boronic acid has the theoretical capacity to bind lysine and form a complex.[18-20] However, these two scenarios were primarily inspected for their effect on the affinity associated with ligand binding. Evidence that they can also modify binding kinetics is not provided in those studies. The introduction of both units (benzaldehyde and boronic acid, Figure 8A) has been found to give covalent binding to lysine[21, 22] and even prolongation of RT.[21] The introduction of α-aminoboronic acid unit provides two potential scenarios for covalent binding as seen from Figure 8B. These scenarios could not be unequivocally assessed in the current study. It is important to note that the linker plays a critical role for the postulated covalent engagement. Primary non-covalent docking using the X-ray structure of H$_1$R will be useful to help targeting the proposed ligand-protein interaction by selecting the optimal linker. Utilization of boron-containing covalent ligands in studying binding kinetics can then be expanded on H$_1$R.
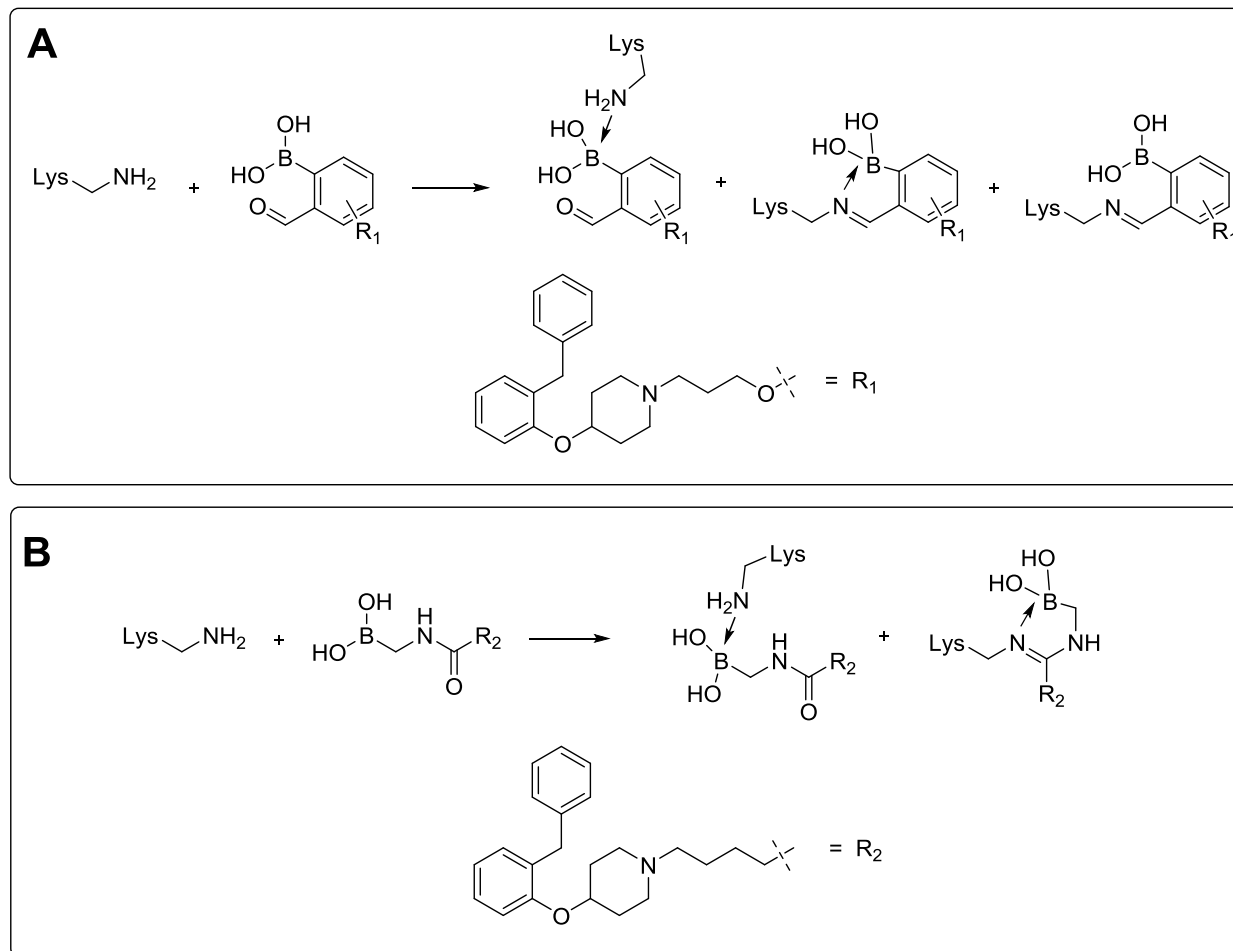
Figure 8. Different scenarios using the theoretical capacity of a boron atom to bind lysine residues, including dative complexes and formation of imines. (A) The proposed engagement between a benzaldehyde boronic acid and a lysine residue. (B) The proposed engagement between an α-aminoboronic acid unit and a lysine residue, ranging from a dative complex to a condensation product.

Development of photocaged H$_1$ receptor antagonists for GPCR photopharmacology

The previous chapters use kinetic binding properties of small-molecule ligands as a means to modulate GPCR signaling. Photochemical control (photopharmacology) provides an alternative means for modulating GPCR signaling. Utilization of photons can achieve the control of ligand activity and enhance pharmacological selectivity with spatial and temporal regulation of GPCR signalling.[23, 24] Incorporating a photosensitive functional group into ligands can enable this photocontrol.[25-28] One of the subareas in this field is photocaging, in which a key functional group in a ligand is caged (i.e. protected with a photoprotective group PPG) which can be deprotected with light to restore the affinity of the ligand.

In **chapter 6**, photocaging as a means of modulating H$_1$R signaling is explored. Specifically, modulation of ligand binding to the amine binding region and to the upper aromatic region was

pursued. Three strategies were undertaken. Firstly, olopatadine was chosen as a key parent compound as the carboxylate group on the phenyl moiety is accommodated in the upper aromatic sub-pocket. Caging of the carboxylate group was envisioned to result in a steric clash with the transmembrane helixes in the upper sub-pocket (Figure 9A). Secondly, *ortho-*, *meta-* and *para*-substituted carboxybenzyl analogs (i.e. VUF16874-16876) of an in-house hit were hypothesized to fit, but caged analogs were postulated not to fit the relatively small space in the amine-binding region (Figure 9B). Thirdly, the introduction of a PPG directly on the piperidine ring of desloratadine was proposed to reduce the basicity of the amine and therefore most likely affect ligand binding at the H_1R. Moreover, the resulting caged desloratadine with the bulky PPG group may experience a steric clash with nearby residues (Figure 9C).

Pharmacological results show that caged olopatadine (VUF25163) still has the propensity to bind to the H_1R pocket (Figure 9A). Evidently, a charged carboxylic acid moiety is not substantially contributing to the binding affinity of olopatadine. The high affinity of caged olopatadine implies that the coumarin moiety can fit efficiently into some space in the H_1R pocket. Binding to the extracellular vestibular region of the H_1R is most likely possible. The nanomolar binding affinity of caged olopatadine prevents a further detailed inspection as photopharmacology tool. Caged VUF16875 and 16876 (VUF25247 and 25248, respectively) also still have good binding affinity at the H_1R and no loss of affinity was observed when compared to parent compounds (Figure 9B). Caged VUF16875-16876 still harbor the basic amine and may change their conformation to fit the limited space in the amine-binding region. However, caged desloratadine (**10**) has a 2.2 log unit shift compared to desloratadine (Figure 9C). The appreciable drop in binding affinity may result from the combination of reduced basicity of the amine and steric clash of the bulky PPG group. Photo-uncaging at 400 nm leads to the release of desloratadine with concomitant formation of several byproducts, as identified by LCMS and NMR analyses. The uncaging affords an increase in observed H_1R affinity. In contrast and as expected, the binding affinity of desloratadine itself is retained after illumination. Caged desloratadine was selected for further exploration in a functional assay (H_1R mediated NFAT activation). Also in this functional assay the caged compound shows a lower antagonist potency compared to the parent desloratadine. Yet, illumination of the caged compound at 400 nm resulted in potent antagonism of histamine responses. Future *in vivo* assays with optical modulation of H_1R antagonism are therefore warranted with the new caged desloratadine analog.

Functionalisation of the basic amine of the piperidine ring has proven successful in the case of caged desloratadine. The results on the caged ligand suggests that more bulky PPGs such as BODIPY[29] can be selected to induce potentially bigger steric clash with residues in binding pocket. While in this chapter the amine binding region and upper aromatic region were addressed, the lower aromatic sub-pocket of H_1R with limited space can potentially also be targeted with this

strategy by installing the presented PPG or BODIPY on H_1R antagonists, for instance by replacing the chloro atom of desloratadine/ levocetirizine by a PPG on e.g. a phenol.

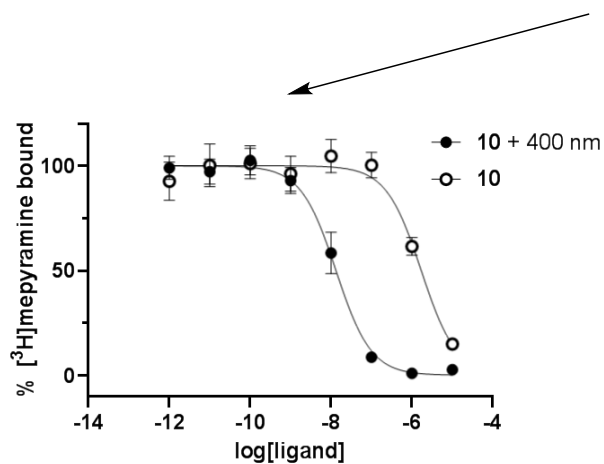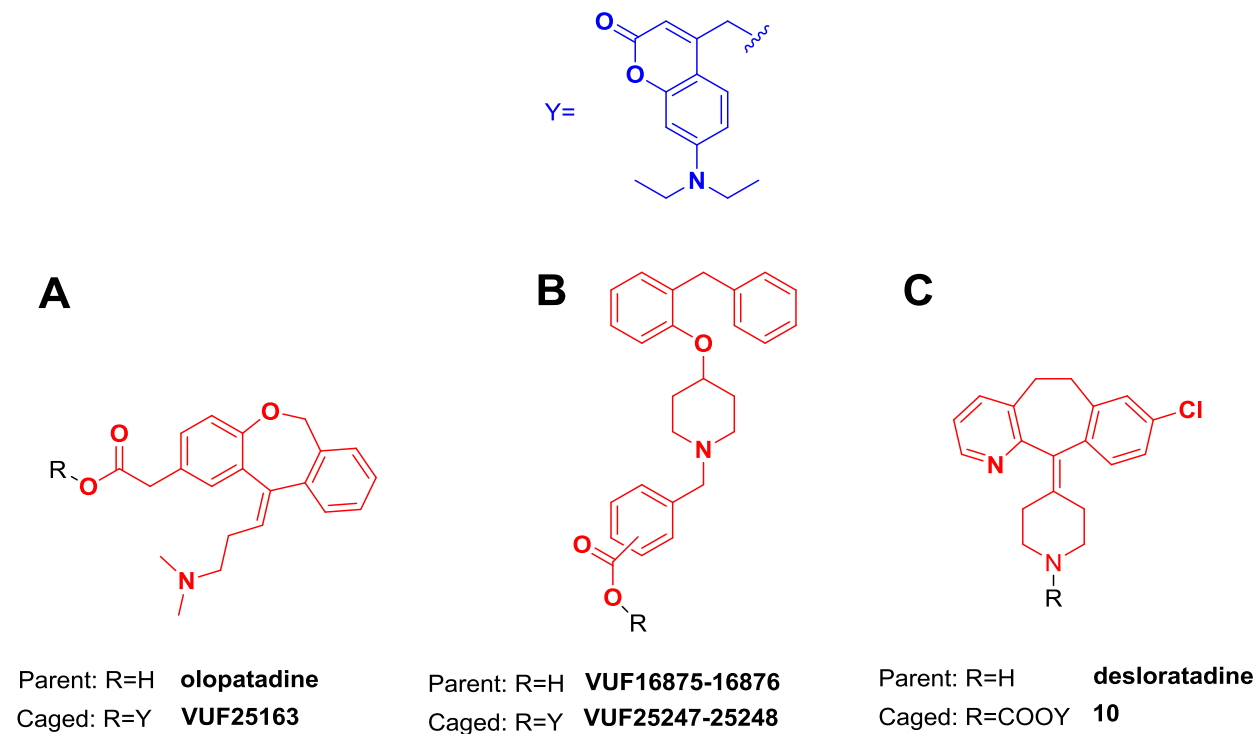**Figure 9.** Several classes of coumarin-based photocaged H_1R antagonists, which upon illumination release parent compound olopatadine (A), VUF16875-16876 (B) and desloratadine (C).

Final perspectives

Throughout this thesis, it has been shown that GPCR modulation can be achieved by strategic use of binding kinetics. The studies in **Chapters 2**, **3**, **4** and **5** have provided structural factors that

affect the kinetics of ligand-target interaction. These detailed structure-kinetics relationships help in understanding H_1R pharmacology. In this thesis the starting point has been either a VS hit (VUF14544) (**Chapter 4**, **5**) or rupatadine (**Chapter 2**). Different starting scaffolds may result in a broader variety of SKRs. Thus, in follow-up studies, other starting scaffolds can be considered. Indeed, there are more than 45 clinically used antihistamines targeting H_1R, which offer a wealth of opportunities to develop more tool compounds. Starting points can also be based on virtual screening. In this thesis, H_1R photopharmacology was also explored. The successful application of a photocaged desloratadine paves the way for furthering H_1R photopharmacological knowledge. Again, other H_1R scaffolds can be considered and, moreover, the three binding sub-pockets in H_1R also provide more chances to develop more and different types of photosensitive tool compounds.

It is of interest to discuss the potential broader applicability of the results described in this thesis. H_1R was used as an ideal "work horse" class A GPCR. The different approaches and concepts studied on H_1R can find their ways to broader applicability. GPCRs being the largest drug target family, the pharmacology of other GPCRs can be explored by these developed approach/concepts in refined manners. The study of binding kinetics of small-molecule ligands has received increased interest recently. In this thesis, we have used isosteric replacements, covalent binding and cyclization approaches to study binding kinetics at H_1R for the first time. These SKR approaches have not been thoroughly studied in many other GPCRs and these concepts could be expanded to other GPCRs. However, the exploration of these approaches/concepts would be challenging without thorough pharmacological tools such as existing for H_1R. For example, mutational studies can offer more detailed insights in the binding process. Also, the availability of crystal structures of the target plays an important role. Yet, as mentioned in the introductory chapter of this thesis, despite major advances in the crystallography field crystal structures have been disclosed for a limited number of GPCRs only. In combination with such crystal structures, computational methods such as docking and molecular dynamic will be able to help in understanding the process of binding and unbinding.

The detailed profiles of binding kinetics for existing antihistamines in this thesis has proven important as these provided a primary selection for initial explorations. Ideally, the factors underlying slow off-rate binding kinetics of small-molecule ligands are taken into consideration in a broader fashion and for other GPCR targets. However, it is likely that these factors need to be inspected on a case-to-case basis. It is not guaranteed that the factors found for H_1R ligands can modulate binding kinetics for any particular GPCR case. For a thorough understanding of binding kinetics for a given GPCR, crystal structures of receptors and computational methods are beneficial or even necessary.

The successful application of photocaging on H_1R, as shown in this thesis, is a good start for other targets and it may pave the way for photopharmacology for other GPCRs. In studies on photopharmacology, both crystal structures and computational methods can play similarly crucial roles as in binding kinetics studies, as does knowledge of detailed SAR. Thus, in photopharmacology studies on other GPCRs, the combined knowledge of various sources (crystal structures, computational work, existing SAR, design of molecules, pharmacological study and mutational study) form primary guidelines. However, these general guidelines will be challenging to follow for every GPCR target. The difference in affinity between caged and parent compound determines further exploration. As the work in this thesis shows, such affinity differences are not always present even when anticipated based on ligand-based models. Also, efficient photochemical uncaging reactions need to be ensured in photopharmacology and this includes improved irradiation times and product profiles compared to the case in this thesis. The used wavelength can be fine-tuned with regard to different photoremovable protecting groups and compatibility with the biological system under study. Moreover, the carboxylate, secondary/primary amine and hydroxy groups, frequently present in successful H_1R antagonists and good starting points for photocaging, can be used in other GPCR ligands if these functional group are present.

References

1.   Miller, D. C.; Lunn, G.; Jones, P.; Sabnis, Y.; Davies, N. L.; Driscoll, P., Investigation of the effect of molecular properties on the binding kinetics of a ligand to its biological target. *MedChemComm* **2012,** *3* (4), 449-452.

2.   Tresadern, G.; Bartolome, J. M.; Macdonald, G. J.; Langlois, X., Molecular properties affecting fast dissociation from the D2 receptor. *Bioorganic & Medicinal Chemistry* **2011,** *19* (7), 2231-2241.

3.   Schmidtke, P.; Luque, F. J.; Murray, J. B.; Barril, X., Shielded hydrogen bonds as structural determinants of binding kinetics: application in drug design. *Journal of the American Chemical Society* **2011,** *133* (46), 18903-18910.

4.   Veber, D. F.; Johnson, S. R.; Cheng, H.-Y.; Smith, B. R.; Ward, K. W.; Kopple, K. D., Molecular properties that influence the oral bioavailability of drug candidates. *Journal of Medicinal Chemistry* **2002,** *45* (12), 2615-2623.

5.   Treherne, J. M.; Young, J. M., Temperature-dependence of the kinetics of the binding of [3H]-(+)-N-methyl-4-methyldiphenhydramine to the histamine H1-receptor: comparison with the kinetics of [3H]-mepyramine. *British Journal of Pharmacology* **1988,** *94* (3), 811-822.

6.   Wallace, R. M.; Young, J. M., Temperature dependence of the binding of [3H]mepyramine and related compounds to the histamine H1 receptor. *Molecular Pharmacology* **1983,** *23* (1), 60-66.

7.   Gillard, M.; Chatelain, P., Changes in pH differently affect the binding properties of histamine H1 receptor antagonists. *European Journal of Pharmacology* **2006,** *530* (3), 205-214.

8.   Kanba, S.; Richelson, E., Histamine H1 receptors in human brain labelled with [3H]doxepin. *Brain Research* **1984,** *304* (1), 1-7.

9.	Gillard, M.; Van Der Perren, C.; Moguilevsky, N.; Massingham, R.; Chatelain, P., Binding characteristics of cetirizine and levocetirizine to human H1 histamine receptors: contribution of Lys191 and Thr194. *Molecular Pharmacology* **2002,** *61* (2), 391-399.

10.	Malany, S.; Hernandez, L. M.; Smith, W. F.; Crowe, P. D.; Hoare, S. R., Analytical method for simultaneously measuring ex vivo drug receptor occupancy and dissociation rate: application to (R)-dimethindene occupancy of central histamine H1 receptors. *Journal of Receptor and Signal Transduction Research* **2009,** *29* (2), 84-93.

11.	Slack, R. J.; Hart, A. D.; Luttmann, M. A.; Clark, K. L.; Begg, M., In vitro characterisation of the duration of action of the histamine-1 receptor antagonist azelastine. *European Journal of Pharmacology* **2011,** *670* (2), 586-592.

12.	Slack, R. J.; Russell, L. J.; Hall, D. A.; Luttmann, M. A.; Ford, A. J.; Saunders, K. A.; Hodgson, S. T.; Connor, H. E.; Browning, C.; Clark, K. L., Pharmacological characterization of GSK1004723, a novel, long-acting antagonist at histamine H(1) and H(3) receptors. *British Journal of Pharmacology* **2011,** *164* (6), 1627-1641.

13.	Wittmann, H.-J.; Seifert, R.; Strasser, A., Influence of the N-terminus and the E2-loop onto the binding kinetics of the antagonist mepyramine and the partial agonist phenoprodifen to H1R. *Biochemical Pharmacology* **2011,** *82* (12), 1910-1918.

14.	Bosma, R.; Stoddart, L. A.; Georgi, V.; Bouzo-Lorenzo, M.; Bushby, N.; Inkoom, L.; Waring, M. J.; Briddon, S. J.; Vischer, H. F.; Sheppard, R. J.; Fernández-Montalván, A.; Hill, S. J.; Leurs, R., Probe dependency in the determination of ligand binding kinetics at a prototypical G protein-coupled receptor. *Scientific Reports* **2019,** *9* (1), 7906.

15.	Procopiou, P. A.; Ford, A. J.; Gore, P. M.; Hancock, A. P.; Hodgson, S. T.; Holmes, D. S.; Looker, B. E.; Vile, S.; Clark, K. L.; Saunders, K. A.; Slack, R. J.; Watts, C. J., Identification of selective 8-(piperidin-4-yloxy)quinoline sulfone and sulfonamide histamine H1 receptor antagonists for use in allergic rhinitis. *Bioorganic & Medicinal Chemistry Letters* **2017,** *27* (21), 4914-4919.

16.	Lai, J. H.; Liu, Y.; Wu, W.; Zhou, Y.; Maw, H. H.; Bachovchin, W. W.; Bhat, K. L.; Bock, C. W., Synthesis and structural investigation of internally coordinated α-amidoboronic acids. *The Journal of Organic Chemistry* **2006,** *71* (2), 512-519.

17.	Bhat, K. L.; Braz, V.; Laverty, E.; Bock, C. W., The effectiveness of a primary aliphatic amino group as an internal Lewis base on the formation of a boron–oxygen–carbon linkage: a computational study. *Journal of Molecular Structure: THEOCHEM* **2004,** *712* (1), 9-19.

18.	Whyte, G. F.; Vilar, R.; Woscholski, R., Molecular recognition with boronic acids-applications in chemical biology. *Journal of Chemical Biology* **2013,** *6* (4), 161-74.

19.	Migneault, I.; Dartiguenave, C.; Bertrand, M. J.; Waldron, K. C., Glutaraldehyde: behavior in aqueous solution, reaction with proteins, and application to enzyme crosslinking. *BioTechniques* **2004,** *37* (5), 790-802.

20.	Dal Corso, A.; Catalano, M.; Schmid, A.; Scheuermann, J.; Neri, D., Affinity enhancement of protein ligands by reversible covalent modification of neighboring lysine residues. *Angewandte Chemie International Edition* **2018,** *57* (52), 17178-17182.

21.	Akçay, G.; Belmonte, M. A.; Aquila, B.; Chuaqui, C.; Hird, A. W.; Lamb, M. L.; Rawlins, P. B.; Su, N.; Tentarelli, S.; Grimster, N. P.; Su, Q., Inhibition of Mcl-1 through covalent modification of a noncatalytic lysine side chain. *Nature Chemical Biology* **2016,** *12* (11), 931-936.

22.	Cal, P. M. S. D.; Vicente, J. B.; Pires, E.; Coelho, A. V.; Veiros, L. s. F.; Cordeiro, C.; Gois, P. M. P., Iminoboronates: a new strategy for reversible protein modification. *Journal of the American Chemical Society* **2012,** *134* (24), 10299-10305.

23.	Berizzi, A. E.; Goudet, C., Strategies and considerations of G-protein-coupled receptor photopharmacology. *Advances in Pharmacology* **2020,** *88*, 143-172.

24.   Ricart-Ortega, M.; Font, J.; Llebaria, A., GPCR photopharmacology. *Molecular and Cellular Endocrinology* **2019,** *488*, 36-51.

25.   Silva, J. M.; Silva, E.; Reis, R. L., Light-triggered release of photocaged therapeutics - Where are we now? *Journal of Controlled Release* **2019,** *298*, 154-176.

26.   Brieke, C.; Rohrbach, F.; Gottschalk, A.; Mayer, G.; Heckel, A., Light-controlled tools. *Angewandte Chemie International Edition* **2012,** *51* (34), 8446-8476.

27.   Klán, P.; Šolomek, T.; Bochet, C. G.; Blanc, A.; Givens, R.; Rubina, M.; Popik, V.; Kostikov, A.; Wirz, J., Photoremovable protecting groups in chemistry and biology: reaction mechanisms and efficacy. *Chemical Reviews* **2013,** *113* (1), 119-191.

28.   Ellis-Davies, G. C. R., Caged compounds: photorelease technology for control of cellular chemistry and physiology. *Nature Methods* **2007,** *4* (8), 619-628.

29.   Kand, D.; Liu, P.; Navarro, M. X.; Fischer, L. J.; Rousso-Noori, L.; Friedmann-Morvinski, D.; Winter, A. H.; Miller, E. W.; Weinstain, R., Water-soluble BODIPY photocages with tunable cellular localization. *Journal of the American Chemical Society* **2020,** *142* (11), 4970-4974.

Summary

Drug discovery and development is a long trajectory involving many disciplines and stages. During the stages of hit-to-lead and lead optimization, design, synthesis, and pharmacological evaluation of molecules play important roles. During these stages, medicinal chemists often use Structure-Activity Relationships (SAR) or more recently emerging strategies, such as Structure-Kinetics Relationships (SKR) studies. In parallel, chemical biology tools as used in photopharmacology approaches are becoming available. As one of largest drug target families, G protein-coupled receptors (GPCRs) offer a wealth of opportunities to study these approaches and concepts.

In this thesis, SKR have been thoroughly studied for antagonists of a prototypic family A GPCR, the histamine H_1 receptor (H_1R). The photopharmacology approach has also been investigated for H_1R in a proof-of-concept study. Utilization of these concepts to study this archetypical GPCR will facilitate better understanding of small-molecule modulation of GPCRs and pave the way for the application of these approaches to other GPCRs and other protein targets.

The binding kinetics of a ligand is a metric that has been proposed to predict better *in vivo* efficacy. It provides a more detailed description of the ligand binding interaction than the binding affinity under equilibrium conditions. Correlating the structural parts responsible for the binding kinetics of a ligand has proven challenging to generalize. Some factors, such as the numbers of rings, involvement of shielded hydrogen bonds and number of rotatable bonds, have been found to be correlated to binding kinetics in specific cases.

In this thesis, the SKRs of various sets of designed compounds targeting H_1R are explored and additional factors that can modulate binding kinetics of GPCR ligands have been found (**chapter 2-5**). Steric clash events in the limited space nearby the amine-binding region in the H_1R binding pocket were found to be able to modulate binding kinetics in **chapter 2**. [^{3}H]levocetirizine was chosen to analyse the kinetics of binding of unlabeled ligands with a much longer residence time. The hypothesized steric clash may help the dissociation of the ligands from the binding pocket and therefore shorten residence time. In **chapter 3**, analysis of benchmark H_1R ligands led to the notion that tricyclic antagonists have a longer residence time at H_1R than non-tricyclic ones. To further explore this molecular feature, twelve tailored antagonist analogs were synthesized and their kinetic profile investigated. The detailed SKR results show that cyclization of the aromatic groups of such analogues has a pronounced effect on the ligand-target RT, while the cyclisation effect of the basic amine moieties on the binding kinetics is less pronounced. In **chapter 4**, the kinetic profiles of ligands were explored using isosteric replacements of a carboxylic acid. While isosteric replacements have often been used in SAR studies, it will be important to know the effect of isosteric replacements in modulating binding

kinetics. The binding affinities of non-acidic and acidic isosteres of carboxylic acids as well as a tailored set of sulfonyl-containing ligands were found to be similar. However, acidic isosteres tend to have higher KRI values (a reciprocal measure for rate of unbinding) than most non-acidic ones. Finally, covalent binding is an approach to modulate binding kinetics in a more defined way. In **chapter 5**, covalent binding to modulate binding kinetic profiles was explored through boron-containing ligands. The unique chemical properties of boron were hypothesized to affect ligand binding kinetics via reversible covalent binding with key lysine K191 residue in H_1R. The obtained data on two sets of boron-containing ligand series indicate that kinetic profiles can be affected modestly by an α-aminoboronic acid, but does not suggest that covalent labeling is occurring on a second class of ligands comprising a benzaldehyde-boronic acid unit.

Next to the exploration of kinetic binding parameters of small-molecule ligands to address modulation of GPCR, photochemical modulation (photopharmacology) provides a new approach to GPCR modulation. Photocaging, i.e. protecting a ligand with a photoremovable group, has proven to be successful in obtaining optical control of ligand activity. In **chapter 6**, we took advantage of such a photocaging strategy on H_1R. A designed coumarin-caged H_1R antagonist has a ~100-fold lower affinity for the human H_1R. Uncaging with 400 nm light results in release of the parent compound desloratadine and an associated efficient blockade of H_1R.

In summary, this thesis presents the design and synthesis of tool compounds with tailored kinetic binding profiles or photopharmacological features, that can help in the future understanding of H_1R pharmacology and in the development of novel ligands.

Nederlandse Samenvatting (Summary in Dutch)

Het ontwikkelen van medicijnen is een tijdsintensief proces met vele stadia en berust op verschillende disciplines. Tijdens de hit-to-lead en lead optimization stadia spelen het ontwerp, synthese en farmacologisch testen van moleculen een belangrijke rol. Gedurende deze stadia gebruiken chemici vaak structuur-activiteit relaties (SAR) of recenter ontwikkelde strategiën zoals structuur-kinetiek relaties (SKR) voor het ontwikkelen van een nieuw medicijn. Daarnaast zijn er steeds meer bruikbare concepten op het raakvlak van de chemie en biologie, zoals photo-farmacologie. De familie van G eiwit-gekoppelde receptoren (GPCR) biedt veel kansen om de beschreven concepten te onderzoeken.

In dit proefschrift wordt SKR bestudeerd voor antagonisten van een klasse A GPCR, te weten de intensief bestudeerde histamine H1 receptor (H_1R). Daarnaast wordt ook photo-farmacologie toegepast op de H_1R in een proof-of-concept studie. Het toepassen van deze concepten op een archetypische GPCR zal de kennis omtrent het moduleren van GPCRs met kleine moleculen vergroten en zal de weg banen voor het gebruik van de onderzochte concepten op GPCRs en andere groepen van eiwitten.

In de literatuur is gesuggereerd dat de bindingskinetiek van liganden een belangrijke maat is om de in vivo efficacy van een medicijn te kunnen voorspellen. Het geeft een gedetailleerdere beschrijving van de interactie tussen een eiwit en ligand dan verkregen door de bindingsaffiniteit onder evenwichtscondities. Het is gebleken dat de correlatie tussen de structurele eigenschappen van een ligand en de bindingskinetiek niet makkelijk te generaliseren is. Echter, in specifieke gevallen zijn er correlaties gevonden tussen structuurelementen van het ligand en de bindingskinetiek, zoals de hoeveelheid ringstructuren, afgeschermde waterstofbruggen en het aantal roteerbare bindingen.

In dit proefschrift is de SKR van H_1R liganden onderzocht door het ontwerpen en testen van verschillende groepen liganden. Aanvullende factoren die bepalend zijn voor de bindingskinetiek van liganden op een GPCR zijn daarbij gevonden (hoofdstuk 2-5).

Sterische hindering in de compacte bindingsholte voor amine-groepen in H_1R is bepalend voor de bindingskinetiek van liganden (hoofdstuk 2). In dit hoofdstuk is [^{3}H]levocetirizine gekozen als radioligand om de kinetiek van liganden met een lange residence time te onderzoeken. Op basis van het onderzoek in dit hoofdstuk kan geconcludeerd worden dat de introductie van moleculaire structuurelementen die sterische hindering met de receptor geven kan worden toegepast om de residence time te verkorten.

In hoofdstuk 3 leidt een analyse van bekende medicijnen voor H_1R tot de observatie dat tricyclische liganden een langere residence time hebben dan niet-tricyclische liganden. Dit is verder onderzocht door het synthetiseren en testen van twaalf H_1R antagonisten die stapsgewijze veranderingen in de structuur bevatten. De gedetailleerde SKR laat zien dat het cycliseren van de aromatische groepen van deze liganden een groot effect heeft op de residence time maar dat het cycliseren van het basische amine niet een duidelijk effect lijkt te hebben.

In hoofdstuk 4 zijn de kinetische eigenschappen van liganden onderzocht na het vervangen van carboxylaat groepen door bioisosteren. Het vervangen van moleculaire groepen door bioisosteren is vaak onderzocht in de context van SAR-studies maar het is belangrijk om het effect hiervan ook te onderzoeken in SKR-studies. Zowel de bindingsaffiniteit van zure en neutrale isosteren van de carboxylaat groep als de bindingsaffiniteit van specifiek ontworpen liganden met een sulfonyl groep laten vergelijkbare waarden zien voor H_1R. Zure isosteren vertonen echter een hogere KRI waarde (een reciproke maat voor de dissociatie snelheid) dan neutrale isosteren.

Het gebruik van covalente interacties biedt een beter gedefinieerde manier om de bindingskinetiek van liganden te moduleren. In hoofdstuk 5 is geprobeerd covalent bindende liganden te ontwerpen door boor-bevattende groepen te introduceren. De onderliggende hypothese is dat de unieke chemische eigenschappen van boor kunnen zorgen voor een reversibele covalente interactie tussen het ligand en de lysine op positie 191 van H_1R, hetgeen de bindingskinetiek zou kunnen beïnvloeden. De data van twee groepen boor-bevattende liganden geeft aan dat een bescheiden effect op de bindingskinetiek behaald kan worden door het introduceren van een α-aminoboorzuur maar laat niet zien dat liganden met een benzaldehyde-boorzuur een covalente interactie aangaan met H_1R.

Naast het gebruik van de bindingskinetiek van liganden vormt optische modulatie (photo-farmacologie) een nieuwe manier om GPCRs te moduleren met lichtgevoelige liganden. Photocaging, een biologisch actief ligand inactief maken met een chemische groep die verwijderd kan worden met licht, is in een aantal gevallen succesvol in het optisch moduleren van biologische systemen. In hoofdstuk 6 is een photocage strategie toegepast op liganden voor H_1R. De ontworpen liganden zijn op cruciale posities gesubstitueerd met coumarine als lichtgevoelige beschermgroep. Deze substitutie zorgt in het beste geval voor een ~100 keer lagere affiniteit van deze liganden voor H_1R. Het afsplitsen van de coumarine door te bestralen met licht met een golflengte van 400 nm resulteert in het vrijkomen van de actieve stof desloratadine en een effectieve blokkade van H_1R.

Samengevattend kan gesteld worden dat de in dit proefschrift ontwikkelde moleculen met op maat ontworpen bindingskinetiek en photo-farmacologische eigenschappen kunnen helpen om de H_1R farmacologie verder te begrijpen en om nieuwe liganden te ontwikkelen.

Acknowledgements

After five years of living in Amsterdam, the end is here. The adventure has been tough and full of challenges. However, I have to say, it has been an amazing time. I am genuinely happy that, during this adventure, so many people have helped and supported me, or have been by my side throughout. It is those people that have made my five years in the Netherlands such an enjoyable and unforgettable experience. In this last chapter of my thesis I would like to express my gratitude to those great people.

Rob Leurs, my promoter, thank you so much for offering me the opportunity to pursue my PhD in your group. The opportunity has meant a lot to me and I believe this will be important for my future. I am sincerely grateful for your trust and support as a person, and grateful for your supervision and support throughout my research. **Maikel Wijtmans**, my co-promoter, I thank you for your trust and for letting me pursue a PhD in this group in Amsterdam. Throughout the four years of research and half a year of writing, you have supervised me intensely. The time and effort that you have invested in me seems endless. Your critical thinking and insight have shaped me as a researcher. **Iwan J. P. de Esch**, thank you for your strong support and supervision in these four years. **Chris**, **Henry**, **Barbara**, I am grateful to all of you. I would like to thank you all for your support in different projects. The constructive suggestions always helped me. Working with all of you has been enjoyable.

Reggie, **Sebastiaan**: two colleagues from K4DD: My two collaborators/partners within the VU and MedChem group. It was such a great pleasure to work with the both of you. Thank you for your endless assistance and help. The two of you set a good example for me and I gained a lot from you. Your way of thinking and speaking inspired me deeply. Your way of performing science and making friends also influenced me a lot. I am so grateful for all of this. Moreover, I would like to send my best wishes to you two and hope to see you again. **Niels**, **Tamara**, **Tiffany**, **Ivana and Daniel da Costa Pereira**: colleagues from photopharmacology: I would like to thank each of you for your help and assistance. I have learnt so much from each of you. Working with you guys was also enjoyable. I wish each of you good luck and a nice future. **Rick**, **David**, **Lorena**, **Pierre**: we spent over three years in the lab together. There are so many beautiful moments with you in my mind that I will never forget. MTB, skydiving, pizza time, swimming, laser tag, food festival, Düsseldorf Christmas markets, lab-outing days, BBQs, so on and so forth. Thank you for your care and support when I felt down or frustrated. I will remember all of this. I wish to see you guys again in the future and I wish you guys good luck with your science and future. **Albert**, **Márton**: two computational chemists: I would like to thank you for your assistance and

help. Without your support I would not have been able to manage some projects. I wish both of you a nice future. **Shanliang**, **Yang**, **Miaomiao**, **Xiaoyuan**: Chinese colleagues in the MedChem group. It's been great to meet you guys here in Amsterdam. I appreciated your kind help and care. Good luck to all of you and I wish all of you a nice future. **Marta**, **Ilze**, **Stephanie**, **Gábor**, **Maarten**, **Erik**, **Ton**: It's so nice to meet you guys in the MedChem group and to be friends. So many beautiful moments we spent together will be in my heart forever. I have appreciated all of your help in my daily life and research. Thank you guys, it means more to me than words can describe. We will see each other soon in the Netherlands and I send my best wishes to you guys. **Xavi**, **Sophie**, **Andrea**, **Jessica**, **Guido**, **George**, **Kerstin**, **Mounir**, **Inna**: I am very glad to have met you guys in the MedChem group. Working with you guys has been such an enjoyable time. I thank all of you for your assistance and help here and there. I hope you are enjoying your current work and I send my best wishes. **Hans**, **Andrea** and **Elwin**: I thank all three of you for the technical help in LCMS, HPLC, HRMS, NMR, the compound library and even in the dark room. You guys have always been glad to help me out during my study here and took care of me at the beginning. I wish you all good luck and enjoyment in your work and life. My master students: **Wrej**, **Jay**, **Mark**, **Karan**, **Marieke**, **Lady**: it has been such a great pleasure to have you four as my trainee students. Thank you for all of your collaboration and contributions in projects. I really appreciated your guys' hard work and help. Some of your work is not present in chapters, but they may be present in manuscripts in the near future. I hope you guys did learn a lot from your internships. It was lots of fun to work together with you. Last but not least, I wish you guys all good luck in the future. I would like to thank other master students I met in lab: **Sara**, **Rilana**, **Evgenia**, **Tom**, **Elina**, **Amid**, **Steven**, **Lydia**, **Maria**, **Joep**, **Anna**, **Alba**, **Dominik**, **Muhan Zhao** and **Maral**. It was a great pleasure to study with you. I am sincerely grateful for all of the support and help from you all. I wish you all a nice future.

Jian Lin, it has been awesome to have met you in Amsterdam and to be friends. You are such a nice person that I would like to share almost all things with you. I can't remember how many times we were at your place, drinking and telling jokes. Since you are studying Chinese media, you always could help me out of some confusion and come up with new ideas. I learnt so much from you. I am really grateful for this friendship. I am so glad that you found an assistant professor position at the University of Groningen. I wish you all the best at your job. **Wei Zhang** and **Yang Liu** - such a nice couple! We first met each other three and a half years ago, and we got to know each other so rapidly since we all joined the bus trip to Germany and Austria. Later, we traveled together with other friends in the summers of 2016 and 2017. We always helped each other by discussing issues from projects. Both of you can cook incredible food and invited me many times. We will definitely see each other again in China. I would like to be invited when you have your wedding ceremony. **Bin Sun** and **Benchi Wang**, I am so glad to have met you two in Amsterdam and to be friends with you. You two were amazing hosts for food and drink, and even BBQs. Bin showed me the best way to cook food. Benchi showed me the best way to work hard and play

hard. Both of you are such smart guys. I learnt so much from you two. I grew up in a poor family, which had such an effect on me. I was always really jealous of what you guys had before, but I will not be jealous any longer. Hopefully you guys are enjoying your jobs and lives. We will definitely see each other in China and drink over and over when we meet. **Yongzhi Gao**, my ex-roommate and ex-colleague from the same supervisor. Thank you for so much support. I am very grateful for this. I always believe that you can go further and beyond with your ambition. I wish that you will enjoy the rest of your PhD and find a nice job in the Netherlands. **Yiwen Tang**, **Yipeng Song** and **Shaotao Bai**, I am so lucky to have met you guys in Amsterdam. As same-year PhD students, you guys always encouraged me and showed me endless support. All three of you guys have so many strengths. I have definitely learned a lot from each of you and I am thankful for the opportunity to be friends with you. I wish you guys all the best and enjoyment in what you are doing. I would like to also thank other friends I met in Amsterdam and in China: **Yaya Liu, Jiming Li**, **Jinlan Wang**, **Biwen Wang**, **Hao Li**, **Yumei Wang**, **Luting Song**, **Xiaojuan Zhao**, **Chuan Wu**, **Huiqin Gao**, **Yuanqing Wang**, **Sheng Zhou**, **Chao Ding**, **Lina Jiang**, **Huan Li**, **Yao Tong**, **Na Li**, **Yanhao Lin**, **Ting Liu**, **Yujing Ma**, **Dongdong Zhen**, **Yansong Feng**, **Aaron**, **Xiang Zhen**, **Ken**, **Suzy**, **Fangying Chen**, **Shuguang Yuan**, **Jena**, **Edgar**, **Mary**, **Mia**. I have to thank some of my ex-roommates: **Tianfen Wang**, **Liya Yang**, **Yisha Bu**, **Sheng Xu**, **Yongmei Sun**. Your support and care made my PhD days so enjoyable and unforgettable. I wish you all the best in the future. **Yongjie Zhang**, it was so nice to meet you at the VU. I am still grateful that at the beginning of my PhD study, you instructed me a lot, telling me how to get along with colleagues and how to improve my English and manage projects. In the first two years, we liked making jokes with each other. That was lots of fun. I wish you all the best. **Zhiqing Zhang** and **Meichen Yu**, I am very glad to know you two. Thanks for many suggestions and for being supportive to me. **Zhigang Rao**, my ex-roommate of three years during my master study. We talked a lot about science and projects. Thanks for visiting me in Amsterdam in April 2017. I hope you also can manage your PhD graduation in Germany soon. We will of course see each other in China. **Peipei**, such a nice and kind Chinese friend. I can still recall the time that we drank together and played lots of games. Hope you find a job here and enjoy the rest of your time in Amsterdam. **Yanfang Li**, **Mengjia Li**, **Chuli Zhou**, thanks for sharing plenty of valuable talks with me. I really enjoyed the moments that we talked to each other on the phone. Best wishes with your PhD in China (Mengjia). **Xiaoqi**, the first Chinese friend I made outside of university in Amsterdam. You were also my first roommate for half a year. I hope you enjoy your work and time in the Netherlands. **Irina**, thanks for plenty of valuable support and care when I felt down. I wish to visit you in Ukraine in the near future. **Difei Yu** and **Wenjia Liu**, I am so happy to have met you two during different periods of my PhD days. Thanks for sharing all of the good times with me here in Amsterdam. **Yufang Zhao** and **Qin Zeng**, many thanks for your strong support and talks at the beginning of the PhD. I really appreciated all of the enjoyable moments we had. **Xin Zhao**, such a nice Chinese PhD. We both stayed in Wuhan University for master study, but we did not meet each other. Thanks for your

strong support and companionship during the first two years. I hope that you enjoy your work and I wish you all the best. **Danwei Gu, Mengjie Ying**, thanks for your strong support and companionship. Together with you, I got to know myself better and better. **Juliana**, my best neighbor in Amsterdam. Thanks for your huge support and help. The beautiful moments we shared are unforgettable. Hopefully you are enjoying your job in Brazil. I am ready to visit you in Brazil. I am also ready to welcome you in China. I wish to see you sooner rather than later. **Henriette Schoemaker**, I would like to give my special thanks to Henriette. You helped me to improve my English a lot. That made my following PhD days smoother and much more enjoyable. **Hui Zhu**, thanks for your financial support. You are the best teacher I have ever met. I can still clearly recall all of your words from when I was a little middle-school student. I am sincerely grateful for your trust, inspiration and encouragement. What you taught me in the past 17 years has enlightened and motivated me to be strong, and to confront all future challenges, both in my life and in academia. Right now I am your friend and always will be. I wish you all the best, and hope that we will see each other in China sooner rather than later!

Xiaodan Wang, **He Lei** and **Jinchun Xiao**, my best three friends from high school. Thanks for your guys' endless love and unconditional support. In the past 14 years, we have shared so many enjoyable and unforgettable moments. You are my life-long friends. It's the greatest pleasure to have you guys in my life. I've learned so much from each of you. I felt guilty that I could not attend He's wedding ceremony, but I will for sure attend Xiaodan's and Jinchun's wedding ceremonies. Hopefully, you guys will not miss mine. We will definitely see each other in China!

Hailing Hu, I will see you in China soon.

Last, but definitely not least, I would like to thank my parents for their endless love and unconditional care. I knew you did not agree with me going abroad for the PhD, but now you can be proud to know that I am the first person in my village who is awarded a PhD degree from abroad. I thank my siblings for their care and love. I am so lucky to have two older sisters and two brothers.

List of Publications

Publications related to this thesis:

1. The route to prolonged residence time at the histamine H_1 Receptor: growing from desloratadine to rupatadine
Zhiyong Wang*, Reggie Bosma*, Albert J. Kooistra, Nick Bushby, Sebastiaan Kuhne, Jelle van den Bor, Michael J. Waring, Chris de Graaf, Iwan J. de Esch, Henry F. Vischer, Robert J. Sheppard, Maikel Wijtmans and Rob Leurs
J. Med. Chem. **2019**, *62,* 6630-6644 (**co-first author**)

2. Exploring the effect of cyclization of histamine H1 receptor antagonists on ligand binding kinetics.
Zhiyong Wang*, Reggie Bosma*, Sebastiaan Kuhne*, Jelle van den Bor, Wrej Garabitian, Henry F. Vischer, Maikel Wijtmans, Rob Leurs and Iwan J. P. de Esch
Manuscript submitted.

3. Bioisosteric replacements of carboxylic acid to explore binding kinetics on the histamine H_1 receptor.
Zhiyong Wang, Sebastiaan Kuhne, Reggie Bosma, Daniel Da Costa Pereira, Philipp Fronik, Marc Stroet, Melanie van der Woude, Ivana Josimovic, Loretta Inkoom, Mounir Andaloussi, Henry F. Vischer, Iwan J. P. de Esch, Maikel Wijtmans and Rob Leurs
Manuscript to be submitted.

4. Design and synthesis of photocaged H_1 receptor antagonists for GPCR photopharmacology.
Zhiyong Wang, Ivana Josimovic, Tiffany K van der Meer, Hans Custers, Andrea van de Stolpe, Karan Pultoo, Henry F. Vischer, Iwan J. P. de Esch, Maikel Wijtmans and Rob Leurs
Manuscript in preparation.

Publications not related to this thesis:

1. Selenophenes: introducing a new element into the core of non-steroidal estrogen receptor ligands
Zhiyong Wang*, Silong Zhang*, Zhiye Hu, Changhao Li, Chu Tang, Kathryn E. Carlson, Junjie Luo, Chune Dong, John A. Katzenellenbogen, Jian Huang and Hai-Bing Zhou
ChemMedChem **2017**, *12,* 235-249 (**co-first author**)

2. C_2-symmetric BINOL-squaramide as efficient organocatalyst for the enantioselective alpha-amination of 1,3-dicarbonyl compounds with dialkyl azodicarboxylates
Zhi-yong Wang*, Shi Tang*, Bin Liu and Chun-E. Dong
Chin. Chem. Lett. **2015**, *26,* 744–748 (**co-first author**)